DOE/NASA/0008-12
NASA CR-165139

CERAMIC REGENERATOR SYSTEMS DEVELOPMENT PROGRAM — FINAL REPORT

C. A. Fucinari, C. J. Rahnke, V. D. N. Rao, J. K. Vallance
Research Staff
Ford Motor Co.

(NASA-CR-165139) CERAMIC REGENERATOR SYSTEMS DEVELOPMENT PROGRAM Final Report, 1 Oct. 1976 - 31 Dec. 1979 (Ford Motor Co.) 264 p HC A12/MF A01 CSCL 10B

N81-22982

Unclas
G3/85 21923

October 1980

Prepared for
NATIONAL AERONAUTICS AND SPACE ADMINISTRATION
Lewis Research Center
Under Contract DEN 3-8

For
U.S. DEPARTMENT OF ENERGY
Automotive Technology Division

DOE/NASA/0008-12
NASA CR-165139

CERAMIC REGENERATOR SYSTEMS DEVELOPMENT PROGRAM — FINAL REPORT

C. A. Fucinari, C. J. Rahnke, V. D. N. Rao, J. K. Vallance
Research Staff
Ford Motor Co.

1980

Prepared for
National Aeronautics and Space Administration
Lewis Research Center
Cleveland, Ohio 44135
Under Contract DEN 3-8

For
U.S. DEPARTMENT OF ENERGY
Automotive Technology Division

TABLE OF CONTENTS

TABLE OF CONTENTS — Continued

LIST OF ILLUSTRATIONS

LIST OF ILLUSTRATIONS — Continued

LIST OF ILLUSTRATIONS — Continued

LIST OF ILLUSTRATIONS — Continued

LIST OF ILLUSTRATIONS — Continued

LIST OF ILLUSTRATIONS — Continued

LIST OF ILLUSTRATIONS — Continued

LIST OF ILLUSTRATIONS — Continued

LIST OF ILLUSTRATIONS — Continued

LIST OF ILLUSTRATIONS — Continued

LIST OF ILLUSTRATIONS — Continued

LIST OF ILLUSTRATIONS — Continued

LIST OF ILLUSTRATIONS — Continued

LIST OF ILLUSTRATIONS — Continued

LIST OF ILLUSTRATIONS — Continued

LIST OF ILLUSTRATIONS — Continued

LIST OF ILLUSTRATIONS — Continued

LIST OF TABLES

LIST OF TABLES — Continued

SUMMARY

This is the final report for the NASA/Ford Ceramic Regenerator Systems Development Program. It describes all of the results obtained in this program, which started October 1, 1976 and was completed December 31, 1979.

TASK I. CORE DURABILITY TESTING AT 800°C (1472°F)

Approximately 77,296 core hours of engine durability test at 800°C (1472°F) were completed under this program. This exceeds the Task I objectives which was 76,000 hours at this temperature.

Turbine engine durability tests on aluminum silicate regenerator cores show that this material is relatively impervious to chemical attack. Fourteen cores of this material have each accumulated over 5000 hours of engine test at 800°C (1472°F), and five cores have each attained the durability objective of 10,000 hours with a minimal amount of chemical attack damage.

One thin-wall AS core has now accumulated 10,000 hours of engine test.

A Supplier D first-generation MAS core has accumulated 5381 hours at 800°C (1472°F). A Supplier D MAS core made from a more advanced material having lower thermal expansion characteristics and greater strength has now accumulated 3518 hours. This latter core shows no evidence of thermal or chemical attack damage.

A MAS core made by Supplier I from extruded segments has now accumulated 2474 hours at 800°C (1472°F). This core also shows no evidence of thermal or chemical attack distress.

Little problem has been encountered with the elastomer which bonds the ring gear to the regenerator matrix for thick-wall AS or MAS assemblies. The elastomer cut from an assembly after 7000 hours of engine test, shows little sign of aging.

Separations in the elastomer-matrix bond region have occurred on all of the weaker thin-wall AS cores bonded using the conventional technique. Utilization of a high-compliance elastomer system shows promise of solving this problem. Two different high compliance elastomer configurations were tested with a maximum of 7954 hours accumulated on one core.

The cement holding the hub inserts in place failed in eight out of the first eighteen AS cores that have undergone engine test. A re-designed hub configuration which utilizes a solid ceramic ring around the hub insert was tested and appears to have corrected this problem. Approximately 35,000 hours have been accumulated on a sample of eleven of these re-design hubs with the highest hour one completing 7200 hours of engine test.

At the present time, thirteen engines have been on test with the current three-point support or rim-mounting system. No major difficulties have been encountered after 61,114 hours.

The spring and fixed roller ball bearings in the mounting system in all the engines were replaced by solid graphite bearings which do not require lubrications. None of these bearings failed, and wear rate appears to be satisfactory with some graphite bearings having now accumulated 3600 hours.

TASK II. CORE DURABILITY TESTING AT 1000°C (1832°F)

Twelve different regenerators have been tested at 1000°C (1832°F) and this sample has accumulated 28,834 hours at this temperature. This accumulation exceeds the Task II program objective of 28,000 hours.

About 8071 hours of engine test at an average regenerator inlet temperature of 982°C (1800°F) have been accumulated on a Supplier A first-generation, thick-wall aluminum silicate core, and 5411 hours at this temperature have been accumulated on a thin-wall core of the same material. Neither core shows any signs of thermal or chemical attack damage after this exposure. A total of four AS cores have each exceeded 5000 hours of engine test at this temperature without distress.

A second-generation AS material from Supplier A, which has higher temperature capability (1100°C, 2012°F), has accumulated 310 hours at 1000°C (1832°F). This advanced material shows good mechanical integrity, seal compatability and no signs of distress after this exposure.

A core of Supplier D's second-generation MAS and another fabricated by Supplier I from extruded MAS segments were placed on test at 1000°C (1832°F). These cores accumulated 437 and 236 hours, respectively. Neither core showed any sign of chemical or thermal distress after operation at this temperature.

TASK III. MATERIAL SCREENING TESTS

The laboratory tests are more severe than the corrosive conditions prevalent during normal engine operation. Thus, the test sequence provides an excellent screening procedure for determining likely materials that can survive engine durability testing.

Based on test results from this task, the MAS matrix materials provide the best resistance to chemical attack in the engine environment for the regenerator application.

TASK IV. AEROTHERMODYNAMIC PERFORMANCE

Since the start of this program in October 1976 nineteen matrices were evaluated in a shuttle rig, which exceeds the twelve sample task objective. Together with the twenty matrices evaluated previously the existing matrix sample size is thirty-nine. Twenty-five rectangular, eight sinusoidal, four isosceles triangular, and two hexagonal configuration comprise the present matrix sample size.

In addition, the present sample size represents a good cross-section of the different manufacturing processes which are currently being evaluated as follows:

1. Supplier A — Corrugating or extrusion
2. Supplier B — Stacked extruded tubes
3. Supplier C — Corrugating
4. Suppliers D and E — Calendering
5. Supplier I — Extrusion
6. Supplier J — Embossing or stamped sheets

Several factors that merit design considerations in the utilization of this test data were illustrated as follows:

1. Matrix Quality
2. Fin Geometry
3. Aspect Ratio
4. Length to Hydraulic Diameter

Aerothermodynamic performance characteristics can be significantly altered by variations in fin shape uniformity, bond quality and surface roughness. Based on the present matrix sample size, up to 25% variation in overall fin efficiency can occur due to manufacturing process limitations.

Utilizing overall fin efficiency (J/F) as a basis for comparison, and considering matrix fin configurations with equivalent hydraulic diameter, wall material thickness, and flow length, the effect of fin geometry can be summarized as follows:

1. The sinusoidal triangular structure appears to be the least efficient fin configuration. An increase in heat transfer efficiency accompanied by an increase in pressure drop can be obtained by reducing the aspect ratio of this type of surface geometry to approach the extruded isosceles triangular structure.

2. For embossed rectangular structures, heat transfer and pressure drop characteristics appear to increase with increasing aspect ratio.

When selecting a matrix fin geometry for a fixed size heat exchanger the effect of length to hydraulic diameter should be considered. If the L/DH of the particular application is significantly different than the matrix test sample flow conditions, the performance characteristics of the matrix fin geometry should be adjusted accordingly.

The first attempt to evaluate the effect of a wavy flow passage was completed. The wavy flow passage increased the heat transfer and pressure drop characteristics 20% and 17.5% respectively for a 2% improvement in overall fin efficiency.

The examples in this section have served to illustrate the important factors that must be considered when selecting an optimum fin configuration for a given heat exchanger application. When selecting the best existing fin geometry for a given heat exchanger size and flow conditions, the passage geometry, material thickness

and limitations of the method of fabrication must all be considered. Utilization of the alternate heat transfer (A) and pressure drop (C) characteristics accounts for all of these factors for matrices fabricated from existing tooling.

When selecting the most efficient fin shape for a new set of tooling, the standard heat transfer (J) and pressure drop (F) characteristics can be utilized, since the material wall thickness is factored out. Once the desired fin geometry is selected, the fabrication technique must be capable of producing the required material wall thickness and sample quality. This explains how an apparently less efficient fin shape (sinusoidal) can yield improved performance for a specific regenerator application due to the ability of the fabrication method to produce a much thinner structure.

TASK V. DESIGN STUDIES OF ADVANCED REGENERATOR SYSTEMS

Three matrix types have been characterized in terms of radial and tangential MOR and MOE and radial compressive strength: the Supplier A wrapped, sinusoidal passage AS; the Supplier D wrapped, rectangular passage MAS-2; and the Supplier I extruded triangular passage MAS. Weibull distribution of these data indicates the variation in properties for each supplier are the result of processing variations between cores rather than fundamental material property differences.

Three-dimensional finite element stress anaylsis of the above matrix configurations indicated stress relief slots substantially reduce tangential stress in the rim of a regenerator, compared to an unslotted regenerator. Localized high stress regions do occur at the slot below the hot face, but they diminish rapidly with distance. Consequently, they usually do not propagate to the hot surface of the core.

The maximum stress is a function of the number of equally spaced slots and the slot geometry. The slot geometries evaluated consist of a one inch radial depth at the hot face which is tapered axially to 25%, 50% or 100% of the core thickness.

Tangential stress safety factors are defined as the ratio of maximum stress to average strength. Due to the large variance in physical properties of cellular ceramic structures, there is an equally large variance in thermal stress safety factors. Consequently these values should be compared on a relative basis to determine durability potential for various designs.

An axisymmetric finite element analysis indicates that in order to successfully bond a ring gear to a thin-wall AS core, a minimum reduction of 70% in apparent elastomer modulus is required. The interrupted elastomer configuration, which has operated successfully in the engine, has been shown to provide a 90% reduction in apparent modulus compared to the standard configuration.

A preliminary test evaluation indicates that with the exception of the inner seal crossarm, current state of the art seal coatings appear to be acceptable for 1200°C (2192°F) regenerator inlet temperature operation. Additional testing is required to establish the upper temperature limitation of the crossarm coating.

A material with higher temperature capability, such as silicon nitride, may be required for regenerators where the inlet temperature exceeds 1100°C (2012°F) or 1200°C (2192°F). Increased axial length and hydraulic diameter would have to be incorporated into regenerators of these materials to control pressure loss and still compensate for the axial conductivity loss inherent with these high conductivity materials.

TASK VI. THERMAL STABILITY TESTS OF CERAMICS

The laboratory test data generated provides a basis for the determination of the potential service temperature capability of the various materials available for the regenerator application.

The first-generation AS material appears to have insufficient thermal stability above 1000°C service. The second-generation AS material appears to have sufficient thermal stability for 1100°C applications.

Properly fired MAS matrices have demonstrated thermal stability and excellent resistance to sodium ion attack at temperatures up to 1200°C.

TASK VII. MANUFACTURING COST STUDIES

An initial cost study was updated to include more recent process developments and to account for inflation and rising energy costs. In addition, two additional heat exchanger sizes applicable to automotive gas turbine engines were also evaluated.

A cost comparison of two fabrication techniques (conventional and zero-wind) was completed. Data for two regenerator core configurations indicate a production cost increase ranging from 15% to 26%, depending on core configurations.

TASK VIII. CORE MATERIAL AND DESIGN SPECIFICATION

A core material and design specification for a regenerative heat exchanger intended for operation in a gas turbine engine with a maximum of 1000°C (1832°F) inlet temperature was completed. This procurement specification evolved from experience accumulated over the last thirteen years in laboratory and engine testing of ceramic materials proposed for service as regenerator cores in the Ford 707 Gas Turbine at 800°C (1472°F) and 1000°C (1832°F) maximum inlet temperature.

The specification was written in a general sense and is intended to include a wide variety of ceramic materials fabricated into high open area cellular structures by any one of a number of viable processes. These fabrication techniques include extrusion, wrapped paper, calendering, embossing, glass tube bundling and others.

TASK IX. PROJECT MANAGEMENT

Program emphasis was directed to increased engine testing at 1000°C (1832°F) during the second quarter of 1978. In order to increase confidence level in B_{10} life projections for AS cores, the original program was extended an additional year at no additional cost to NASA.

Based on an empirical reliability relationship from Weibull distribution theory the confidence level for AS cores varies from 47% to 80% for a B_{10} life at 800°C (1472°F) of 10,000 and 5000 hours, respectively.

INTRODUCTION

Since 1965, Ford Motor Company has been engaged in developing a ceramic regenerator system for use in gas turbine engines. Over 100,000 hours of engine operating experience have been accumulated on a sample of approximately 1,000 regenerator cores fabricated of lithium aluminum silicate (LAS) and produced by two suppliers.

By 1971, when Ford started limited production of the 707 series industrial gas turbine engine, it was believed that the regenerator system had a durability life of at least 4000 to 5000 hours. Because of unexpected sporadic failures in applications such as generator sets and pleasure boat installations, a new series of controlled durability tests was started. When these tests were terminated in August, 1973, 11 core failures had occurred out of a sample of 30 cores on test. It was determined that the failures were primarily caused by a severe chemical attack on the lithium aluminum silicate material used. This test data showed that these regenerators had a B_{10} life of 600 hours and an average life of 1600 hours.

Late in 1973, an engineering research program was initiated to solve the regenerator core failure problem. The primary objective of this program is to develop ceramic regenerator cores that can be used in passenger car gas turbine engines, Stirling engines, industrial/truck gas turbine engines and other industrial waste heat recovery systems. Specific durability objectives are defined as achieving a B_{10} life of 10,000 hours on a truck/industrial gas turbine engine duty cycle at a regenerator inlet temperature of 800°C (1472°F).

In late 1973 Ford funded several companies to develop new ceramic regenerator materials. By 1974, new materials, including aluminum silicate (AS) and a magnesium aluminum silicate (MAS) were screened in laboratory and engine tests and found to have acceptable resistance to chemical attack. Regenerator cores made from new materials were placed on durability test late in 1974 and early in 1975.

The Ford 707 industrial turbine was used as the test bed to evaluate these new regenerator materials and concepts. Since 1974, over 109,126 engine test hours (218,252 core hours) have been accumulated on regenerator systems.

Late in 1974, the Alternate Automotive Power Systems Division of the Environmental Protection Agency joined with Ford Motor Company in an "Automotive Gas Turbine Ceramic Regenerator Design and Reliability Program." In early 1975, this program was transferred to the newly-formed Energy Research and Development Administration (ERDA), and since October 1, 1976 this program has been under the direction of the National Aeronautics and Space Administration (NASA). A description of the work conducted in these programs is contained in References 1 through 8.

The present DOE/NASA cost-sharing program with Ford Motor Company continues the ceramic regenerator design and development work that was started under the original EPA/FORD contract. This latest program is subdivided into ten major tasks. These tasks are:

Task I — Core Durability Testing at 800°C (1472°F)
Task II — Core Durability Testing at 1000°C (1832°F)
Task III — Material Screening Tests
Task IV — Aerothermodynamic Performance
Task V — Design Studies of Advanced Regenerator Systems
Task VI — Ceramic Thermal Stability Tests
Task VII — Manufacturing Cost Studies
Task VIII — Core Material and Design Specifications
Task IX — Program Management
Task X — Reporting Requirements

The technical progress in each of these tasks for the period from October 1, 1976 to December 31, 1979 is recorded in the following sections of this report.

DISCUSSION OF RESULTS
TASK I. CORE DURABILITY TESTING AT 800°C (1472°F)
I.A. INTRODUCTION

Reference 1 describes the engine test results obtained by Ford Motor Company on lithium aluminum silicate ceramic regenerators used in the 707 turbine engine up to the end of 1973. These regenerator cores were mounted at the hub and driven through ceramic pins cemented into the rim. These data showed that chemical attack was the major cause of failure, and that this type of regenerator core configuration would have a B_{10} life of 600 hours and a B_{50} life of 1600 hours. A B_{10} life of 600 hours was obtained from a Weibull Analysis of the failures in this sample, and means that 10% of the regenerators of this configuration will fail in less than 600 hours of engine test. A B_{50} life of 1600 hours means that 50% of the regenerators will fail in less than 1600 hours of engine exposure.

By 1975 AS and MAS regenerators had been successfully fabricated, and these materials showed promise in both laboratory and accelerated engine tests. They were placed on long term durability tests and the results are reported in References 2 to 8. The total accumulation of engine test hours since the start of the test program on January 1, 1974 is 109,126 hours (218,252 core hours). With respect to the current program with NASA, a total of 77,296 core hours have been accumulated at 800°C (1472°F) since the program was started on October 1, 1976. This test hour accumulation exceeds the program objective for Task 1, which was an accumulation of 76,000 core hours.

I.B. DISCUSSION

I.B.1 Durability Record of Aluminum Silicate Regenerators

To date, 23 aluminum silicate (AS) regenerators, fabricated by Supplier A, from their original AS composition have been engine tested in the Ford 707 turbine. While all these cores contain the same material they can be broken down into two classifications depending upon their fin geometry and wall thickness. The original AS configuration was a thick-wall matrix containing about 900 holes per square inch. As part of a program to fabricate higher performance rotary heat exchangers, Supplier A developed a thin-wall, aluminum silicate material. The thick-wall aluminum silicate has an average matrix wall thickness of 0.11mm (.0043 inch) while the thin-wall has a thickness of 0.07mm (.0026 inch) and contains 1300 holes per square inch. A performance comparison, which is based on shuttle rig test results, shows that the thin-wall matrix will have an effectiveness at part power that is about 1-2% higher than that of the thick-wall matrix. This could be translated into about 5-10% gain in part power fuel economy when a thin-wall regenerator is operated in the 707 turbine engine.

Eleven thick-wall AS cores were tested at 800°C (1472°F) under identical operating conditions and these cores make up the control sample on which durability projections will be based. The durability status of these cores is shown in Figure I.B.1.1. About 68,000 core hours of engine test have been accumulated on this aluminum silicate sample with four cores having attained the durability objective of 10,000 hours.

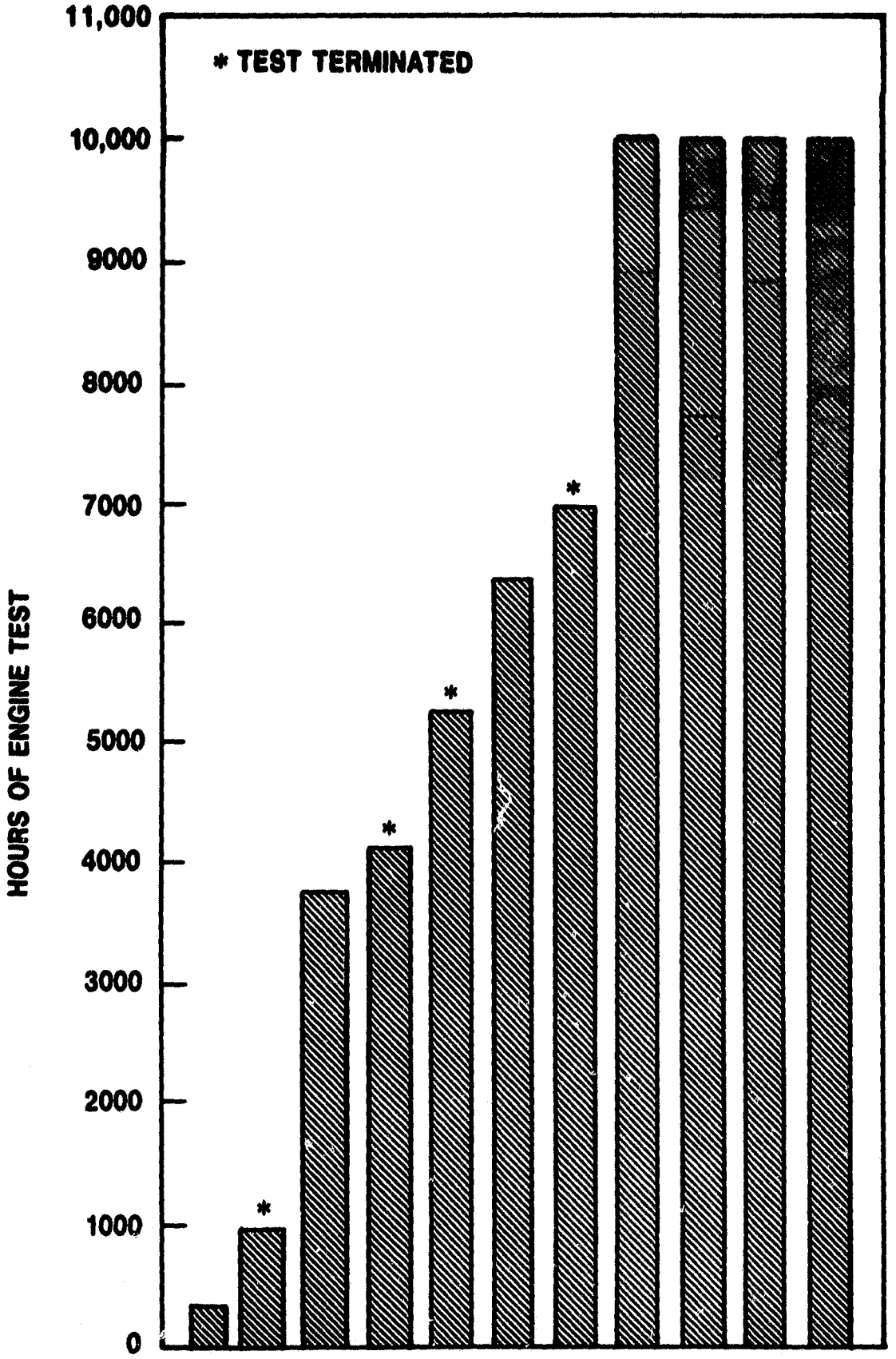

Figure I.B.1.1 **Durability Record of Thick-Wall AS Regenerators Operating at 800°C (1472°F)**

Five thin-wall AS cores have also been engine tested at 800°C (1472°F) as shown in Figure I.B.1.2 and one core has accumulated over 10,000 hours.

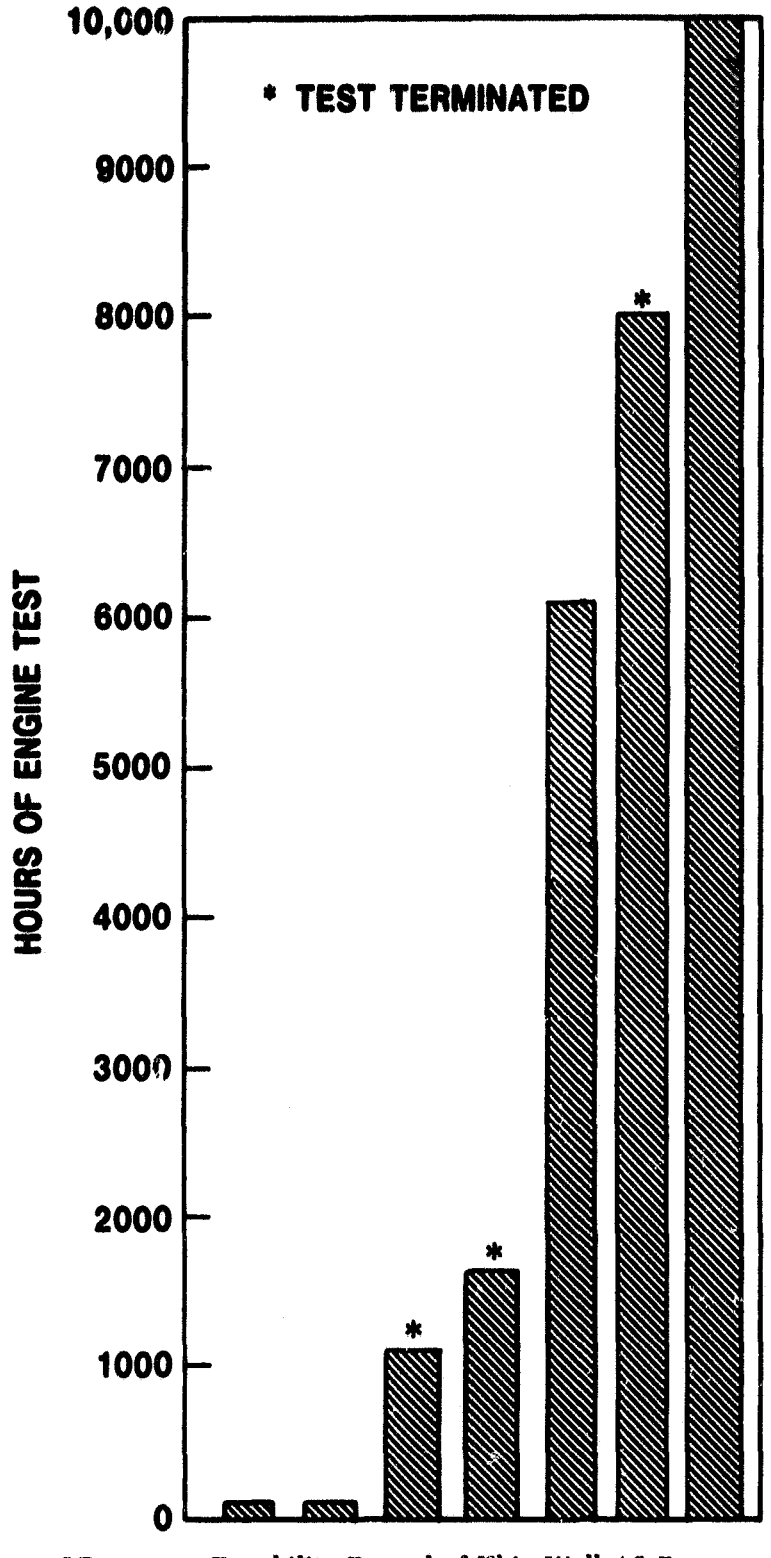

Figure I.B.1.2 Durability Record of Thin-Wall AS Regenerators Operating at 800°C (1472°F)

The running history of all Supplier A's AS cores that have been engine tested are shown in Figure I.B.1.3. This figure also includes the seven cores tested at 1000°C (1832°F) and described in Section II.B. Over 125,000 hours of engine test have been accumulated on this material. None of these cores show any serious signs of thermal distress or chemical attack damage. To date, a total of fourteen AS cores have accumulated over 5,000 hours and eight cores have each accumulated over 7,000 hours of engine test without visual distress.

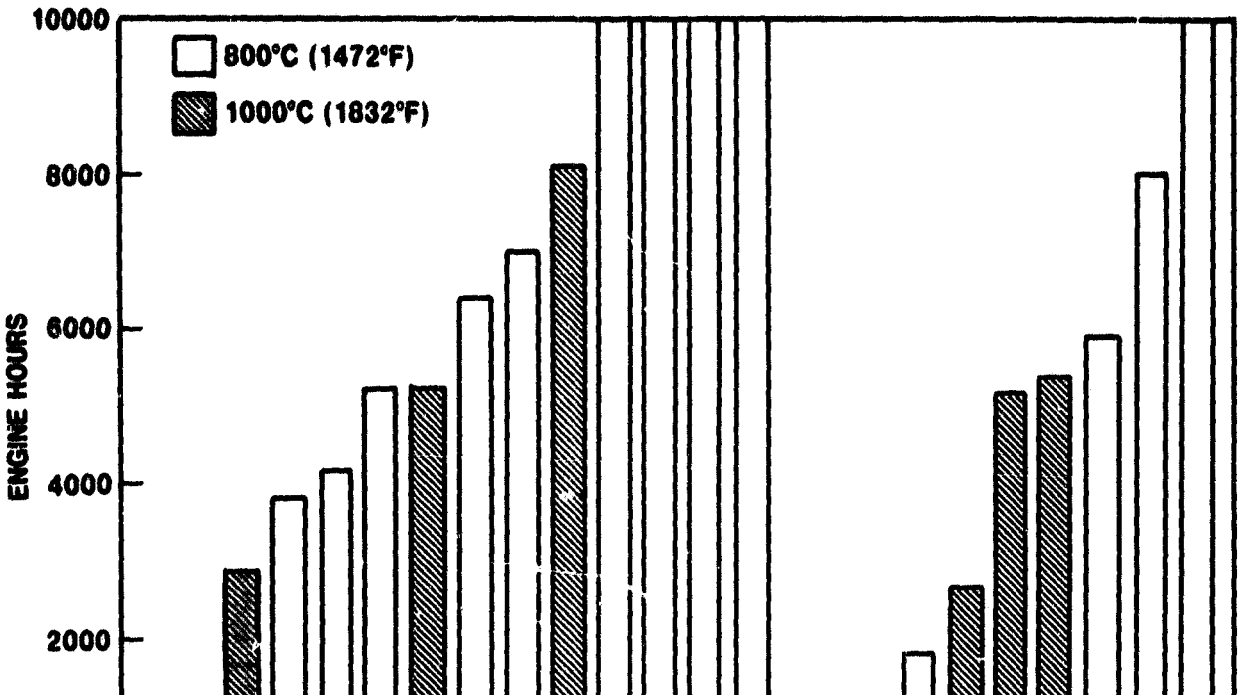

Figure I.B.1.3 **Durability Record of All AS Regenerators Engine Tested in the Ford 707 Turbine**

At least two failures are required before a Weibull failure analysis can be made. Since there have been no true core failures of matrices made from this material, a failure analysis cannot be initiated. Utilizing the current individual core hours of all of the AS cores together with an empirical reliability relationship from Weibull distribution theory, the projected confidence level for various B_{10} life objectives were estimated as illustrated on Figure I.B.1.4.

This durability record of AS regenerators, and the fact that there were no failures of AS cores in over 125,000 hours of engine test, can be compared to the durability record of LAS regenerators. The Weibull plot shown in Figure I.B.1.5 and taken from Reference 1 is presented as background data to show the level of durability that could be expected with a Lithium-Alumina-Silicate (LAS) ceramic regenerator in 1973. It is based on a sample of 30 regenerators that were tested in 13 different

Ford 707 turbine engines. Approximately 38,000 hours of core durability were accumulated on the regenerators used in this sample. The hours at which each of the eleven failures occurred is also tabulated in this figure. The failure data suggests that a B_{10} life of 600 hours and a B_{50} life of 1600 hours would probably be representative of the durability of the 1973 LAS ceramic regenerators in most gas turbine applications. The AS test data, on the other hand, shows an 80% confidence in achieving a B_{10} life of 5000 hours.

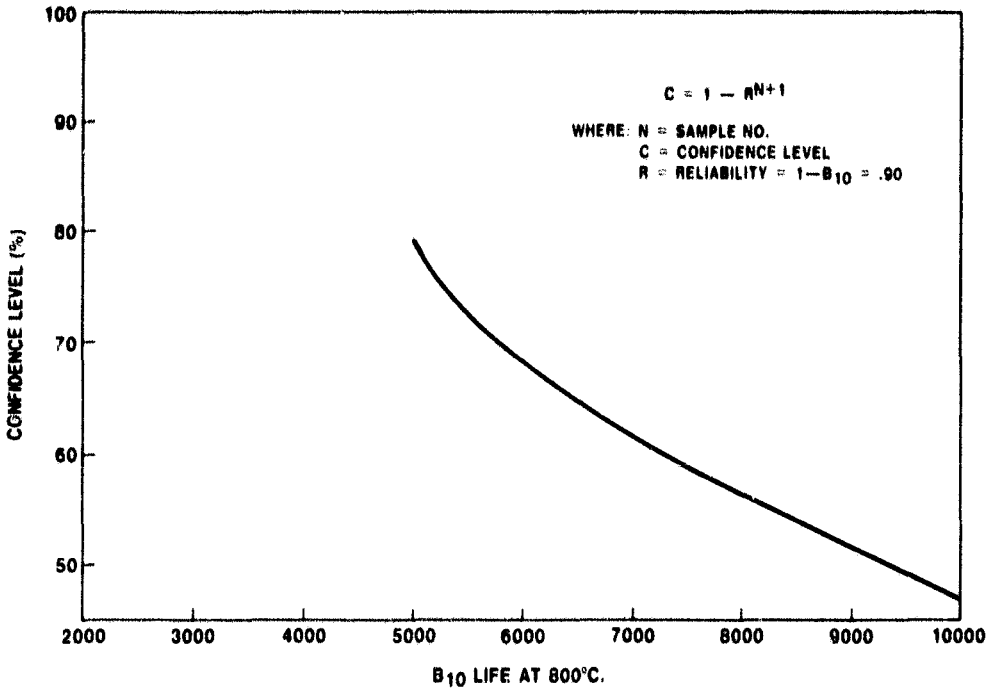

Figure I.B.1.4 Reliability Confidence Level for AS Regenerators at 800°C (1472°F)

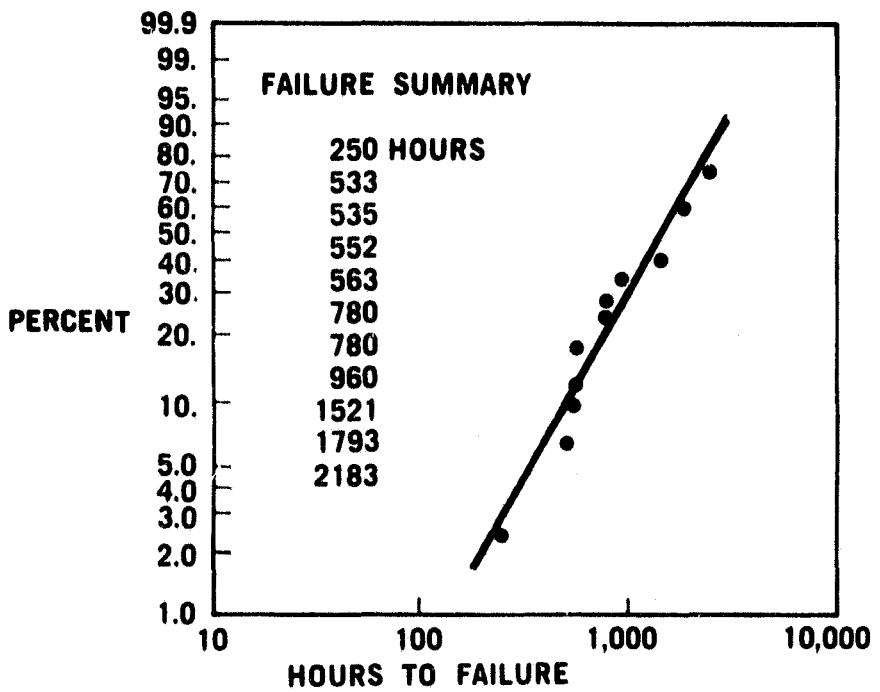

Figure I.B.1.5 Durability Record of 1973 LAS Regenerators

I.B.2 Wear of Aluminum Silicate Regenerators

Since the thin-wall AS material has 1/3 the strength of the old thick-wall LAS material, there was some concern that a regenerator seal system that had been developed for the stronger thick-wall LAS material would damage the surface of the thin-wall AS material. A comparison of the core surface wear under the peripheral seal rubbing shoe for both thick and thin-wall AS cores is shown in figure I.B.2.1. It is believed that, with the Ford seal shoe peripheral coatings, most of the core wear occurs when foreign debris is trapped or passes between the rubbing shoe and the core. Such debris may consist of powdered insulation that has eroded off the main housing insulation blankets, other ceramic dust, or rust. This debris embeds itself in the softer, cold-side rubbing shoe coating, and as a consequence no core wear is observed on this face. The debris cannot embed itself in the harder, hot-side rubbing shoe coating and will cause core surface wear in this location. The large scatter in the hot-side data reflects the random pattern in which wear occurs as well as measurement difficulty. Within the accuracy of these results it appears that the thin-wall core does not exhibit a significantly higher surface wear under the peripheral rubbing seal than does the thick-wall core.

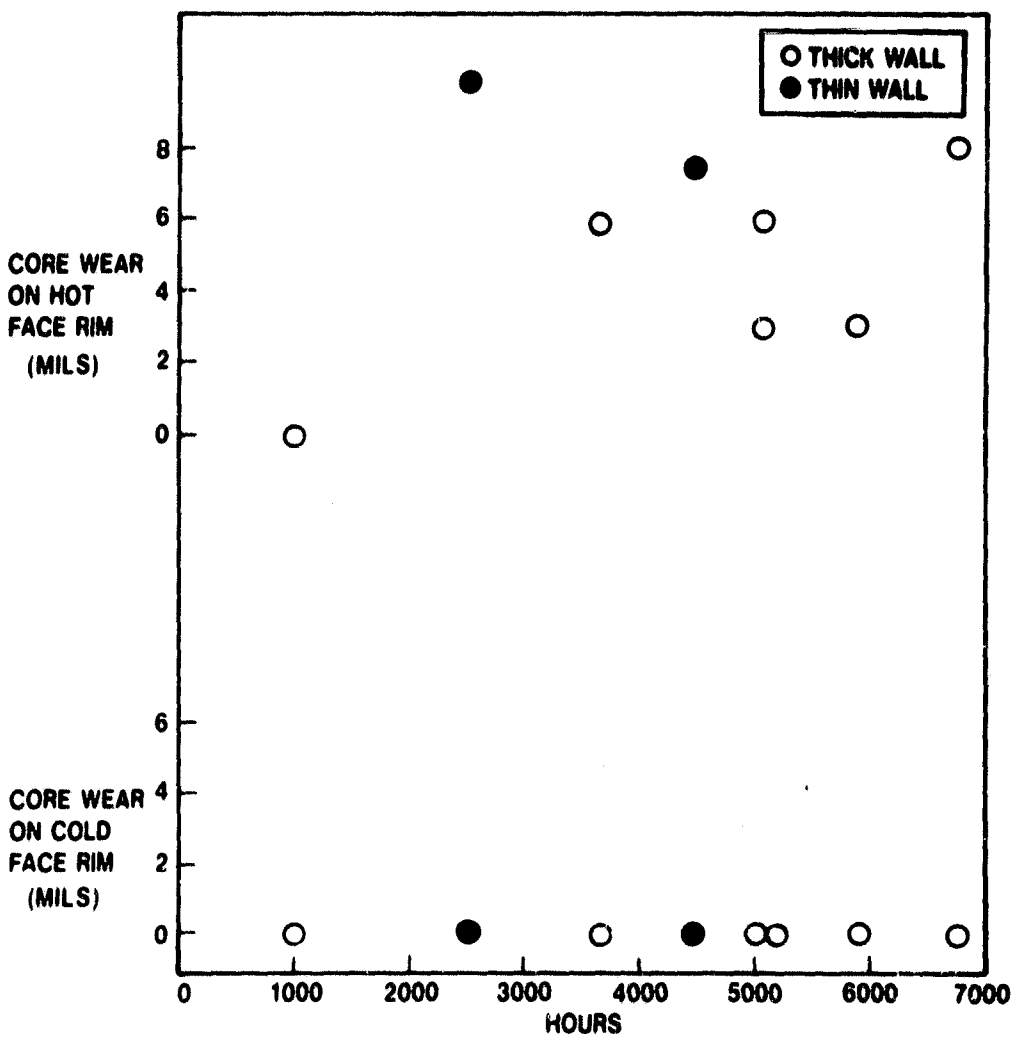

Figure I.B.2.1 Surface Wear of AS Regenerators vs. Operating Hours in an Engine

Because of the core "dishing," which will be discussed in the next section, it is almost impossible to precisely measure core surface wear due to the crossarm rubbing shoe. The measurements taken to date would suggest that neither the thick nor thin-wall cores show any measurable sign of surface wear due to the crossarm seal. While more data are needed, the thin-wall material appears to have enough integrity to withstand normal seal shoe rubbing forces.

I.B.3. Chemical Attack Measurements on AS Regenerators

None of these aluminum silicate cores exhibit any of the signs of serious distress which are typical of chemical attack. Two such signs are: the chemical composition remaining in the core after service and the amount the core has distorted or dished in its cold or free state. Chemical attack will cause lithium leaching or a change in the chemical composition on both the hot and cold side of the core. This lithium oxide loss or composition change in turn will cause a change in the crystal structure of the material resulting in a change in thermal expansion behavior and the generation of microcracks. As a consequence, one face of the core will grow more than the other, causing a dish or out-of-flatness in the core when it is cold.

Ten thick-wall aluminum silicate cores were examined for chemical attack by measuring their dishing or out-of-flatness in the free state. These values, along with the engine hours at which the measurement was made, are shown in Figure I.B.3.1. LAS regenerators usually dish 15 to 25 mils in 2,000 hours before they fail. All ten AS cores show little distortion which suggests that they have undergone little if any chemical attack damage. Since measurements were made on the cores that had accumulated 10,000 hrs. of test, these results are very encouraging. These data support the conclusions reached in the accelerated engine tests (discussed in Section III.B.3 of this report), and it appears that the aluminum silicate cores are relatively insensitive to chemical attack.

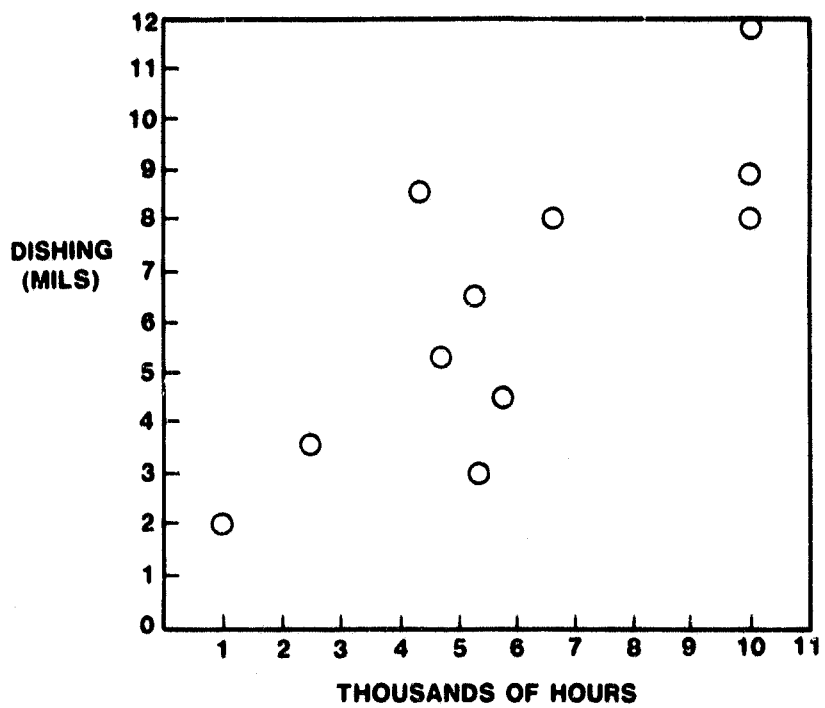

Figure I.B.3.1 Dishing History of Thick Wall AS Cores

I.B.4. Suspended Tests of Certain Cores

In determining the statistical life of a component utilizing the Weibull theory, both failed and operational components are considered in the analysis. The operational or "suspended" components, as they are called in statistical analysis, can be of two different types: those components which are still running when the testing is terminated and those components which have been failed or damaged accidentally by an external source. In this latter category are components that have been damaged by failures of the test equipment itself. In this regenerator program cores which have failed because of mechanical loads, thermal stresses or chemical attack are considered to be true failures. There have been no such failures of AS or MAS regenerators. Cores that have been damaged as a result of mishandling or because of a failure somewhere else in the engine are considered "suspended" items and will be treated as such in the Weibull Analysis. Nine such suspensions (Table I.B.4.1) occurred during the time interval covered by this program.

		REASON FOR TEST TERMINATION				
CORE NO.	DURABILITY (HOURS)	CRACKS FROM HUB CEMENT FAILURE	POWER TURBINE FAILURE	INSULATION FAILURE	GLAZED	HANDLING
34	5188	•				
54	7954	•				
56	1737	•				
53	1064	•				
32	6935		•			
27	8071			•		
51	5250			•		
57	5411				•	
47	4115					•

Table I.B.4.1 Suspended Durability Matrices

A power turbine failure occurred in engine 506 and the two cores, No. 32 and No. 45 were damaged by debris. Only the surface was damaged in Core No. 45 (Figure I.B.4.1) and it was returned to service. A cone-shaped hole (Figure I.B.4.2.) was punched in Core No. 32 by high velocity debris. Attempts to patch this hole and return the core to service resulted in a complete breakup of this core (Figure I.B.4.3). Testing of Core No. 32, which was a thick-wall AS core and had accumulated 6935 hours, was terminated, therefore, by the accidental failure of a power turbine.

Testing of another core, No. 53, was terminated when this core was damaged in shipment. This core was being returned from the Supplier after having its hub repaired (this problem is discussed in Section I.B.6) when it was broken in transit. Core No. 53 was a thin-wall AS core, and had accumulated 1064 hours of engine test.

Figure I.B.4.1 AS Core No. 45 Showing Surface Damage from Power Turbine Failure

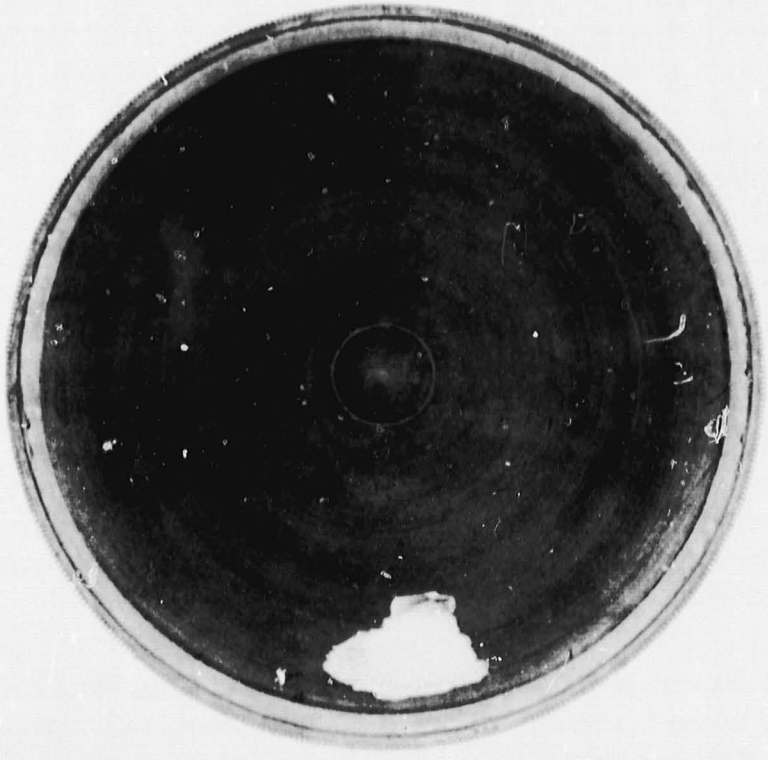

Figure I.B.4.2 AS Core No. 32 Showing Hole Made in Core by Debris from Power Turbine Failure

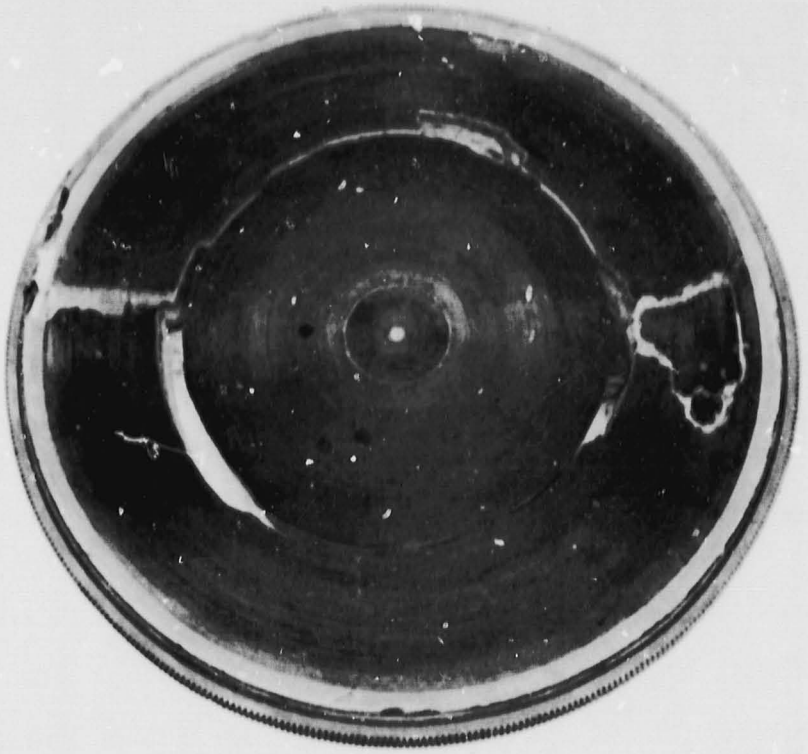

Figure I.B.4.3 AS Core No. 32 Showing Final Failure of Core Initiated in Region Damaged by Power Turbine Failure

Core No. 34 was terminated at 5188 hours when cracks which were formed during rebonding of the hub propagated to the rim and caused a segment to jam under the crossarm seal (Figure I.B.4.4). The hub cement first failed in this core after 4750 hours, causing the hub to come loose and creating three radial cracks in the matrix. This type of failure is attributed to improper processing during fabrication and is not considered a true core failure. This failure mode and the corrective action are discussed in Section I.B.6 of this report. An experimental hub held in place with three ceramic pins was then cemented into place in this core. It failed after an additional 38 hours of engine test, and this failure caused an additional growth of the three cracks initiated during the first hub failure. A third hub, incorporating a ceramic ring, was then cemented in place and the matrix cracks propagated almost to the rim during this processing. After 400 hours of additional engine test, these cracks allowed a segment to shift axially, jamming a crossarm seal.

Core No. 47 was installed backwards in an engine. Since the ring gear extends closer to the cold face than the hot face of the core, this improper installation resulted in the ring gear striking the main housing when the engine was started. The axial load imparted to the core by this housing-ring gear interference caused the core to fail (Figure I.B.4.5). The similarity between this failure and the axial load failure shown in Figure A.2.2 of Reference 1 is apparent.

Testing of thin-wall AS Core No. 56 was terminated after 1737 hours for the same reason Core No. 34 was terminated. The hub failed in Core No. 56 after 11 hours of engine test, and when it was re-cemented back in place, radial cracks were generated in the hub region (Figure I.B.4.6.). The hub came loose again after an additional 38 hours, and it was again re-cemented, aggravating the existing cracks. Final failure occurred after 1731 hours when these cracks finally propagated to the rim.

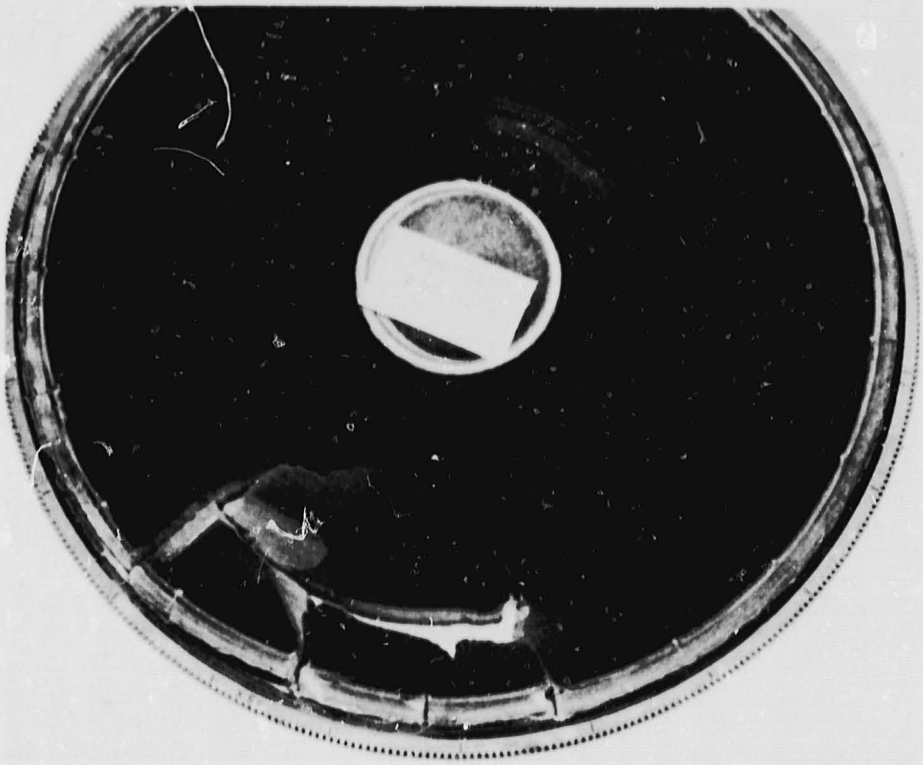

Figure I.B.4.4 Thick-Wall AS Core No. 34 Which Failed Due to Cracks That Were Initiated During Rebonding of Hub

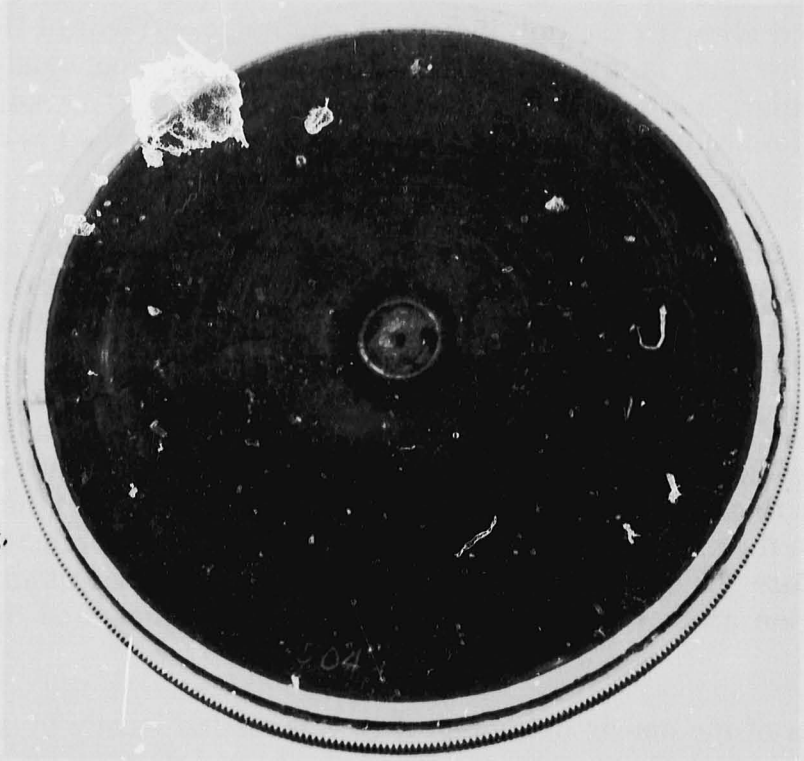

Figure I.B.4.5 Thick-Wall AS Core No. 47 Damaged Due to Improper Engine Installation

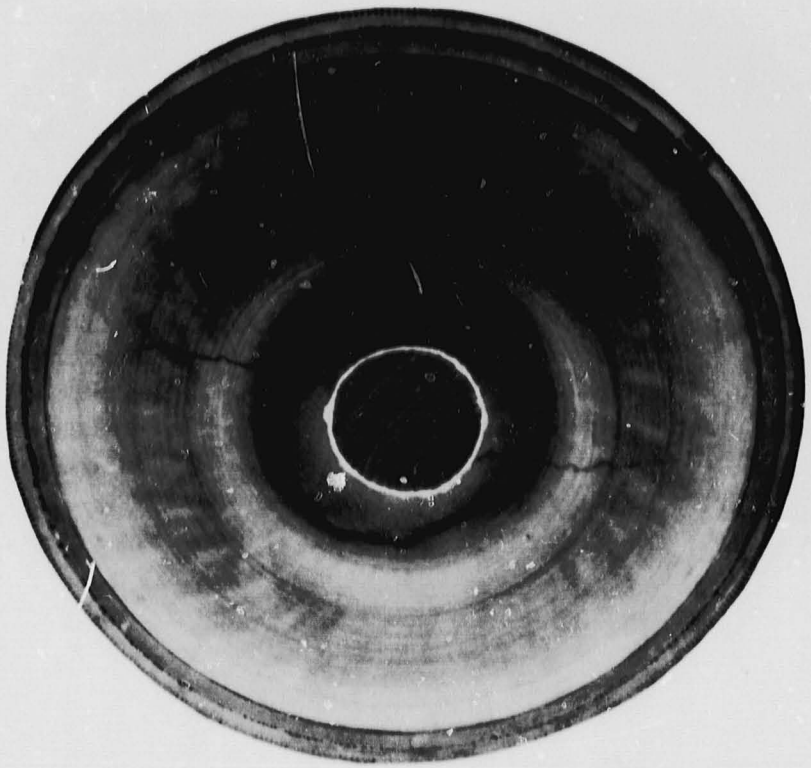

Figure I.B.4.6 **Thin-Wall AS Core No. 56 Showing Cracks Introduced When Hub Was Recemented After 11 Hours of Engine Test**

Thin-wall AS Core No. 54 was terminated after 7954 hours when a hub cement failure occurred allowing the hub insert to become loose (Figure I.B.4.7). Although this was the first hub failure for the particular core, the poor quality of the hub cement, particularly on the hot face, had been noted earlier. The radial cracks generated in this failure were serious enough, so that it was decided to retire this core also.

Four of the nine suspended tests were associated with a hub cement failure. These hub cement failures are a function of the quality of the assembly processing. This problem is discussed in detail in Section I.B.6 and a satisfactory solution, which has been proven by engine test, appears to exist.

Two cores No. 27 and No. 51 were damaged when insulation attached to metal parts in the hot flow path came loose and abraded against the matrix surface. Core No. 27 was a thick-wall AS core which had operated for 8071 hours at 1000°C (1832°F), when the surface became so badly damaged by this foreign material that it was retired. Core No. 51 was also a thick-wall AS core and had attained 5250 hours before insulation eroded the matrix material severely enough so that it also was retired.

The hot face of the matrix in another core was melted locally by a failure of the fuel control and combustion systems. During an aborted start, raw fuel impinged on this core while it was hot. The fuel ignited and the surface of the core was melted or "glazed" to a depth of 6mm (.15 inch) over 10% of the surface. This matrix, Core

No. 57, had accumulated 5411 hours at 1000°C (1832°F) when it was damaged. It was a thin-wall AS matrix.

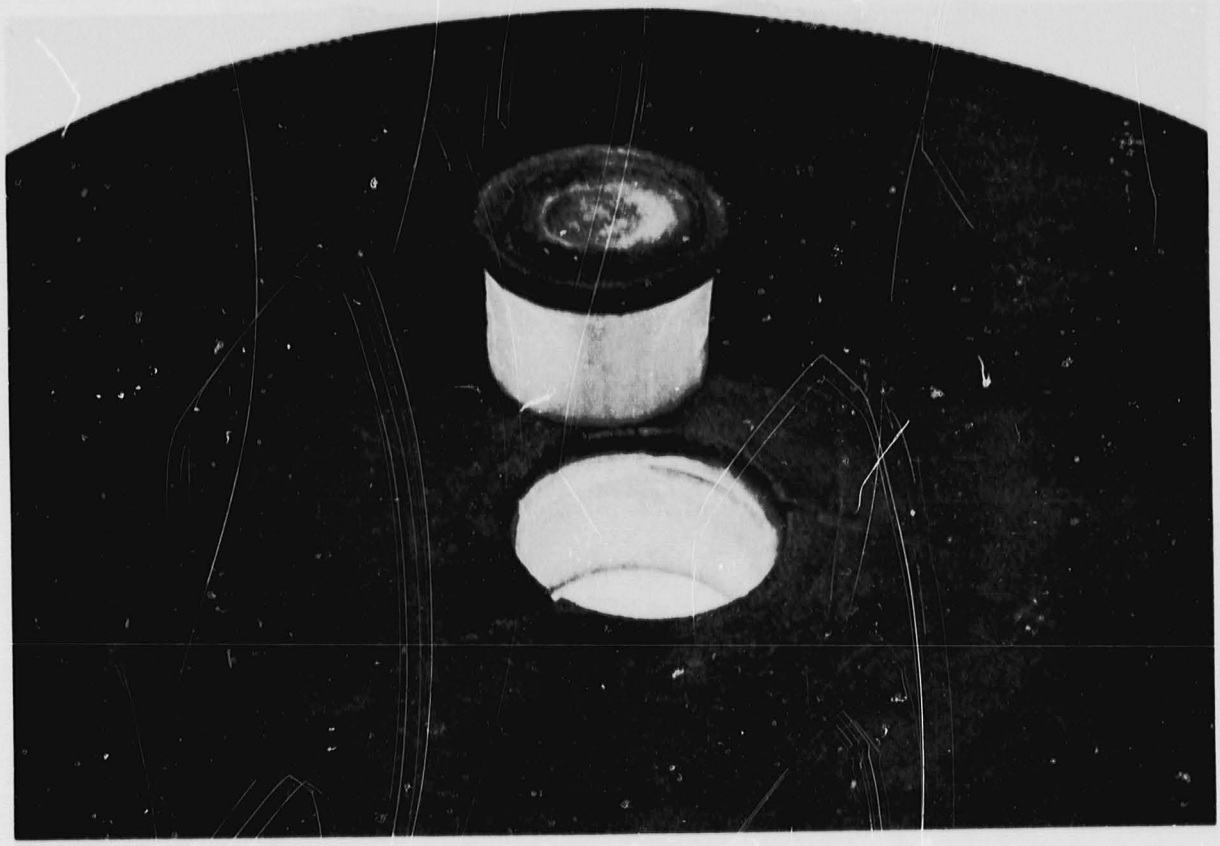

Figure I.B.4.7 **Thin-Wall AS Core No. 54 Showing Failure of Cement Bonding Hub Insert in Place**

All nine "suspended" regenerators were retired because they were damaged by a failure in the test gas turbine engine itself or because of poor quality control during the assembly of the core. No true chemical attack, mechanical load, or thermal stress failures were observed in any of these cores.

I.B.5 Durability Test of a Magnesium Aluminum Silicate Regenerator

Engine tests of two early MAS regenerators are described in Section M of Reference 1. One of these early MAS cores accumulated 426 hours of engine test before it was retired. The testing of this core was terminated when the cement holding the hub or center section in place failed and caused damage in this region. Subsequently, an improved procedure for bonding the center insert to the rest of the matrix was developed. This procedure was used to cement the center insert into a MAS core fabricated by Supplier D. This core, which is shown in Figure I.B.5.1 was evaluated in both the accelerated chemical attack engine test and long term engine durability tests (Reference 2). It has now accumulated 5381 total hours of engine test.

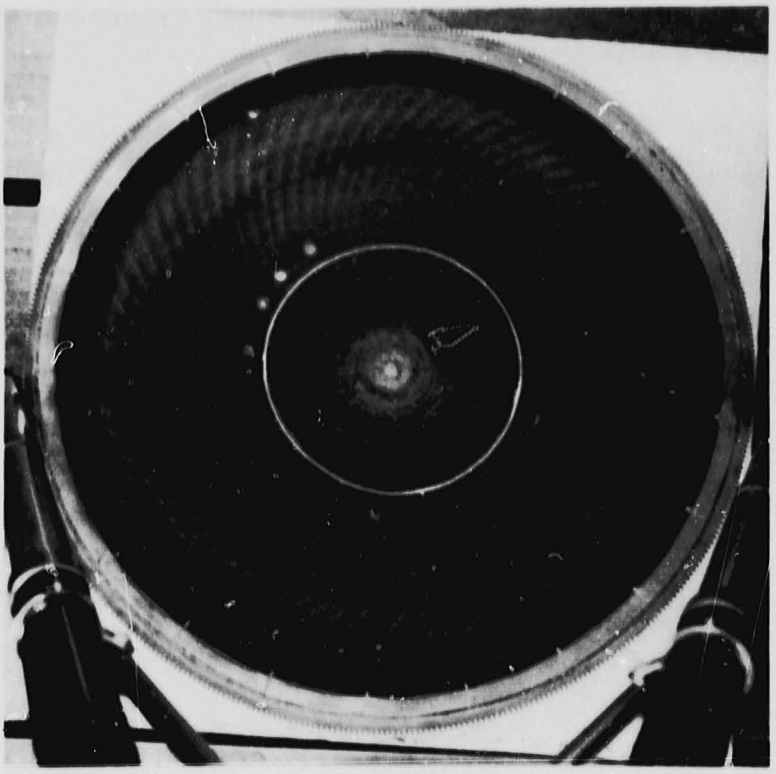

Figure I.B.5.1 **First Generation MAS Regenerator Fabricated by Supplier D**

The core had developed thermal stress cracks in the space between the stress relief slots. These cracks, which were noted after 200 hours of testing, are shown in Figure I.B.5.2. The cracks are attributed to thermal stresses, because the MAS material used in this core has a relatively high coefficient of thermal expansion and the core was operated at temperatures up to 800°C (1472°F). The analysis conducted in Section V.B.2 of this report on this same high expansion MAS material with a slotted rim showed that at these temperatures the rim thermal stress safety factor could be substantially below unity. The material in the rim area, therefore, would be expected to fail and develop thermal cracks. These cracks propagated into a region below the regenerator seal shoe inner diameter, where the ceramic is in a state of compression, and then they stabilized.

After 1552 hours on the MAS core, a safety device caused the engine to shut down automatically because of an overtemperature which was caused by clogged engine air inlet filters. On teardown inspection, it was found that several of the rim cracks in the MAS core had propagated radially inward. These cracks can be seen in the photograph taken after the emergency shutdown and presented in Figure I.B.5.3. An examination of the recorded engine data showed that the cores operated at progressively higher temperatures, in excess of 850°C (1562°F), for the last 25 hours as the filters clogged. These higher temperatures increased the thermal stress and reduced the rim safety factor an additional 15 to 25%, so that it was well below unity. Apparently the added thermal strain induced in the rim of this MAS core caused the original cracks to propagate.

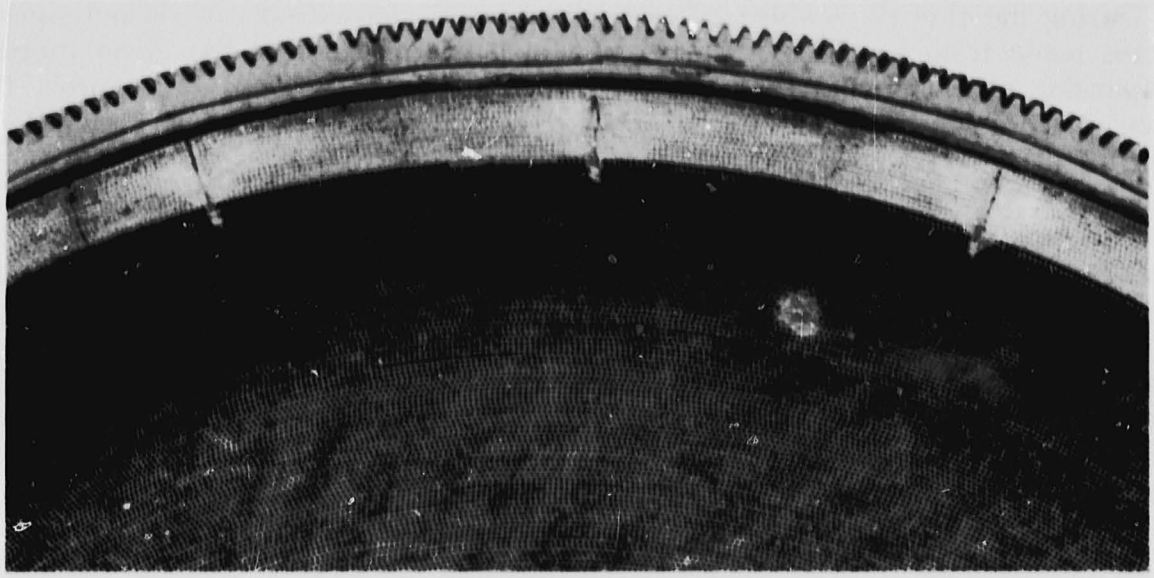

Figure I.B.5.2 MAS Regenerator Rim Showing Thermal Stress Cracks Located Between Stress Relief Slots After Operation at 800°C (1472°F)

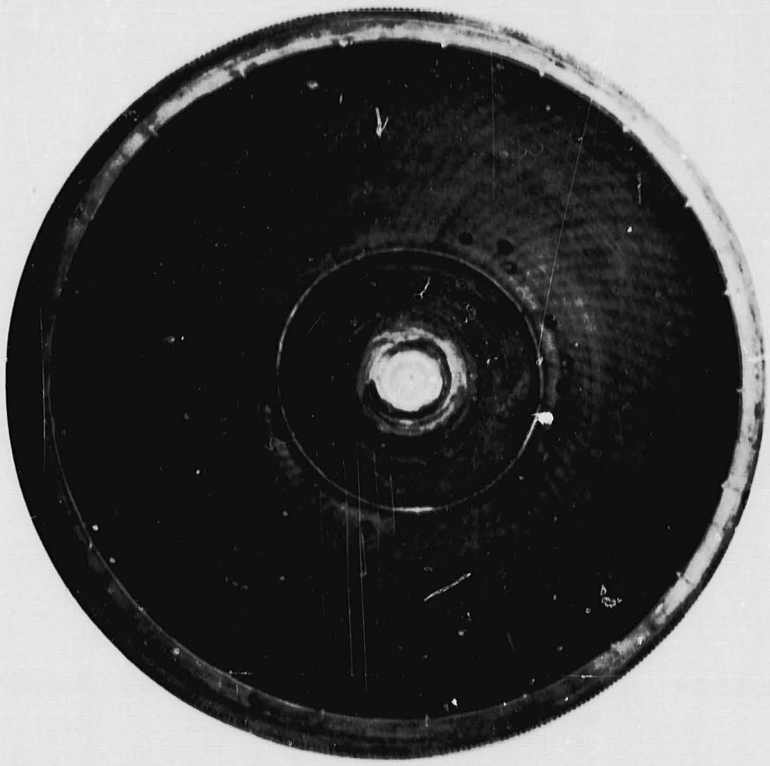

Figure I.B.5.3 Thermal Stress Cracks in MAS Core After Operation at 850°C (1562°F)

Even with elongated cracks, the regenerator was still operational and it was returned to service. It accumulated an additional 3829 hours at 800°C (1472°F) by the end of the report period for a total engine life of 5381 hours. As described in Section I.B.6 of this report, the hub of this core came loose due to a cement failure after 3752 hours, but the hub was repaired and the core returned to service.

During the first six months of 1977, Supplier D successfully fabricated several cores made from a new MAS material which is stronger and has lower thermal expansion characteristics than the material used in the original three cores. The first of these second-generation MAS cores was placed on engine test toward the end of 1977.

This new core is shown in Figure I.B.5.4., and it is apparent that the hub insert is smaller than that of the original MAS core shown in Figure I.B.5.1. This should decrease the likelihood of problems in the hub area. The new core has essentially a square passage with a hydraulic diameter of .655 mm (.026 in) and a cell count of 140 holes/square cm (900 holes/square inch), while the older core had a hydraulic diameter of 1.092 mm (.043 in) and a cell count of 51.5 holes/square cm (332 holes/square inch). The geometry of the passage in the new core is more desirable for use in a gas turbine application.

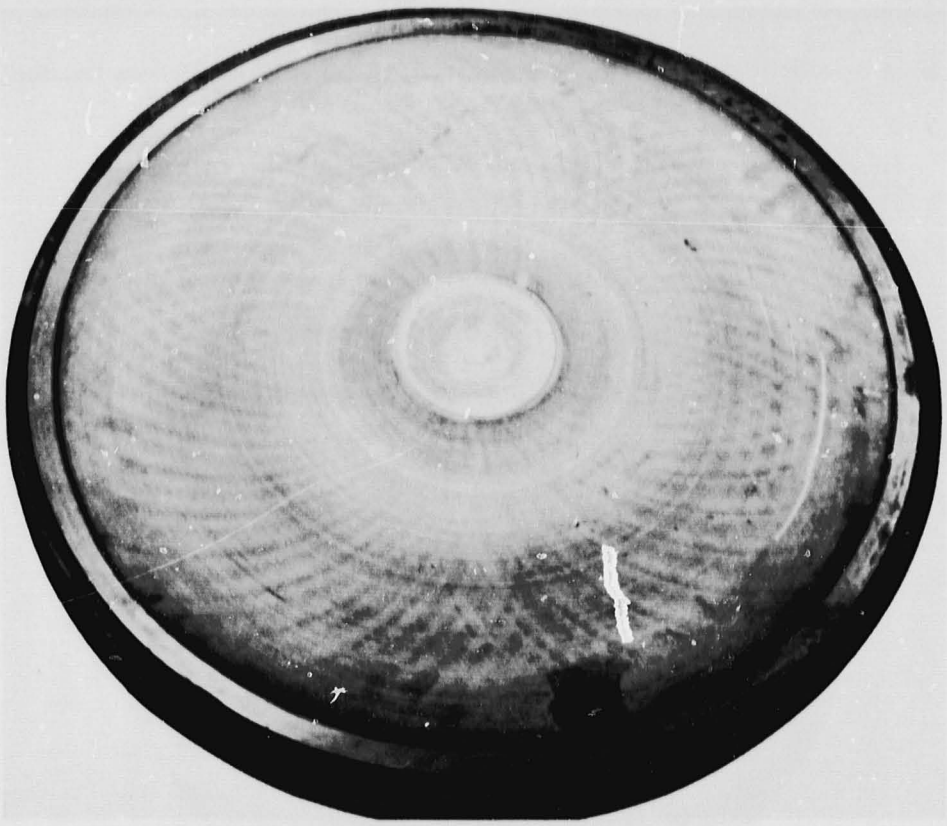

Figure I.B.5.4 **Second Generation MAS Core Made by Supplier D with an Advanced Material**

Although it is not apparent from the photograph, the stress relieving slots extend all the way to the cold face and the ring gear is bonded to the core with a greater compressive preload in the assembly of the new core. Both of these changes were incorporated to increase the rim thermal-stress safety factor and are analyzed in detail in Section V.B.2 of this report. This analysis suggests that this new second-generation MAS material with the improved stress relief techniques will result in a regenerator that is capable of operation at 1000°C (1832°F). This core accumulated 3518 hours by the end of the program.

Early in 1979 Supplier I successfully fabricated a full-size MAS material core, which consists of 35 extruded segments as shown on Figure I.B.5.5. This core, which features the desirable isosceles triangular matrix geometry, has a stress relief slot between each of the 22 outer segments which essentially means that the rim has 44 stress relieving slots. This core is also bonded to the ring gear with a large compressive pre-load to reduce tangential thermal stresses. Since this MAS material also has a relatively low thermal expansion characteristic, analysis shows that it too is capable of operation at 1000°C (1832°F). In fact, as described in Section II.B, a core of this configuration has been successfully operated at this temperature. This particular core attained 2474 hours at 800°C (1472°F) by the end of the program.

Figure I.B.5.5 Supplier I Full-Size MAS Regenerator Fabricated from Extruded Segments

During the latter part of 1979 a full-size MAS material core was received from Supplier E. This core was fabricated by the embossing process and consists of rectangular flow passages with a nominal 5:1 aspect ratio. A total of 120 hours at 800°C (1472°F) were accumulated on this core.

Figure I.B.5.6 summarizes the operating experience with MAS regenerators. Supplier D's first-generation regenerator accumulated 5381 hours and their second-generation accumulated 3518 hours by the end of the program. The segmented core of Supplier I had accumulated 2474 hours when this ceramic regenerator development program was completed in December 1979. Although a larger core sample and more test hours would be desirable, all the data accumulated to date indicates that MAS is a viable material for a rotary, ceramic heat exchanger.

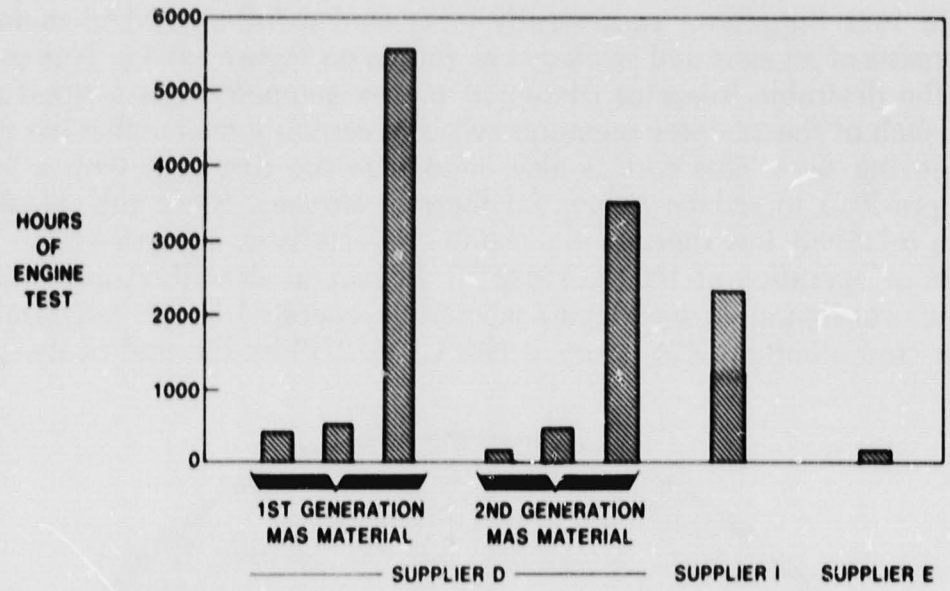

Figure I.B.5.6 Durability Record of MAS Regenerators

I.B.6 Hub Cement Failures of AS Regenerators

During the third quarter of 1976 under an earlier program, the cement holding the hub insert in place failed in three different thick-wall AS cores. These cores had accumulated 9 hours, 68 hours, and 2368 hours at the time of failure. Photographs of the 2368 hour failure and the hub insert are shown in Figures I.B.6.1. and I.B.6.2. In each case the failure was attributed to improper composition or improper processing of the cement itself.

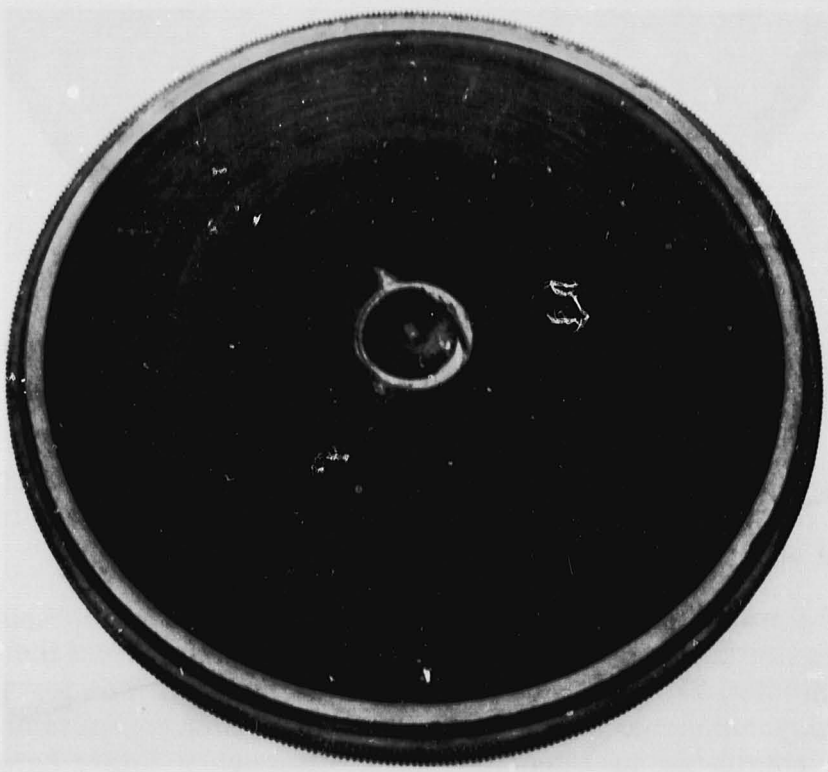

Figure I.B.6.1 AS Core No. 43 After Failure of Cement Bonding Hub Insert in Place

During this program, five additional hub cement failures occurred. Two were thick-wall AS cores with 58 and 4750 hours and the three others were thin-wall AS cores with 11, 1604 and 7954 hours. All eight failures contained the same cement and processing procedure. Thus, eight failures have occurred in the twenty-three AS cores of this configuration that have been tested in the Ford 707 turbine.

This cement, which was developed specially for use with AS material, relies on a foaming action or expansion when it is fired to properly bond the two ceramic pieces together. An examination of Figure I.B.6.2 shows that this foaming action occurred at both faces of the insert, but did not take place in the center. The cement actually shrank away from the ceramic in the center portion of the matrix. The insert was held in place, therefore, by a thin band of cement at each core face. As the engine housing distorts or creeps with operating hours, slight additional seal rubbing forces are applied to this section of the matrix. These slight additional forces may have caused this thin band of good cement to fail.

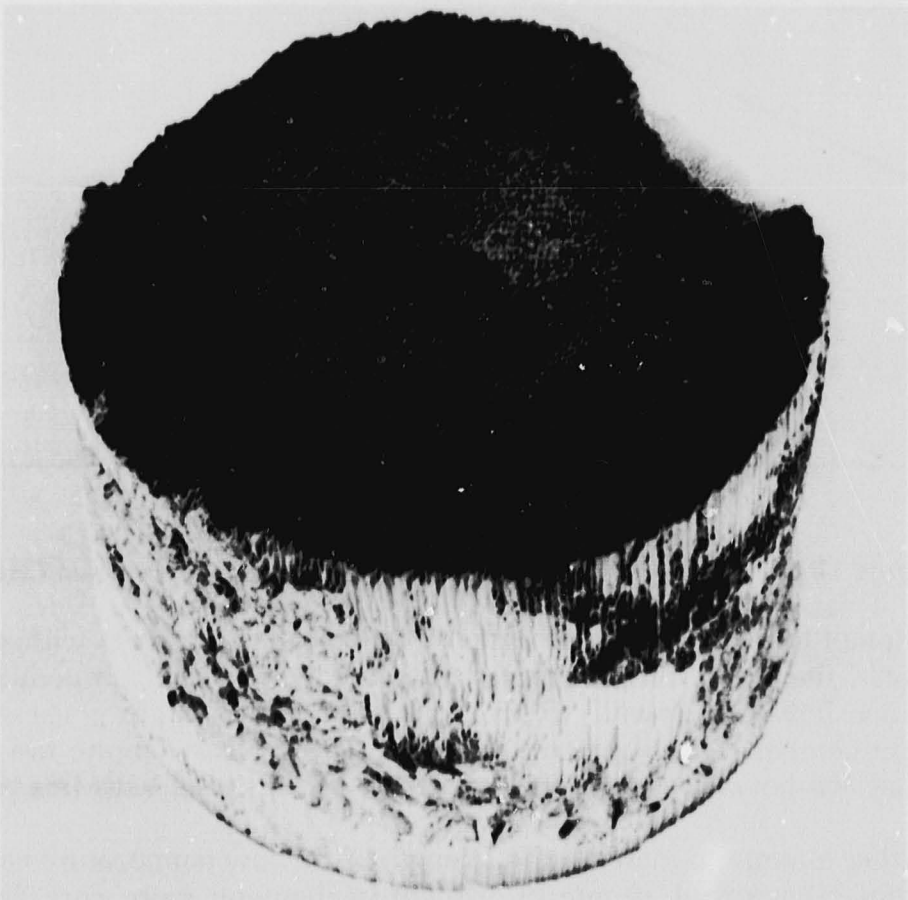

Figure I.B.6.2 **Hub Insert from Core No. 43 with Non-Foamed Cement in Center**

The failure of the cement that attaches the matrix hub insert is primarily a quality control problem. When properly processed the cement has good durability potential as evidenced by the Weibull distribution for these cores, Figure I.B.6.3. Based on Weibull distribution theory, 10% of these matrix inserts would be expected to separate after 30 hours of engine test. Conversely, four of the five cores that have attained 10,000 hours durability contain the original matrix insert hub.

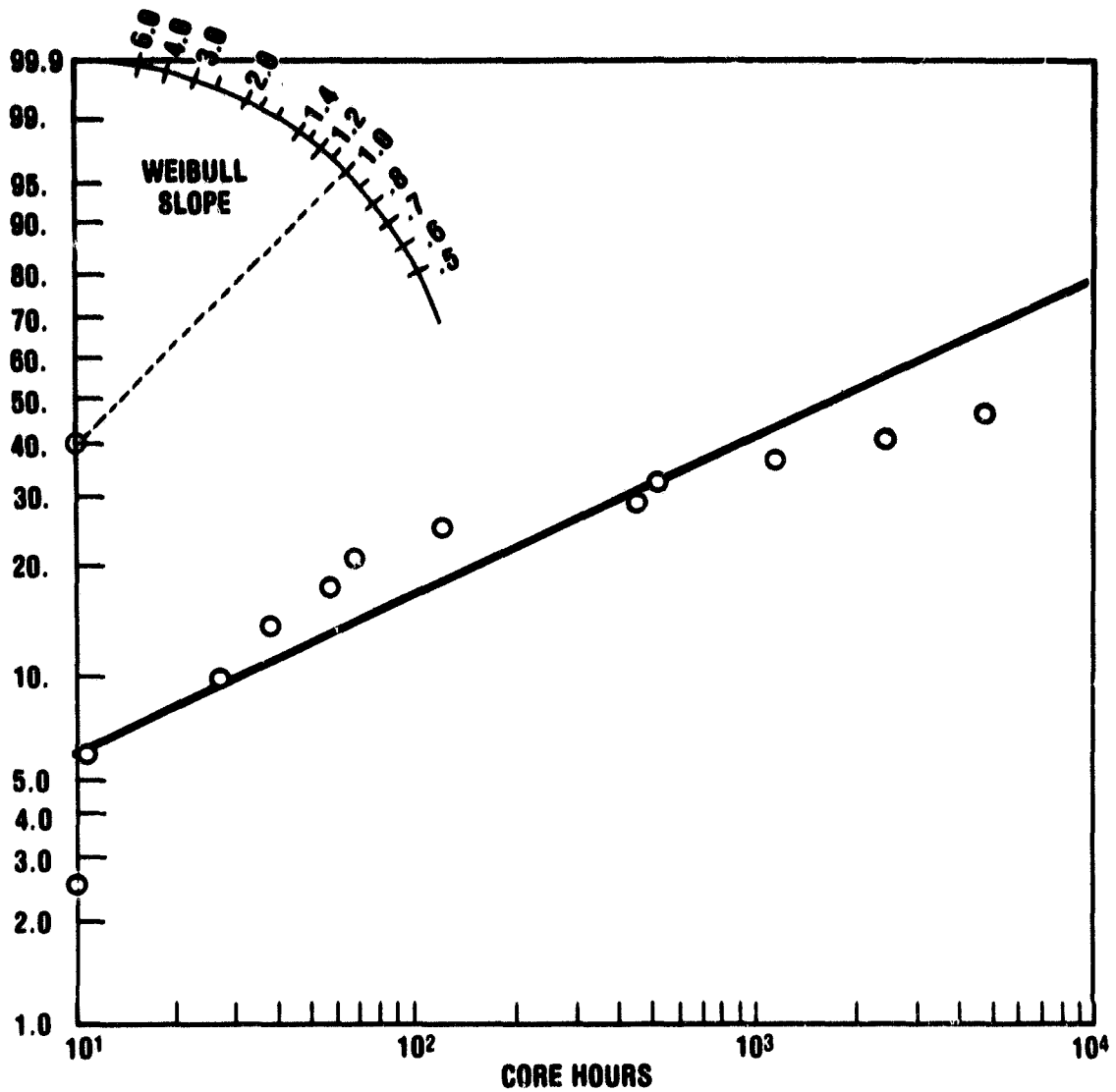

Figure I.B.6.3 Failure History of AS Cores with Supplier A Foam Cement

In an attempt to return the cores with the failed hubs to service without removing the ring gear, the hubs were cemented in place with a low temperature cement. Figure I.B.6.4 shows a thin-wall AS core with a new hub held in place with this low temperature cement. This approach was abandoned when engine test experience showed that 500 hours was the best that could be expected with this procedure.

As a further attempt to increase the strength of the low temperature cement bond, three or four holes about 19 mm (0.75 inch) in diameter were core drilled at the point between the hub insert and the matrix. Then ceramic "roll pins" were cemented into these holes. Since this latter approach resulted in no additional durability gain, the low temperature cement was abandoned.

It has been necessary to remove the ring gears and return the cores to the Supplier for installation of a new hub using a high temperature cement. This approach destroys the elastomer and the running history accumulated on it. A thick-wall core that has a new hub held in position with a high temperature cement is shown in Figure I.B.6.5.

Figure I.B.6.4 Thin-Wall AS Core with Hub Repaired with Low Temperature Cement

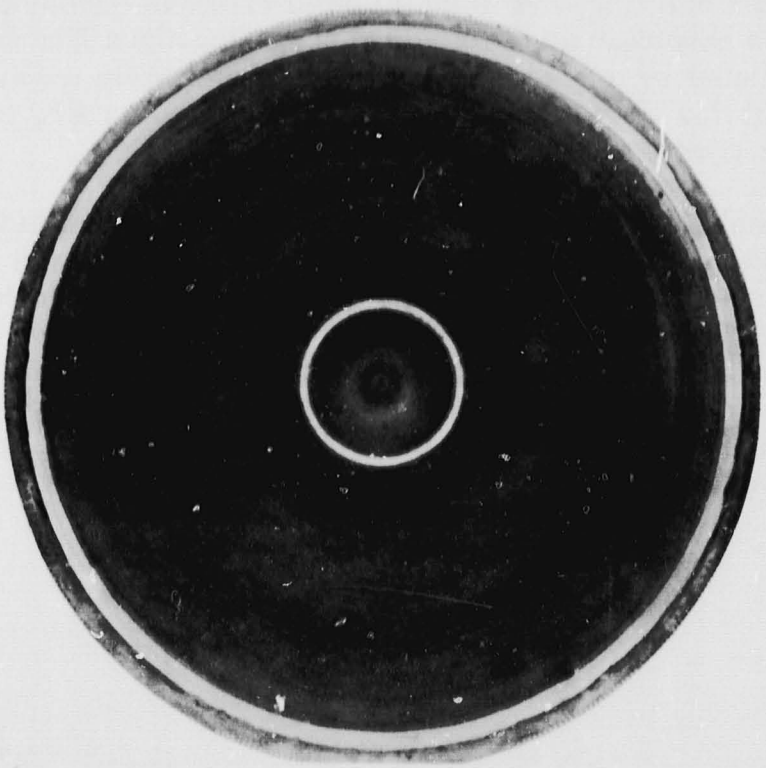

Figure I.B.6.5 Thick-Wall AS Core No. 43 with Hub Repaired with High Temperature Cement and Solid Ceramic Ring

In this arrangement the hub is cemented into a thin, 50 mm (.25 inch) wide, solid ceramic ring and this sub-assembly is then cemented into the matrix. The ceramic ring allows better control of temperature during the firing of the cement, and it also provides a better match of the thermal expansion characteristics of the insert-matrix bond area to the rest of the matrix.

As described in Section I.B.4 the cores can be damaged when the hubs fail and/or during the subsequent repair. This fact is illustrated by comparing Figure I.B.6.1. and I.B.6.5 taken of Core No. 43 before and after hub repair. Small radial cracks are seen in Figure I.B.6.1 after the initial hub failure. The additional processing and another high temperature firing which are required to recement a new hub in place have caused these cracks to grow significantly as shown in Figure I.B.6.5. As noted in Section I.B.4 this damage, which occurred during the hub failure and subsequent repair, eventually caused the failure of Cores No. 34 and No. 56. New cores with the ceramic ring holding the hub insert in place do not show any distress in the hub region.

Since late 1977 all active AS cores that have undergone hub failures have been repaired to this configuration, and all new cores received from Supplier A have been built with this design. As a result, eleven cores with this new hub configuration have been on durability test since 1977, and their durability record is shown in Figure I.B.6.6. One of these cores has accumulated over 7200 hours, but one low-hour failure occurred in late 1977. In this failure the ceramic ring and the hub insert itself were shattered into tiny fragments. The cause of this failure remains unexplained, since the cement bond between the insert and ring, as well as between the matrix and ring, was found to be in excellent condition. The ring itself was well within expansion and compositional specifications. The failure appears to have been initiated by an unknown external source. More engine test hours are needed to see if this kind of failure will recur, but the durability record of the rest of this sample is very good.

A Weibull analysis of the original hub cement configuration indicates a B_{10} life of 30 hours. The redesigned hub, which consists of the hub insert cemented into a thin ceramic ring which is then cemented into the matrix, appears to have corrected this problem. Although one early hour failure of this configuration is still without explanation, the other ten hubs of this configuration have accumulated 35,000 hours of engine test without distress. Since at least two failures are needed before a Weibull failure analysis can be made, a projection on the B_{10} life of the redesigned hub cannot be made. Its durability and reliability, however, appears to be adequate.

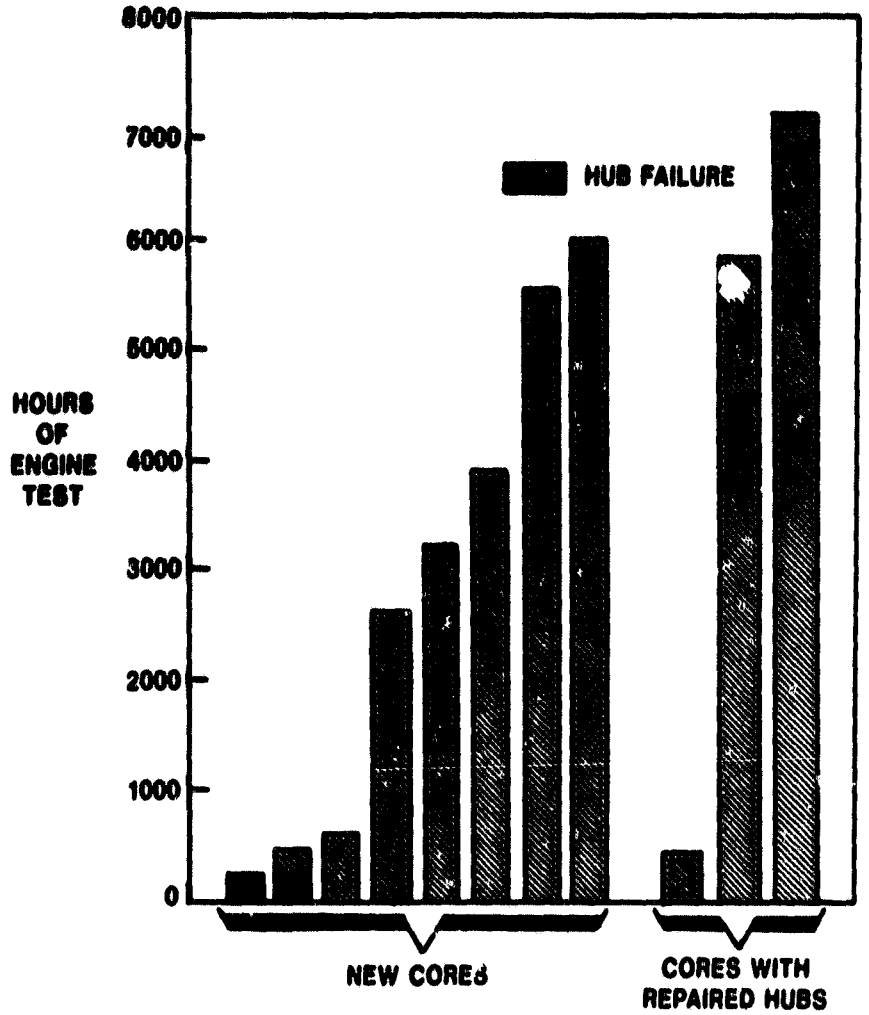

Figure I.B.6.6 **Durability Record of Cores with Solid Ceramic Ring Around Hub Insert**

I.B.7 Hub Cement Failures of MAS Regenerators

Hub cement failures have occurred in MAS regenerators, causing the hub insert to come loose. All of the MAS cores tested to date have had their hubs assembled with a cement that cures at a low temperature. This type of cement is similar to that used unsuccessfully with the AS cores as illustrated in Figure I.B.6.4. The durability record of this class of cement with the MAS regenerator hubs is much better than with AS hubs. The better performance of this cement in the MAS core is attributed to the fact that the expansion of this material more nearly matches that of the cement, and this MAS material is stronger in the radial direction and better able to withstand any additional matrix-cement expansion mismatch.

Figure I.B.7.1 shows the hub cement failure that occurred in the Supplier D's first-generation MAS core described in the previous section. The hub in this core had been cemented in place with the same low temperature cement used with the AS core shown in Figure I.B.6.4. The cement used in the MAS core lasted 3752 hours before it failed. The hub in this core was recemented with low temperature cement and has accumulated another 1628 hours. Figure I.B.7.2 shows a hub failure that occurred in Supplier D's second-generation MAS regenerator after 473 hours.

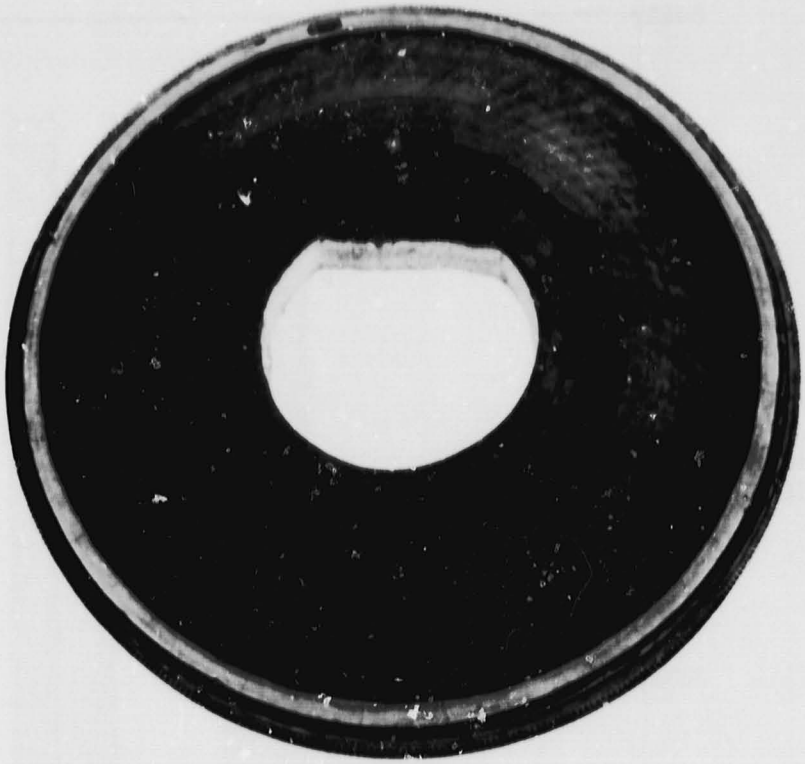

Figure I.B.7.1 Supplier D First Generation MAS Core with Hub Cement Failure After 3752 Hours

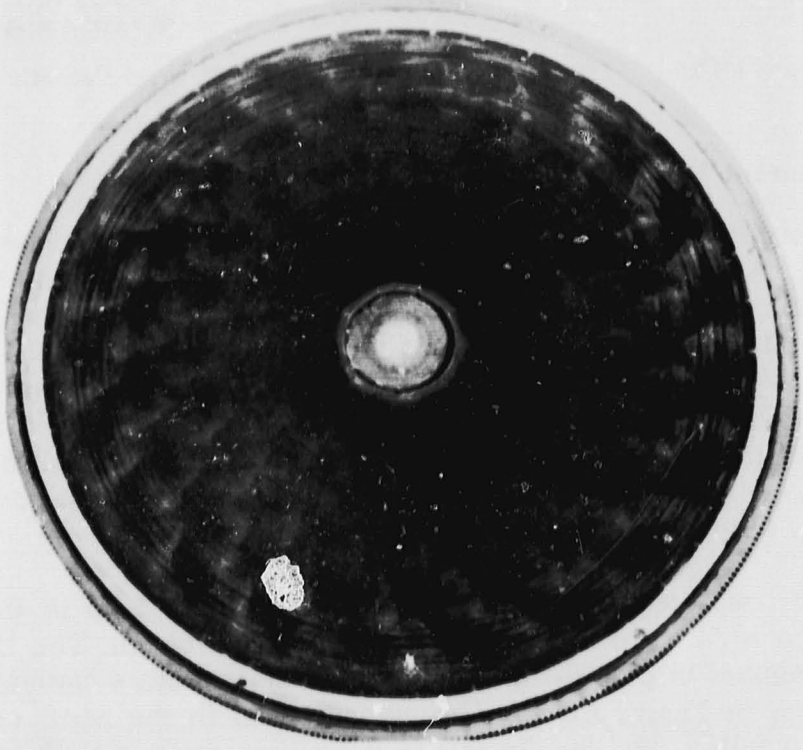

Figure I.B.7.2 Supplier D Second Generation MAS Core with Hub Cement Failure After 473 Hours

The other second-generation hubs were operational after 110 and 3514 hours. It should be noted that only a limited number of these MAS cores were fabricated, and the hub cementing techniques and processing were still in the early stages of development. It is believed that the test data acquired to date on MAS cores shows that the potential exists for utilizing a low-cost, low-temperature-curing cement to assemble the hub insert to the matrix. More process development is required on this approach.

These hub failures are still not considered to be a serious, fundamental problem. Low temperature cement has shown reasonable durability in MAS cores, and with improved processing control may be adequate for this material.

I.B.8 Matrix-Elastomer Bond Separation

Reasonably good durability has been obtained with the elastomer bonded ring gear on the thick-wall AS core. Although separation did occur as low as 315 hours, the separations, for the most part, were traced to installation of the core in an engine with a worn pinion. The step wear pattern on these pinions introduced an axial load on the ring gear and elastomer which eventually caused a separation in the matrix-elastomer interface region.

As reported in Section B of Reference 2, the elastomer shows little deterioration with running hours. This was confirmed recently when measurements of elastomer hardness (durameter) were taken from the core that had accumulated 6935 hours before it was irreparably damaged by a power turbine failure. The average durameter values radially and axially throughout the elastomer after 6935 hours of engine test are shown in Figure I.B.8.1. The approximate initial hardness after curing is about 70. This elastomer tends to soften slightly during initial exposure to temperature, followed by a gradual increase in hardness. The data from the 6935 hour regenerator shows that on the exposed cold and hot faces the elastomer hardness has exceeded its initial value. The data also show that it is still softer than its initial value in the inside of the elastomer where it was not exposed to an oxidizing atmosphere. This indicates good stiffness stability at operating temperatures for the present polymer after almost 7000 hours of test. Since hardening with time at temperature is not excessive, the elastic modulus should also be stable. Consequently, for a given ring gear deflection during engine operating conditions, the radial tensile load on the core should be unchanged.

The results obtained with the same elastomeric drive on the thin-wall AS core have not been as successful. Since the thin-wall matrix has a thinner cross section, it will be weaker and have less capability for carrying thermal and mechanical loads. Every thin-wall AS core, bonded with the same procedure used with the thick-wall cores, has had a separation in the elastomer-matrix bond area.

Some separations even occurred during bonding; an example of this is illustrated in Figure I.B.8.2 which shows the rim damage suffered by a thin-wall core in the bonding fixture. Every one of these thin-wall elastomer-matrix bond area separations occurred in the weaker matrix material. This is illustrated in Figure I.B.8.3 which shows the matrix securely attached to the elastomer. A more detailed examination shows that separation occurred in the second or third ceramic corrugation under the one attached to the elastomer.

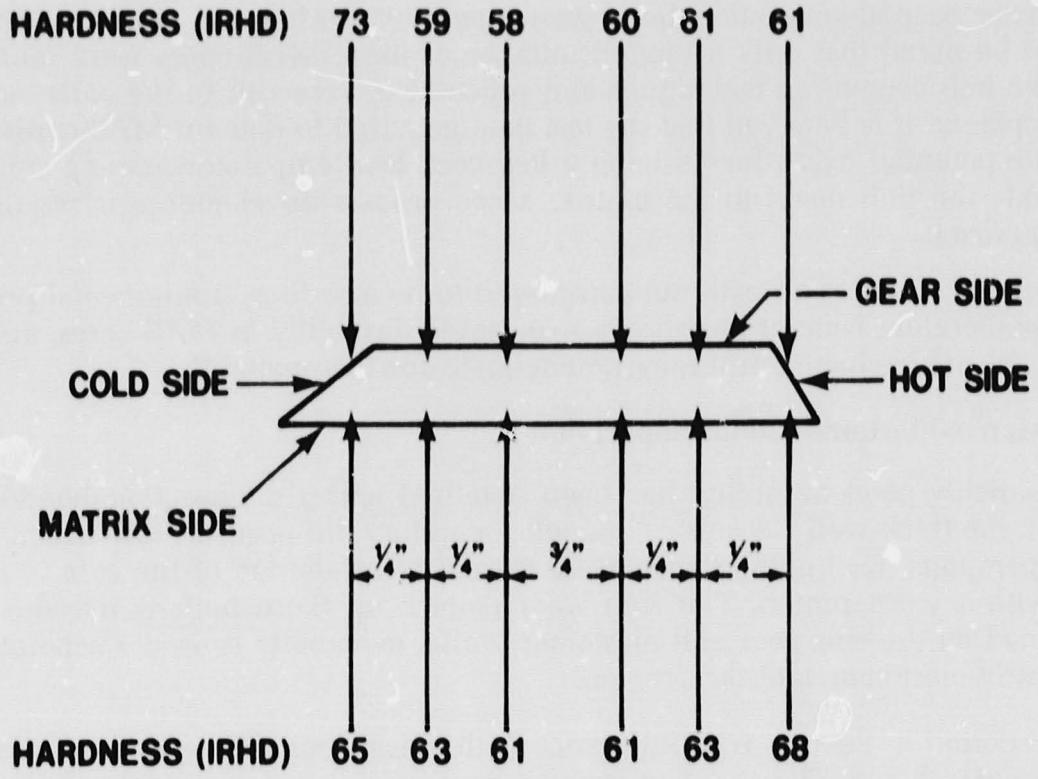

Figure I.B.8.1 Hardness Readings in Elastomer After 6935 Hours of Engine Operation

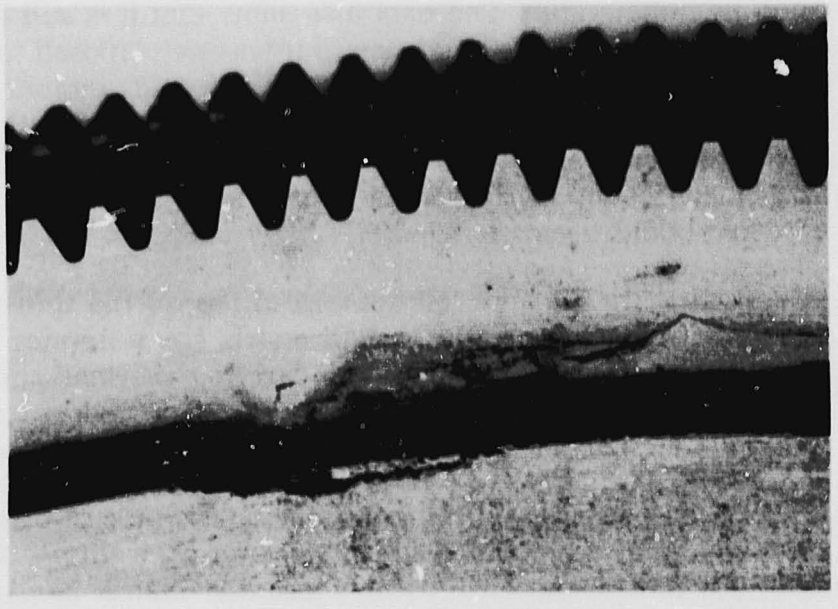

Figure I.B.8.2 Circumferential Crack in the rim of a Thin-Wall AS Regenerator Initiated During Elastomer Bonding of the Ring Gear

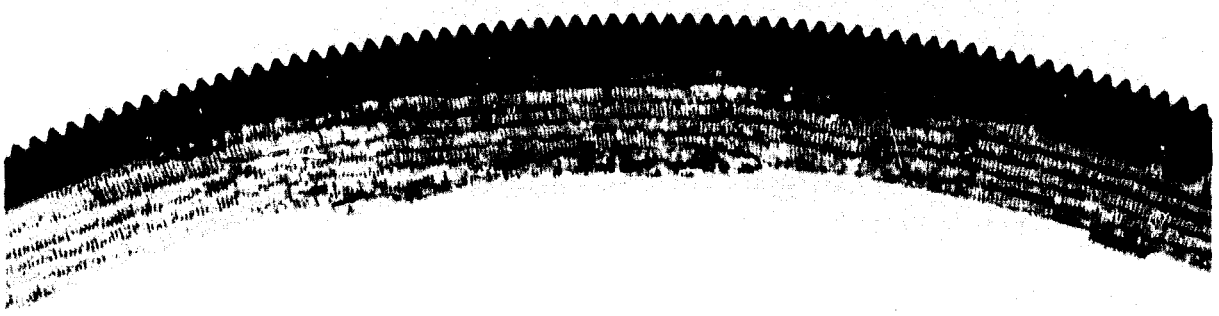

Figure I.B.8.3 **Elastomerically Bonded Ring Gear Which Has Separated from a Thin-Wall AS Core During Engine Operation**

The transient stress in a ceramic regenerator can be reduced by introducing a compressive load at the rim to counteract the operating tensile thermal stresses. This is accomplished in the Ford regenerator by bonding the ring gear to the core at an elevated temperature. The resulting contraction of the ring gear on cool down, after the elastomer has been allowed to cure at the higher temperature, provides a radial compressive preload on the regenerator. The amount of preload can be adjusted by changing the bonding temperature or by modifying the configuration of the elastomer. Three different levels of compressive preload have been applied to the thin-wall core with inconclusive results.

The zero compressive preload is accomplished by bonding the gear and curing the elastomer at room temperature. This results in a maximum operating radial tensile load being applied to the core by the more rapidly-expanding metal gear during engine transients. The single thin-wall AS core bonded with zero preload separated after 239 hours of engine test.

Three thin-wall cores were bonded at an intermediate temperature resulting in an intermediate compressive preload on the core at room temperature and a reduced radial tensile load on the core during transient operation. Two separated at low hours while the third was on the verge of separation at 1064 hours when the hub of this particular core came loose.

A maximum compressive preload is accomplished by bonding and curing the elastomer at its maximum possible temperature. This compressive preload neutralizes the greater growth of the ring gear during transients so that the elastomer is in a low stress state under these conditions. Two cores were bonded with a maximum compressive preload. One core developed so many cracks as it cooled down that it could not be used for engine test. The other core developed a crack but was placed on engine test. A separation in the elastomer-matrix bond region occurred in this core after 3885 hours.

Recent measurements of the thin-wall AS matrix physical properties shows a large variation in strength. In addition, both the tensile and compressive radial

strength of this matrix is very low, so that even moderate compressive or tensile loads during bonding or during engine operation will cause cracks and/or separation. This material data is presented in Section V.B.1 of this report. The eventual solution to this problem is the development of a high-compliance, low modulus elastomer system to reduce the stress on the core during bonding and during engine operation. The chemical development of a high-compliance elastomer has not been pursued at Ford because of the significant amount of time and effort that may be required for this approach to become feasible.

Alternate approaches for increased compliance utilizing mechanical changes, but still retaining the same elastomer, are shown in Figure I.B.8.4. The upper configuration in the illustration incorporated over 300 holes in the elastomer and results in a 50% reduction in the radial modulus of the elastomer. The lower configuration utilizes slots to reduce the radial modulus by almost 95%. Both are discussed in greater detail in Section V.B.3.

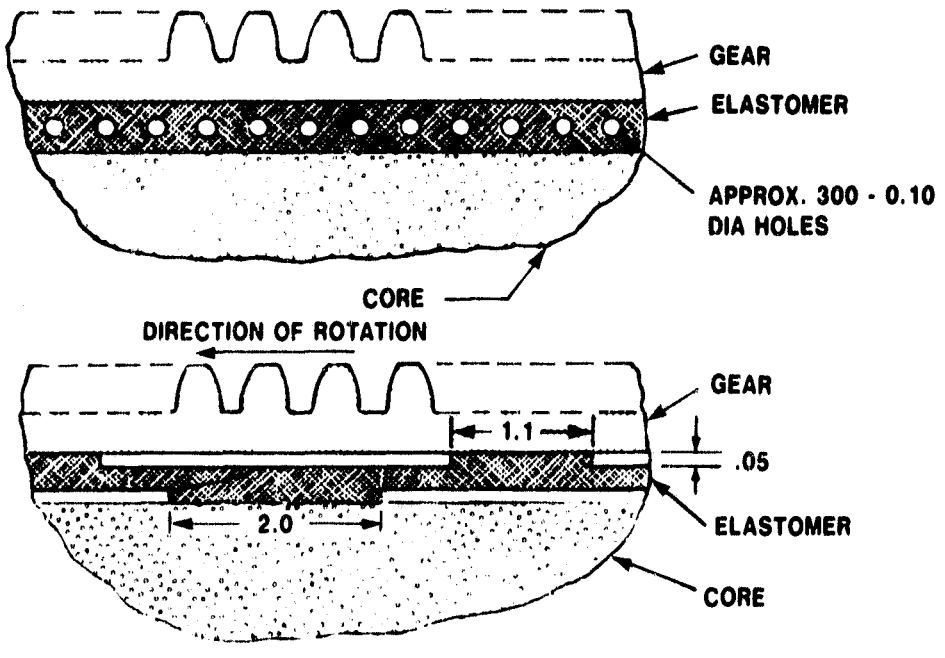

Figure I.B.8.4 Compliant Elastomer Schemes

The test results obtained to date on these various approaches are summarized in Figure I.B.8.5. The cores shown on the left hand side of the figure are those that were described earlier and were bonded at three different levels of preload, utilizing conventional bonding techniques. Separation ranged between 239 and 3885 hours. The middle group is the elastomer containing the 300+ holes and having a modulus reduction of 50%. One early hour separation suggests that this approach is marginal and a greater reduction in modulus is required. Experimental and analytical evidence presented in Section V.6.3 shows that the eventual solution to this problem is the development of a high-compliance elastomer system in which the modulus of the elastomer is reduced at least 70%. This conclusion is supported by engine operating experience, presented in Figure I.B.8.5, which shows that a 50% reduction in modulus is inadequate and failures will occur with this arrangement.

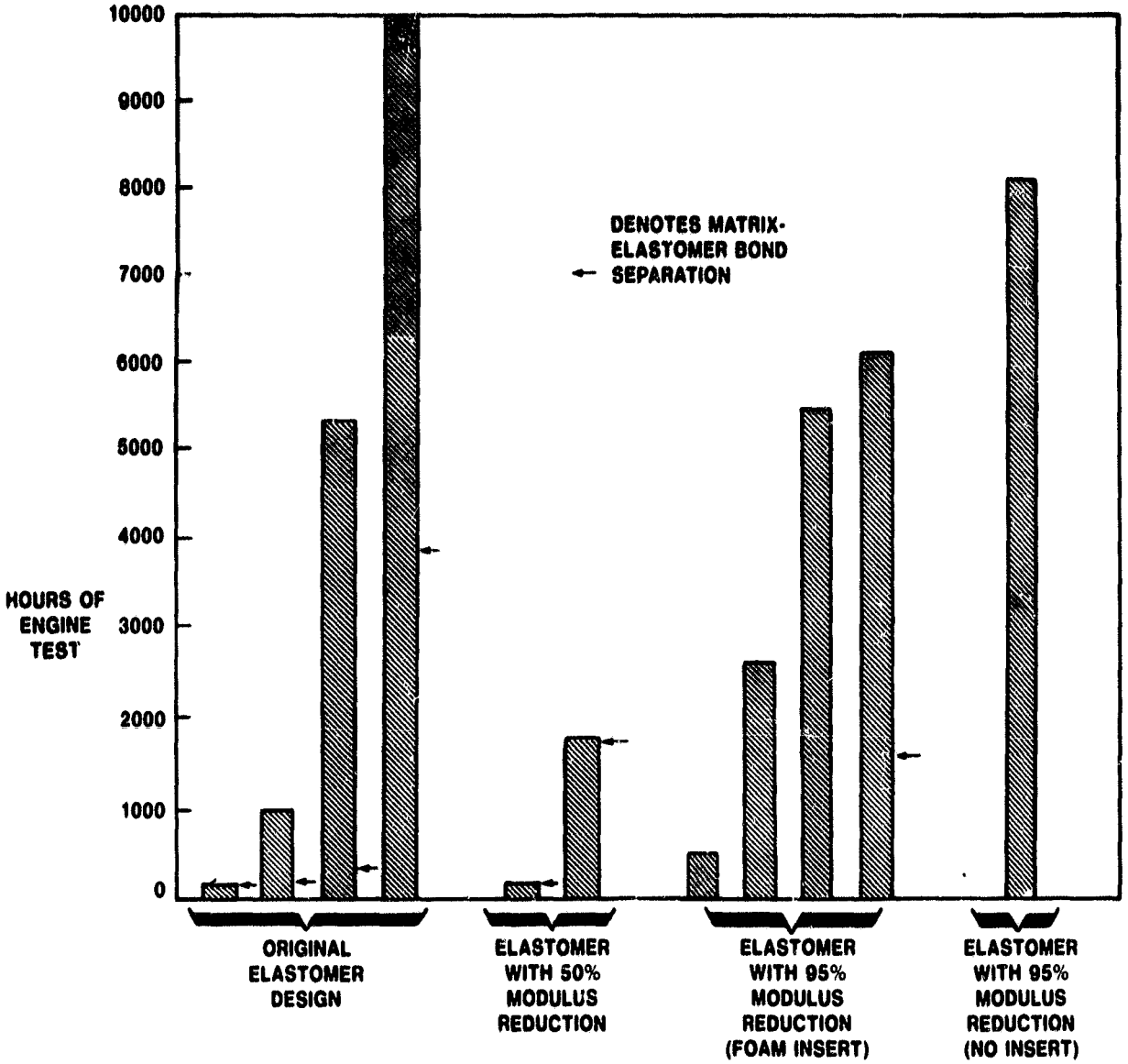

Figure I.B.8.5 **Durability Record of Thin-Wall AS Regenerators Utilizing Different Elastomer Bonding Approaches**

Two different slotted regenerator configurations are now on test in which the modulus of the elastomer has been reduced by 90-95%. One of these assemblies has now accumulated 7954 hours of engine test (Figure I.B.8.5). This configuration incorporates slots in the elastomer (Figure I.B.8.6) to reduce the modulus. In the other configuration these slots are filled with foam rubber. It is believed that the second configuration with the foam rubber functions identically to the first during engine operation, provided the foam is not continuously bonded to the matrix or ring gear. One separation occurred with the foam-filled slots in which the foam was securely bonded to both matrix and ring gear. Use of the foam rubber simplifies the gear-elastomer assembly process.

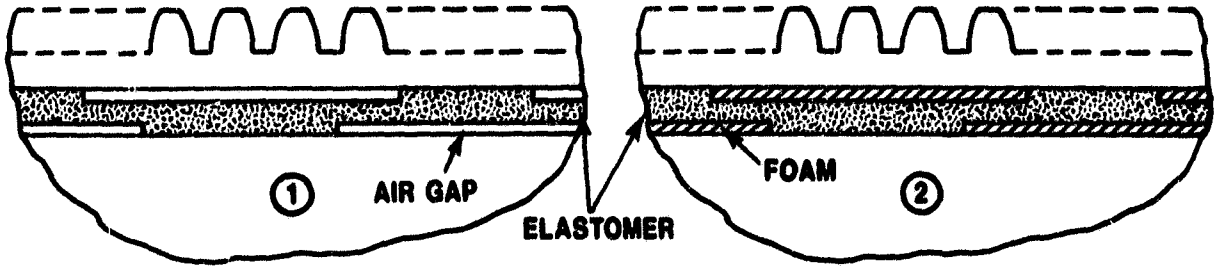

Figure I.B.8.6 High Compliance Elastomer Designs

Since 1978, all thick and thin-wall AS cores have been elastomerically bonded with the high-compliance, slotted configuration. The data accumulated to date suggest that this approach will result in the successful elastomeric bonding of the ring gear to thin-wall AS cores. There have been no matrix-elastomer bond separations with MAS cores, which are bonded with a continuous strip of elastomer.

I.B.9 Drive and Support System

Until the end of 1973, the Ford 707 regenerator drive and support system consisted of cylindrical solid ceramic pins cemented into the rim of the core. Spring clips provided an attachment between the ring gear and the solid ceramic pins in the rim. The core was mounted at the center through a solid ceramic center hub. This drive and support system is described in detail in Sections J and K of Reference 1.

In 1974, the design and development of a rim mount or three-point support system was initiated to facilitate the development of new chemically resistant ceramic materials. With this drive and support system, parallel development efforts for solid ceramic and cement technology were eliminated. Consequently, the present three-point support system contains a regenerator matrix which does not contain solid ceramic pins or a solid hub. The ring gear, which is attached to the rim with an elastomer, is supported at three points (Figure I.B.9.1.). In addition to the main design impetus of maximizing the effort to develop new ceramic matrix materials, the elastomeric, rim-support system has the following advantages when compared to the earlier spring clip, hub-support system:

1. Reduces the possibility of cracks initiated by mechanical, thermal, or chemical stress from propagating to a center hub, and/or pins which ultimately separate from the matrix causing ring gear disengagement and engine shutdown.

2. Eliminates the need for a costly second firing of the matrix, which is required to cement the solid ceramic pins and hub to the core.

3. Permits the effective use of a continuous rim core with stress relief slots, which will be discussed in detail in Section V.B.2.

The present three-point system design (Figure I.B.9.1) has eliminated the bearing, ring gear and matrix problem areas which were associated with the first two design attempts. The early design configurations are described in detail in Section B of Reference 1.

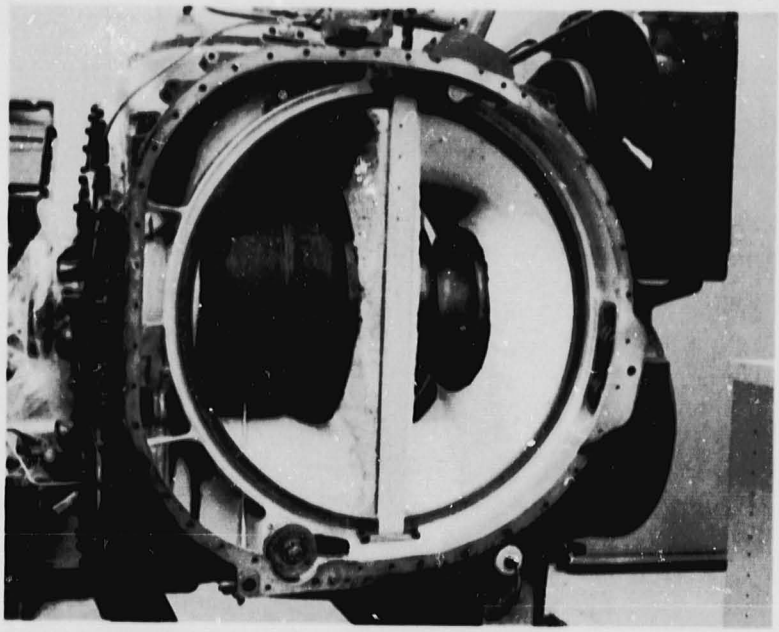

Figure I.B.9.1 **Photograph of Ford 707 Turbine Engine Housing Showing Modifications Required to Incorporate the Present Rim Support System**

Figure I.B.9.2 illustrates the force diagram of the present design. Since the major reaction force is at the fixed roller location, a yoke with two rollers is utilized (Figure I.B.9.3) at this point. The lightly loaded spring roller and pinion locations are shown on Figures I.B.9.4 and I.B.9.5, respectively. Except for the pinion location the roller assemblies contain an outer race support ring (Figure I.B.9.6) for the bearing. This provides additional rigidity, reduced bearing speeds, and lower contact stresses in the bearing.

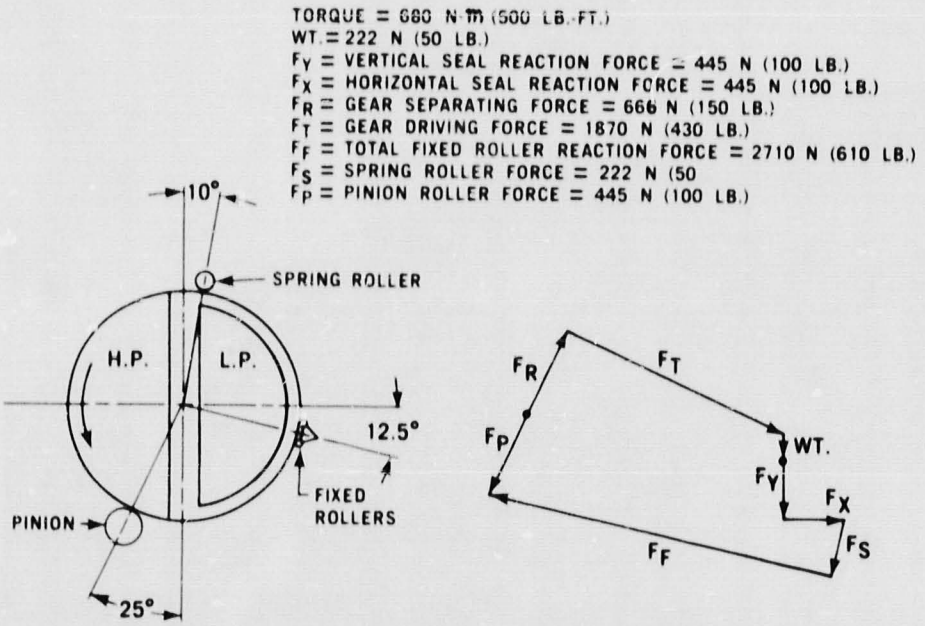

Figure I.B.9.2 **Regenerator Force Resolution for the Modified Rim Support System at 680 Nm (500 ft-lbs) Torque Condition**

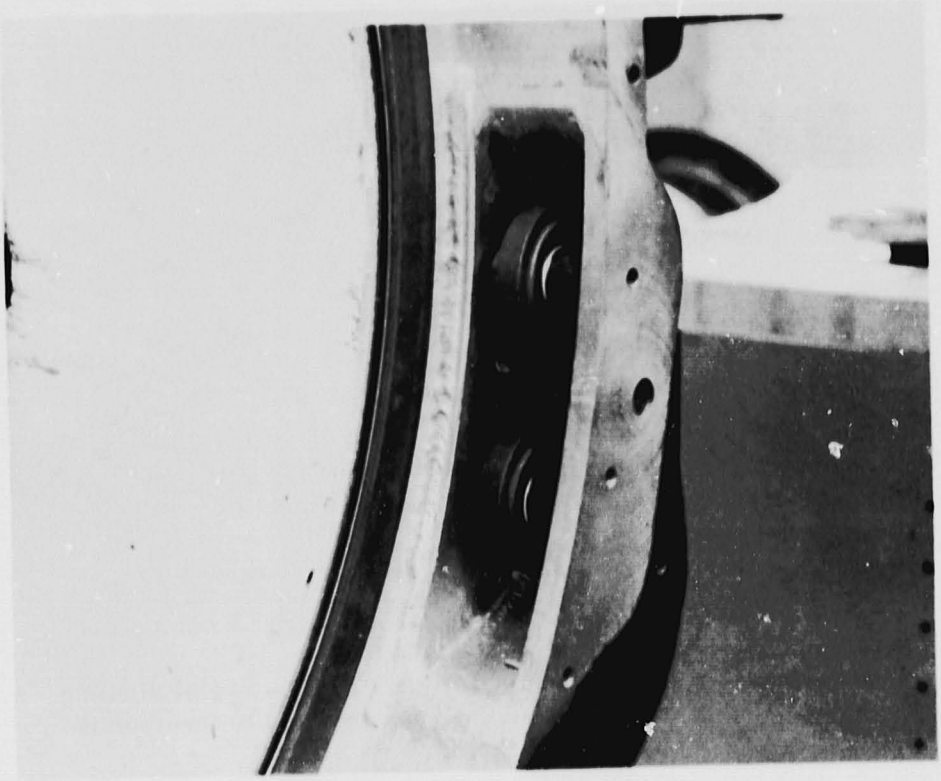

Figure I.B.9.3 Photograph of Ford 707 Turbine Engine Housing Showing Location of Fixed-Support Rollers

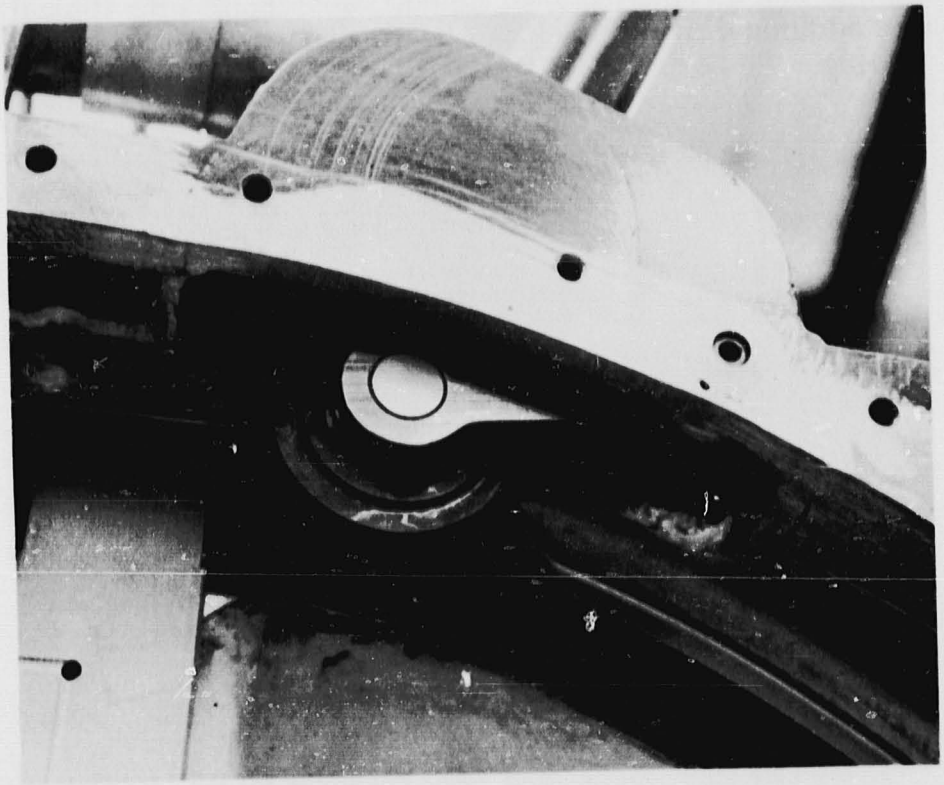

Figure I.B.9.4 Photograph of Ford 707 Turbine Engine Housing Showing Location of Spring-Loaded Roller

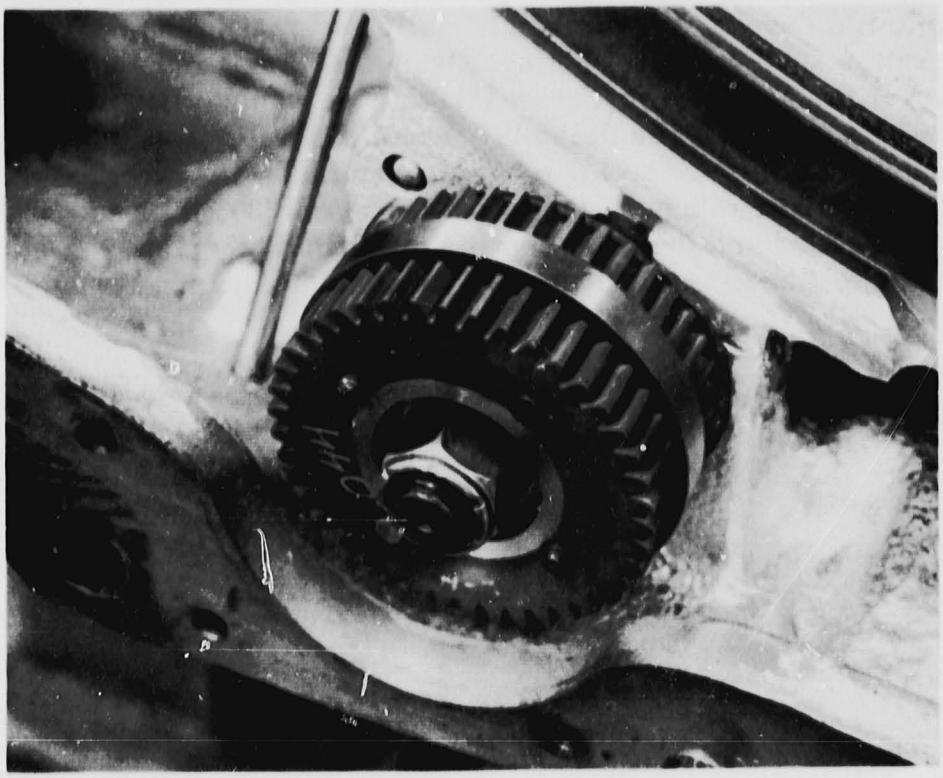

Figure I.B.9.5 Photograph of Ford 707 Turbine Engine Housing Showing Location of Drive Pinion Assembly

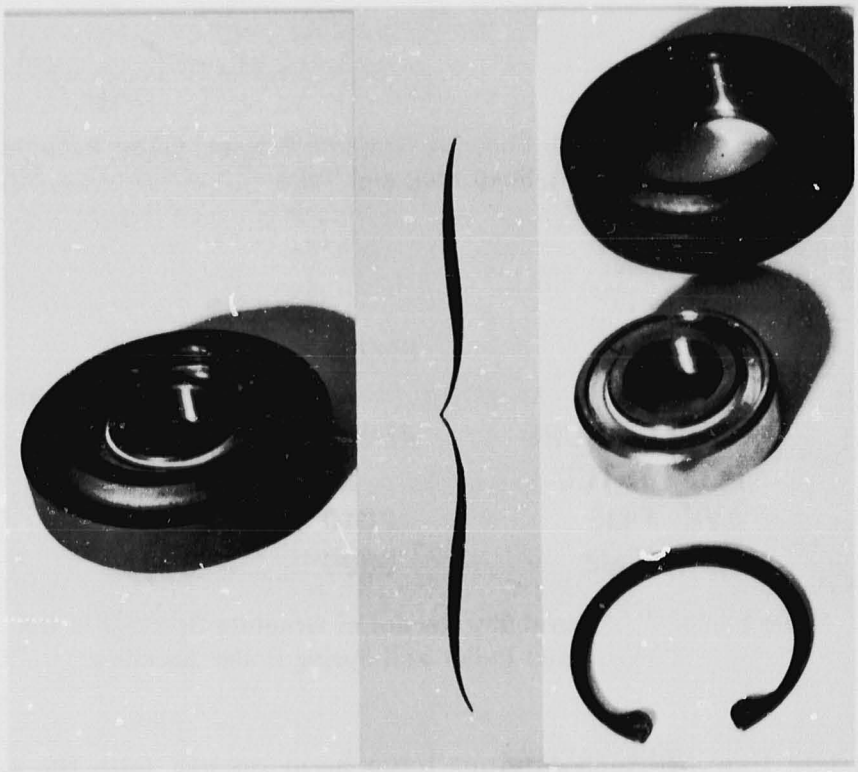

Figure I.B.9.6 Photograph Showing Ball Bearing, Outer Race Support Ring and Snap Ring

In an effort to develop a more maintenance-free system, the ball bearings were replaced with a solid graphite bearing. This graphite bearing along with its outer steel roller or tire is shown in Figure I.B.9.7. The graphite bearing is held in the steel tire with snap rings. The durability record of these graphite bearings is tabulated in Table I.B.9.1. In the spring roller location the bearing carries a 222N (50 lb) load and in the fixed roller location it carries 1355N (305 lb) load. None of these bearings have failed and the wear appears satisfactory. By mid-1978, all of the engines then on test had been converted to the graphite bearing system.

Figure I.B.9.7 Photograph Showing Graphite Bearing, Outer Race Support Ring, Shaft, Snap Ring and Yoke

	ROLLER	
	FIXED	SPRING
TOTAL HOURS	48287	37296
NO. TESTED	24	20
AVE. TIME	2010	1865
MAX. TIME	3600	3600

Table I.B.9.1 Durability Record of Graphite Bearings in the Fixed Roller and Spring Roller Locations

At the present time, thirteen engines have been on test with the current three-point support system. No major difficulties have been encountered after 61,114 hours.

I.C. TASK SUMMARY

Approximately 77,296 core hours of engine durability test at 800°C (1472°F) were completed under this program. This exceeds the Task I objective which was 76,000 hours at this temperature.

Turbine engine durability tests on aluminum silicate regenerator cores show that this material is relatively impervious to chemical attack. Fourteen cores of this material have each accumulated over 5000 hours of engine test at 800°C (1472°F), and five cores have each attained the durability objective of 10,000 hours with a minimal amount of chemical attack damage.

One thin-wall AS core has now accumulated 10,000 hours of engine test.

A Supplier D first-generation MAS core has accumulated 5381 hours at 800°C (1472°F). A Supplier D MAS core made from a more advanced material having lower thermal expansion characteristics and greater strength has now accumulated 3518 hours. This latter core shows no evidence of thermal or chemical attack damage.

A MAS core made by Supplier I from extruded segments has now accumulated 2474 hours at 800°C (1472°F). This core also shows no evidence of thermal or chemical attack distress.

Little problem has been encountered with the elastomer which bonds the ring gear to the regenerator matrix for thick-wall AS or MAS assemblies. The elastomer cut from an assembly after 7000 hours of engine test shows little sign of aging.

Separations in the elastomer-matrix bond region have occurred on all of the weaker thin-wall AS cores bonded using the conventional technique. Utilization of a high-compliance elastomer system shows promise of solving this problem. Two different high compliance elastomer configurations were evaluated, with one assembly having accumulated 7954 hours.

The cement holding the hub inserts in place failed in eight out of the first eighteen AS cores that have undergone engine test. A re-designed hub configuration which utilizes a solid ceramic ring around the hub insert appears to have corrected this problem. Approximately 35,000 hours have been accumulated on a sample of eleven of these re-design hubs with the highest hour one completing 7200 hours of engine test.

At the present time, thirteen engines have been on test with the current three-point support or rim-mounting system. No major difficulties have been encountered after 61,114 hours.

The spring and fixed roller ball bearings in the mounting system in all the engines have been replaced by solid graphite bearings which do not require lubrications. None of these bearings have failed, and wear rate appears to be satisfactory with some graphite bearings having now accumulated 3600 hours.

TASK II. CORE DURABILITY TESTING AT 1000°C (1832°F)

II.A. INTRODUCTION

A regenerator inlet temperature of 1000°C (1832°F) is a short-term goal that is needed for use in the current Stirling and gas turbine engines now under development. As a result of this projected need, in the fourth quarter of 1975, a special 707 turbine engine was assembled with high temperature regenerator seals and additional compressor discharge air cooling of the main frame bulkhead. Previous testing had shown these changes were needed to prevent seal coating failures and thermal distortion of the main frame. This engine contained the rim-support regenerator core mounting system. A thick-wall aluminum silicate regenerator core was installed on the left hand side and a thick-wall core of Supplier A's CPD-6 material was installed on the right hand side. Both cores were rim mounted with elastomer bonded ring gears and stress relieved rims. During the first year of testing, the engine was operated at an average regenerator inlet temperature of 982°C (1800°F) with excursions of 30°C (52°F) above and below this value being permitted. These regenerator inlet temperatures were obtained by operating the engine at higher-than-design turbine inlet temperatures at 60 to 65% gasifier spool speed and low power turbine speeds. It was possible by operating at these conditions with turbine inlet temperatures of 1065-1080°C (1950-1975°F) to expose the regenerator to inlet temperatures up to 1020°C (1850°F). Since this elevated test program was initiated, it was necessary to completely rebuild the engine many times. On several other occasions it was necessary to replace nozzles, turbine rotors, and sheet metal ducting as these parts distorted, oxidized, or crept under thermal loads.

The original objective of Task II of this Program was to accumulate 1000 core-hours during each quarter at an inlet temperature of 1000°C (1832°F). Because of the increased interest in higher temperature operation of the regenerator, NASA initiated a program change in the first quarter of 1978 so that in the second quarter two of the 800°C (1472°F) engines would be converted to 1000°C (1832°F) engines. This would increase the number of hours of test at 1000°C (1832°F) per quarter from 1000 core-hours to 3000 core-hours. The conversion of the two engines was completed in the second quarter of 1978.

During the current program with NASA a total of 28,834 core-hours have been accumulated at 1000°C (1832°F) which is above the final Task II program objective of 28,000 hours.

II.B. DISCUSSION

As noted above, the first engine operated at elevated temperatures contained a thick-wall, Supplier A, AS core on one side and a thick-wall, Supplier A, CPD-6 core on the other side. Early in this test, thermal rim cracks were detected in the rim of the CPD-6 core. These cracks which were first observed at 418 hours are shown in Figure II.B.1. Radial cracks emanate from the base of the stress relief slots. These cracks are believed to be caused by high rim thermal stresses, and not totally unexpected in light of the fact that the rim safety factor for this design is just above unity. The thermal stress safety factors for aluminum silicate and CPD-6 ma-

terial at these temperatures are listed in Table II.B.1. These values suggest that the CPD-6 material will be marginal at these elevated temperatures. Providing the material is thermally stable, the aluminum silicate regenerator should have no problems with thermal stresses at 1000°C (1832°F).

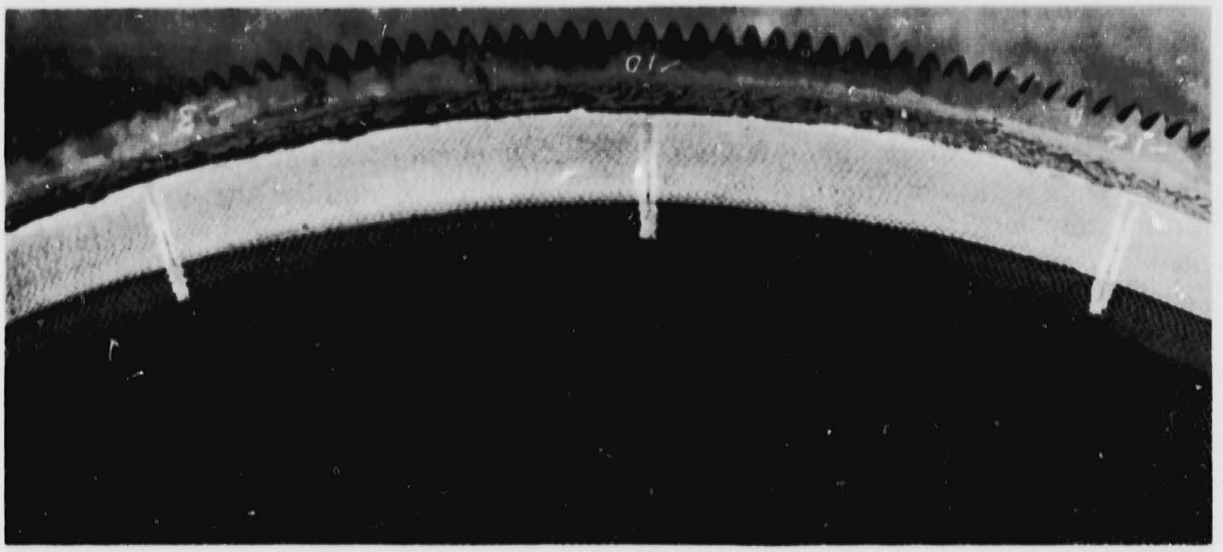

Figure II.B.1 Supplier A's CPD-6 Regenerator After 418 Hours at 982°C (1800°F)

RIM CONFIGURATION	MATERIAL	THERMAL STRESS SAFETY FACTOR
STRESS RELIEF, CONTINUOUS RIM	CPD6	1.5
STRESS RELIEF, CONTINUOUS RIM	ALUMINUM SILICATE	7.5

Table II.B.1 Safety Factor Comparison for Two Different Ceramic Materials at 982°C (1800°F)

The cracks in the CPD-6 material did not grow radially in the next 1400 hours. Figure II.B.2 shows the same cracks after 1710 hours. The width of the cracks appear to have increased, but this is merely fretting or crumbling of the edge of the crack caused by the rubbing action of the crossarm seal shoe. This edge fretting has been observed previously in cracks that survive long periods of engine exposure. The fact that the length of the crack has not changed appreciably indicates that the crack may have propagated to a region where the matrix is in compression. The crack then appears to have stabilized at this position.

After 2307 hours of operation at an average inlet temperature of 982°C (1800°F), the CPD-6 core failed, and a photograph of this failure is shown in Figure II.B.3. The failure mode is typical of a chemical attack failure with mid-radius cracks formed on both faces. This material had shown only marginal improvement in chemical attack resistance when compared to LAS in engine tests that were con-

ducted at 800°C (1472°F) (Reference 2). It had also shown only a small improvement over LAS in laboratory test at 1000°C (1832°F) with sodium present (Reference 2). Eventual failure due to chemical attack, therefore, was expected in these high temperature engine tests. This material was then dropped from the engine test program.

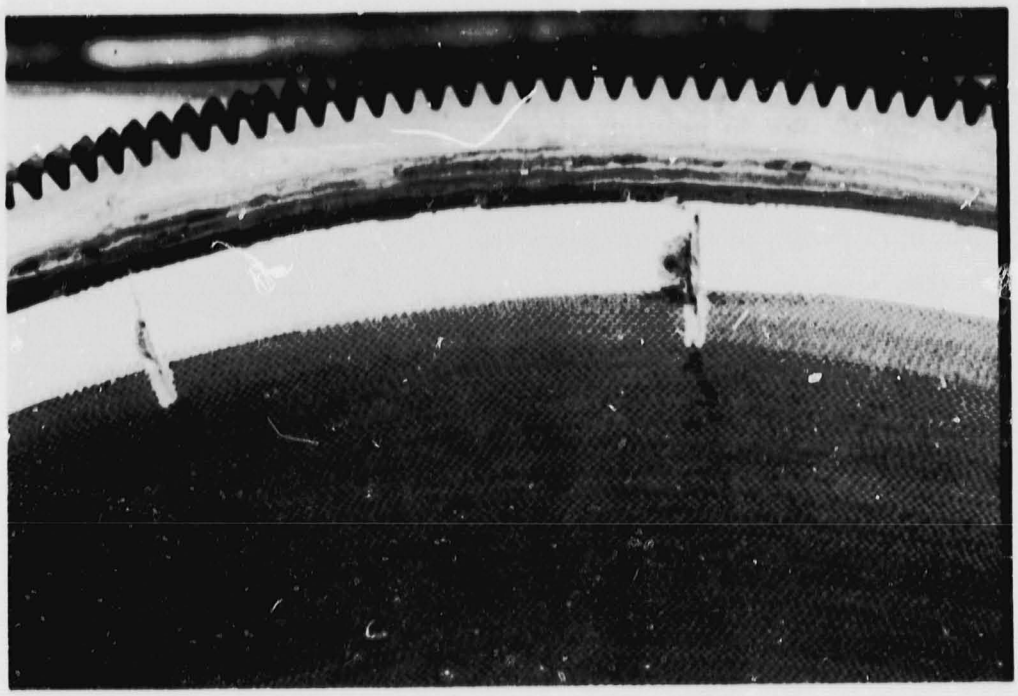

Figure II.B.2 Supplier A's CPD-6 Regenerator After 1710 Hours at 982°C (1800°F)

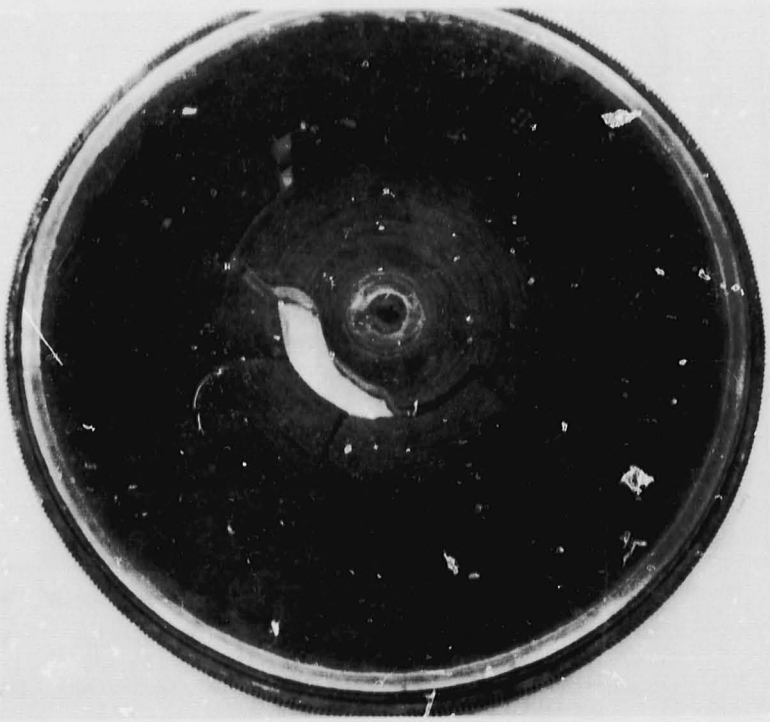

Figure II.B.3 Failed CPD-6 Core After 2307 Hours at 982°C (1800°F)

The CPD-6 core was replaced with a thin-wall AS core and the test was continued. When two additional engines were available for 1000°C (1832°F) testing in 1978, one additional thick-wall AS core, two additional thin-wall AS cores and one of Supplier D's thick-wall MAS cores were put on test. Over a period of time it has been necessary to replace some of these cores with others.

The present Task II status is summarized in Figure II.B.4 and shows that the highest-hour thin-wall AS core has accumulated 5411 hours at an average inlet temperature of 982°C (1800°F). This core was removed from test when the hot side surface was glazed due to ignition of fuel deposits during a false engine start. A second thin-wall core was terminated after 443 hours when excessively damaged by a MAS core failure on the opposite side of the engine. The highest hour thick-wall AS core has 8071 hours at this temperature.

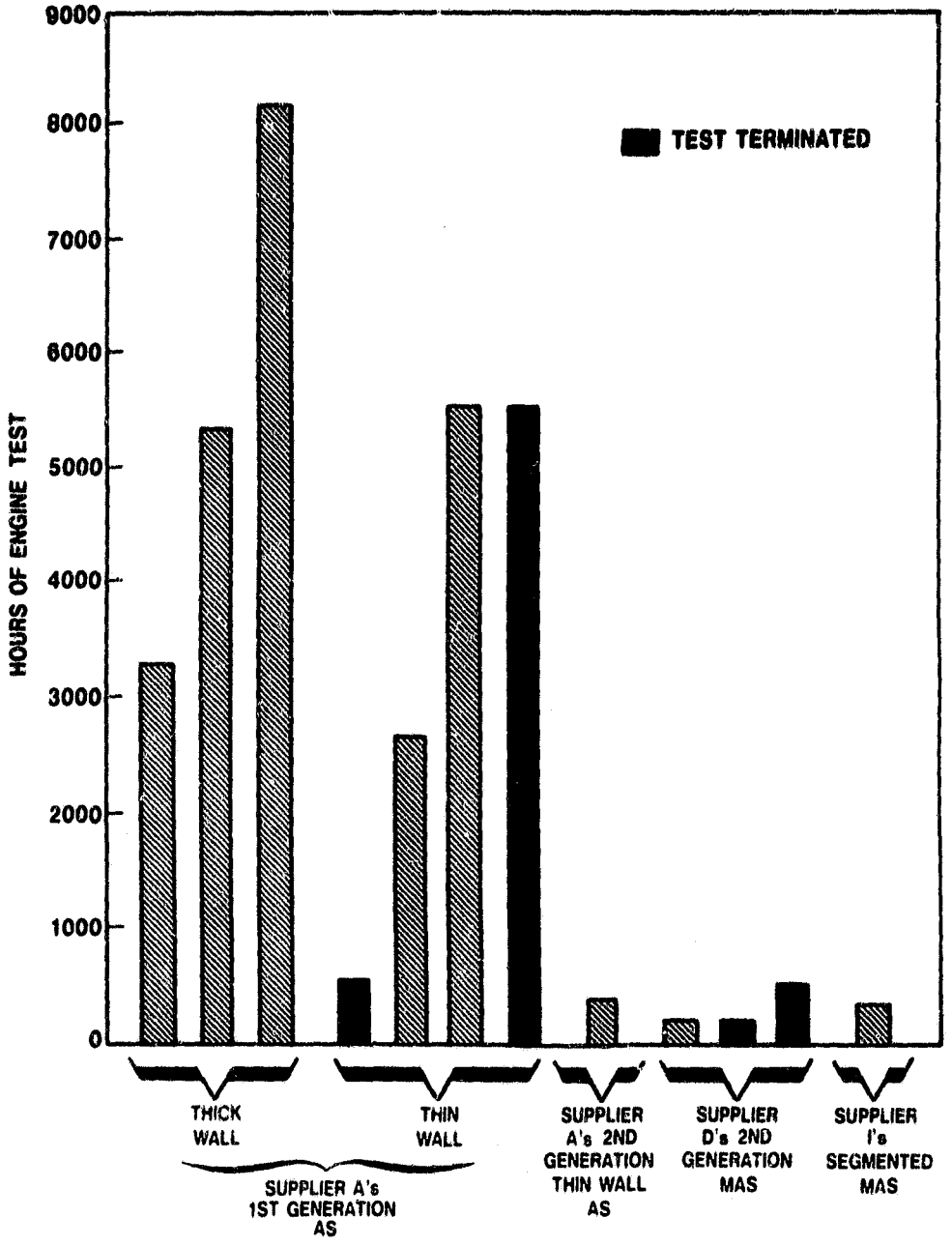

Figure II.B.4 Durability Record of Regenerators Operating at 1000°C (1832°F)

The first MAS core tested at this temperature was terminated after a hub cement failure. The core, which was fabricated with the Supplier D MAS-2 material, appeared to be void of thermal cracks in the rim after 473 hours. A second core of this material was installed in the high temperature engine and accumulated 110 hours before experiencing circumferential separation at mid-radius due to marginal matrix bonding in that region. A third core has accumulated 101 hours at this time.

During the last few months of the test program, a core of Supplier A's new, second-generation AS material became available for engine test. All of the other Supplier A AS cores, described in Tasks I and II of this program, have been made from Supplier A's first-generation AS material. Elevated temperature tests conducted in the laboratory and reported in Section VI have shown that this material is thermally stable only up to temperatures slightly above 1000°C (1832°F). The second-generation AS material has higher temperature capability, and this is desired for the Advance Gas Turbines now under design for automotive applications. Although the Ford 707 engine could not be operated at regenerator inlet temperatures above 1000°C (1832°F), the limited testing of the second-generation AS in the 707 turbine showed that it has sufficient mechanical integrity to withstand the mechanical loads imposed by a turbine drive and seal system. This core showed no distress after 310 hours of operation at 1000°C (1832°F).

Late in the final months of the program a second MAS core assembled from extruded segments was received from Supplier I. It is similar to the one shown in Figure I.B.5.5 and described in Section I.B.5. This core also is desired in the future Advance Gas Turbine automotive engines because of its good performance and low cost. It also was placed on test at 1000°C (1832°F) and accumulated 236 hours without distress before the NASA/Ford test program was completed.

It is interesting to note that although the thermal stress safety factor for the MAS regenerators was close to unity none showed any indication of thermal rim cracks. The compressive preload of the ring gear and the stress relieving slots result in a satisfactory containment of these thermal stresses. These stress relieving techniques are described in detail in Section V.B.2.

II.C TASK SUMMARY

Twelve different regenerators have been tested at 1000°C (1832°F) and this sample has accumulated 28,834 hours at this temperature. This accumulation exceeds the Task II program objectives of 28,000 hours.

About 8071 hours of engine test at an average regenerator inlet temperature of 982°C (1800°F) have been accumulated on a Supplier A first-generation, thick-wall aluminum silicate core, and 5411 hours at this temperature have been accumulated on a thin-wall core of the same material. Neither core shows any signs of thermal or chemical attack damage after this exposure. A total of four AS cores have each exceeded 5000 hours of engine test at this temperature without distress.

A second-generation AS material from Supplier A, which has higher temperature (1100°C, 2012°F) capability, has accumulated 310 hours at 1000°C (1832°F). This ad-

vanced material shows good mechanical integrity, seal compatability and no signs of distress after this exposure.

A core of Supplier D's second-generation MAS and another fabricated by Supplier I from extruded MAS segments were placed on test at 1000°C (1832°F). These cores accumulated 437 and 236 hours, respectively. Neither core showed any sign of chemical or thermal distress after operation at this temperature.

TASK III. MATERIAL SCREENING TESTS

III.A. INTRODUCTION

The material screening tests represent a three-step program which formed the basis for the screening of ceramic materials for the heat-exchanger application in the gas turbine engine. The candidate materials were first subjected to laboratory tests simulating conditions at the hot face and the cold face of the regenerator in service. Those materials deemed promising were tested next as inserts in a host core running in an engine operating in an accelerated corrosion mode. In this test, common road salt (sodium chloride) is ingested into the engine operating with a regenerator inlet temperature of 800°C (1472°F). The materials that showed good resistance to corrosion were then fabricated into full size regenerators and evaluated in the engine operating in the same accelerated corrosion mode. The emphasis in this test program is on the physical and chemical stability of the candidate materials under the most severe engine conditions and the test sequence identifies the materials with potential capability to meet the 10,000 hour durability requirement in the gas turbine engine.

III.B DISCUSSION

III.B.1 Laboratory Tests

The initial part of the materials screening tests is the laboratory testing. The laboratory tests are designed to evaluate a candidate material's resistance to attack by sodium and sulphur compounds. Specifically, the tests are aimed at quantifying the sodium ion exchange and sulphuric acid leaching of the materials as they occur under engine operating conditions at the regenerator hot face and cold face respectively. The regenerator hot face environment consists of high pressure discharge air with low pressure inlet gas. High pressure inlet air and low pressure exhaust gas exist at the cold face of the regenerator.

In the cold face chemical attack test the specimens of the candidate materials are subjected to a 2-hour leaching in 1% sulphuric acid at 25°C. The specimens are then heated to 315°C (600°F), which approximates the regenerator cold face temperature. The degree of stability is determined by measuring the changes in the sample length as well as 25°C-800°C (RT-1472°F) thermal expansion behavior as related to a series of such exposures.

In the hot face chemical attack test the matrix specimens are soaked in 3.5% sodium chloride solution and dried in air at 200°C (392°F) for 2 hours. The specimens are then exposed to 800°C (1472°F) and thermal stability is periodically determined by measuring changes in specimen length and thermal expansion in the 25°-800°C (RT-1472°F) range.

The standard specimens for testing are obtained in the form of 25.4 mm x 25.4 mm x 76.2 mm (1 inch x 1 inch x 3 inch) rectangular parallel-pipeds cut from bulk matrix with the axial faces ground parallel to each other within 0.025 mm (0.001 inch). Prior to testing, the specimens are degreased by a five minute ultrasonic

treatment in ACS acetone. The samples are then washed in distilled water for five minutes in an ultrasonic cleaner, air dried with filtered oil-free compressed air and oven dried at 200°C for at least thirty minutes. The specimens are then heated to 500°C for at least fifteen minutes to drive off any occluded volatile impurities and cooled to room temperature. This completes the cleaning procedure and the specimens are stored in a dry environment. The initial length measurements of the cleaned specimens are obtained by means of Sheffield Visual Comparator with 5000:1 amplification. The lengths are measured to nearest 2.5×10^{-5} mm (within 1 millionth of an inch) and the measurements are accurate to within $\pm 1.3 \times 10^{-4}$ mm (± 5 millionths of an inch). After each period of testing (i.e., hot face or cold face test), the surface of the axial faces are cleaned by means of a soft brush to remove extraneous material and length measurements are obtained. At the end of each test 6.35 mm x 6.35 mm x 50.8 or 25.4 mm (1/4 inch x 1/4 inch x 2 inch or 1 inch) specimens are cut and thermal expansion ($\frac{\Delta L}{L}$) from 25°C to 800°C (RT-1472°F) is measured utilizing Theta dilatometer. The precision of this dilatometer has been checked periodically by means of standard specimens and is within ±20 ppm in the 25°C-800°C temperature range

During this test program sixteen materials from various suppliers around the world have been evaluated. These materials belong to three basic families. (1) Lithium aluminum silicate (LAS), (2) Magnesium aluminum silicate (MAS) and (3) modifications of these two types; e.g., AS, aluminous silicate-keatite which is derived from LAS by leaching out lithium and LAS/MAS which is essentially a mixture or solid solution of LAS and MAS materials. The test matrices evaluated are listed in Table III.B.1.1.

Material	Fabrication	Supplier Code	Symbol
LAS STANDARD	WRAPPED	A	×
LAS/MAS	WRAPPED	K	Δ
LEACHED LAS (AS)	WRAPPED	A	▲
MAS	EXTRUDED	I	□
MAS	WRAPPED	E	◪
MAS	WRAPPED	J	■
MAS	WRAPPED	C	◊
MAS	WRAPPED	D	♦
SiC	WRAPPED	L	*
LAS	BONDED TUBES	B	O
LEACHED LAS (AS)	BONDED TUBES	B	●
MAS	WRAPPED	A	▼
MAS	EXTRUDED	A	⊙
LAS/MAS	WRAPPED	K	⊡
MAS	WRAPPED	E	▽
Zr./MAS	WRAPPED	K	◬

Table III.B.1.1 Materials Evaluated

The results of the cold face test program are summarized in Figure III.B.1.1. With the exception of Supplier J MAS all materials showed a remarkably low susceptibility to sulphuric acid attack when compared to the standard Supplier A LAS matrix. The Supplier B LAS matrix suffered shrinkage while all others showed growth. The leached LAS matrices from Suppliers A (▲) and B (●) both are practically unaffected. All the MAS matrices with the exception of those Suppliers of I (□), J (■) and D (♦) also showed very little growth. The Supplier K LAS/MAS matrices of a later process (⊡) showed a greater susceptibility to acid attack than the matrices furnished during the early part (Δ) of the program. It is evident from these data the Supplier K LAS/MAS matrices are only marginally better than the standard LAS matrices. The MAS matrices are produced by two different processes; e.g., wrapping — Supplier A (▼), C (◊), D (♦), E (◪), E (▽) and J (■), extruded — Supplier A (⊙) and I (□). In spite of the difference in processing, the materials showed little or no difference in corrosion behavior under sulphuric acid attack. Since the Supplier J matrix material is not significantly different from that of the Supplier E — which showed no sulphuric acid attack — the higher susceptibility of the Supplier J matrix is attributed to processing. The thermal expansion behavior of these matrices in the as-received condition and after the simulated cold face attack test are summarized in Figures III.B.1.2 — III.B.1-15. All the LAS matrices showed a significant change in the thermal expansion behavior after the cold face test. This is consistent with the ion-exchange ($Li^+ — H^+$) mechanism and the resultant crystal lattice distortion attributed to the LAS β-Spodumene solid solution compositions and is manifested by the dimensional changes shown in Figure III.B.1.1. The MAS matrices also exhibited a change in thermal expansion after the sulphuric acid attack. The change is particularly large in the materials evaluated during the early part of the program; e.g., Supplier E (◪), C (◊) and J (■). The MAS materials evaluated towards the end of the program, e.g., Supplier A (⊙), (▼), E (▽) represent the state-of-the-art material and processing technology and are practically immune to sulphuric acid attack as shown both by the absence of dimensional change (Figure III.B.1.1.) and very little change in thermal expansion behavior (Figures III.B.1.12, III.B.1.13 and III.B.1.14).

The results of the hot face corrosion test program are summarized in Figure III.B.1.16. The thermal expansion behavior of these materials before and after the simulated hot face corrosion test are summarized in Figures III.B.1.17 to III.B.1.30. Many of the materials showed a sharp dimensional change initially (during the first 50 hours) followed by a more gradual change during the subsequent test period.

Even though many materials experienced an initial growth, and while some continued to grow (e.g., Supplier A LAS (X), C MAS (◊), D MAS (♦), K-ZrIMAS (Δ)) the others exhibited a gradual shrinkage. After approximately 150 to 350 hours of testing even those materials that have been experiencing shrinkage reversed to growth behavior (e.g., A MAS (▼), I MAS (□), A-Leached LAS (▲), B-Leached LAS (●)). This phenomenon appears to be related to the transformation of residual glass in the matrix in case of the MAS materials since little or no absorption of Na into the matrix has been observed. The growth in case of the LAS and leached LAS matrices is attributable to interaction with sodium which will be discussed in subsequent sections. The growth in the Supplier K LAS/MAS materials (Δ, earlier composition ⊡ later composition) is very high and is much higher than that of standard

LAS (X) matrix. The later composition, presumably an improved version of the composition evaluated during the early part of the program, showed highest growth of all the materials evaluated. These materials appear to be inherently unstable as evidenced by their thermal expansion behavior before and after test (Figure III.B.20 and III.B.1.30) in addition to the growth observed (Figure III.B.1.16). Among all the LAS matrices evaluated, the Supplier B LAS (O) showed the least growth which is less than half that of the standard — Supplier A LAS matrix (X). The growth in the leached LAS matrices of Supplier A (▲) and B (●) are comparable. The thermal expansion behavior of these materials before and after the hot face test (Figures III.B.1.17 (X), III.B.1.22 (O), III.B.1.18 (▲) and III.B.1.24 (●)) show that the new materials including Supplier A leached LAS (▲) have increased susceptibility to hot face chemical attack than the standard LAS (A (X)) matrix. It is interesting to note that the thermal expansion of the leached LAS from Supplier A became increasingly negative while that of the Supplier B (●) became increasingly positive as is the case with the standard (A — (X)). In case of the standard LAS and the Supplier B LAS and leached LAS the increase in thermal expansion seems to indicate Na absorption into the lattice. The observed negative expansion trend with the Supplier A leached LAS appears to be due to dilatation resulting from consolidation and sintering of the skeletal β Spodumene structure. All the MAS matrices with the exception of Supplier J (■) matrix showed very little dimensional change following the initial growth. In all cases the dimensional change is less than 100 ppm during the last 400 hours of the test. The MAS matrix materials evaluated during the last part of this program (e.g., Supplier A MAS, wrapped (▼), extruded (⊙), Supplier E MAS wrapped (∇)) showed remarkably low growth. The thermal expansion behavior of these materials (Figure III.B.1.27 to III.B.1.29) showed very little change after the simulated hot face corrosion test. It should also be noted that in all these materials the thermal expansion after the test is higher, however only slightly, compared to the fresh material. This is in contrast to fairly large changes after the test and somewhat inconsistent nature, i.e., some of the materials showed higher and others lower thermal expansion after the test, of expansion behaviors of the MAS matrices evaluated during the early part of the test program. These results show a marked improvement in the MAS materials and processing technology since the initial stages of this program, and the state-of-the-art MAS materials are practically immune to the chemical attack environment presented by the gas turbine engine on both the hot and cold side of the regenerator.

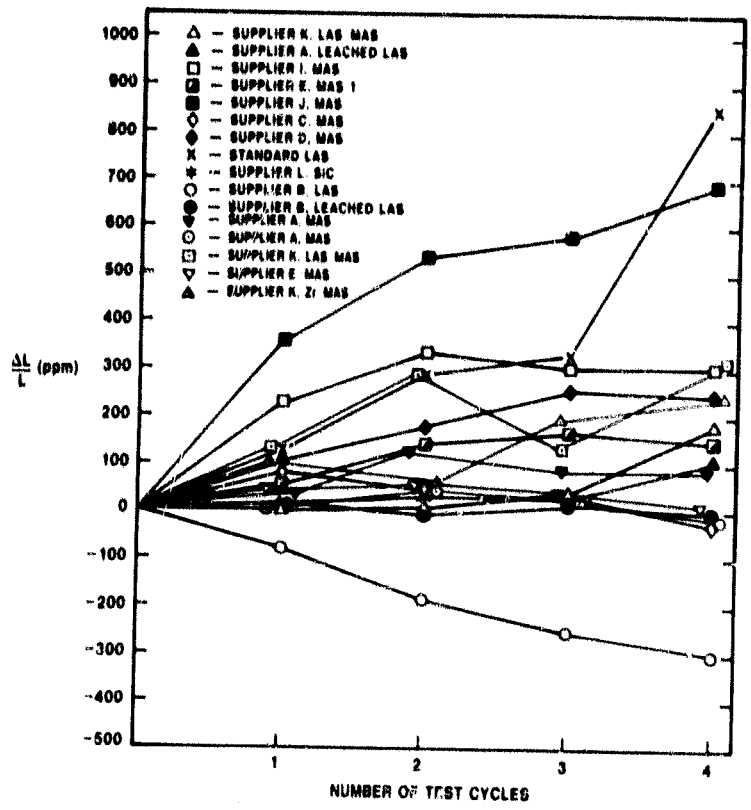

Figure III.B.1.1 **Physical Stability of Various Materials Under Cold Face Test Conditions.**

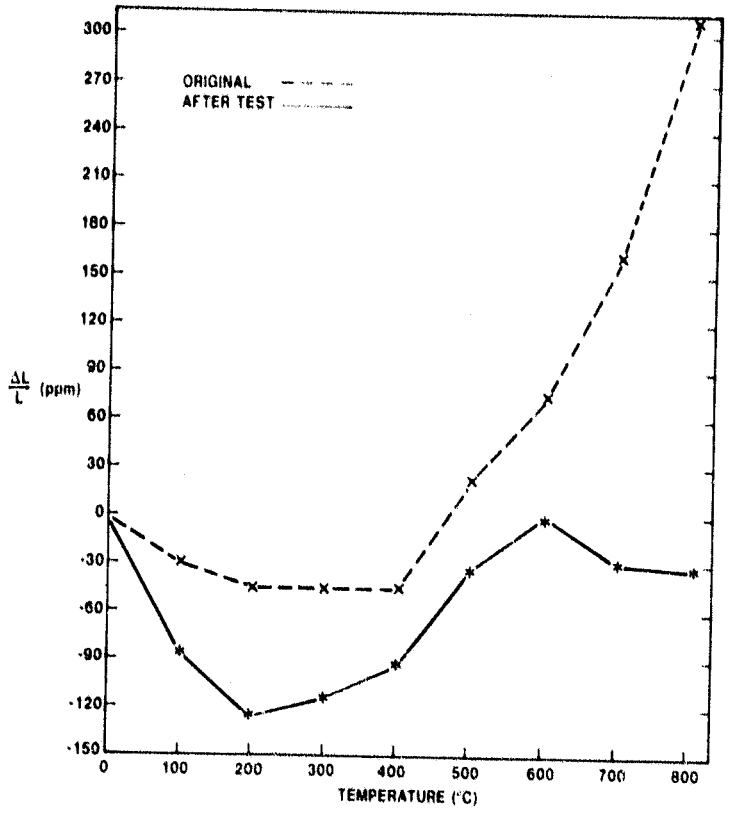

Figure III.B.1.2 **9455 LAS Standard; Thermal Expansion Before and After Cold Face Testing.**

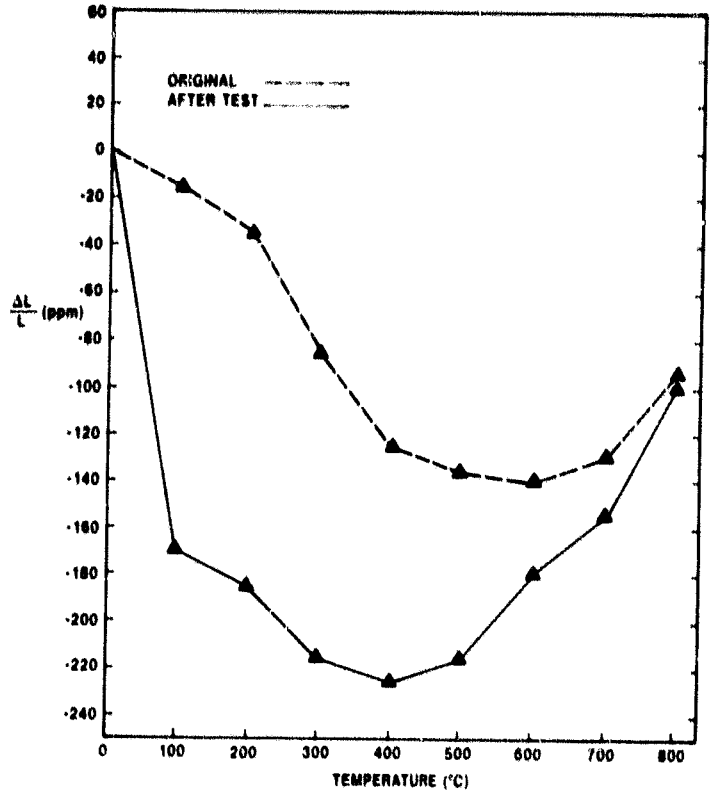

Figure III.B.1.3 Supplier A Leached LAS; Thermal Expansion Before and After Cold Face Testing.

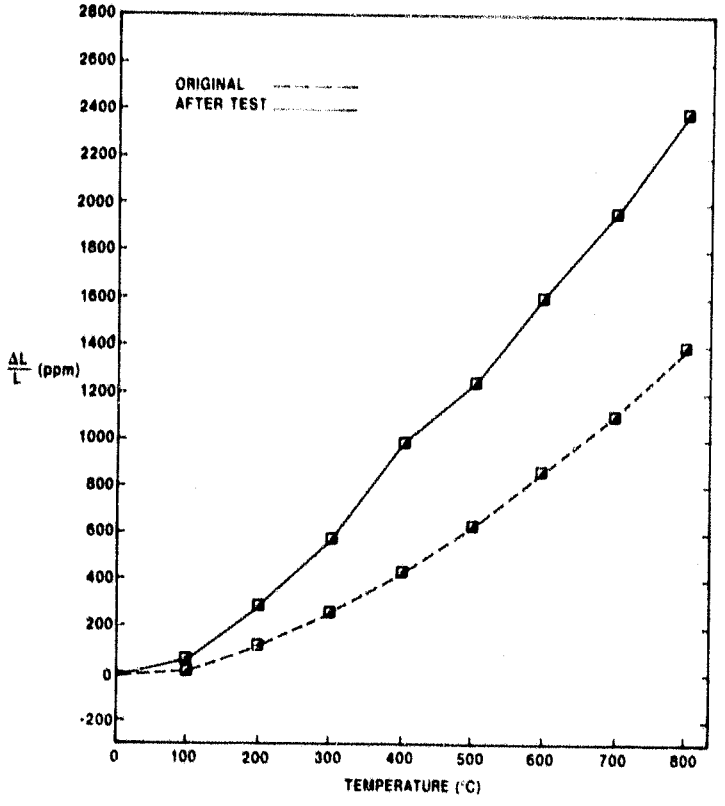

Figure III.B.1.4 Supplier E MAS; Thermal Expansion Before and After Cold Face Testing.

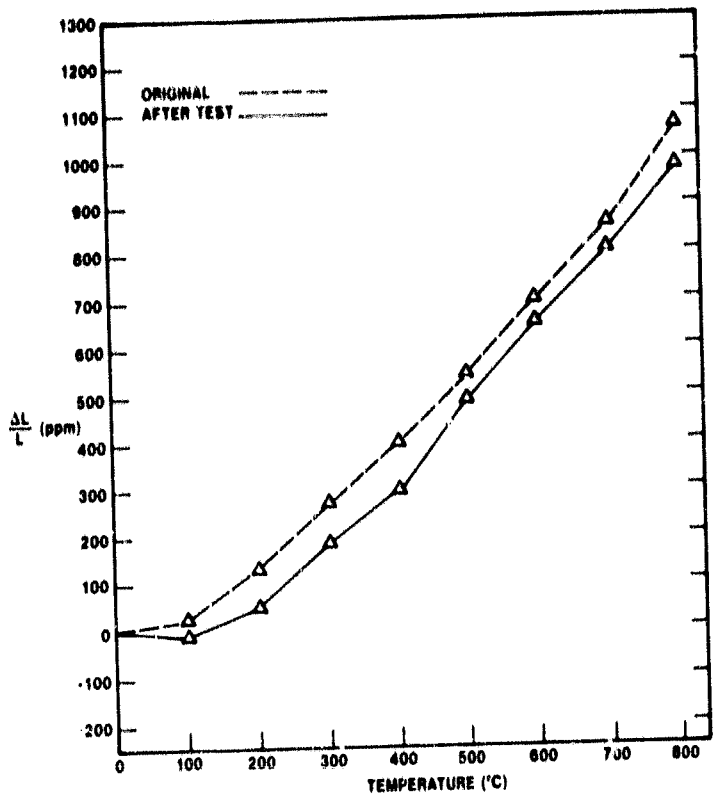

Figure III.B.1.5 Supplier K LAS/MAS; Thermal Expansion Before and After Cold Face Testing

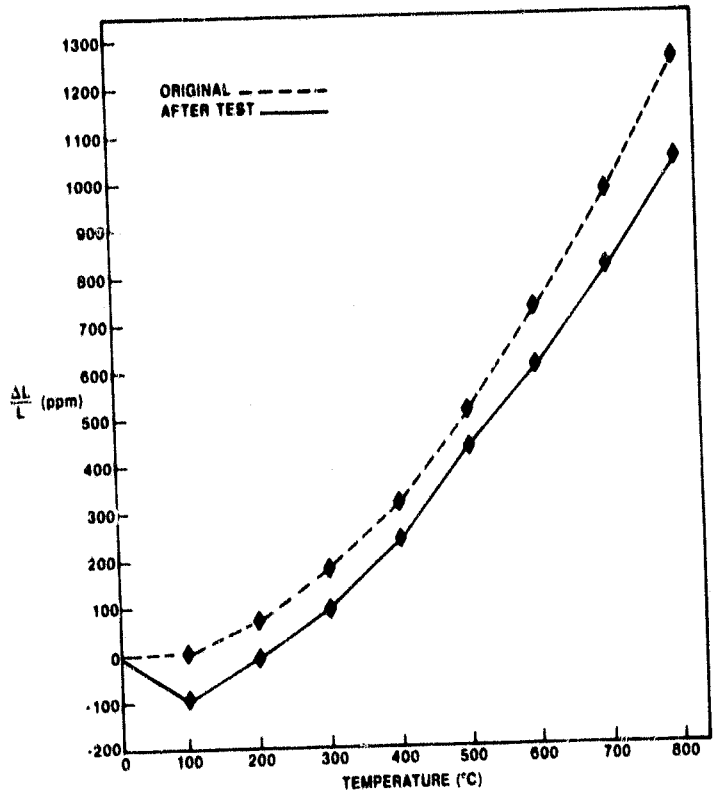

Figure III.B.1.6 Supplier D MAS; Thermal Expansion Before and After Cold Face Testing.

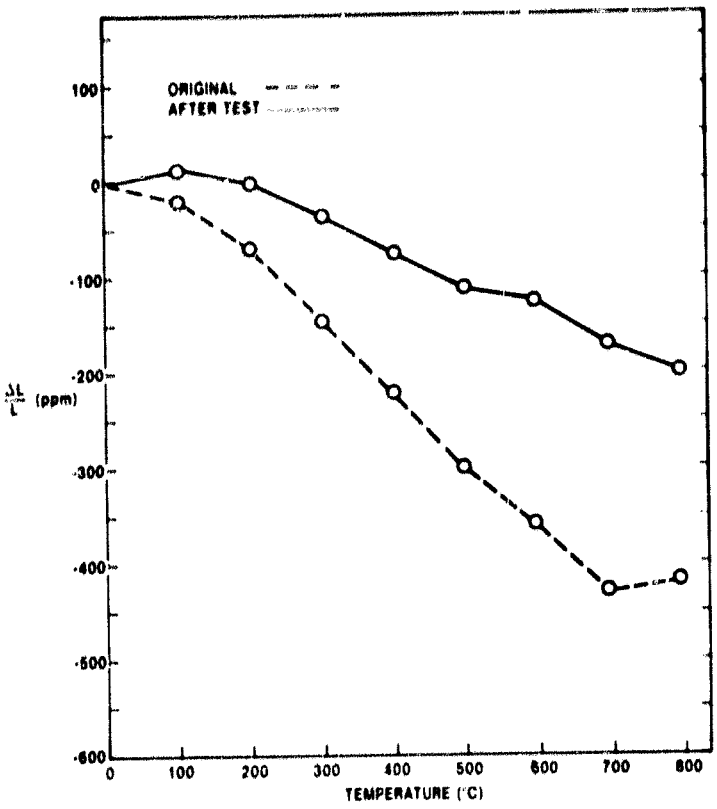

Figure III.B.1.7 **Supplier B LAS; Thermal Expansion Before and After Cold Face Testing.**

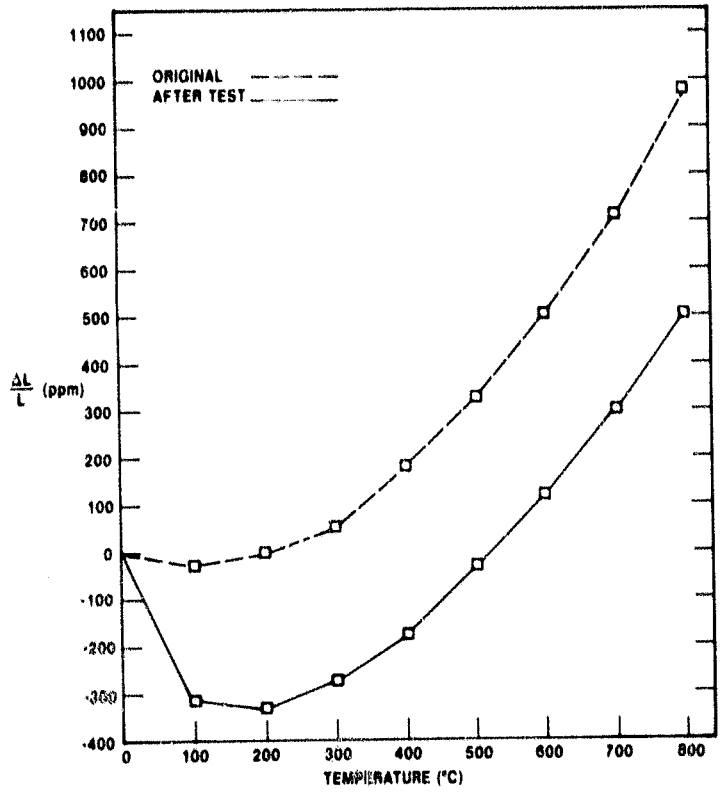

Figure III.B.1.8 **Supplier I MAS; Thermal Expansion Before and After Cold Face Testing.**

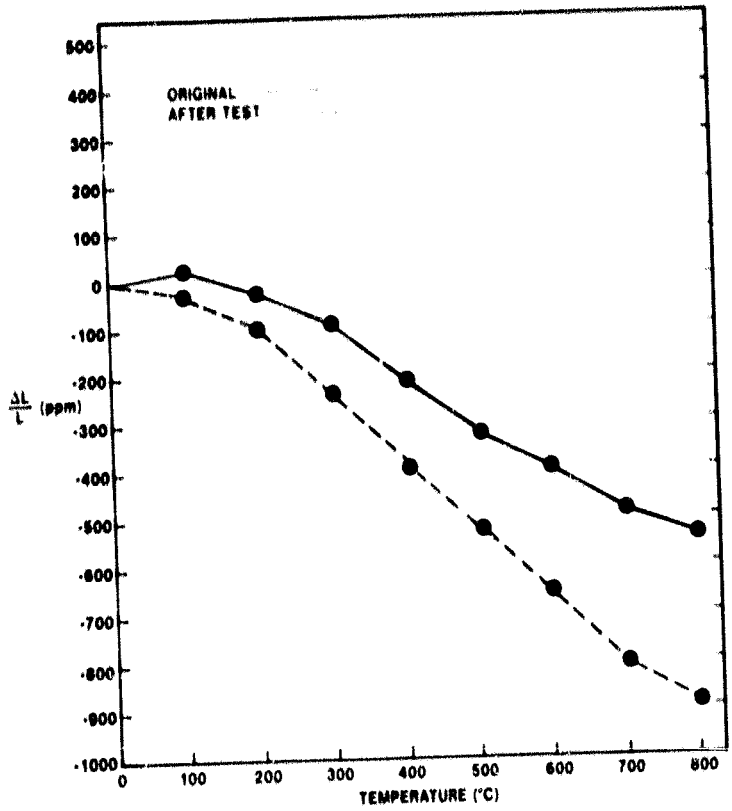

Figure III.B.1.9 **Supplier B Leached LAS; Thermal Expansion Before and After Cold Face Testing.**

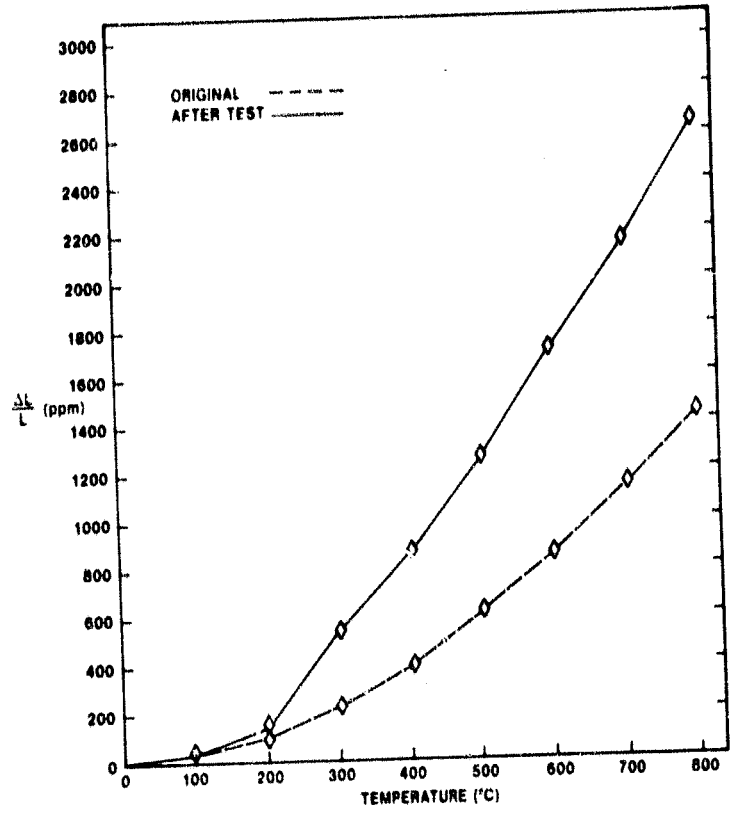

Figure III.B.1.10 **Supplier C MAS; Thermal Expansion Before and After Cold Face Testing**

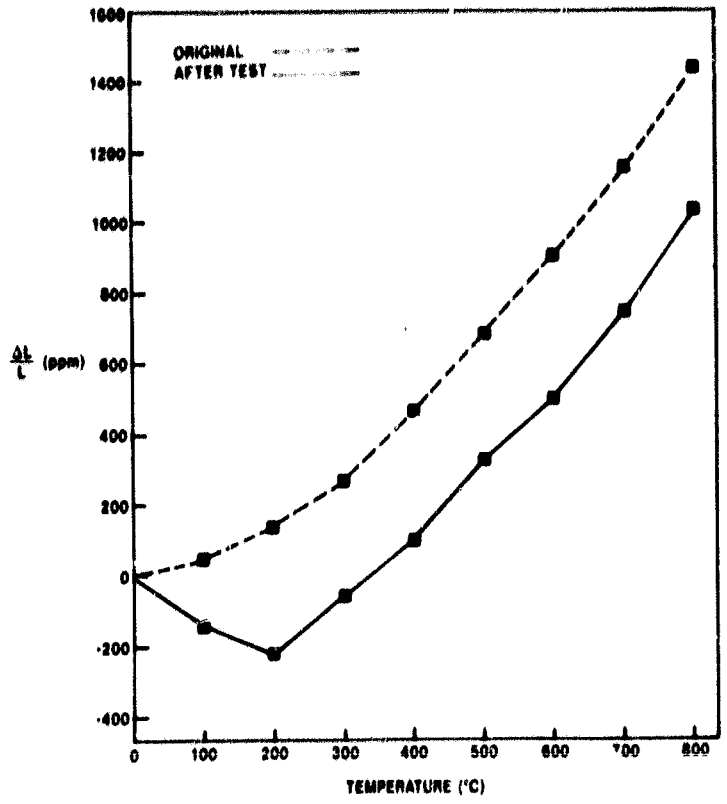

Figure III.B.1.11 Supplier J MAS; Thermal Expansion Before and After Cold Face Testing

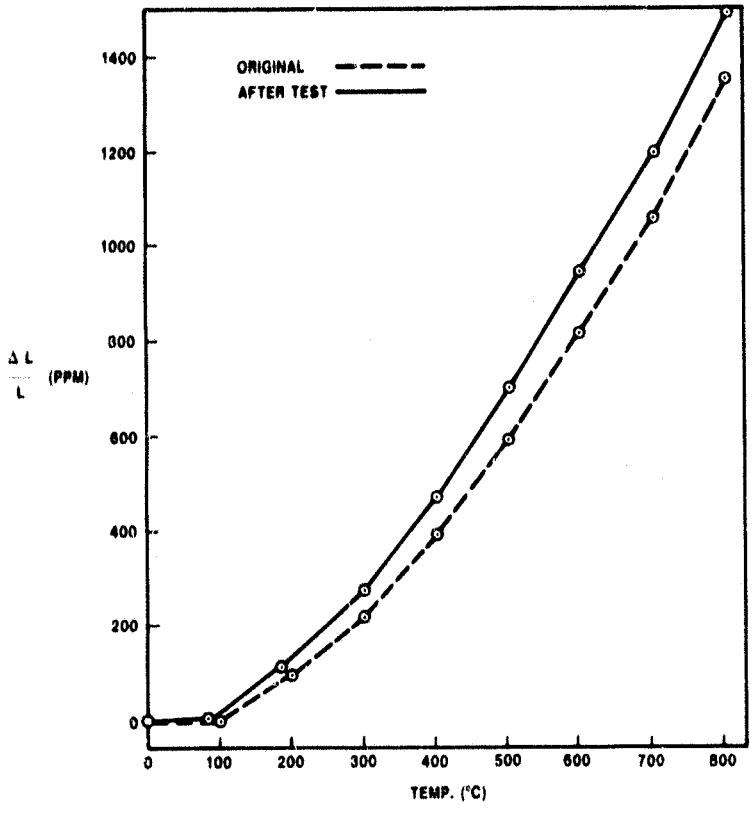

Figure III.B.1.12 Supplier A, MAS (Extruded); Thermal Expansion Before and After Cold Face Test Conditions

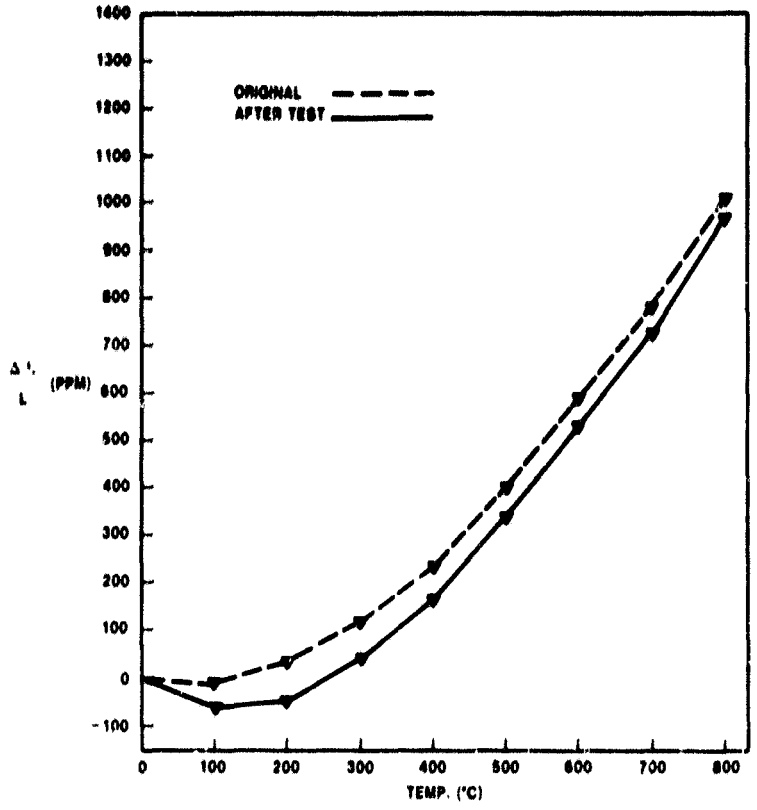

Figure III.B.1.13 Supplier A, MAS (Wrapped); Thermal Expansion Before and After Cold Face Test Conditions

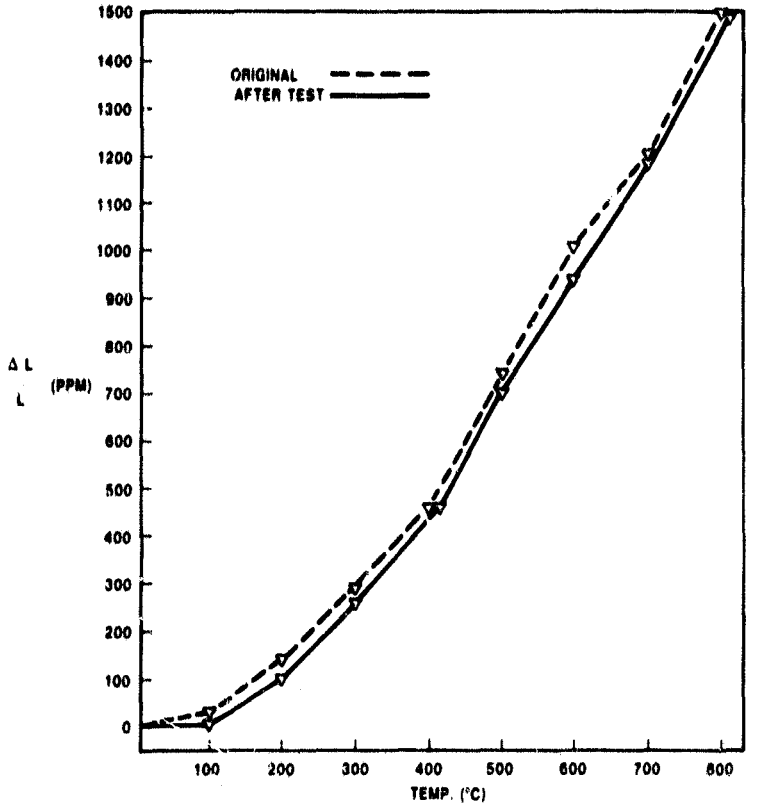

Figure III.B.1.14 Supplier E, MAS Thermal Expansion Before and After Cold Face Test Conditions

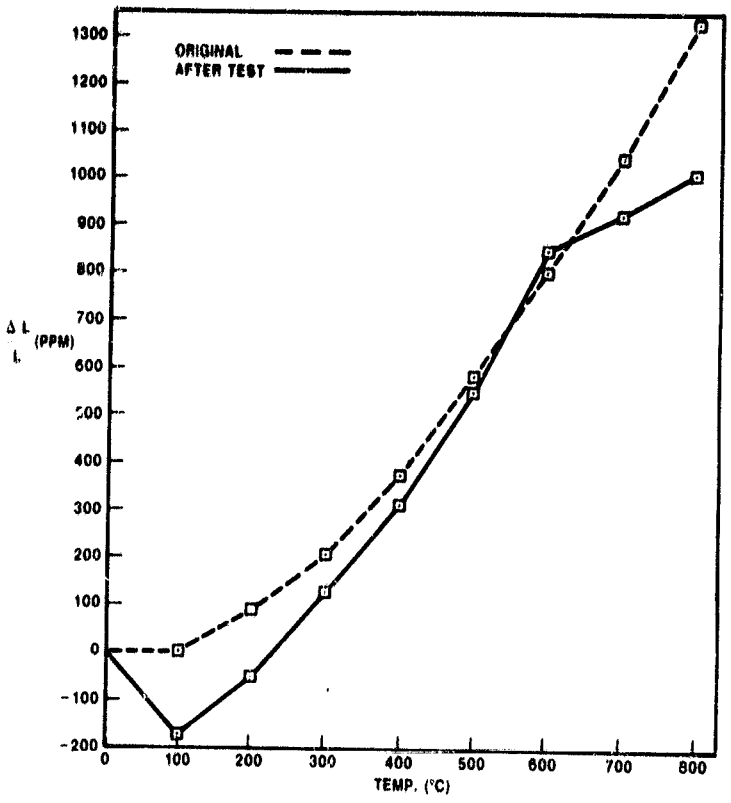

Figure III.B.1.15 **Supplier K, LAS/MAS; Thermal Expansion Before and After Cold Face Test Conditions**

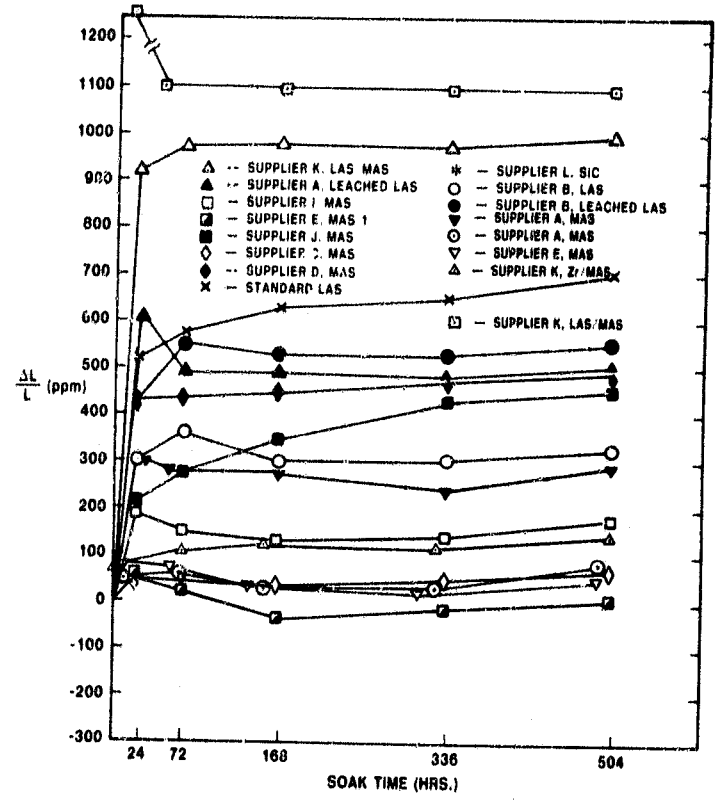

Figure III.B.1.16 **Physical Stability of Various Materials Under Hot Face Test Conditions**

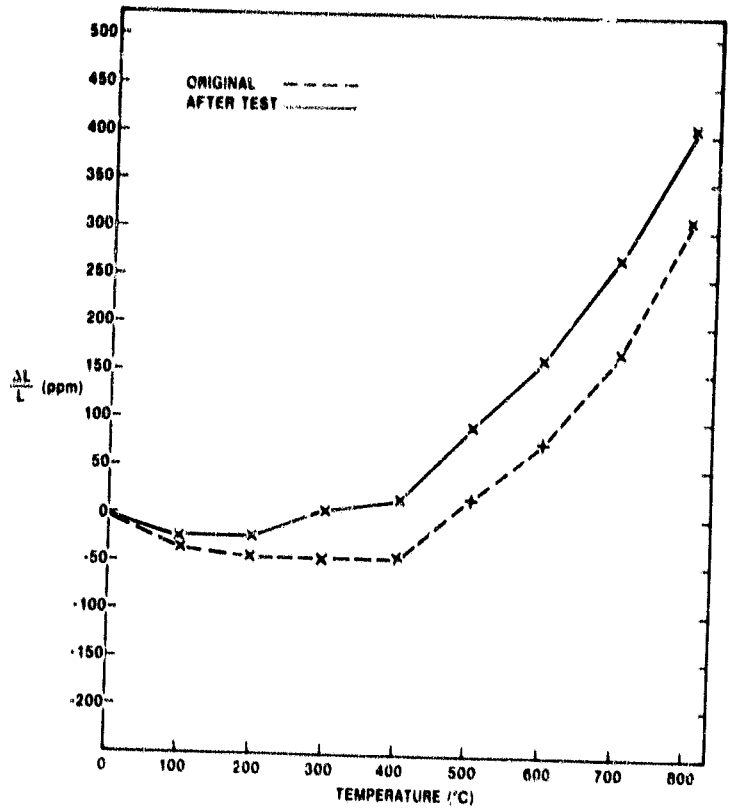

Figure III.B.1.17 9455 LAS Standard; Thermal Expansion Before and After Hot Face Testing.

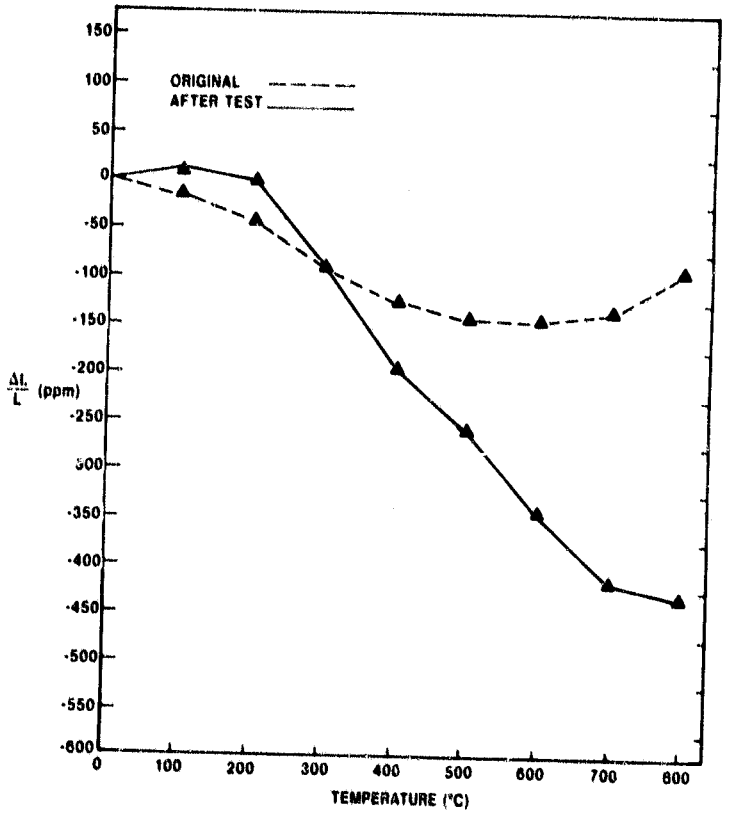

Figure III.B.1.18 Supplier A Leached LAS; Thermal Expansion Before and After Hot Face Testing.

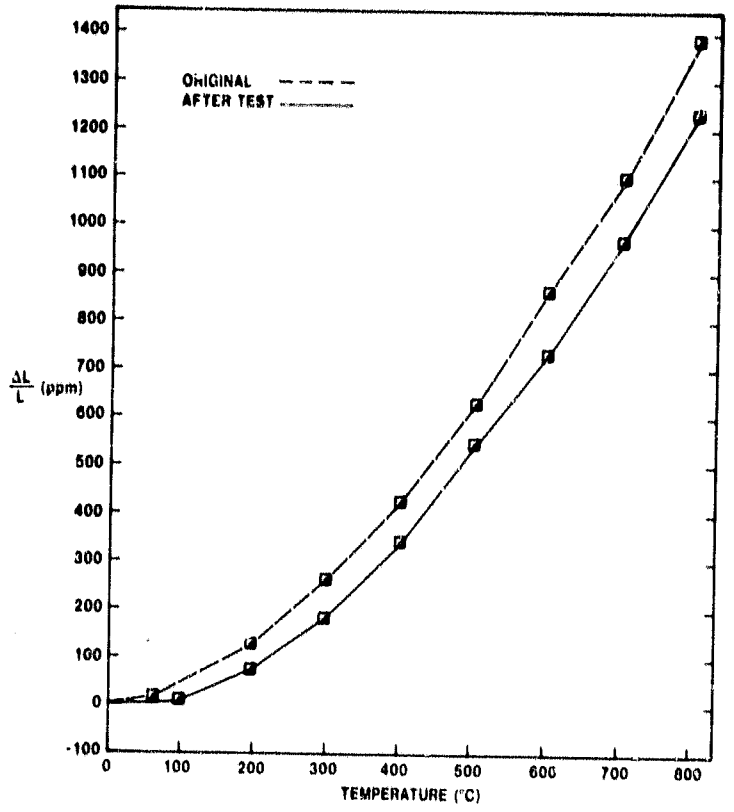

Figure III.B.1.19 **Supplier E MAS; Thermal Expansion Before and After Hot Face Testing.**

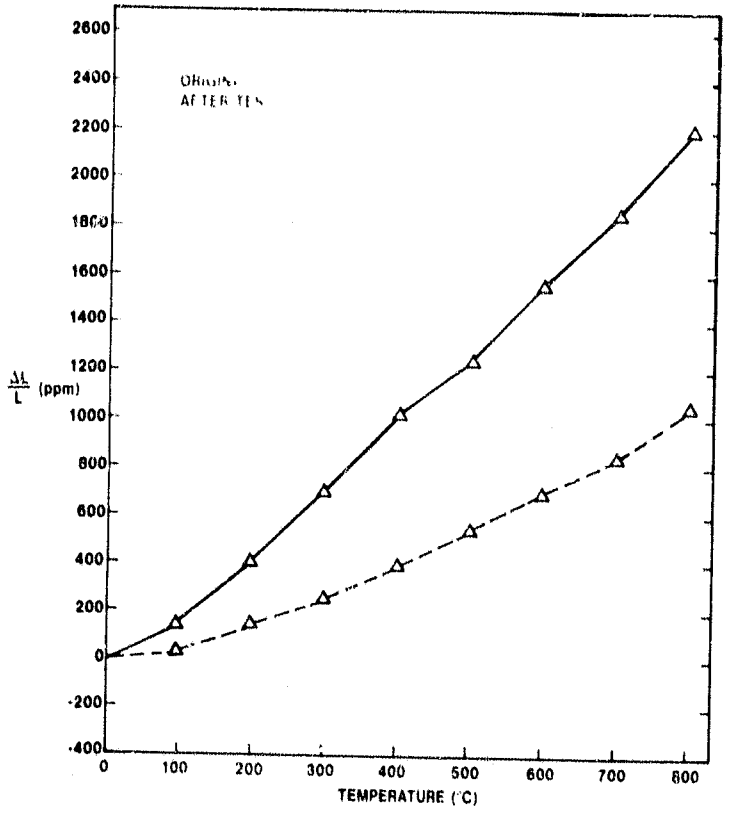

Figure III.B.1.20 **Supplier K LAS/MAS; Thermal Expansion Before and After Hot Face Testing.**

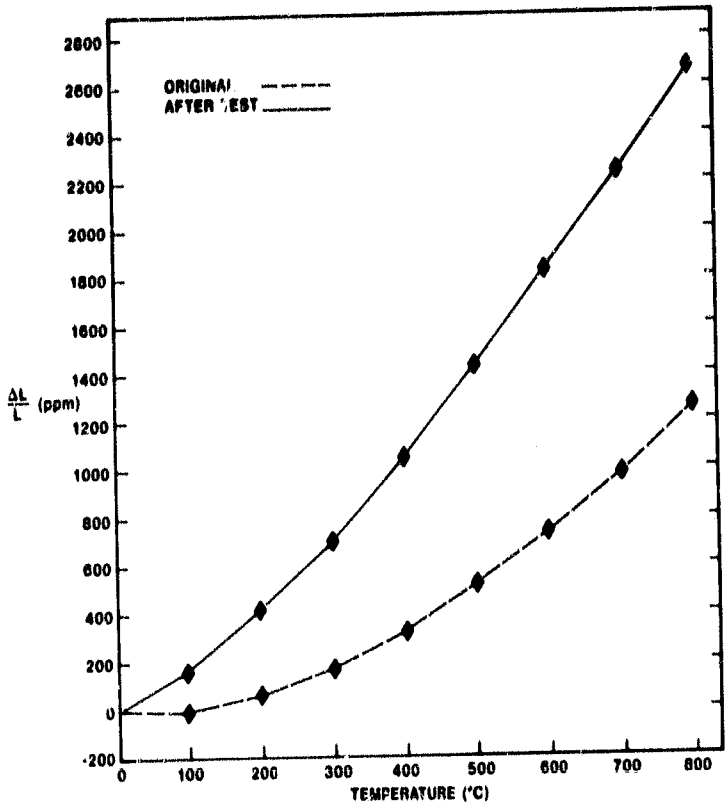

Figure III.B.1.21 **Supplier D MAS; Thermal Expansion Before and After Hot Face Testing.**

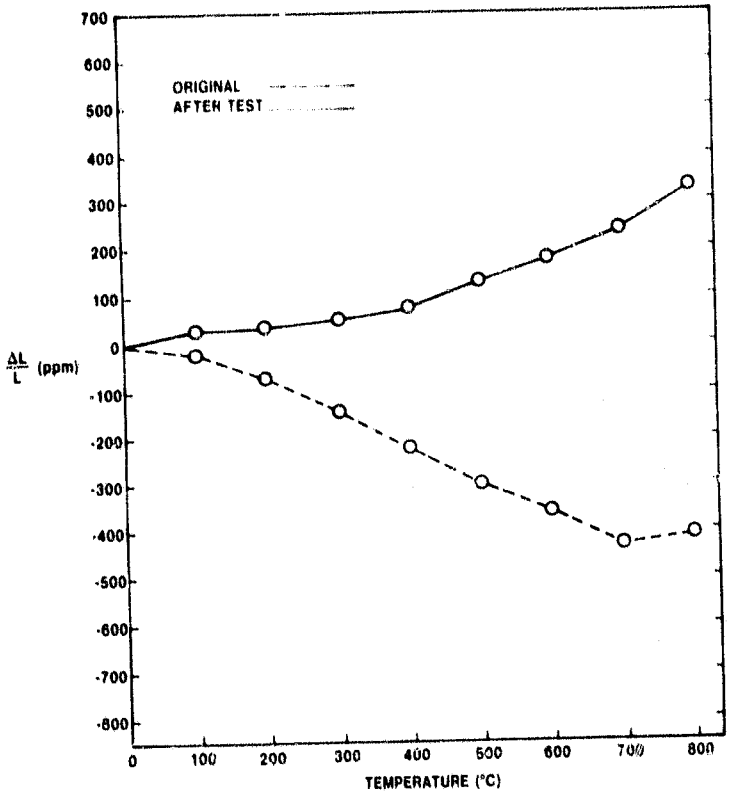

Figure III.B.1.22 **Supplier B LAS; Thermal Expansion Before and After Hot Face Testing.**

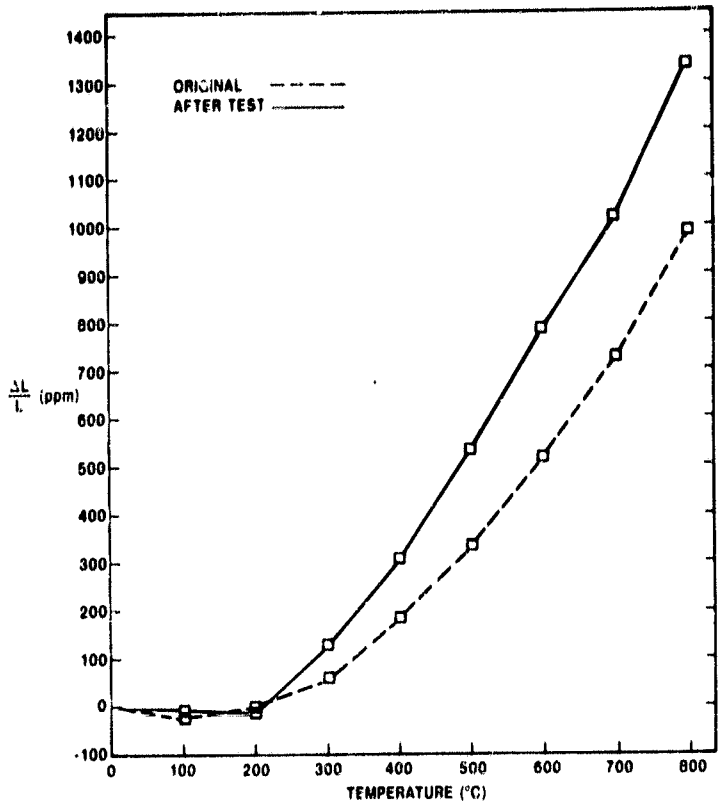

Figure III.B.1.23 **Supplier I MAS; Thermal Expansion Before and After Hot Face Testing.**

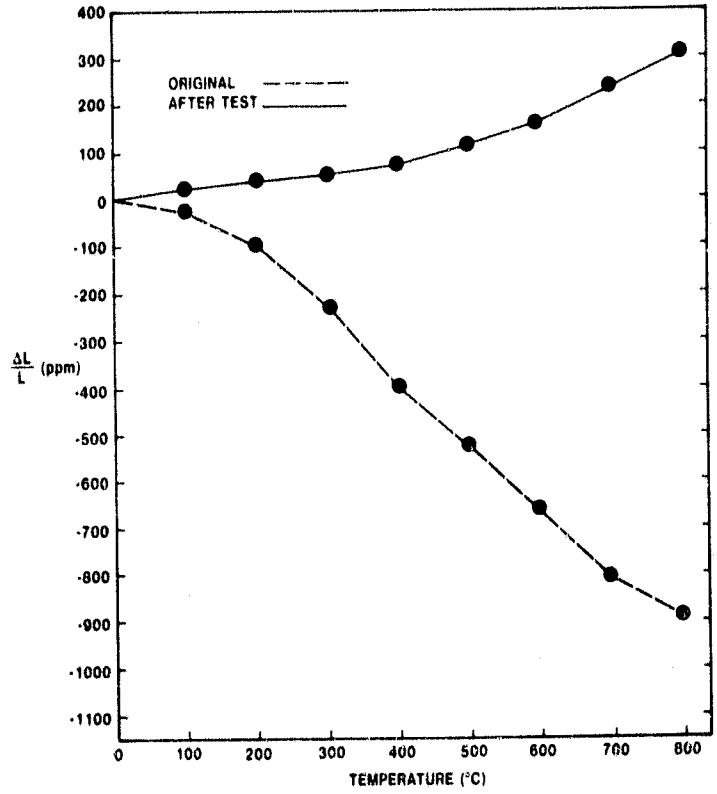

Figure III.B.1.24 **Supplier B Leached LAS; Thermal Expansion Before and After Hot Face Testing.**

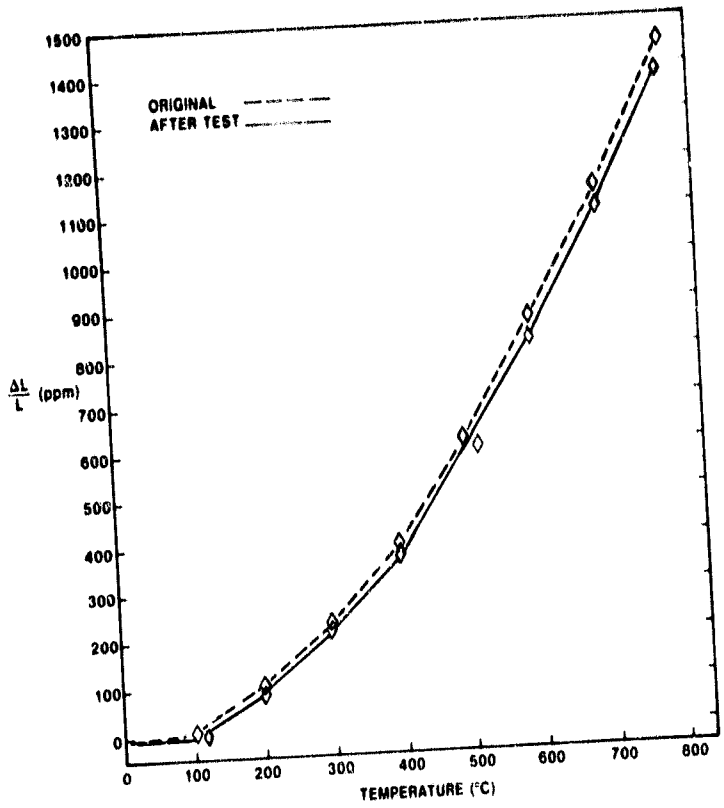

Figure III.B.1.25 Supplier C MAS; Thermal Expansion Before and After Hot Face Testing.

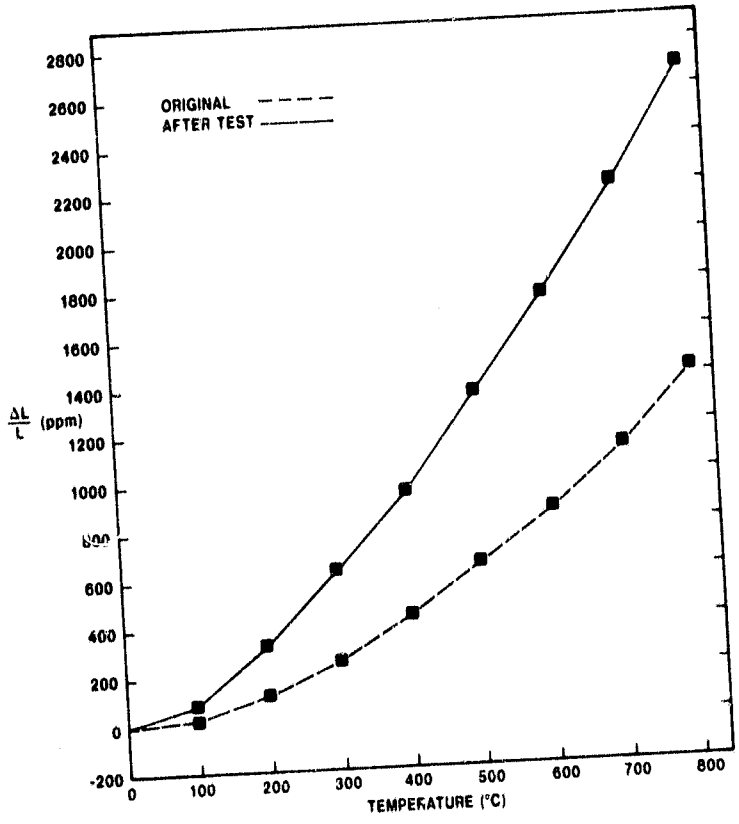

Figure III.B.1.26 Supplier J MAS; Thermal Expansion Before and After Hot Face Testing.

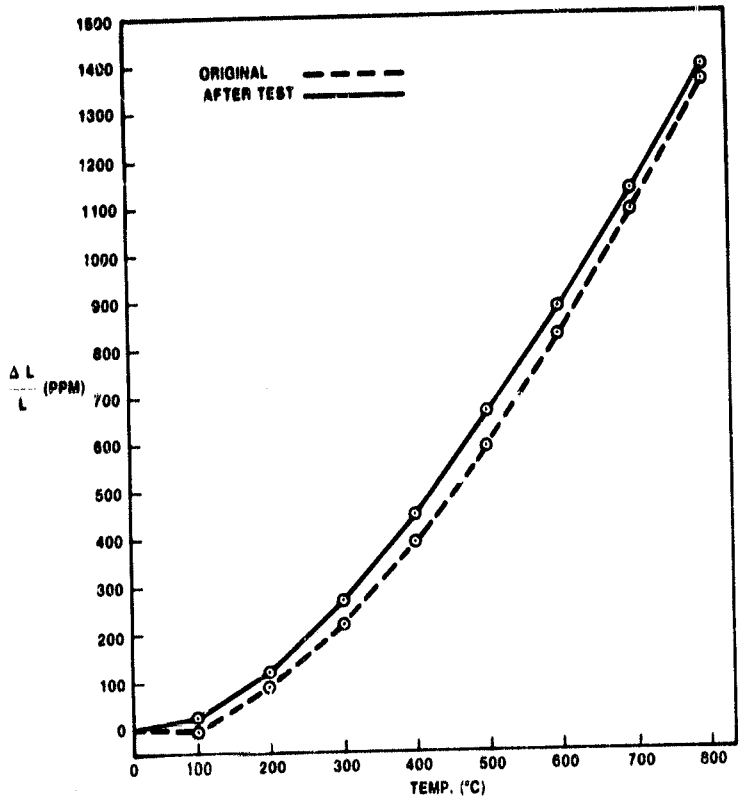

Figure III.B.1.27 Supplier A, MAS (Extruded); Thermal Expansion Before and After Hot Face Test Conditions

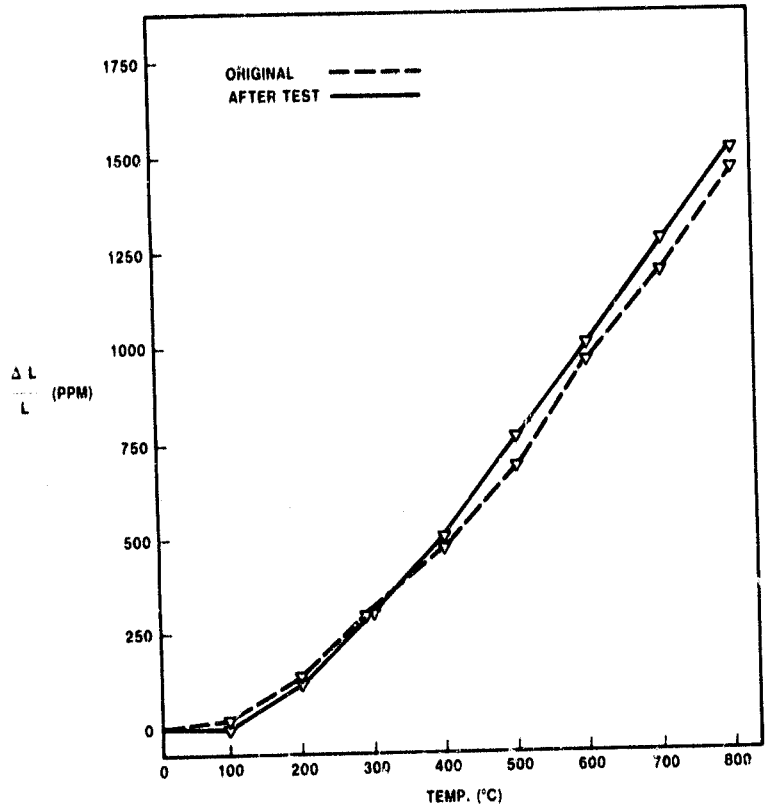

Figure III.B.1.28 Supplier E, MAS; Thermal Expansion Before and After Hot Face Test Conditions

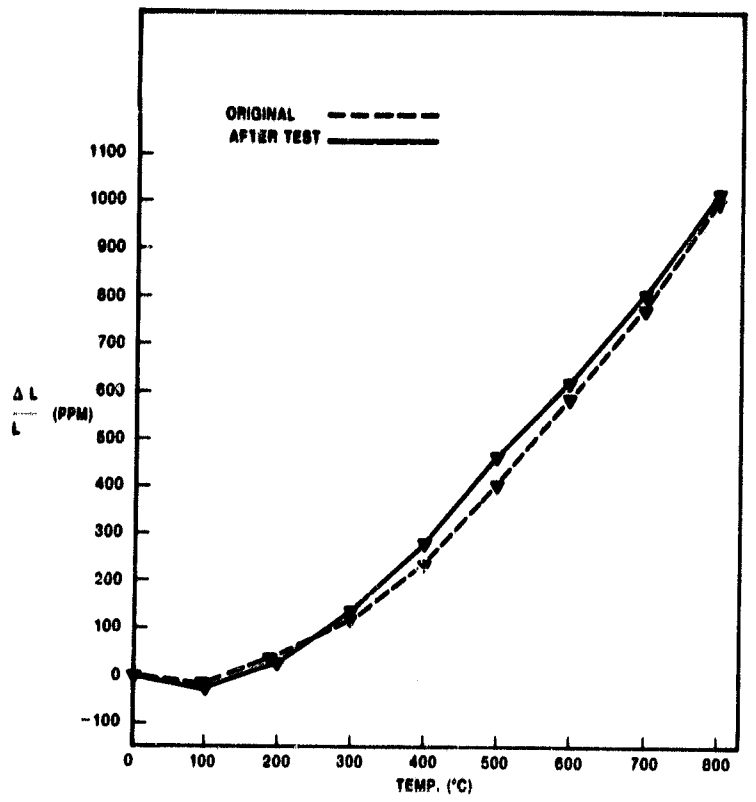

Figure III.B.1.29 Supplier A, MAS (Wrapped); Thermal Expansion Before and After Hot Face Test Conditions

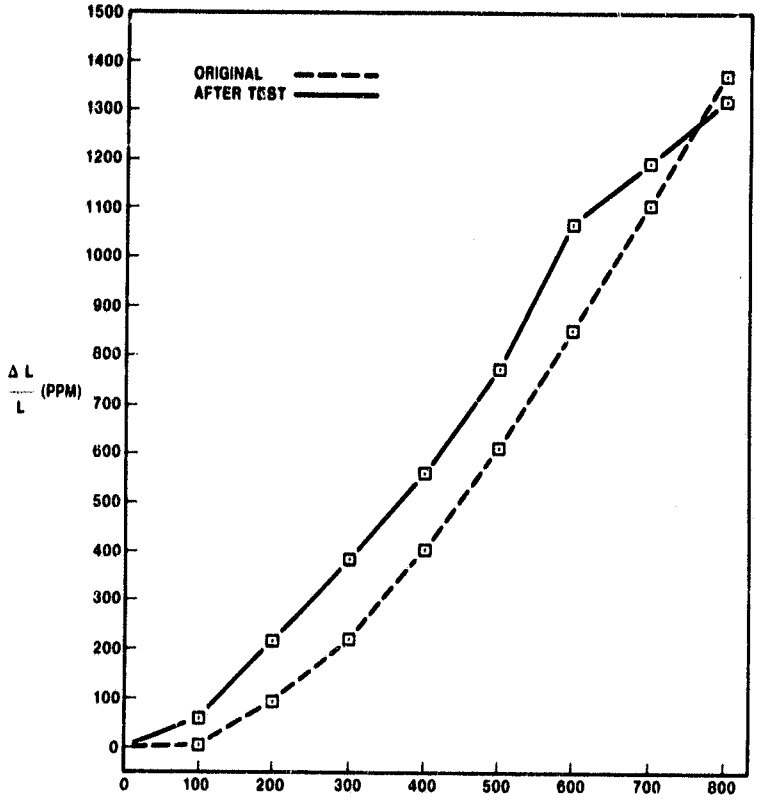

Figure III.B.1.30 Supplier K, LAS/MAS; Thermal Expansion Before and After Hot Face Test Conditions

III.B.2 Accelerated Corrosion Testing: Matrix Inserts

In this test candidate materials obtained as cylindrical matrices are inserted in a standard regenerator utilizing an appropriate cement. The core is then run in a Ford 707 gas turbine engine with a regenerator inlet temperature of 800°C (1472°F) for 120 hours. Common road salt, primarily sodium chloride, is ingested into the engine in a controlled manner. Samples from the test matrix surface are periodically (every 40 test hours) analyzed for sodium absorbed into crystal lattice. Thermal expansion data is obtained at the end of the test.

The specimen size used for inserts is 50.8 mm — 101.6 mm dia. by 71.12 mm — 71.37 mm long (2-4 inch dia. by 2.8-2.81 inch long). The host core, a standard 707 engine LAS regenerator is core drilled at 178 mm (7 inch) radius location to accommodate the test matrix specimens. The specimens are aligned such that the faces are parallel to the host regenerator faces and are slightly recessed to avoid contact with regenerator seals in service. The inserts are secured in the host matrix by means of a hydraulic cement (calcium aluminate or aluminum silicate). The ring gear is installed on the core utilizing a standard procedure and the regenerator assembly is readied for engine testing. A typical regenerator assembly with inserts of test matrices is shown in Figure III.B.2.1. These test cores are run on either side or both sides of a Ford 707 gas turbine engine with salt ingestion.

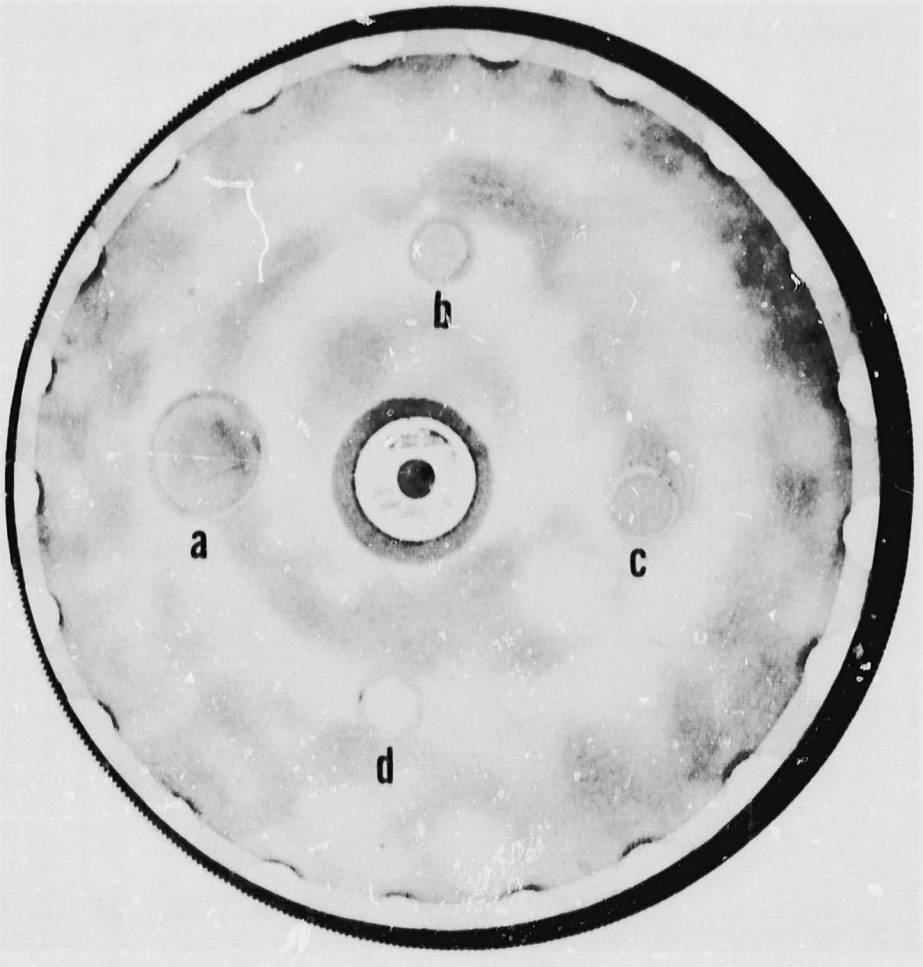

Figure III.B.2.1 Accelerated Corrosion Test Core 1 with Matrix Inserts

An apparatus specially designed to deliver salt powder at controlled rate is used to insure reproducible salt ingestion into the engine. Common road salt is ground and screened (±150 mesh particle size) to yield a free flowing powder. The apparatus is shown in Figures III.B.2.2 and the ingesting arrangement is shown in Figure III.B.2.3. The salt is carried into the engine by means of throttled air heated and kept dry by means of heat lamps (a). The salt is fed into the hopper (b) of the apparatus provided with dessicant to avoid moisture pickup. The salt powder is passed into an aspirator by means of a screw-tap feeding mechanism located at the bottom of the hopper and is carried away into the engine through pipe (c) by means of throttled air warmed up by heat lamps. Screw-tap speed settings control the feed rate and the throttle air pressure is controlled to assure uniform delivery and timer (d) controls the feed time. This system provided a reliable means for ingesting salt in a controlled and reproducible manner.

Two host cores with test matrix inserts have been evaluated during this program. The first core was a standard LAS core with (1) Supplier K LAS/MAS, (2) Supplier J MAS, (3) Supplier I MAS and (4) Supplier E MAS test matrix inserts. The second host core was a Supplier A leached LAS matrix with (1) Supplier C MAS, (2) Supplier D MAS, (3) Supplier B leached LAS, (4) Supplier E MAS and (5) Supplier B LAS test matrix inserts. The core is shown in Figure III.B.2.4.

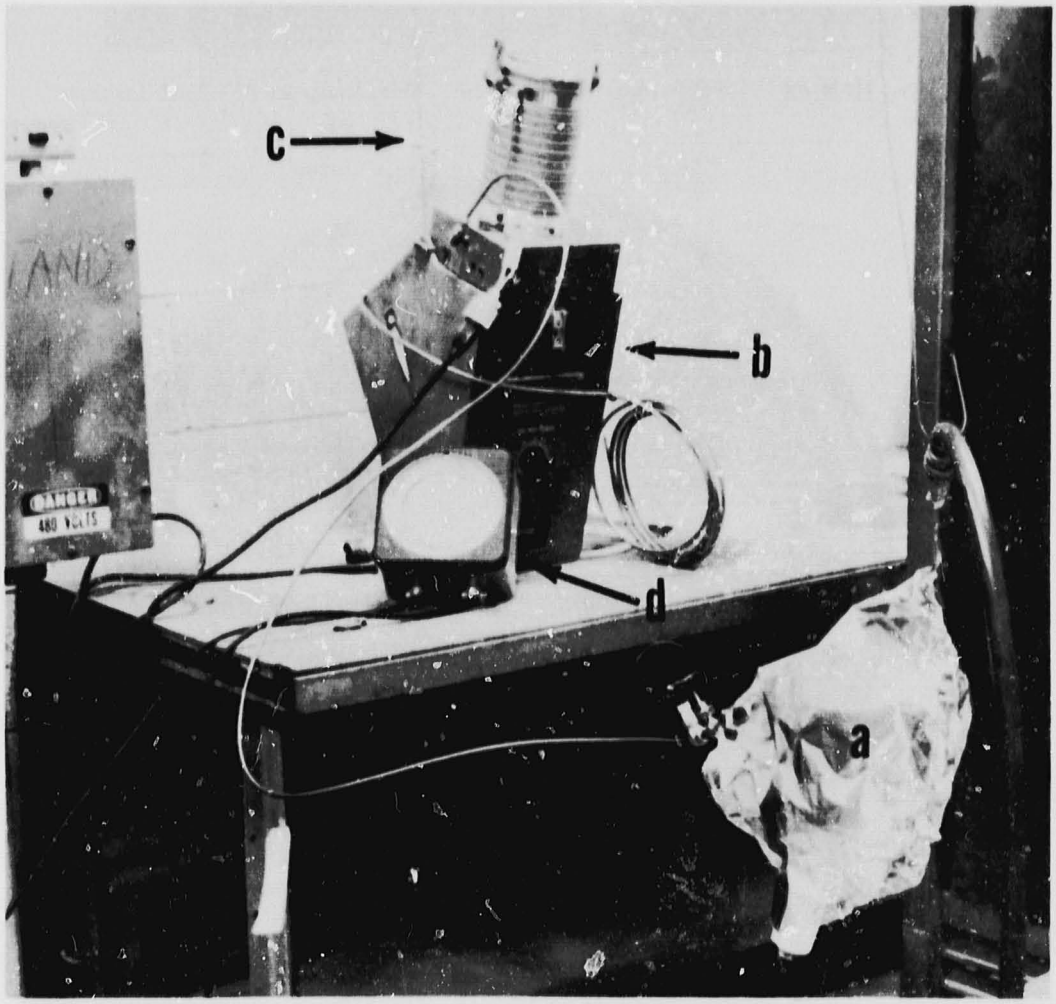

Figure III.B.2.2 Salt Ingestion System — Measurement and Transportation

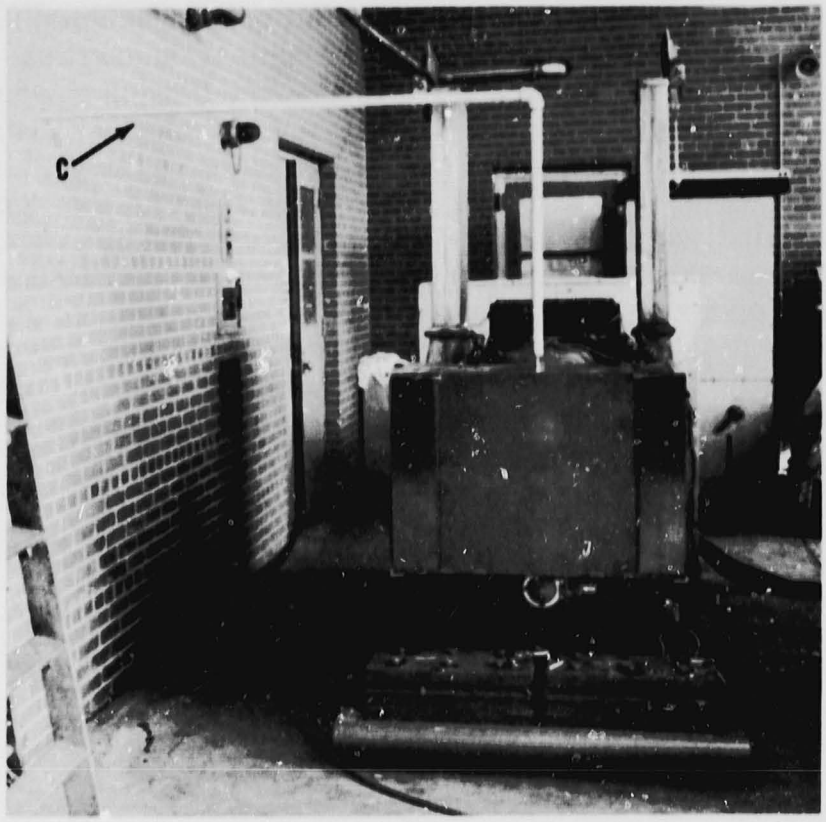

Figure III.B.2.3 Salt Ingestion System — Hook up to 707 Test Engine

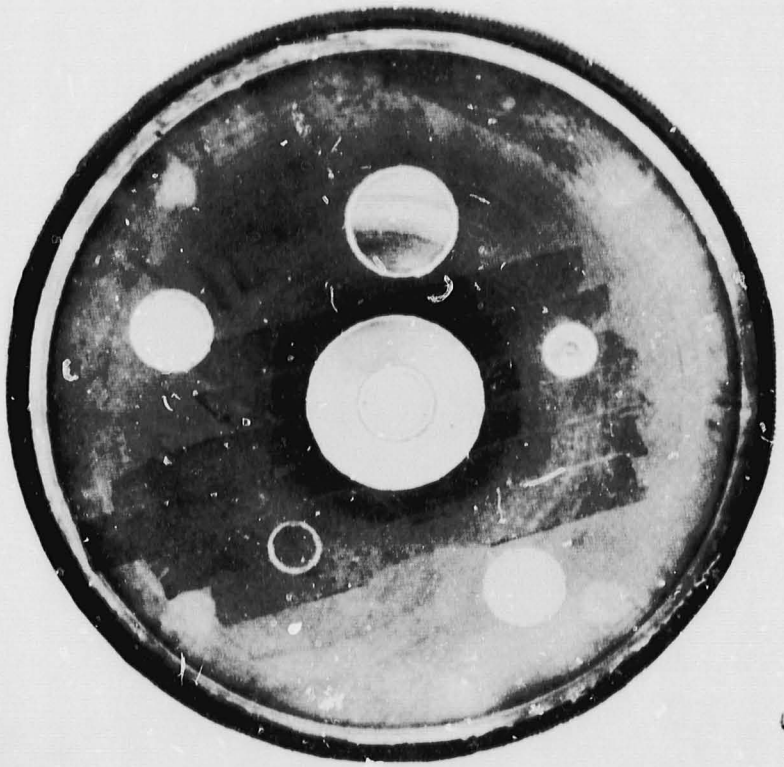

Figure III.B.2.4 Test Core-2 Accelerated Corrosion Leached LAS Host Matrix with Matrix Inserts for Accelerated Corrosion Testing

The first host core, i.e., standard LAS with test matrix inserts, was evaluated in the accelerated corrosion test for 120 hours. Test samples for chemical analysis for each test interval were obtained from both hot face and the cold face of the host matrix as well as the test matrices. Two sets of analyses are carried out for the major constituents of interest that are subject to sodium ion exchange, namely NA_2O, Li_2O and MgO. The specimens are boiled in water to obtain the constituents adhering to the matrix and the remaining matrix is then dissolved in appropriate carrier to determine the quantities absorbed into the matrix crystal lattice. Both the solutions were analyzed by means of atomic absorption spectrophotometer utilizing calibrated standards solutions. The chemical analyses of the matrix samples obtained at 25 hr., 39 hr., 80 hr. and 120 hr. exposure are summarized in Tables III.B.2.1, III.B.2.2, III.B.2.3 and III.B.2.4 respectively.

As one examines Tables III.B.2.1 — III.B.2.4, the higher reactivity of the hot face of the regenerator becomes apparent, as the sodium uptake (acid solution) for each material is higher at the hot face. When the 25 hour, 39 hour, 80 hour and 120 hour data are compared, the Supplier K LAS/MAS material seems to be taking up sodium as engine testing continues, while the MAS materials seem relatively impervious to salt attack under the conditions of this test.

SAMPLE	POSITION	SOLUTION	% Na_2O	% Li_2O	% MgO
SUPPLIER K	COLD FACE	WATER	0.18	0.05	N.D.*
LAS/MAS	COLD FACE	ACID	0.51	2.67	5.51
SUPPLIER K	HOT FACE	WATER	0.03	N.D.	N.D.
LAS/MAS	HOT FACE	ACID	0.78	2.76	5.49
SUPPLIER I	COLD FACE	WATER	0.25		0.01
MAS	COLD FACE	ACID	0.22		10.01
SUPPLIER I	HOT FACE	WATER	0.16		N.D.
MAS	HOT FACE	ACID	0.35		13.64
SUPPLIER E	COLD FACE	WATER	0.11		N.D.
MAS	COLD FACE	ACID	0.38		13.62
SUPPLIER E	HOT FACE	WATER	0.13		N.D.
MAS	HOT FACE	ACID	0.40		13.65
SUPPLIER J	COLD FACE	WATER	0.05		N.D.
MAS	COLD FACE	ACID	0.02		13.75
SUPPLIER J	HOT FACE	WATER	0.10		0.02
MAS	HOT FACE	ACID	0.35		13.59

*N.D. = NOT DETECTED
BLANKS = NO ANALYSIS

Table III.B.2.1 Chemical Analysis of Test Matrices After 25 Hours Exposure in Engine — Test Core-1

SAMPLE	POSITION	SOLUTION	% Na_2O	% Li_2O	% MgO
SUPPLIER K LAS/MAS	COLD FACE	WATER	0.58	0.15	0.05
	COLD FACE	ACID	0.46	2.98	5.74
SUPPLIER K LAS/MAS	HOT FACE	WATER	0.74	N.D.*	0.11
	HOT FACE	ACID	1.68	3.07	2.46
SUPPLIER I MAS	COLD FACE	WATER	0.85		0.07
	COLD FACE	ACID	0.21		10.18
SUPPLIER I MAS	HOT FACE	WATER	1.64		0.01
	HOT FACE	ACID	0.37		13.05
SUPPLIER E MAS	COLD FACE	WATER	0.28		0.07
	COLD FACE	ACID	0.14		13.60
SUPPLIER E MAS	HOT FACE	WATER	0.76		N.D.
	HOT FACE	ACID	0.53		13.36
SUPPLIER J MAS	COLD FACE	WATER	0.54		0.01
	COLD FACE	ACID	0.01		12.80
SUPPLIER J MAS	HOT FACE	WATER	1.13		0.02
	HOT FACE	ACID	0.29		13.48

*N.D. = NOT DETECTED
BLANKS = NO ANALYSIS

Table III.B.2.2 Chemical Analysis of Test Matrices After 39 Hours Exposure in Engine — Test Core-1

SAMPLE	POSITION	SOLUTION	% Na_2O	% Li_2O	% MgO
SUPPLIER K LAS/MAS	COLD FACE	WATER	0.74	0.10	0.03
	COLD FACE	ACID	0.40	2.11	4.33
SUPPLIER K LAS/MAS	HOT FACE	WATER	3.03	0.06	0.06
	HOT FACE	ACID	1.66	2.43	5.89
SUPPLIER I MAS	COLD FACE	WATER	4.48		0.02
	COLD FACE	ACID	0.16		14.99
SUPPLIER I MAS	HOT FACE	WATER	5.23		0.08
	HOT FACE	ACID	1.20		12.94
SUPPLIER E MAS	COLD FACE	WATER	0.85		0.01
	COLD FACE	ACID	0.04		15.95
SUPPLIER E MAS	HOT FACE	WATER	2.61		0.02
	HOT FACE	ACID	0.34		15.55
SUPPLIER J MAS	COLD FACE	WATER	1.32		0.07
	COLD FACE	ACID	0.04		14.64
SUPPLIER J MAS	HOT FACE	WATER	1.48		0.04
	HOT FACE	ACID	0.52		12.89

Table III.B.2.3 Chemical Analysis of Test Matrices After 80 Hours Exposure in Engine — Test Core-1

SAMPLE	POSITION	SOLUTION	% Na_2O	% Li_2O	% MgO
SUPPLIER K	COLD FACE	WATER	0.85	0.18	0.03
LAS/MAS	COLD FACE	ACID	0.36	2.52	4.53
SUPPLIER K	HOT FACE	WATER	1.62	0.04	0.08
LAS/MAS	HOT FACE	ACID	2.05	2.59	4.73
SUPPLIER I	COLD FACE	WATER	3.73		0.02
MAS	COLD FACE	ACID	0.20		9.46
SUPPLIER I	HOT FACE	WATER	3.10		0.06
MAS	HOT FACE	ACID	0.82		9.07
SUPPLIER E	COLD FACE	WATER	1.04		0.01
MAS	COLD FACE	ACID	0.34		11.58
SUPPLIER E	HOT FACE	WATER	3.28		0.04
MAS	HOT FACE	ACID	0.50		11.06
SUPPLIER J	COLD FACE	WATER	2.05		0.09
MAS	COLD FACE	ACID	0.04		13.71
SUPPLIER J	HOT FACE	WATER	3.29		0.11
MAS	HOT FACE	ACID	0.58		14.17

Table III.B.2.4 **Chemical Analysis of Test Matrices After 120 Hours Exposure in Engine — Test Core-1**

These chemical analysis data corroborate the hot and cold face data discussed in the previous section in that the MAS materials seem quite stable in this sodium engine environment, while the LAS/MAS of Supplier K experiences a continual uptake of sodium during the course of the test. Similar to hot face data, this sodium uptake is rather rapid initially, progresses quite slowly during the middle portion of the test, and finally increases in rate at longer times. There appears to be a complementary decrease in magnesium content of this material with time; however, the magnesium data for the MAS materials would suggest that observed changes are within analytical precision. These data suggest that the MAS materials are unaffected by the accelerated corrosion testing. The magnitude of chemical change occurred in MAS matrix, although quite small when compared to the LAS/MAS material, is not insignificant. This is borne out by the thermal expansion behavior of these materials shown in Figures III.B.2.5 (Δ), III.B.2.6 (□), III.B.2.7 (◪) and III.B.2.8 (■). The MAS materials of Suppliers E (◪) and J (■) (Figures III.B.2.7 (◪) and III.B.2.8 (■), respectively) have experienced very little change in thermal expansion behavior, both from the point of view of the nature of the expansion curves and the magnitude of the change. Each is slightly depressed. The response of the MAS of Supplier E is similar (but smaller in magnitude) to the results of the hot face testing. Material of Supplier I (□) experiences less change than it did under the conditions of the hot face test. The MAS of Supplier I (Figure III.B.2.6) experiences a similar change in thermal expansion behavior (through 600°C) as that resulting from the hot face test. Again, the magnitude of the change after accelerated corrosion testing as matrix inserts is less. The LAS/MAS material of Supplier K (Δ) (Figure III.B.2.5) experiences a larger change in thermal expansion (note scale differences among figures) than did the MAS materials tested concurrently (although not significantly

greater than that MAS of Supplier I). The change in thermal expansion is, like that experienced by the MAS materials, of the same character but smaller in magnitude than the thermal expansion changes observed after the same materials completed the hot face portion of the materials screening tests. In summary, these accelerated corrosion test data of matrix inserts support the conclusions based on the laboratory testing section of this series of materials screening tests. However, these data, when compared to the hot face test data would suggest that the hot face corrosion test is more demanding of the materials than is the accelerated corrosion testing, via the salt ingestion gas turbine engine, of matrix inserts.

The second host core — the Supplier A leached LAS matrix with test matrix inserts of (1) Supplier C MAS, (2) Supplier D MAS, (3) Supplier B leached LAS, (4) Supplier E MAS and (5) Supplier B LAS was evaluated in the accelerated corrosion test for 150 hours. Chemical analysis samples were taken from the hot and cold faces of each matrix insert, as well as the host core, at intervals of 50, 100 and 150 engine hours. The sampling interval was extended from 40 to 50 hours to synchronize the matrix insert chemical sampling with that of a full size MAS core running on the other side of the salt ingestion engine. The thermal expansion behavior of each material after 150 hours of the accelerated corrosion testing was determined by means of differential dilatometer as in the case of the first host core. The atomic absorption analyses of the matrix samples after 50 hour, 100 hour and 150 hour testing periods are summarized in Tables III.B.2.5, III.B.2.6 and III.B.2.7 respectively. As in the case of the first host core, samples for each time interval were obtained from both hot side and cold side of each matrix material.

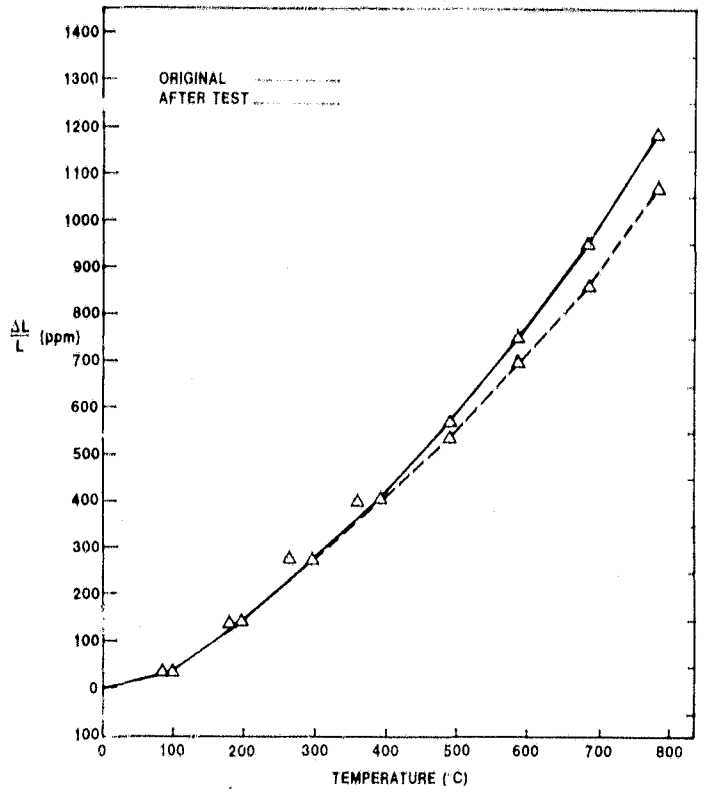

Figure III.B.2.5 Supplier K LAS/MAS; Thermal Expansion Before and After 120 Hours of Accelerated Corrosion Testing as a Matrix Insert.

C-2

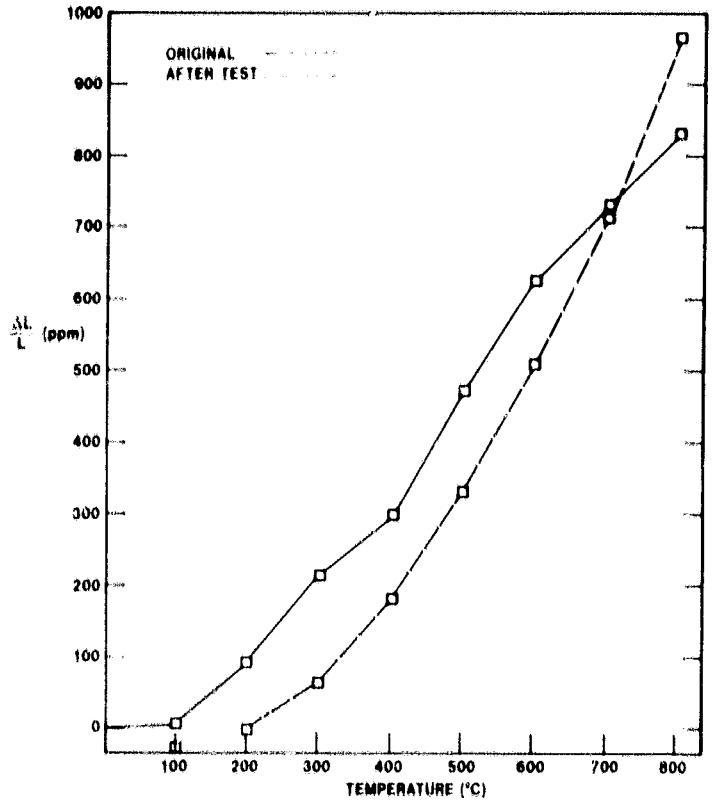

Figure III.B.2.6 **Supplier I MAS; Thermal Expansion Before and After 120 Hours of Accelerated Corrosion Testing as a Matrix Insert.**

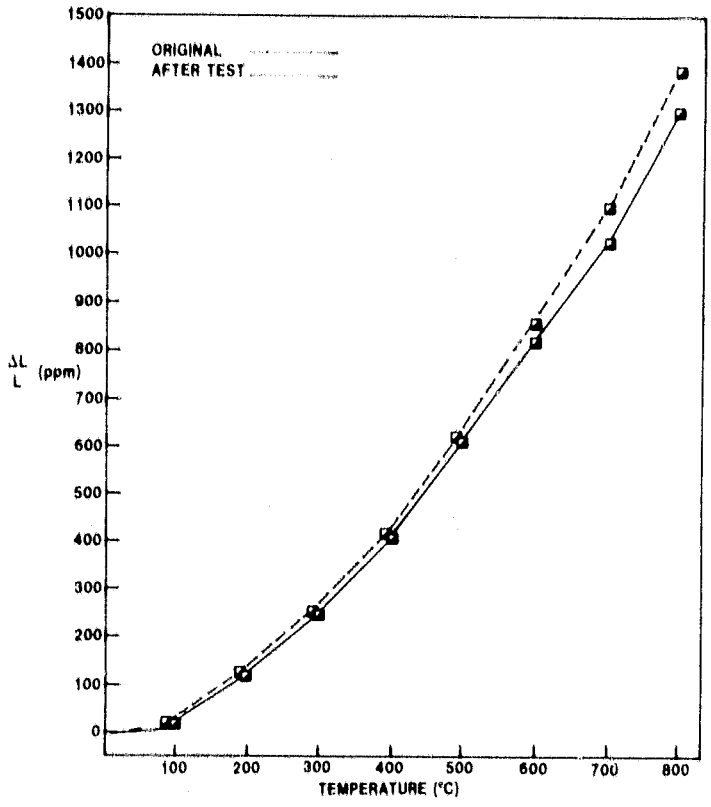

Figure III.B.2.7 **Supplier E MAS; Thermal Expansion Before and After 120 Hours of Accelerated Corrosion Testing as a Matrix Insert.**

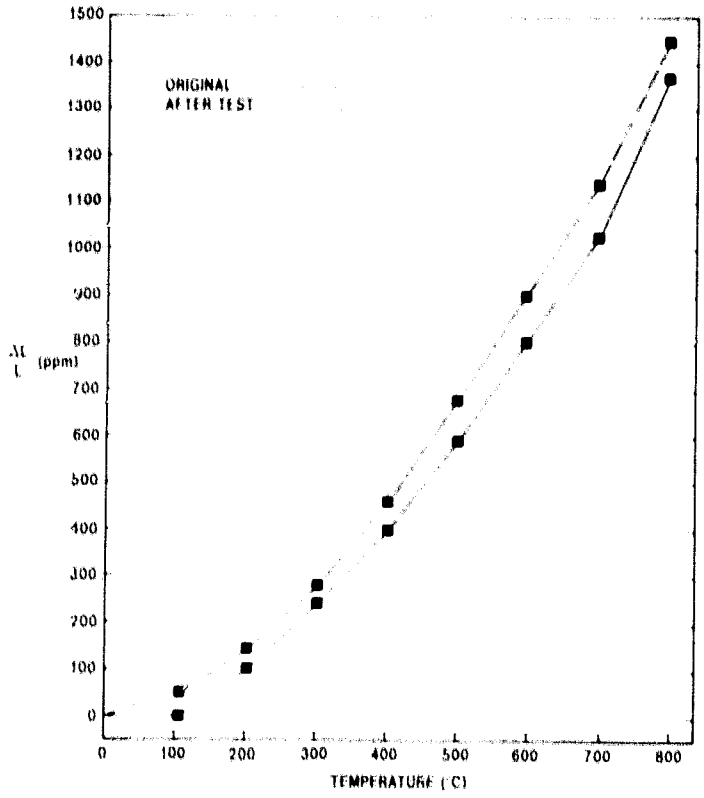

Figure III.B.2.8 **Supplier J MAS; Thermal Expansion Before and After 120 Hours of Accelerated Corrosion Testing as a Matrix Insert.**

Sample	Position	Solution	% Na_2O	% Li_2O	% MgO
Supplier D	Cold Face	Water	0.050		0.013
MAS	Cold Face	Acid	0.041		7.750
Supplier D	Hot Face	Water	0.080		0.005
MAS	Hot Face	Acid	0.066		7.720
Supplier C	Cold Face	Water	0.030		
MAS	Cold Face	Acid	0.062		8.150
Supplier C	Hot Face	Water	0.030		
MAS	Hot Face	Acid	0.065		8.280
Supplier E	Cold Face	Water	0.010		0.001
MAS #2	Cold Face	Acid	0.012		7.750
Supplier E	Hot Face	Water	0.020		0.001
MAS #2	Hot Face	Acid	0.125		7.710
Supplier B	Cold Face	Water	0.030	0.004	
AS	Cold Face	Acid	0.001	N.D.	
Supplier B	Hot Face	Water	0.070	N.D.	
AS	Hot Face	Acid	0.078	N.D.	
Supplier B	Cold Face	Water	0.030	0.030	
LAS	Cold Face	Acid	0.028	1.340	
Supplier B	Hot Face	Water	N.D.	N.D.	
LAS	Hot Face	Acid	0.140	1.590	
Host Core	Cold Face	Water	0.030	0.005	
AS	Cold Face	Acid	0.005	N.D.	
Host Core	Hot Face	Water	0.010	N.D.	
AS	Hot Face	Acid	0.077	N.D.	

N.D = Not Detected
Blank = No Analysis

Table III.B.2.5 **Chemical Analyses After 50 Hours of Accelerated Corrosion Testing as Matrix Inserts — Test Core-2**

Sample	Position	Solution	% Na_2O	% Li_2O	% MgO
Supplier D MAS	Cold Face Cold Face	Water Acid	0.090 0.040		0.010 7.580
Supplier D MAS	Hot Face Hot Face	Water Acid	0.090 0.090		0.005 7.040
Supplier C MAS	Cold Face Cold Face	Water Acid	0.050 0.060		0.001 8.160
Supplier C MAS	Hot Face Hot Face	Water Acid	0.070 0.070		0.001 8.200
Supplier E MAS #2	Cold Face Cold Face	Water Acid	0.020 0.130		N.D. 7.580
Supplier E MAS #2	Hot Face Hot Face	Water Acid	0.040 0.140		N.D. 7.840
Supplier B AS	Cold Face Cold Face	Water Acid	0.070 0.010	N.D. N.D.	
Supplier B AS	Hot Face Hot Face	Water Acid	0.100 0.140	N.D. N.D.	
Supplier B LAS	Cold Face Cold Face	Water Acid	0.070 0.040	0.030 1.540	
Supplier B LAS	Hot Face Hot Face	Water Acid	0.004 0.200	N.D. 1.560	
Host Core AS	Cold Face Cold Face	Water Acid	0.050 0.010	N.D. N.D.	
Host Core AS	Hot Face Hot Face	Water Acid	0.000 0.110	N.D. 0.020	

N.D. = Not Detected
Blank = No Analysis

Table III.B.2.6 Chemical Analyses After 100 Hours of Accelerated Corrosion Testing as Matrix Inserts — Test Core-2

Sample	Position	Solution	% Na_2O	% Li_2O	% MgO
Supplier D MAS	Cold Face Cold Face	Water Acid	0.090 0.040		0.020 7.940
Supplier D MAS	Hot Face Hot Face	Water Acid	0.110 0.070		0.010 7.880
Supplier C MAS	Cold Face Cold Face	Water Acid	0.060 0.060		0.002 8.060
Supplier C MAS	Hot Face Hot Face	Water Acid	0.070 0.060		0.002 8.140
Supplier E MAS #2	Cold Face Cold Face	Water Acid	0.030 0.110		0.001 7.500
Supplier E MAS #2	Hot Face Hot Face	Water Acid	0.050 0.120		0.001 7.730
Supplier B AS	Cold Face Cold Face	Water Acid	0.090 0.010	0.005 N.D.	
Supplier B AS	Hot Face Hot Face	Water Acid	0.120 0.130	N.D. 0.020	
Supplier B LAS	Cold Face Cold Face	Water Acid	0.090 0.030	0.040 1.020	
Supplier B LAS	Hot Face Hot Face	Water Acid	0.030 0.250	N.D. 1.580	
Host Core AS	Cold Face Cold Face	Water Acid	0.050 0.010	0.003 N.D.	
Host Core AS	Hot Face Hot Face	Water Acid	0.030 0.100	N.D. 0.020	

N.D. = Not Detected
Blank = No Analysis

Table III.B.2.7 Chemical Analyses After 150 Hours of Accelerated Corrosion Testing as Matrix Inserts — Test Core-2

A comparison of Tables III.B.2.5, III.B.2.6 and III.B.2.7; representing 50, 100, and 150 hours, respectively, of accelerated corrosion testing of matrix inserts yields several pertinent observations. As is to be expected, the surface accumulation of salt (water solutions) increases with test time. This indicates a sodium chloride buildup on the core surfaces with test time.

The MAS and the AS (leached LAS) materials, including the host core, seem to incorporate a small concentration of sodium into the lattice. This concentration appears to level off after 100 test hours. The Supplier B LAS, a newer and an improved composition, while superior in sodium resistance to the previous LAS compositions does not exhibit a leveling off of sodium pickup, but continues to evidence increasing bulk concentrations of sodium. Of interest is the diminished lithium concentration of the cold face of the Supplier B LAS material relative to the hot face, indicating that acid leaching at the cold face may be a more severe problem at 800°C (1472°F) than is ion exchange at the hot face. The new MAS compositions which represent state-of-the-art material and process technology towards the end of this test program generally appear to be quite resistant to sodium corrosion under these test conditions.

The reaction of these new materials to the accelerated corrosion test is also demonstrated by their thermal expansion behavior before and after the test. The thermal expansion data from room temperature to 800°C for these materials is presented in Figures III.B.2.9 (Supplier D MAS (♦)), III.B.2.10 (Supplier C MAS (◊), III.B.2.11 (Supplier E MAS #2 (∇)), III.B.2.12 (Supplier B AS (●)) and III.B.2.13 (Supplier B LAS (o)).

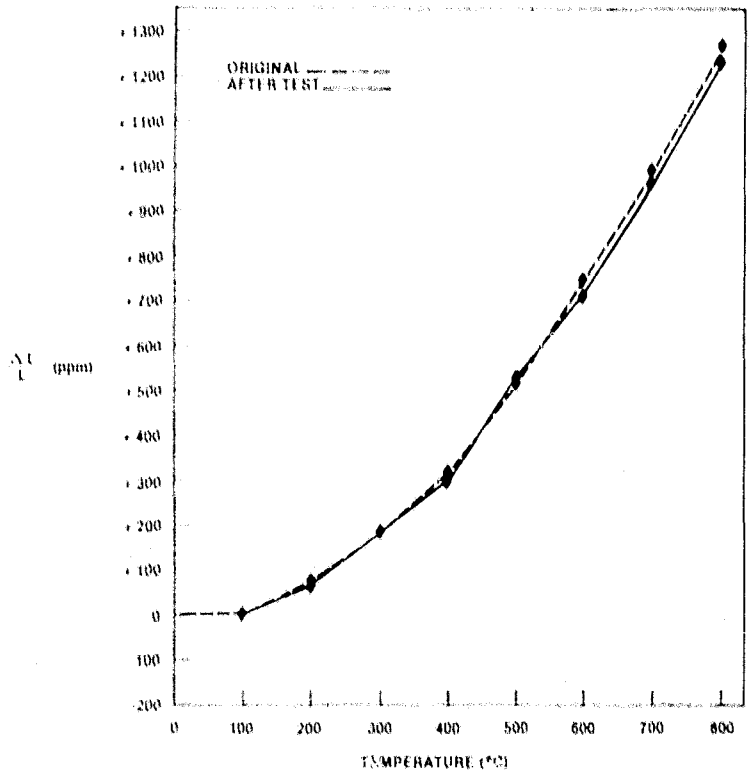

Figure III.B.2.9 Supplier D, MAS; Thermal Expansion Before and After 150 Hours of Accelerated Corrosion Testing as a Matrix Insert

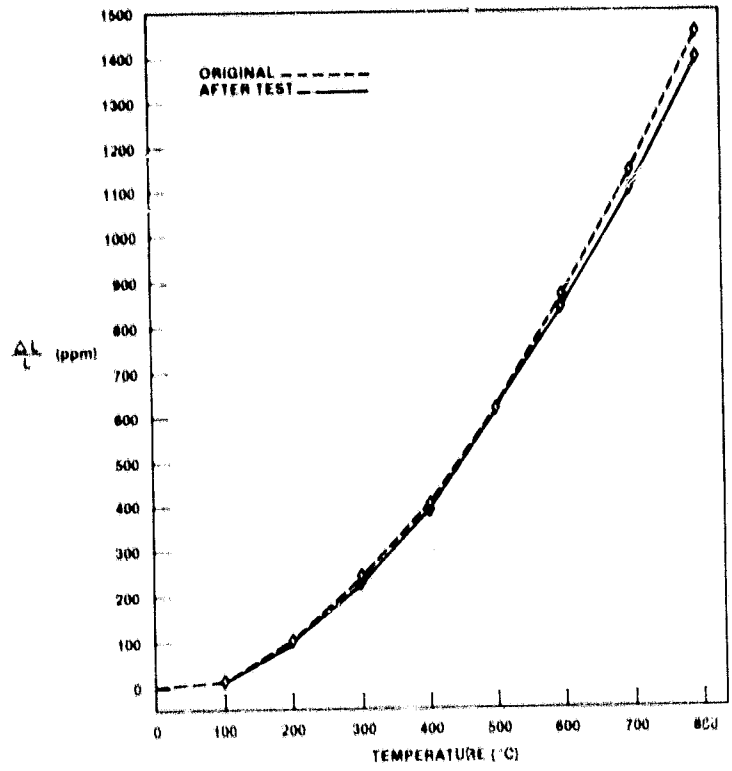

Figure III.B.2.10 **Supplier C, MAS; Thermal Expansion Before and After 150 Hours of Accelerated Corrosion Testing as a Matrix Insert**

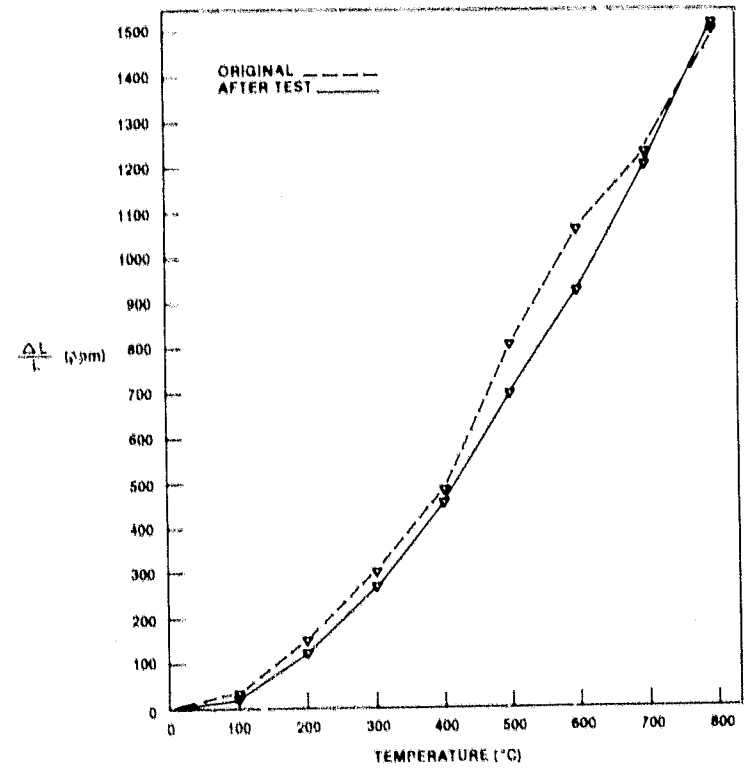

Figure III.B.2.11 **Supplier E, MAS NO. 2; Thermal Expansion Before and After 150 Hours of Accelerated Corrosion Testing as a Matrix Insert**

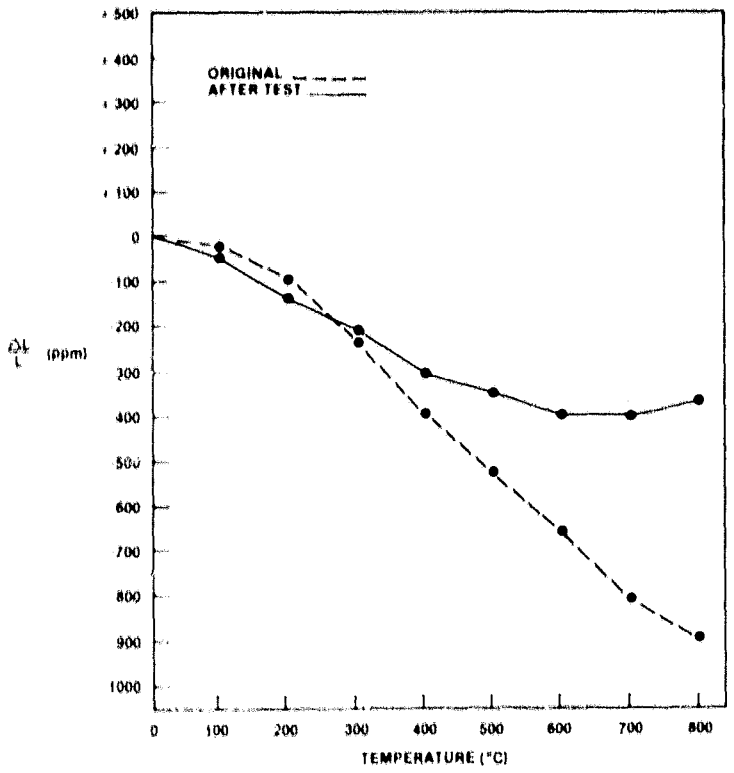

Figure III.B.2.12 **Supplier B, AS; Thermal Expansion Before and After 150 Hours of Accelerated Corrosion Testing as a Matrix Insert**

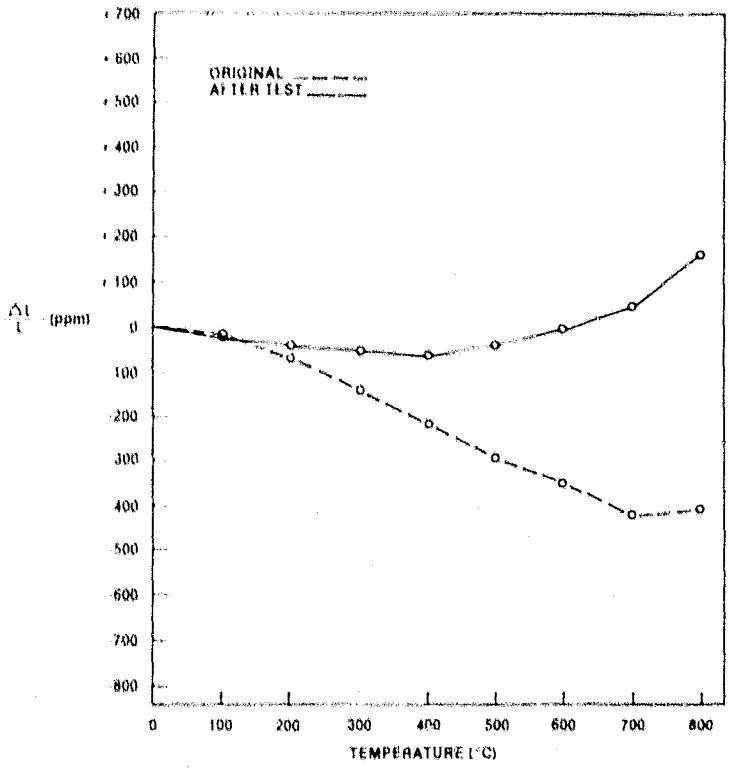

Figure III.B.2.13 **Supplier B, LAS; Thermal Expansion Before and After 150 Hours of Accelerated Corrosion Testing as a Matrix Insert**

An inspection of these figures indicates the relatively benign reaction of the MAS materials to airborne sodium chloride at 800°C (1472°F). The thermal expansion behavior of these materials (Figures III.B.2.9, III.B.2.10 and III.B.2.11) are essentially unchanged by exposure to the accelerated corrosion test conditions for a period of 150 hours.

The thermal expansions of the Supplier B AS (Figure III.B.2.12 (●) and the LAS material (Figure III.B.2.13 (o) have both undergone significant changes as a result of 150 hours of exposure to accelerated corrosion testing as matrix inserts. Both materials have been made less contractive to the point where the LAS is slightly expansive. Evidently the sodium uptake by these materials results in a "stuffing" of the crystalline lattice due to the size disparity between the sodium and the lithium ions. This ionic replacement creates a lattice deformed by residual strain, thereby changing the reaction of the unit cell to changes in temperature. The degree of this change is expected to vary with the magnitude of ion exchange occurred as evidenced by the more pronounced change observed in the LAS material.

The results of the test program indicate that the MAS matrices in general possess superior resistance to the accelerated corrosion test conditions in the engine and particularly the state-of-the-art MAS compositions that became available during the later part of the test program (Supplier C MAS (◇), D MAS (◆), and E MAS #2 (▽) are practically immune to this type of chemical attack.

III.B.3 Accelerated Corrosion Testing: Full Size Cores

Materials deemed promising on the basis of laboratory tests and the accelerated corrosion tests on engine as matrix inserts are evaluated as full size regenerators in a Ford 707 engine operating on accelerated corrosion test mode.

In this test, full size regenerators fabricated from candidate materials are run in the 707 engine with salt ingestion at a regenerator inlet temperature of 800°C. The same salt feed apparatus used for the evaluation of matrix inserts was used in this test. Matrix material from the hot face (regenerator inlet face) and cold face was periodically (every 50 hours) analyzed for sodium absorption into the matrix crystal lattice. The test duration is 500 hours unless terminated due to premature core failure. At the end of the test thermal expansion data from RT-1472°F are obtained for the matrix specimens.

Three full size cores were tested under salt ingestion conditions in this program. The first core, Supplier D MAS, was run at low throttle conditions for over 1200 hours to promote the formation of liquid sulfuric acid on the cold face of the regenerator core and a sample for analysis was obtained. A similar surface sample was taken from a second core, Supplier D MAS, which had been tested at 5000 hours at full throttle; a condition which will produce sulfuric acid vapor rather than liquid at the cold face of the regenerator core. These samples were compared by x-ray diffraction to a similar sample taken from a freshly sintered core of the same material. This comparison was undertaken as some concern was expressed about the chemical stability of cordierite in regenerator applications when the engine was run at power levels where the cold face of the regenerator is below the dew point of sul-

furic acid. These x-ray diffraction data, generated by copper K radiation, are presented in Table III.B.3.1. The data of the standard sample were normalized to the theoretical intensities at each planar spacing, and the experimental data are proportionalized to the actual intensities determined for the standard.

dA°	I/I_0(std.)†	I/I_0(1200 hr.)*	I/I_0(5000 hr.)**
8.58	100	63	32
4.92	40	27	11
4.11	80	46	22
3.38	90	58	46
3.18	80	51	28
3.04	90	64	39
2.65	60	34	22
2.34	40	26	11
1.88	50	25	18
1.69	70	42	25

† Cu K Radiation
* Liquid H_2SO_4
** Vapor H_2SO_4

Table III.B.3.1 Cordierite X-Ray Diffraction Spectrum

A preliminary examination of the x-ray spectra of these samples yielded major cordierite peak intensities which were lower for the high-hour core. Both cores had suffered a decrease in cordierite peak intensities; however, this decrease seems to be related to engine test time rather than the presence (or absence) of liquid sulfuric acid. Additionally, the experimental spectra were searched for peaks corresponding to the reaction products formed by the reaction between sulfuric acid and cordierite. No evidence of aluminum sulfate, magnesium sulfate or silica compounds could be found. The possible time dependence of the cordierite intensity decrease suggests that impurities, possibly from seal coatings, may be diluting the cordierite content of a specific volume of an x-ray powder sample. The x-ray diffraction spectra have been examined in greater detail in an effort to more fully understand the effect of the gas turbine engine environment on MAS regenerator cores. The results of the investigation, however, suggest that MAS is relatively impervious to both liquid and vapor phase sulfuric acid attack, confirming the findings of the laboratory tests simulating chemical attack and the accelerated corrosion tests in engine of matrix inserts.

After the low throttle test time (1200 hours) was completed, the MAS core of Supplier D was introduced into the accelerated corrosion testing program carried out in the Ford 707 gas turbine engine modified for salt ingestion. This core completed 500 hours of salt ingestion engine time. Chemical samples were taken at 50 engine hour intervals, and were analyzed by atomic absorption and results are presented in Table III.B.3.1. This regenerator accumulated an additional 150 hours of accelerated salt corrosion test time when it was run as a baseline standard with other regenerators. The results of chemical analysis of the samples taken during this latter test period are included in Table III.B.3.2.

Test Time	Position	Solution	% Na_2O	% MgO
50 Hours	Cold Face	Water	0.070	0.023
50 Hours	Cold Face	Acid	0.040	7.660
50 Hours	Hot Face	Water	0.030	0.007
50 Hours	Hot Face	Acid	0.162	7.870
100 Hours	Cold Face	Water	0.100	0.032
100 Hours	Cold Face	Acid	0.060	7.720
100 Hours	Hot Face	Water	0.050	0.000
100 Hours	Hot Face	Acid	0.200	7.720
150 Hours	Cold Face	Water	0.130	0.040
150 Hours	Cold Face	Acid	0.040	7.660
150 Hours	Hot Face	Water	0.070	0.000
150 Hours	Hot Face	Acid	0.100	7.870
200 Hours	Cold Face	Water	0.240	0.040
200 Hours	Cold Face	Acid	0.030	7.810
200 Hours	Hot Face	Water	0.060	0.010
200 Hours	Hot Face	Acid	0.170	7.800
250 Hours	Cold Face	Water	0.250	0.040
250 Hours	Cold Face	Acid	0.030	7.830
250 Hours	Hot Face	Water	0.070	0.010
250 Hours	Hot Face	Acid	0.200	7.910
300 Hours	Cold Face	Water	0.360	0.040
300 Hours	Cold Face	Acid	0.030	7.800
300 Hours	Hot Face	Water	0.060	0.010
300 Hours	Hot Face	Acid	0.190	7.870
350 Hours	Cold Face	Water	0.190	0.030
350 Hours	Cold Face	Acid	0.030	7.850
350 Hours	Hot Face	Water	0.050	0.010
350 Hours	Hot Face	Acid	0.230	7.930
400 Hours	Cold Face	Water	0.190	0.030
400 Hours	Cold Face	Acid	0.030	7.930
400 Hours	Hot Face	Water	0.020	0.010
400 Hours	Hot Face	Acid	0.210	7.910
500 Hours	Cold Face	Water	0.370	0.010
500 Hours	Cold Face	Acid	0.270	7.720
500 Hours	Hot Face	Water	0.780	0.040
500 Hours	Hot Face	Acid	0.030	7.790
550 Hours	Cold Face	Water	0.680	0.040
550 Hours	Cold Face	Acid	0.030	7.750
550 Hours	Hot Face	Water	0.040	0.010
550 Hours	Hot Face	Acid	0.710	7.770
600 Hours	Cold Face	Water	0.790	0.040
600 Hours	Cold Face	Acid	0.030	7.740
600 Hours	Hot Face	Water	0.010	0.001
600 Hours	Hot Face	Acid	0.740	7.760
650 Hours	Cold Face	Water	0.670	0.040
650 Hours	Cold Face	Acid	0.030	7.810
650 Hours	Hot Face	Water	0.020	0.004
650 Hours	Hot Face	Acid	0.570	7.830

Table III.B.3.2 Chemical Analyses of Supplier D-MAS Full Size Core During Accelerated Corrosion Testing

The second full size test core, evaluated in the accelerated corrosion testing program was a Supplier C MAS core. After start-up, the engine was run at 50% throttle for 25 hours as a preliminary step to corrosion testing. The core failed when the engine was raised to 100% power. Upon engine disassembly, it was noted that the core had completely delaminated at the boundary between the filled rim and the unfilled matrix. Evaluation of portions of the failed core by Ford and the material supplier indicated that the material was underfired and was weaker than desired. This was attributed to a quality control problem.

The third full size test core, an AS material from Supplier A fabricated in a thin-wall configuration, was introduced into the accelerated corrostion testing program, and the goal of 500 test hours was achieved. The chemical analyses (atomic absorption spectrophotometry) are presented in Table III.B.3.3. The analyses were carried out at 50 hour intervals; however, during periods of extraordinary salt ingestion, the test hours were doubly weighted. This condition occurred once in the course of the test cycle and was traced to a malfunction in the salt feed mechanism which resulted in continuous, rather than periodic, salt ingestion.

The chemical analyses for sodium and magnesium during the accelerated corrosion testing of a full size core of MAS from Supplier D presented in Table III.B.3.2 indicate a salt build-up on the core surface as a function of time. The extreme deposition resulting from the equipment malfunction also was indicated, and the data were corroborated by visual inspections during the sampling procedure, as the salt build-up was quite discernible to the naked eye. The data show that little or no sodium was absorbed by the matrix on the cold face side of the core. Except for the 500 hour sample, the sodium level appears to be constant with time. The 500 hour samples were taken after a heavy salt deposition period.

On the hot face side, however, there is a significant absorption of sodium ion into the matrix crystal lattice. The relative sodium concentrations between the cold side and the hot side data support the contention that one should see more ion exchange at the elevated temperature. It is noteworthy that this MAS core survived 650 hours of accelerated corrosion testing without chemical or physical impairment. This testing was carried out after 1200 previous hours of engine testing at part power to evaluate cold face acid attack. This core continued to function in a durability test engine and accumulated an additional 4000 hours of engine time for a total of 6000 hours.

Sodium analyses during the accelerated corrosion testing of a full size core of the AS composition of Supplier A are presented in Table III.B.3.3. Experience during the matrix insert test program (Section III.B.2) indicated that analyzing for additional constituents was not necessary. The surface deposition of large quantities of sodium is indicated by the initial analyses of the water solutions. The initial test interval (60 hours) is doubly weighted due to excessive salt ingestion. The surface concentrations decrease during subsequent test periods and tend to become constant. Consistent with prior salt ingestion tests, the surface build-up of sodium chloride is more pronounced on the cold face of the regenerator core.

Test Time	Position	Solution	% Na_2O
120 Hours	Cold Face	Water	1.110
120 Hours	Cold Face	Acid	0.030
120 Hours	Hot Face	Water	1.480
120 Hours	Hot Face	Acid	0.070
170 Hours	Cold Face	Water	0.590
170 Hours	Cold Face	Acid	0.090
170 Hours	Hot Face	Water	0.030
170 Hours	Hot Face	Acid	3.030
220 Hours	Cold Face	Water	0.540
220 Hours	Cold Face	Acid	0.070
220 Hours	Hot Face	Water	0.020
220 Hours	Hot Face	Acid	2.820
270 Hours	Cold Face	Water	0.600
270 Hours	Cold FAce	Acid	0.060
270 Hours	Hot Face	Water	0.010
270 Hours	Hot Face	Acid	3.310
320 Hours	Cold Face	Water	0.650
320 Hours	Cold Face	Acid	0.120
320 Hours	Hot Face	Water	0.020
320 Hours	Hot Face	Acid	2.830
370 Hours	Cold Face	Water	0.560
370 Hours	Cold Face	Acid	0.110
370 Hours	Hot Face	Water	0.020
370 Hours	Hot Face	Acid	2.780
420 Hours	Cold Face	Water	0.660
420 Hours	Cold Face	Acid	0.120
420 Hours	Hot Face	Water	0.015
420 Hours	Hot Face	Acid	2.760
500 Hours	Cold Face	Water	0.620
500 Hours	Cold Face	Acid	0.110
500 Hours	Hot Face	Water	0.015
500 Hours	Hot Face	Acid	3.040

Table III.B.3.3 Chemical Analyses of Supplier A-AS Full Size Core During Accelerated Corrosion Testing

A comparison of the sodium levels in the bulk material indicate absorption of sodium into the matrix lattice at both the cold face and the hot face. The cold face concentrations are quite low compared to those found at the hot face. The concentrations at both faces increase with time. Again, it should be pointed out that this core survived the accelerated corrosion testing schedule without any undue deterioration.

The results from the full size core testing program in the accelerated corrosion test mode confirm the findings of the laboratory test phase and the testing of the matrix inserts. The MAS matrices are impervious to ion-exchange and are practically immune to the corrosion attack the engine environment presents on both the hot side and the cold side of the regenerator. The leached LAS also provides adequate resistance to chemical attack and survived the engine environment under accelerated corrosion test conditions.

III.C. SUMMARY

The three phase test program provide an excellent step-wise-screening process for evaluating new matrix materials for the regenerator application in the gas turbine engine.

The laboratory tests in this program are apparently more severe than the corrosion conditions presented in the engine during the accelerated corrosion test program, and thus provide an excellent screening procedure for determining the likely candidates that can survive the engine durability test.

Based on the results of this test program the MAS matrix provides the best chemical attack resistance in the engine environment for the regenerator application. The state-of-the-art MAS materials should provide much better performance than the Supplier D MAS matrix which survived 6000 hour engine test.

TASK IV. AEROTHERMODYNAMIC PERFORMANCE

IV.A. INTRODUCTION

The matrix fin configuration selected for a given heat exchanger, under specific engine conditions, has a significant influence on the level of thermal stress and thermodynamic performance. In order to evaluate thermodynamic performance of prospective fin configurations, a shuttle rig was designed and fabricated.

The essential parameters required for accurate heat exchanger performance prediction are the basic heat transfer (J=Stanton-Prandtl No.=Colburn No.= C_2RE^{X2}) and pressure drop (F=Fanning Friction Factor=C_1/RE) characteristics of the matrix fin geometry being evaluated as a function of a nondimensional flow parameter (RE=Reynold's No.). In order to obtain the basic heat transfer and pressure drop data, a transient technique similar to the "sliding drawer" technique described in Reference 9 was used.

The shuttle rig, shown in Figure IV.A.1, consists of two concentric cylinders fabricated from a material with extremely low thermal conductivity (acrylic plastic). The outer cylinder (Figure IV.A.2) consists of four square ports 90° apart, which contain pressure taps and thermocouples. The inner cylinder (Figure IV.A.3), which contains the matrix sample, is mechanically rotated 90° between the hot and cold air streams. The tight clearance between the concentric cylinders prevents the air from leaking from one stream to the other.

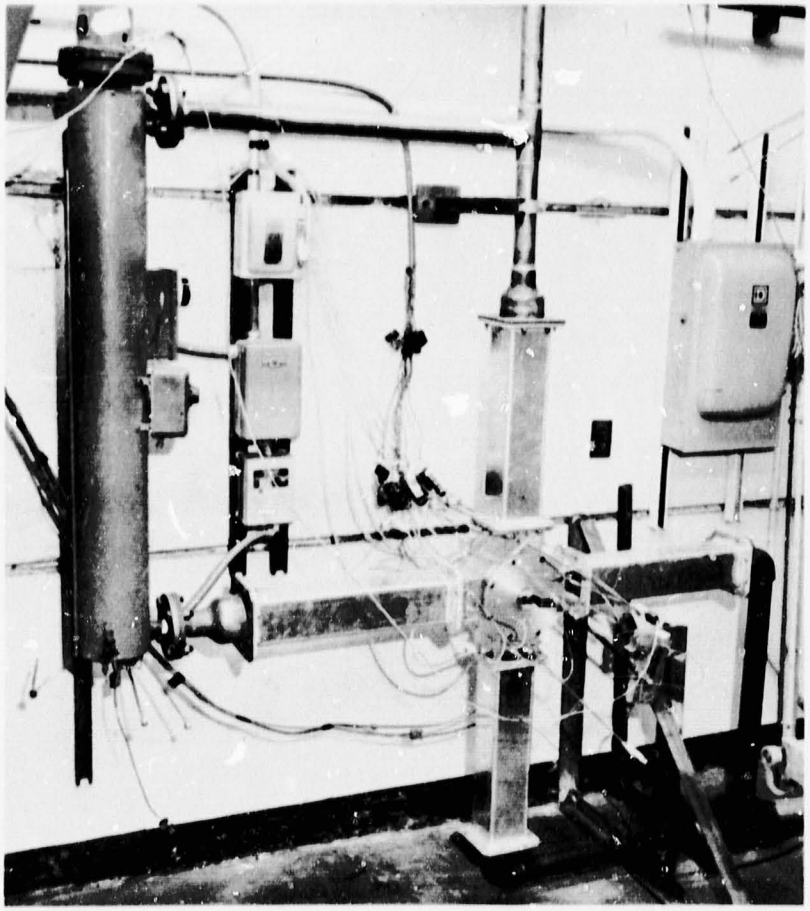

Figure IV.A.1 Photograph of Shuttle Rig

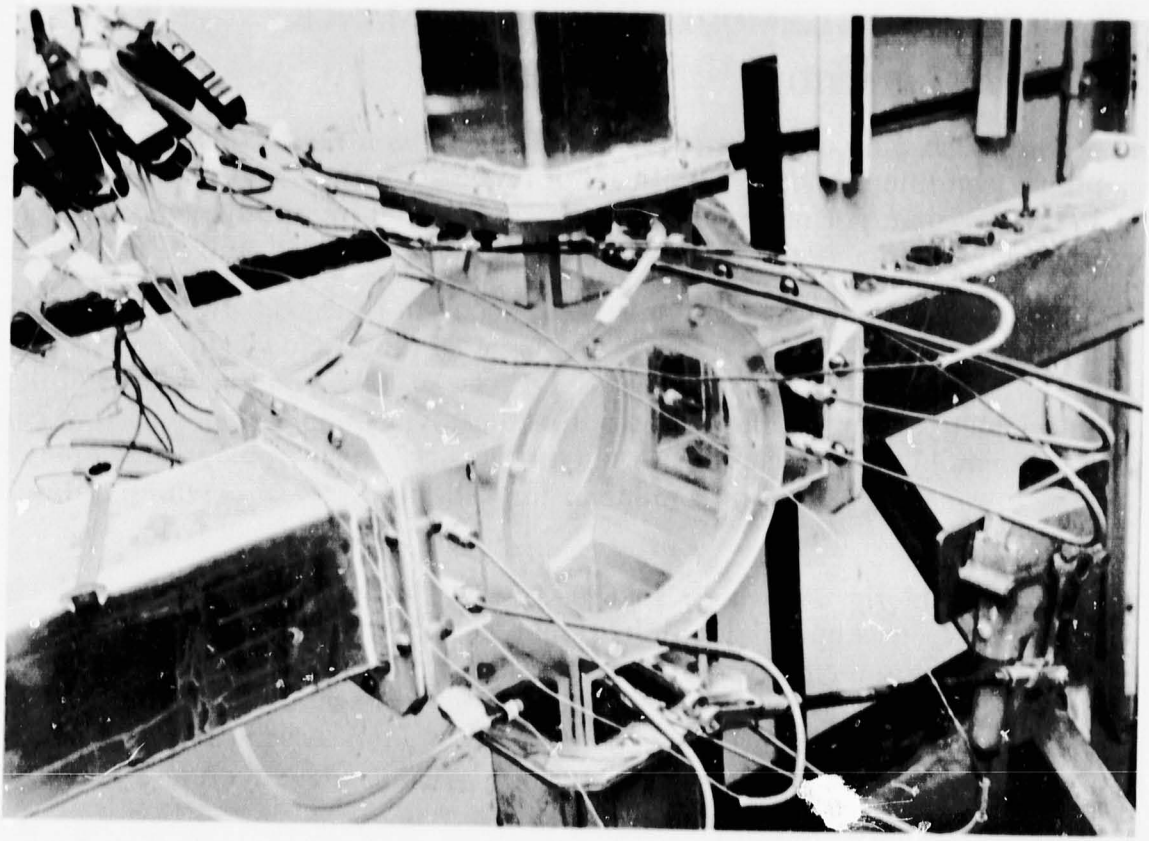

Figure IV.A.2 Photograph of Outer Cylinder Used in the Shuttle Rig

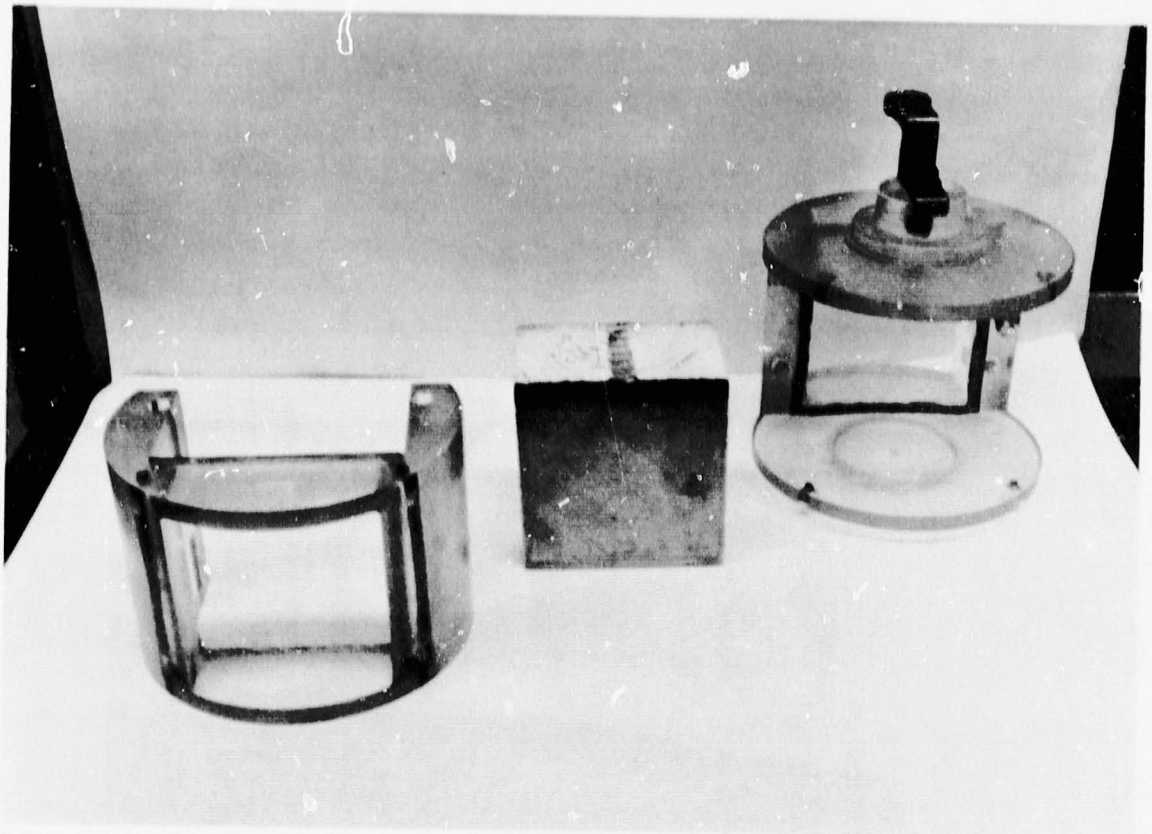

Figure IV.A.3 Photograph of Inner Cylinder Used in the Shuttle Rig

With the inner cylinder exposed to the hot air stream, the test matrix is heated to a uniform temperature of approximately 12°C (22°F) above ambient. A step change in fluid temperature is imposed on the test matrix by rotating the inner cylinder 90°. The downstream fluid temperature, which is referenced to the upstream fluid temperature, is monitored and recorded versus time. By determining the maximum slope of the fluid temperature difference curve during the cooling transient, the Colburn No. of the test matrix can be determined for each flow condition (Reynold's No.). The theoretical basis for this measurement technique is described in Reference 9.

In addition to the dependence on the maximum slope of the fluid temperature difference curve during the cooling transient, the level of the heat transfer characteristics (Colburn No.) is dependent on the fin parameter values utilized for data reduction. This was previously discussed in Section Q in Reference 1. In order to determine the pertinent fin configuration parameters (Figure IV.A.4) required for data reduction, an enlarged photo (Figure IV.A.5) of a 25.4mm (1 inch) square section of the test matrix is taken. From this photo the number of openings per row per inch (X) and the number of rows per inch (Y) is determined. A computer program determines the open area (σ), hydraulic diameter (DH), and heat transfer surface area per unit volume (β) as a function of X, Y, fillet radius, and fin material thickness (S). After measuring the weight and volume of the test matrix, the open area (σ) is determined based on the wall density (ρW) of the matrix material. Once the open area is established, the remaining parameters (DH, β, S) are determined from the computer read-out for the X, Y, and S combination. Consequently, the pertinent fin parameters required (σ and DH) for data reduction are highly dependent on the accuracy of the wall density (ρW) value of the matrix material.

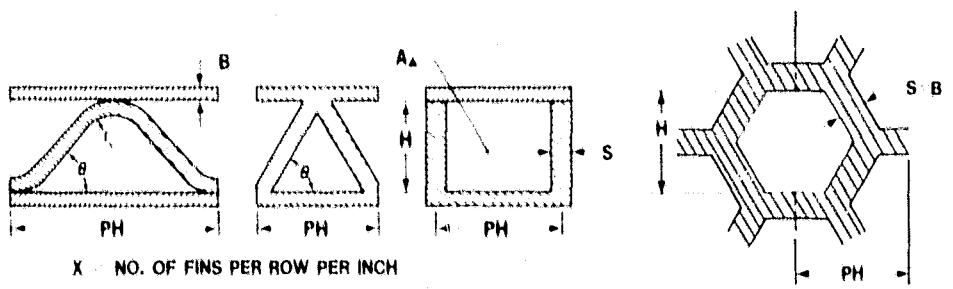

X = NO. OF FINS PER ROW PER INCH

Y = NO. OF ROWS PER INCH

H = FIN HEIGHT = $\frac{1}{Y}$ − B

PH = FIN PITCH = ($\frac{1}{X}$) RECTANGULAR OR HEXAGONAL = ($\frac{2}{X}$) TRIANGULAR

A.R. = ASPECT RATIO = PH / H

B = PLATE THICKNESS

S = FIN THICKNESS

r = RADIUS OF CURVATURE

θ = SHAPE ANGLE

N = NO. OF OPENINGS PER SQ. IN.

A_Δ = CROSS-SECTIONAL AREA OF 1 OPENING

WP = WETTED PERIMETER OF ONE OPENING

DH = HYDRAULIC DIAMETER = $\frac{4 A_\Delta}{W.P.}$

σ = RATIO OF OPEN AREA TO FRONTAL AREA

σ TRIANGULAR = $\frac{2.A_\Delta}{PH\ (H+B)}$ σ RECTANGULAR = $\frac{H\ (PH-S)}{(H+B)\ (PH)}$ σ HEXAGONAL = $\frac{H^2}{(H+B)^2}$

β = HEAT TRANSFER SURFACE AREA PER UNIT VOLUME = $\frac{4\ \sigma}{DH}$

Figure IV.A.4 Definition of Fin Parameters

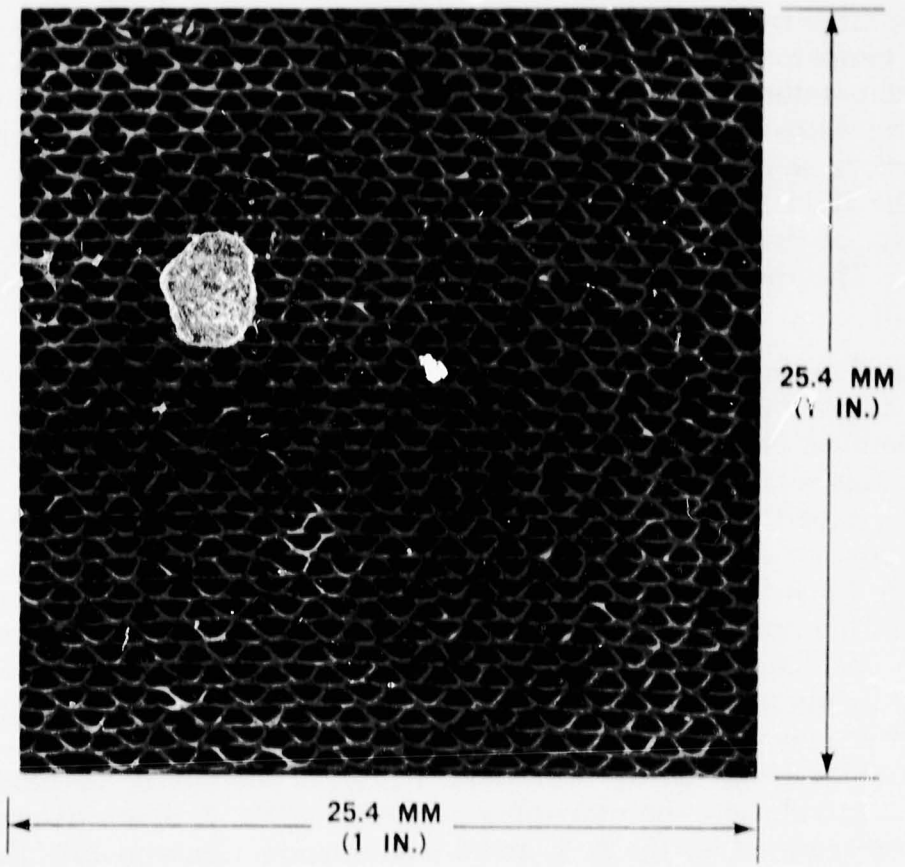

Figure IV.A.5 Photograph Showing One Inch Square Section from Test Matrix

Erroneous estimates of the fin parameters (σ and DH) can introduce significant discrepancies in the F and J curves. Consequently, an alternate method of determining the heat transfer and pressure drop characteristics that eliminates the necessity of estimating fin parameters is desirable. In addition, the alternate characteristics will allow a direct comparison of test data from different sources, since a universal method of determining pertinent fin parameters is non-existent at this time. As previously presented in Section Q.6 of Reference 1, alternate pressure drop and heat transfer characteristics can be expressed in the following forms:

$$\frac{\Delta P \cdot P}{L} = C \frac{\dot{W}^{1.673} T}{A_F}$$

$$\frac{NTU}{L} = \left[A \frac{A_F T^{.673}}{\dot{W}} \right]^{-X_2}$$

Where:

ΔP = Matrix pressure drop — Kpa (PSI)

P = Fluid pressure — KPa (PSIA)

L = Flow Length — CM. (In.)

W = Air Mass flow rate — Kg/Sec. (Lb./Sec.)

T = Fluid temperature — °K. (°R.)

A_F = Matrix frontal area — $M.^2$ ($FT.^2$)

σ = Open area ratio

C_1 = Fanning Friction Factor constant for laminar flow = F·RE

DH = Hydraulic diameter — CM. (In.)

NTU = By definition the number of heat transfer units (determined from the maximum slope of the fluid temperature difference curve during the cooling transient as described in Reference 9)

C_2 = Colburn No. constant for laminar flow = J/RE^{X_2}

X_2 = Reynold's No. (RE) exponent from the Colburn No. ($J=C_2\ RE^{X_2}$)

$$C = 3.56\ (10^{-9})\ \frac{C_1}{\sigma DH^2} \qquad \left[3.506\ (10^{-10})\ \frac{C_1}{\sigma DH^2}\right]$$

$$A = 4.98\left[62.6(10^{-7})\right]^{-X_2}\ \frac{C_2\sigma}{DH}^{\frac{-X_2}{(1-X_2)}} \qquad \left[4.98\left[21.9(10^{-7})\right]^{-X_2}\ \frac{C_2\sigma}{DH}^{\frac{-X_2}{(1-X_2)}}\right]$$

If $X_2 = -1$; then:

$$A = 3.11\ \ (10^{-5})\ \frac{C_2\sigma}{DH^2} \qquad \left[1.09\ \ (10^{-5})\ \frac{C_2\sigma}{DH^2}\right]$$

Once the constants (C and A) have been determined from the equation of the line for the alternate performance characteristics, the pertinent constants (C_1 and C_2) for the basic performance characteristics can be determined from estimated values of σ and DH.

IV.B. DISCUSSION

IV.B.1 Matrix Test Samples

Prior to the start of this program with NASA twenty matrix fin configurations were evaluated in the shuttle rig (Reference 2). These data are repeated on Table IV.B.1.1. During the course of this program an additional nineteen matrix samples were evaluated (Table IV.B.1.2).

CODE:

R — RECTANGULAR
I.T. — ISOSCELES TRIANGULAR
S.T. — SINUSOIDAL TRIANGULAR
H — HEXAGONAL

$$F = C_1 RE^{X_1}$$

$$J = C_2 RE^{X_2}$$

$$\frac{\Delta P.P}{L} = C \frac{WT^{1.673}}{AF}$$

$$\frac{NTU}{L} = A \left[\frac{AFT^{0.673}}{W}\right] - X_2$$

CORE NO	SUP-PLIER	TYPE OF FIN	X FINS / CM (FINS / IN)	Y ROWS / CM (ROWS / IN)	N HOLES / CM 2 (HOLES / IN 2)	S MM (IN.)	B MM (IN.)	H MM (IN.)	PH MM (IN.)	A R PH / H	ρ_w G / CC (LB / FT 3)	L / DH	σ	DH MM (IN.)	β M 2 / M 3 (FT 2 / FT 3)	C X 10^5	A X 10^2	C_1	X_1	C_2	X_2	J/F @ RE = 100	A_c CM 2 (IN 2)
1	A	S.T.	11.8 (28)	13.0 (33)	143 (924)	.109 (.0043)	.109 (.0043)	.660 (.0260)	1.813 (.0714)	2.75	2.20 (137.0)	121	673	.589 (.0232)	424 (1392)	1.30	4.55	13.4	-.1	3.34	-.1	240	183 (.16)
2	D	R	11.4 (29)	12.2 (31)	140 (900)	.193 (.0076)	.193 (.0076)	.627 (.0247)	.879 (.0346)	1.40	1.55 (97.0)	107	599	.655 (.0258)	3654 (1114)	1.23	4.11	14.0	-.1	4.18	-.1	290	183 (.16)
3	D	R	8.3 (21)	8.7 (22)	71.6 (462)	.216 (.0085)	.216 (.0085)	.940 (.0370)	1.211 (.0477)	1.29	1.48 (92.8)	72	669	.960 (.0381)	2765 (843)	.54	2.18	14.9	-.1	4.18	-.1	251	98 (15.2)
4	I	I.T.	15.8 (40)	9.1 (23)	142.6 (920)	.135 (.0053)	.135 (.0053)	.678 (.0382)	1.270 (.0500)	1.34	1.56 (97.3)	121	642	.589 (.0232)	4356 (1328)	1.11	5.11	18.9	-.1	3.83	-.1	381	72 (11.2)
5	C	S.T.	9.8 (25)	15.4 (39)	151 (975)	.135 (.0053)	.135 (.0053)	.516 (.0203)	2.032 (.0800)	3.95	1.43 (89.0)	179	569	.401 (.0158)	5680 (1734)	2.25	18.2	9.1	-.1	62	-.8	171	183 (.16)
6	D	R	6.9 (17.5)	7.5 (19)	51.5 (332)	.300 (.0118)	.300 (.0118)	1.036 (.0408)	1.450 (.0571)	1.48	1.47 (91.4)	87	615	1.092 (.0436)	2253 (687)	515	1.55	16.7	-.1	4.28	-.1	256	46 (7.1)
7	C	S.T.	5.1 (13)	6.3 (16)	32.2 (208)	.178 (.0070)	.178 (.0070)	1.410 (.0555)	3.906 (1.538)	2.77	1.51 (94.3)	53	737	1.316 (.0518)	2240 (683)	33	17.4	18.6	-.1	324	-.5	174	183 (.16)
8	E	R	4.1 (10.5)	14.4 (36.5)	59.4 (383)	.284 (.0112)	.213 (.0084)	.482 (.019)	2.418 (.0952)	5.9	2.40 (149.5)	89	651	.787 (.0310)	3103 (946)	1.18	3.85	18.4	-.1	5.55	-.1	382	98 (9.3)
9	E	R	5.3 (13.5)	15.6 (39.5)	82.6 (533)	.386 (.015)	.228 (.009)	.411 (.0162)	1.88 (.074)	4.57	2.34 (146.3)	109	585	.645 (.0254)	3129 (954)	1.89	4.29	17.5	-.1	5.8	-.1	287	181 (15.6)
10	A	S.T.	14.6 (37)	14.4 (36.5)	209.5 (1351)	.066 (.0026)	.066 (.0026)	.638 (.0248)	1.374 (.0541)	2.18	2.09 (130.4)	128	767	.549 (.0216)	5509 (1797)	1.68	5.9	16.3	-.1	3.29	-.1	282	183 (.16)
11	A	S.T.	6.3 (16)	18.2 (26)	64.5 (416)	.127 (.0050)	.127 (.0050)	.851 (.0335)	3.175 (.1250)	3.73	2.20 (137.3)	91	720	.775 (.0305)	3716 (1133)	76	2.35	14.5	-.1	2.79	-.1	192	183 (.16)
12	A	R	7.8 (17.8)	7.1 (18)	49.6 (320)	.290 (.0114)	.290 (.0114)	1.123 (.0442)	1.427 (.0562)	1.27	1.57 (104.2)	62	634	1.130 (.0445)	2264 (684)	46	1.75	16.5	-.1	5.8	-.1	383	86 (18.2)
13	A	R	5.6 (14.2)	5.6 (14.2)	31.3 (202)	.274 (.0108)	.274 (.0108)	1.514 (.0596)	1.788 (.0704)	1.18	1.63 (101.5)	47	718	1.487 (.0586)	1896 (578)	25	4.43	18.2	-.1	1.44	-.75	250	86 (18.2)
14	E	R	6.1 (15.5)	8.3 (21)	50.5 (326)	.305 (.012)	.381 (.015)	.837 (.033)	1.64 (.0645)	1.88	2.39 (149.3)	70	557	1.02 (.0402)	2181 (665)	62	2.3	15.9	-.1	6.12	-.1	305	62 (9.6)
15	E	R	6.1 (15.5)	11.8 (28)	67.3 (434)	.198 (.0075)	.330 (.013)	.584 (.023)	1.625 (.0645)	2.85	2.34 (145.8)	85	558	.822 (.0324)	2711 (827)	1.88	4.84	16.7	-.1	1.86	-.87	212	64 (9.9)
16	D	R	6.6 (16.8)	6.7 (17.0)	44.2 (286)	.315 (.0124)	.315 (.0124)	1.179 (.0464)	1.511 (.0597)	1.28	1.51 (94.2)	60	625	1.186 (.0467)	2186 (642)	44	1.38	17.1	-.1	4.16	-.1	243	46 (7.1)
17	E	R	3.2 (8.0)	15.4 (39.0)	49.1 (312)	.360 (.0142)	.241 (.0095)	.409 (.0161)	3.175 (.125)	7.76	2.31 (144.4)	98	568	.713 (.0281)	3139 (957)	1.45	8.8	18.3	-.1	3.88	-.88	283	64 (9.9)
18	A	I.T.	7.9 (20)	4.7 (12)	37.4 (240)	.257 (.0101)	.257 (.0101)	1.859 (.0732)	2.540 (.1000)	1.37	1.53 (95.5)	29	653	1.183 (.0458)	2264 (684)	46	6.28	15.6	-.1	1.88	-.72	233	181 (15.6)
19	A	S.T.	15.0 (38)	13.6 (34.5)	203.9 (1311)	.061 (.0024)	.061 (.0024)	.676 (.0266)	1.336 (.0526)	1.98	2.10 (131.0)	122	787	.579 (.0228)	5427 (1653)	1.38	6.58	16.1	-.1	3.94	-.1	245	183 (.16)
20	A	S.T.	10.8 (27.5)	14.6 (37)	157.4 (1018)	.066 (.0026)	.066 (.0026)	.620 (.0244)	1.846 (.0727)	2.98	2.18 (136.3)	107	780	.592 (.0233)	5264 (1605)	1.36	5.83	16.4	-.1	3.19	-.1	195	86 (13.2)

Table IV.B.1.1 Shuttle Rig Matrices (1-20)

CODE

R — RECTANGULAR
I.T. — ISOSCELES TRIANGULAR
S.T — SINUSOIDAL TRIANGULAR
H — HEXAGONAL

$F = C_1 RE^{X_1}$

$J = C_2 RE^{X_2}$

$\frac{\Delta P}{L} \cdot \frac{P}{} = C \frac{WT^{1.673}}{AF}$

$\frac{NTU}{L} = A \left[\frac{AF}{W}^{0.673}\right] X_1$

CORE NO.	SUPPLIER	TYPE OF FIN	X FINS CM (FINS IN.)	Y ROWS CM (ROWS IN.)	N HOLES CM² (HOLES IN.²)	S MM (IN.)	B MM (IN.)	H MM (IN.)	PH MM (IN.)	AR PH H	Pw gM CC (LB. FT.³)	L DH	σ	DH MM (IN.)	β M² M² (FT.² FT.³)	C X10³	A X10²	C_1	X_1	C_2	X_2	J/F @ RE·100	A_F CM² (IN.²)
21	E	R	5.6 (14.3)	10 (25.3)	56.1 (362)	.223 (.0088)	.279 (.011)	.724 (.0285)	1.78 (.070)	2.45	2.02 (126.2)	71	.637	.991 (.0390)	2572 (784)	.62	4.70	17.1	−.1	1.80	−.63	.222	103 (16)
22	E	R	3.9 (10)	15.4 (39)	60.5 (390)	.277 (.0109)	.208 (.0082)	.442 (.0174)	2.54 (.100)	5.75	2.29 (143.2)	94	.608	.739 (.0291)	3290 (1003)	1.28	4.20	18.8	−.1	5.37	−.1	.286	103 (16)
23	E	R	2.4 (6.2)	16.7 (42.3)	40.6 (262)	.381 (.015)	.191 (.0075)	.406 (.016)	4.09 (.161)	10.0	2.39 (149.1)	95	618	.737 (.0290)	3355 (1023)	1.43	8.64	21.2	−.1	1.62	−.61	.184	103 (16)
24	E	R	4.7 (12)	12.6 (32)	59.5 (384)	.417 (.0164)	.279 (.0110)	.516 (.0203)	2.12 (.0833)	4.10	1.94 (121.0)	89	.521	.790 (.0311)	2637 (804)	1.18	2.45	16.9	−.1	4.17	−1	.247	103 (16)
25	C	S.T.	9.8 (25)	12.8 (32.5)	126 (813)	.183 (.0072)	.183 (.0072)	.599 (.0236)	2.03 (.0800)	3.39	2.33 (145.7)	153	.512	.417 (.0164)	4907 (1496)	2.4	4.3	9.4	−.1	2.07	−1	.220	103 (16)
26	I	H	6.8 (17.3)	5.9 (15)	40.3 (260)	.323 (.0127)	.323 (.0127)	1.37 (.054)	1.47 (.058)	1.07	1.62 (101.3)	51	.656	1.37 (.054)	1912 (583)	.32	1.1	17.4	−.1	4.48	−1	.257	46 (7.1)
27	B	H	15 (38.1)	13 (33)	195 (1260)	.071 (.0028)	.071 (.0028)	.699 (.0275)	.665 (.0262)	.95	2.05 (128)	101	.827	.699 (.0275)	4723 (1440)	.81	4.75	14.4	−.1	4.0	−1	.278	46 (7.1)
28	A	R	7.9 (20)	7.9 (20)	62 (400)	.165 (.0065)	.165 (.0065)	1.105 (.0435)	1.27 (.050)	1.15	1.68 (104.6)	64	.756	1.105 (.0435)	2730 (834)	.37	1.85	15.1	−.1	4.25	−1	.281	103 (16)
29	A	R	6.9 (17.5)	6.9 (17.5)	47.5 (306)	.279 (.011)	.279 (.011)	1.17 (.046)	1.45 (.057)	1.24	1.69 (105.6)	61	.653	1.17 (.0462)	2227 (679)	.38	1.75	15.1	−.1	5.25	−1	.348	103 (16)
30	J	R	4.3 (11.0)	7.9 (20)	34.1 (220)	.752 (.0295)	.452 (.0178)	.818 (.0322)	2.31 (.0909)	2.82	1.85 (115.3)	59	.435	1.07 (.0422)	1624 (495)	.72	.93	15.9	−.1	3.49	−1	.219	103 (16)
31	J	R	4.3 (11)	6.7 (17)	29 (187)	.706 (.0278)	.635 (.0250)	.859 (.0338)	2.31 (.0909)	2.69	1.86 (115.8)	62	.398	1.12 (.0440)	1424 (434)	.85	.94	18.7	−.1	4.19	−1	.224	103 (16)
32	J	R	8.5 (21.5)	8.3 (21)	70.1 (452)	.257 (.0101)	206 (.0081)	1.00 (.0395)	1.18 (.0465)	1.21	2.08 (129.5)	59	.649	.963 (.0379)	2696 (822)	.67	2.0	17.8	−.1	4.06	−1	.228	46 (7.1)
33	D	R	10.6 (27)	13.8 (35)	146.5 (945)	.284 (.0112)	.142 (.0056)	.584 (.023)	.94 (.0370)	1.61	1.42 (88.8)	117	.560	.617 .0243	3628 (1106)	1.50	4.1	14.1	−.1	3.97	−1	.302	103 (16)
34	J	R	9.6 (24.5)	21.7 (55)	208.9 (1348)	.218 (.0086)	.218 (.0086)	.244 (.0096)	.818 (.0322)	4.25	2.37 (148.1)	168	.415	.376 (.0148)	4418 (1347)	11.0		28.5					
35	I	I.T.	18.9 (48)	11.0 (28)	208.3 (1344)	.168 (.0066)	.168 (.0066)	.739 (.0291)	1.06 (.0417)	1.43	1.36 (84.6)	166	.496	.429 (.0169)	4622 (1409)	2.75		11.1					
36	A	R			20.2 (130)	.277 (.0109)	.277 (.0109)	1.30 (.0512)	3.15 (1242)	2.43	2.47 (153.8)	40	.753	1.79 (.0705)	1683 (513)	.17		17.6					
37	A	R	9.8 (24.8)	9.8 (25)	96.1 (620)	.147 (.0058)	.147 (.0058)	.869 (.0342)	1.02 (.0403)	1.18	1.57 (98)	82	.731	.871 (.0343)	3352 (1022)	.57		14.0					
38	A	I.T.	7.4 (18.8)	4.3 (10.9)	31.8 (205)	.236 (.0093)	.236 (.0093)	1.98 (.0778)	2.70 (.1064)	1.37	2.43 (151.8)	55	700	1.30 (.0513)	2148 (655)	.28		14.7					
39	A	R	6.3 (16)	6.3 (16)	39.7 (256)	.254 (.010)	.254 (.010)	1.33 (.0525)	1.59 (.0625)	1.19	2.44 (152.1)	53	.707	1.33 (.0525)	2119 (646)	.32		17.8					

Table IV.B.1.2 Shuttle Rig Matrices (21-39)

Photographs of the nineteen samples (matrices 21 thru 39) evaluated during this program are shown on Figures IV.B.1.1. to IV.B.1.20. The standard heat transfer (J) and pressure drop (F) characteristics, which depend on the values determined for open area ratio (σ) and hydraulic diameter (DH), for the first thirteen matrices (matrices 21 thru 33) are listed on Table IV.B.1.2.

Due to instrumentation difficulties the heat transfer data for the last six samples (matrices 34 to 39) contained unacceptable scatter due to instrumentation difficulties. Re-evaluation of these matrices with new instrumentation was not completed before termination of the program. Consequently, only the pressure drop characteristics were completed (Table IV.B.1.2) for the last six matrices.

The alternate heat transfer and pressure drop characteristics, which are based on measured test data, for matrices 21 to 33 are listed on Table IV.B.1.2.

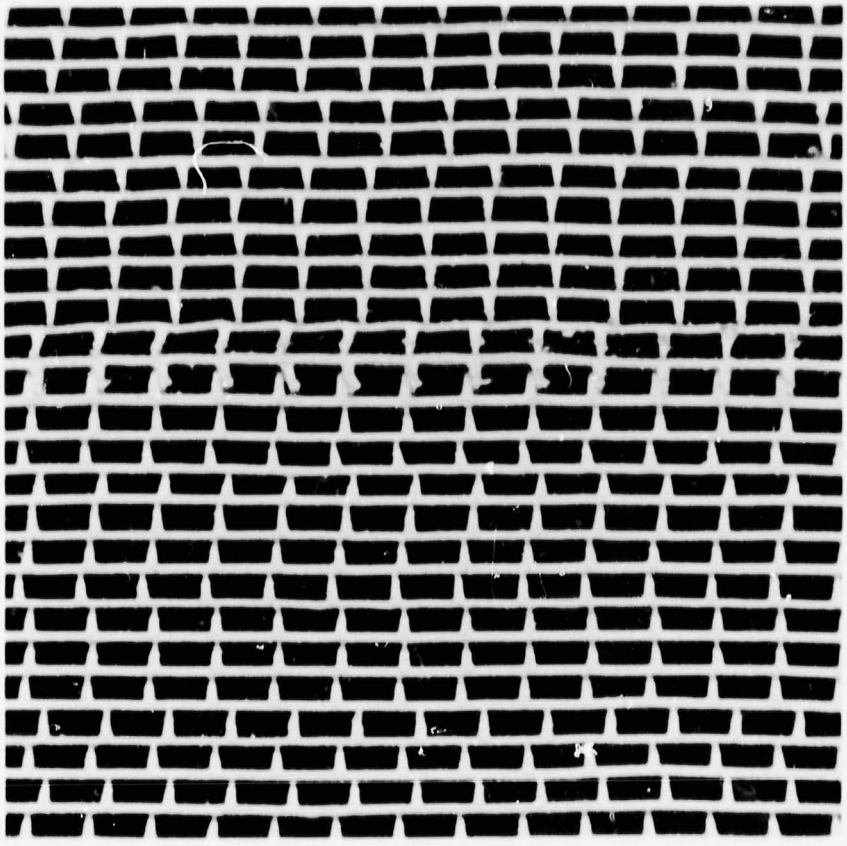

Figure IV.B.1.1 Photograph of Matrix No. 21

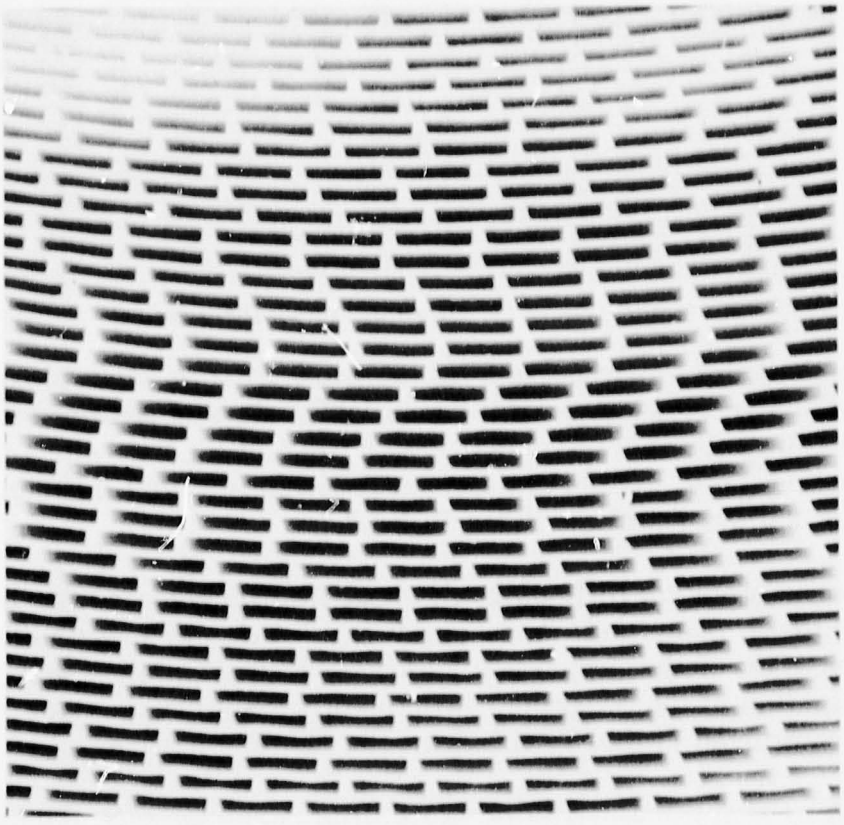

Figure IV.B.1.2 Photograph of Matrix No. 22

Figure IV.B.1.3 Photograph of Matrix No. 23

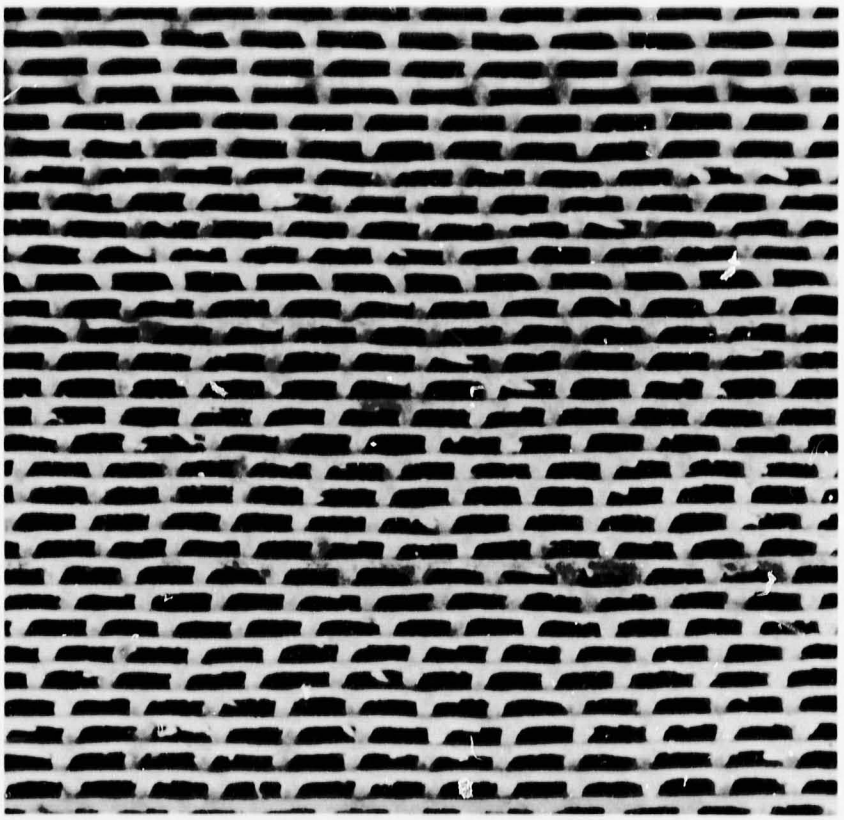

Figure IV.B.1.4 Photograph of Matrix No. 24

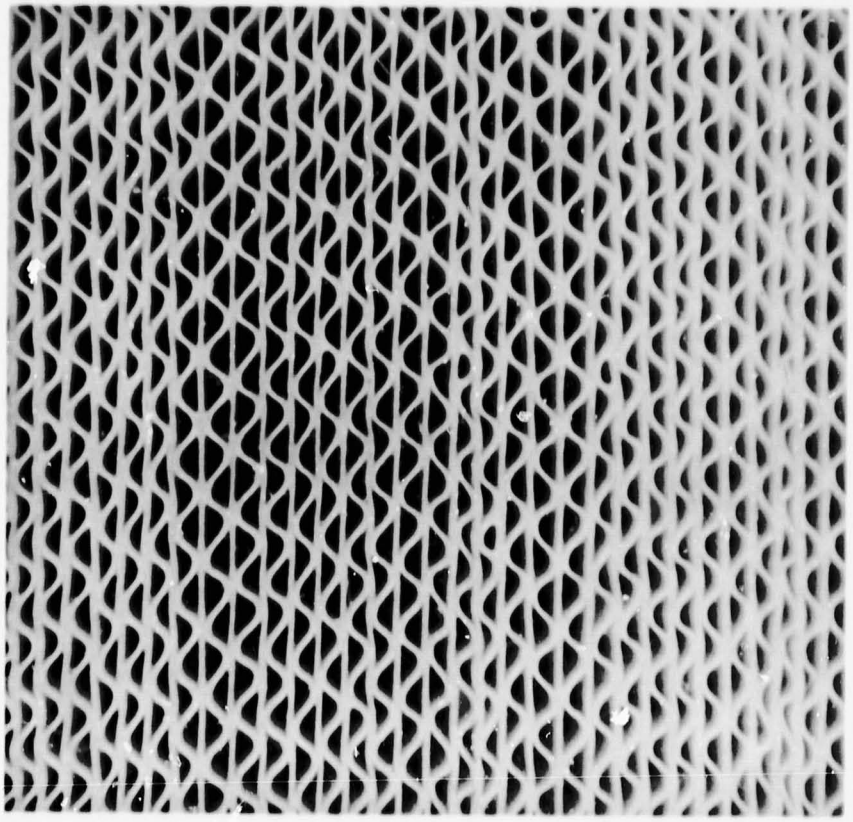

Figure IV.B.1.5 Photograph of Matrix No. 25

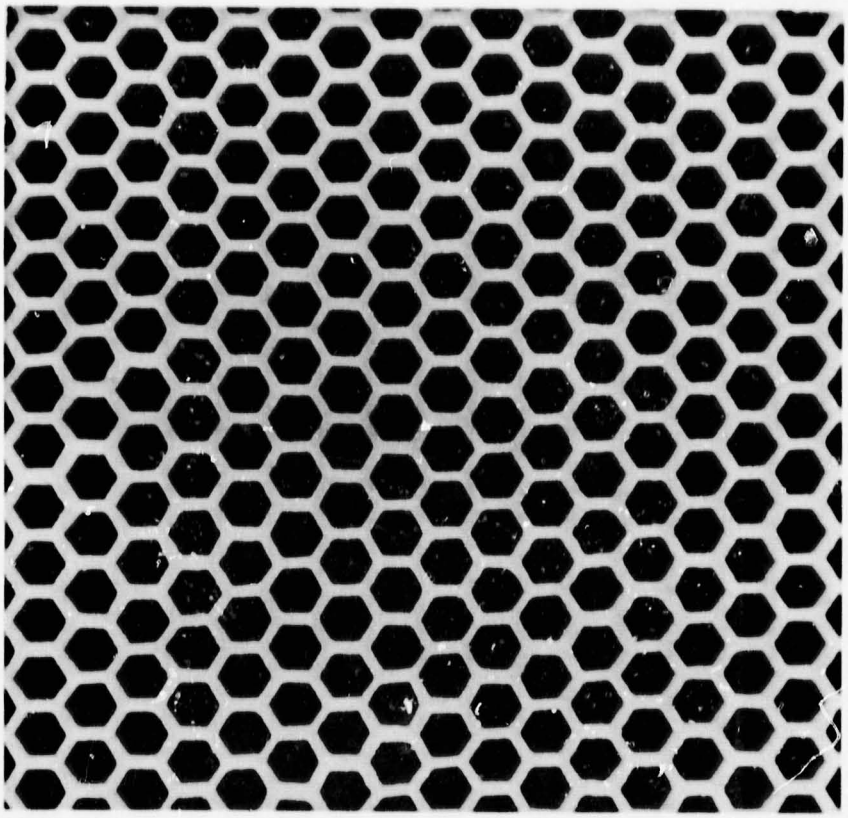

Figure IV.B.1.6 Photograph of Matrix No. 26

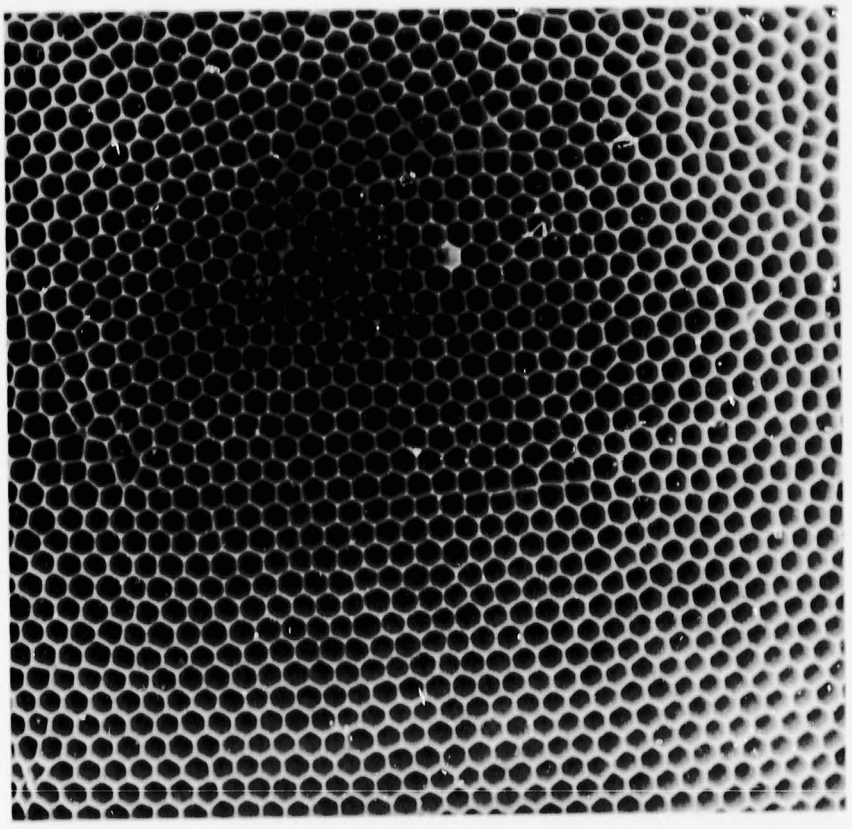

Figure IV.B.1.7 Photograph of Matrix No. 27

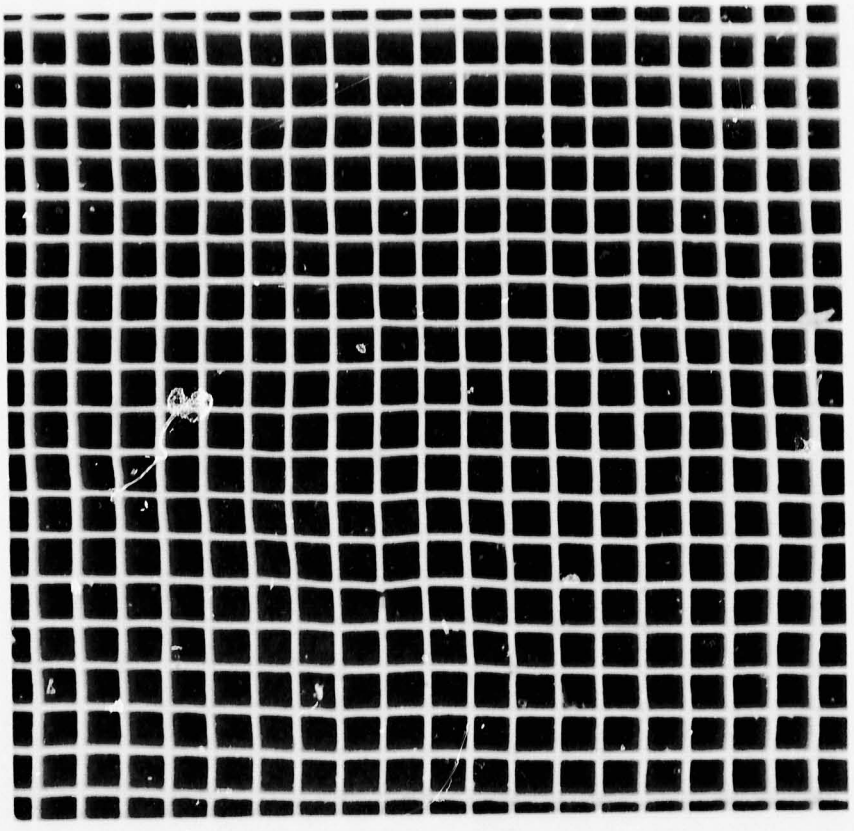

Figure IV.B.1.8 Photograph of Matrix No. 28

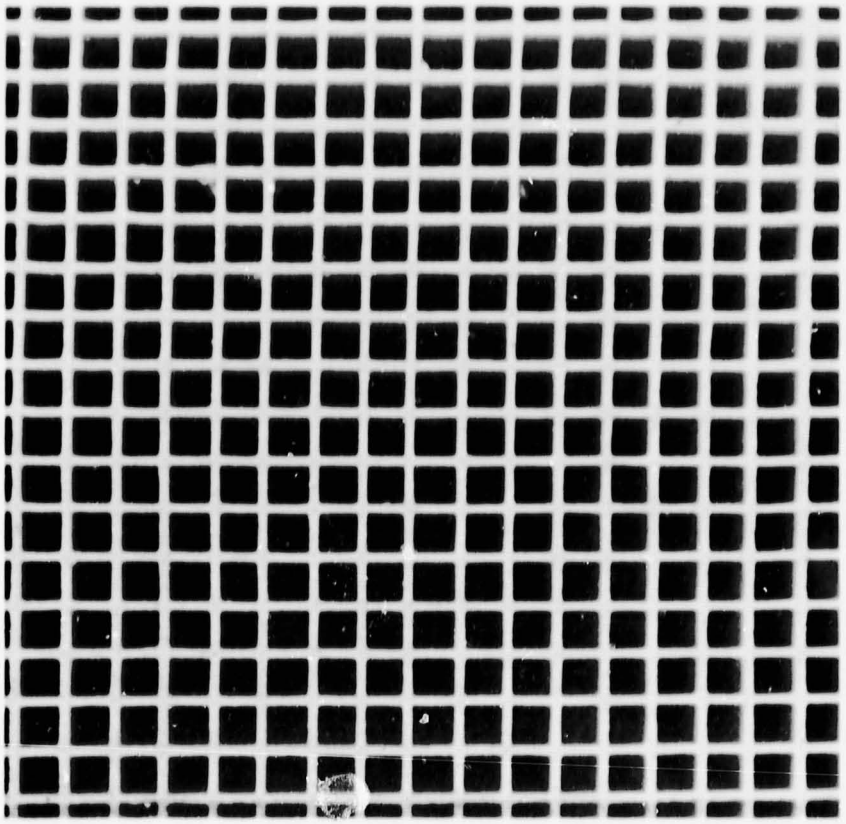

Figure IV.B.1.9 Photograph of Matrix No. 29

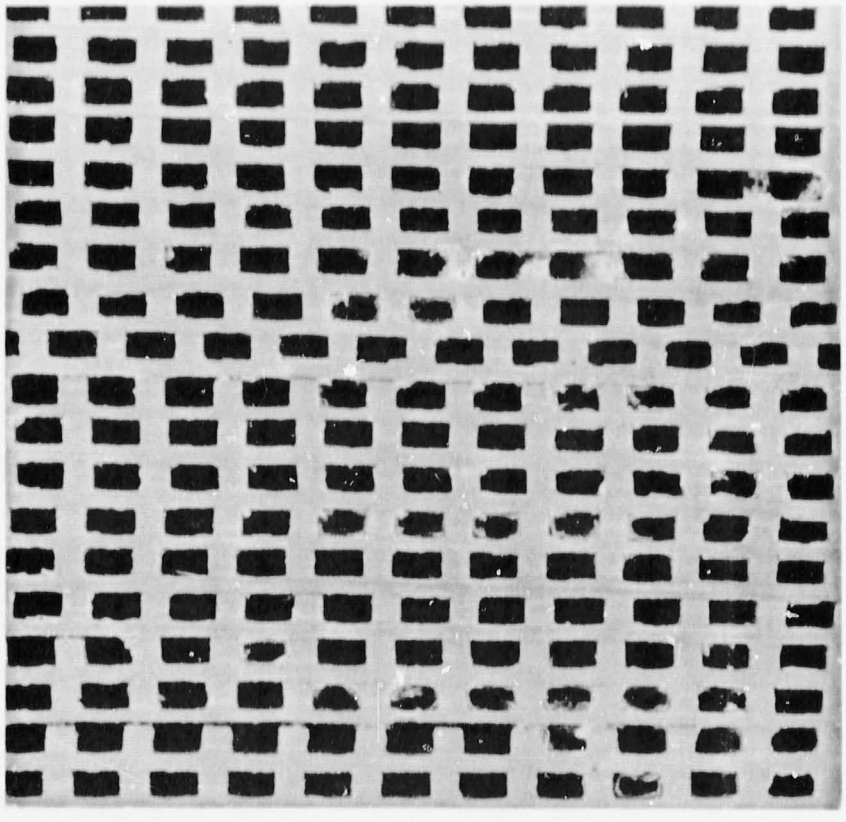

Figure IV.B.1.10 Photograph of Matrix No. 30

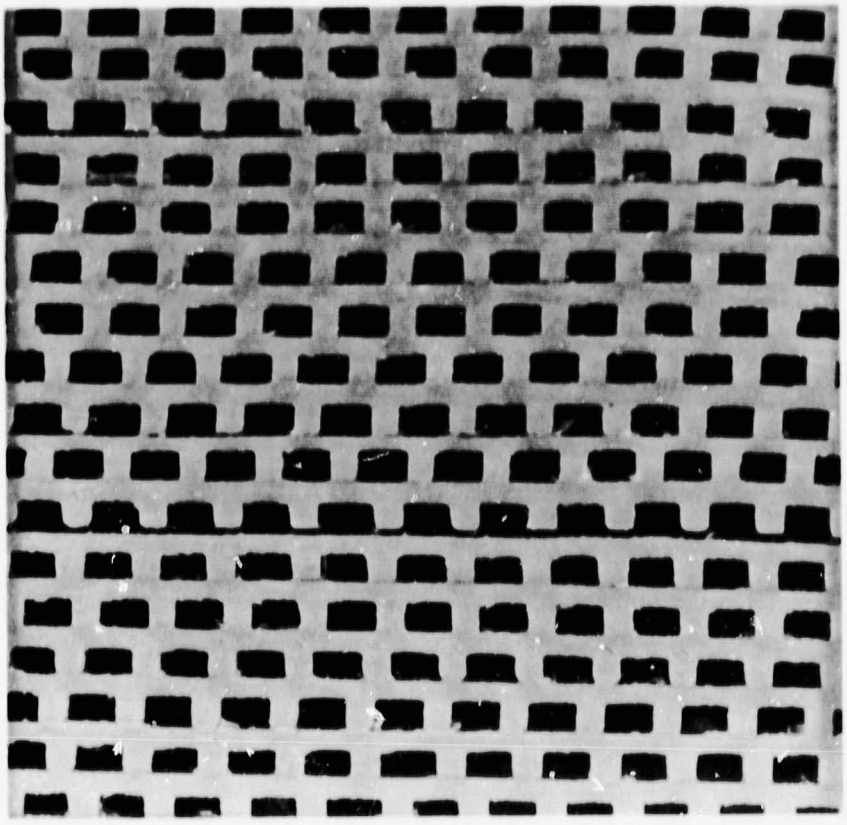

Figure IV.B.1.11 Photograph of Matrix No. 31

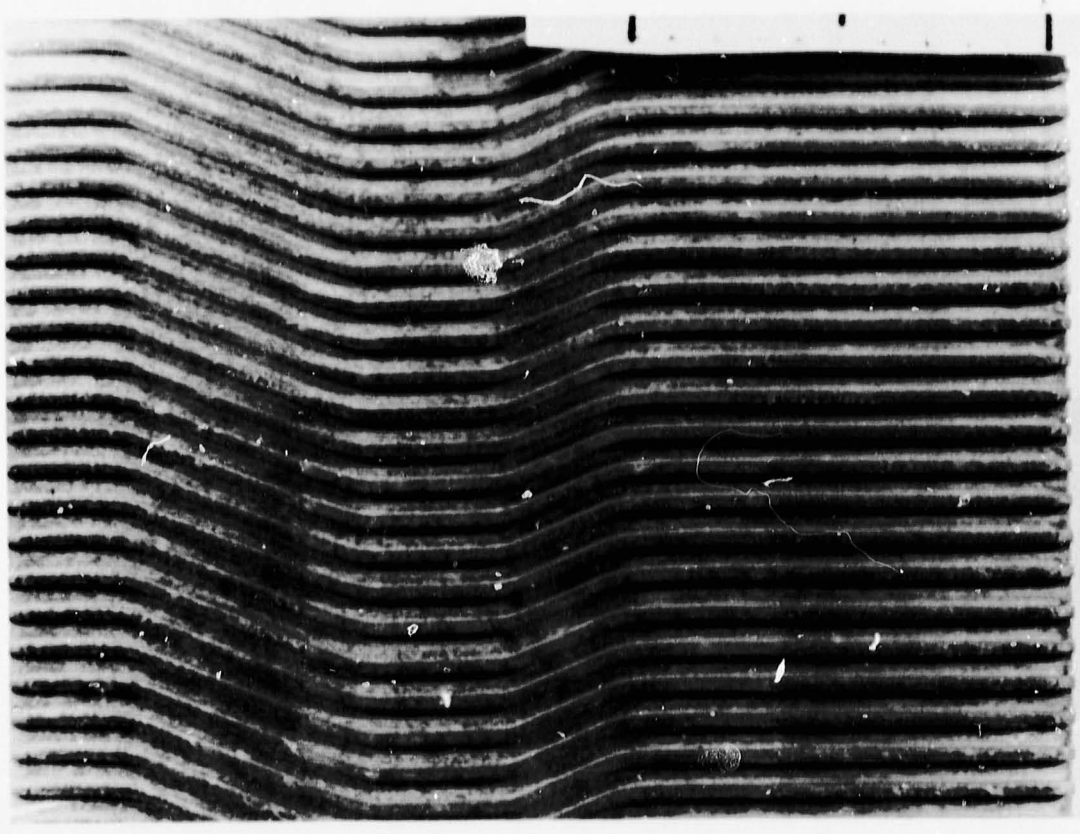

Figure IV.B.1.12 Matrix 31 Wavy Flow Passage

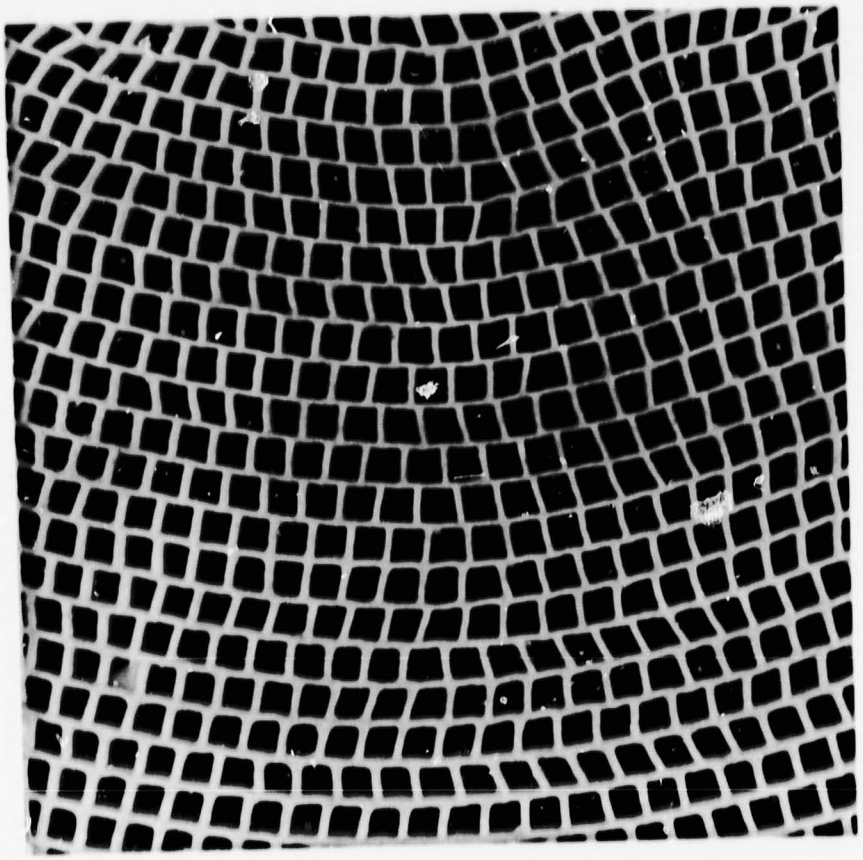

Figure IV.B.1.13 Photograph of Matrix No. 32

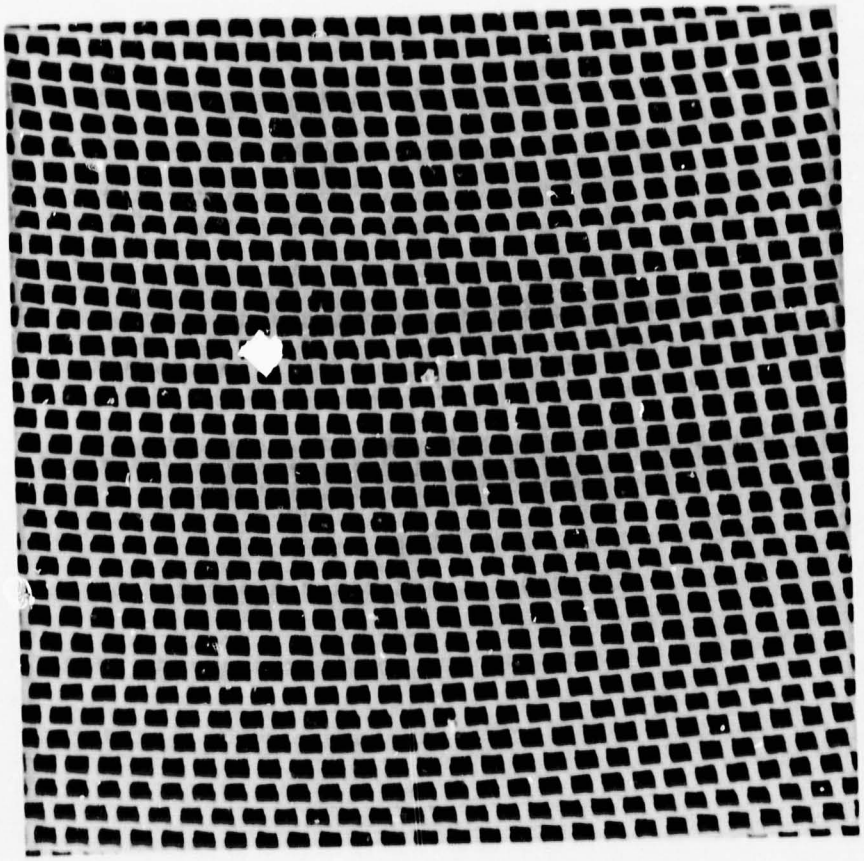

Figure IV.B.1.14 Photograph of Matrix No. 33

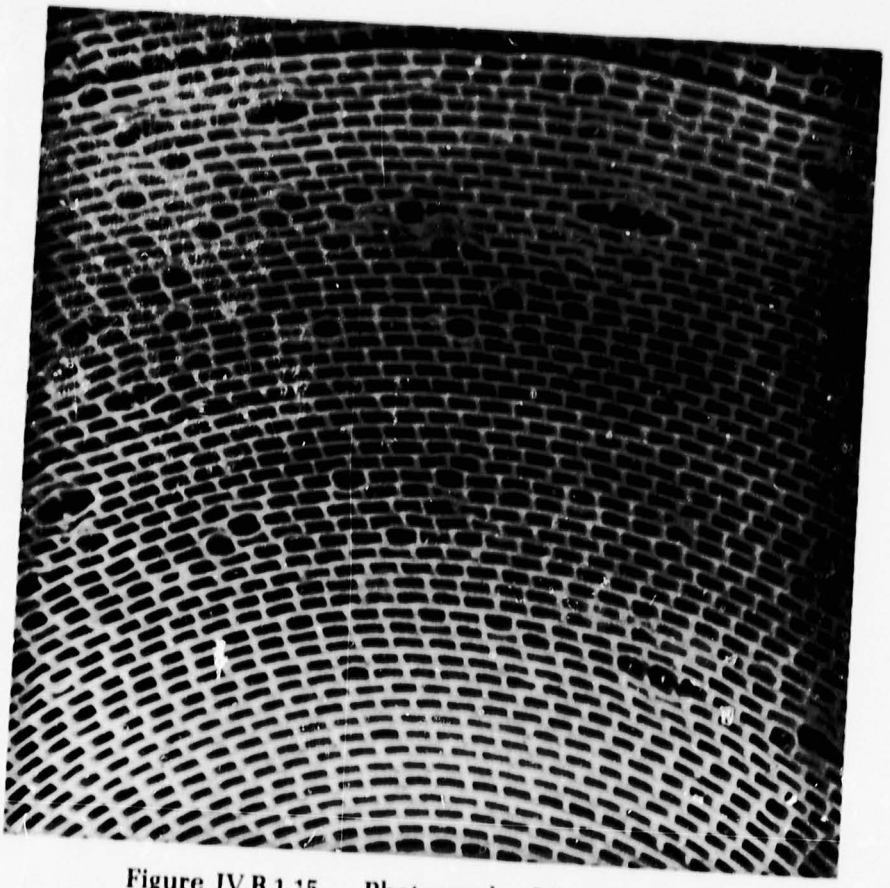

Figure IV.B.1.15 Photograph of Matrix No. 34

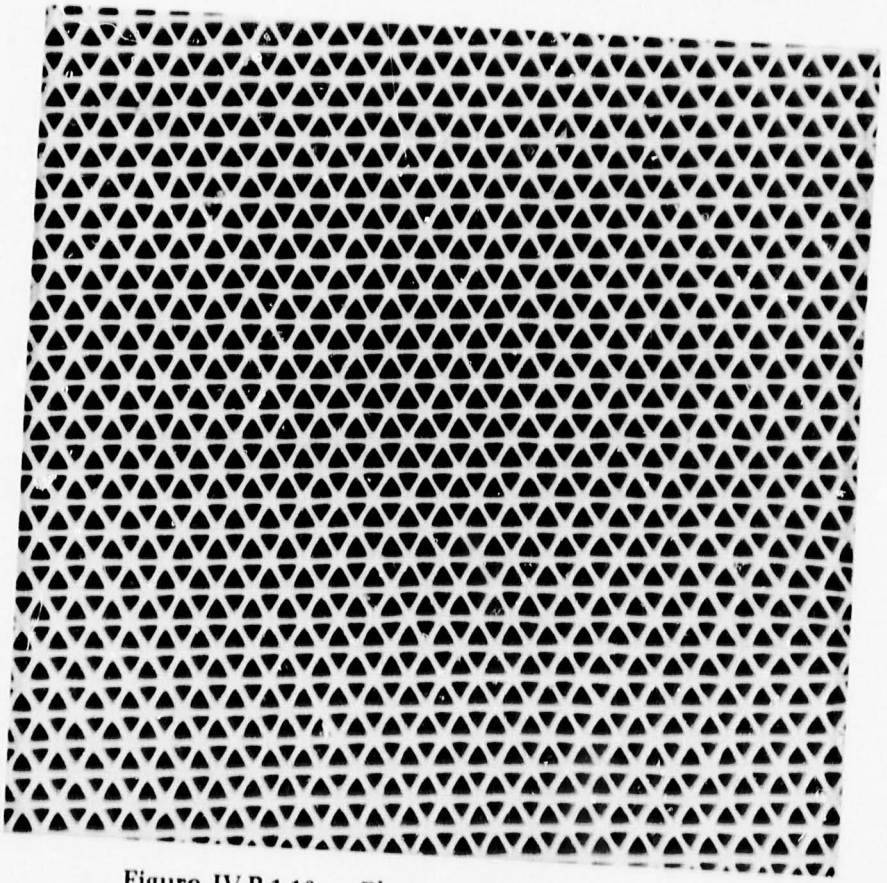

Figure IV.B.1.16 Photograph of Matrix No. 35

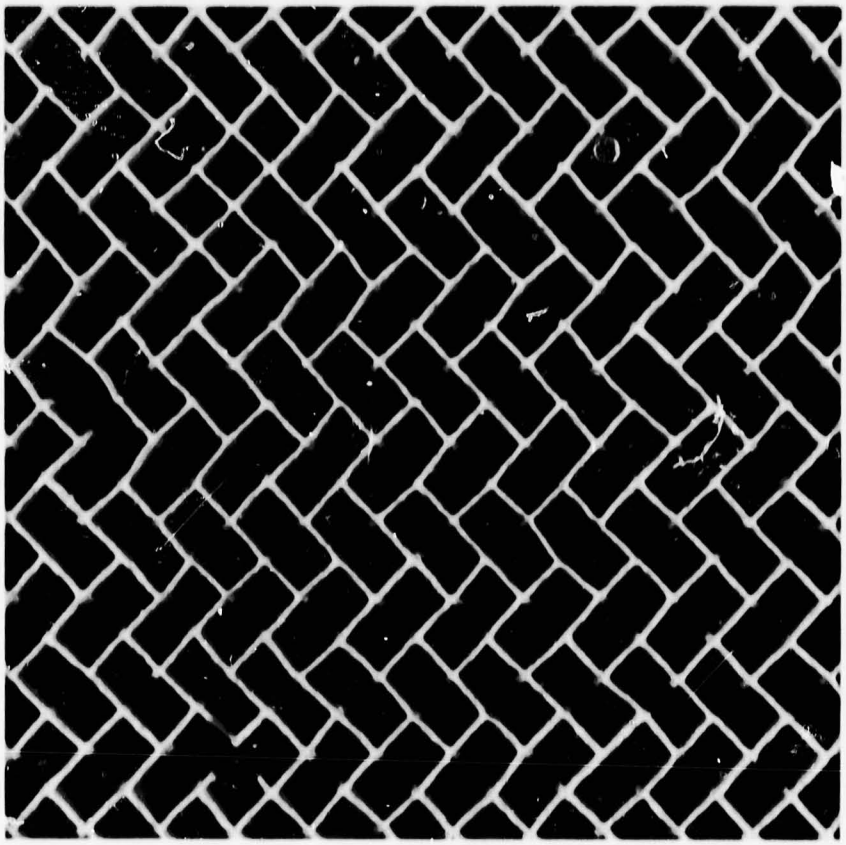

Figure IV.B.1.17 Photograph of Matrix No. 36

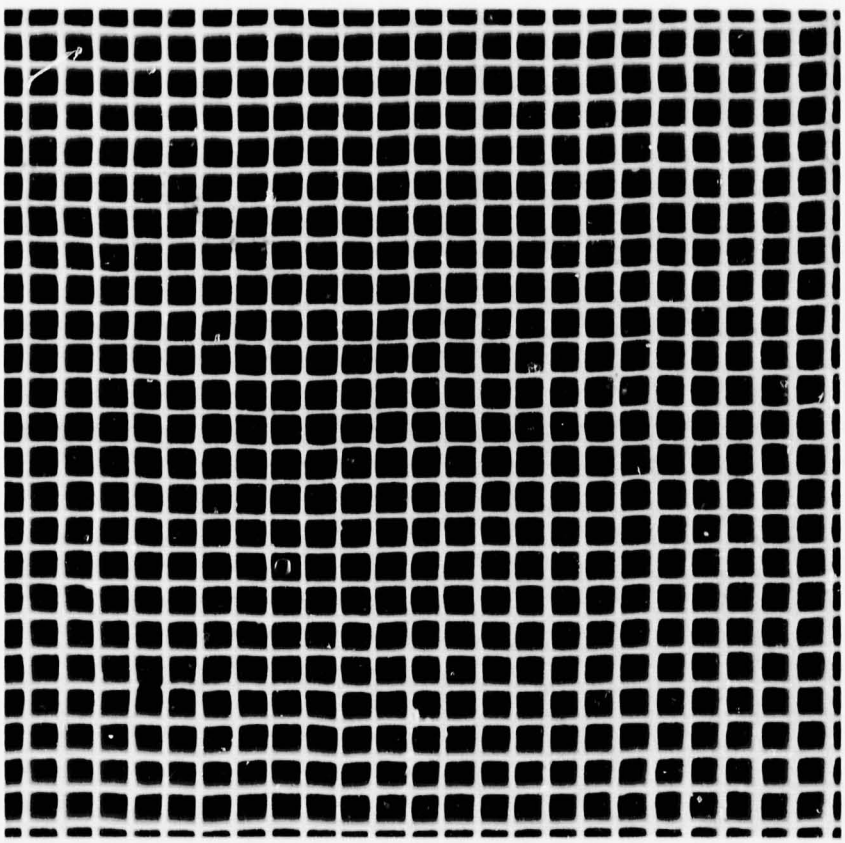

Figure IV.B.1.18 Photograph of Matrix No. 37

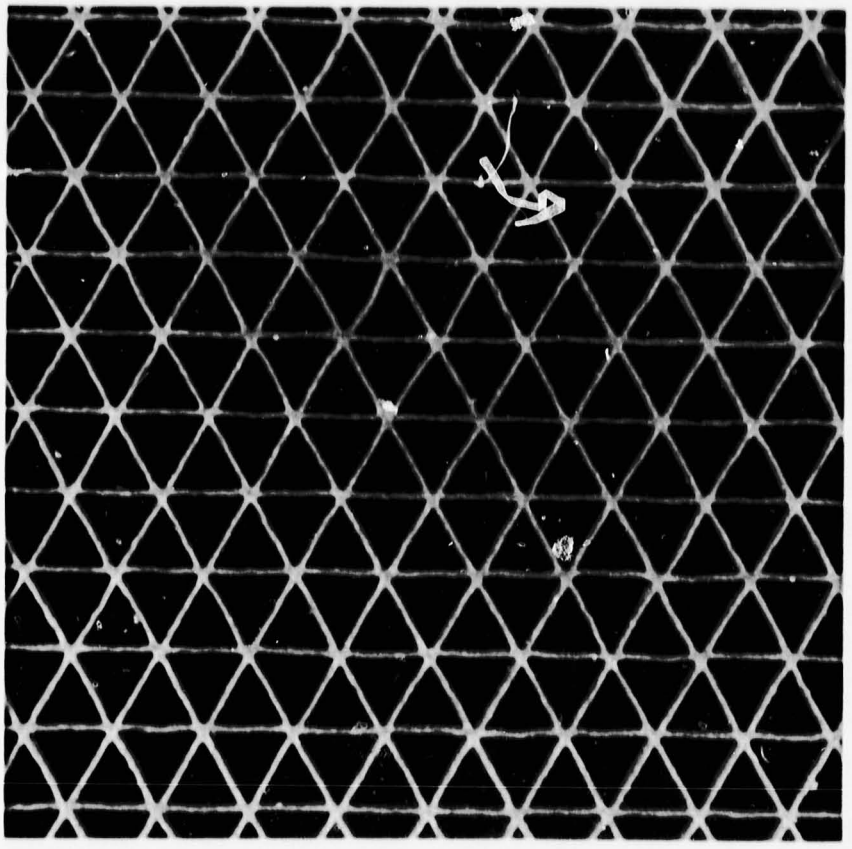

Figure IV.B.1.19 Photograph of Matrix No. 38

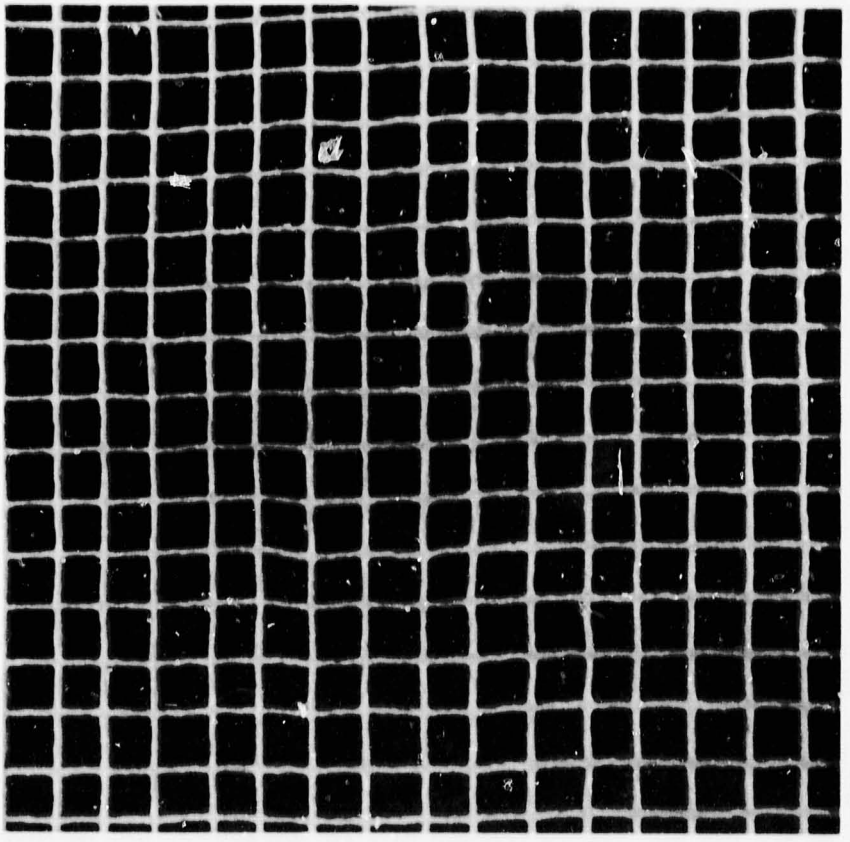

Figure IV.B.1.20 Photograph of Matrix No. 39

The present matrix sample size contains twenty-five rectangular (Core no. 2, 3, 6, 8, 9, 12 thru 17, 21 thru 24, 28 thru 34, 36, 37 and 39), two hexagonal (Core no. 26 and 27), eight sinusoidal (Core no. 1, 5, 7, 10, 11, 19, 20 and 25), and four isosceles triangular (Core no. 4, 18, 35 and 38) fin configurations. In addition, the present sample size represents a good cross section of the different manufacturing processes which are currently being evaluated as follows:

1. Supplier A — Corrugating or extrusion
2. Supplier B — Stacked extruded tubes
3. Supplier C — Corrugating
4. Suppliers D and E — Calendering
5. Supplier I — Extrusion
6. Supplier J — Embossing or stamped sheets

IV.B.2 The Effect of Manufacturing Process on Fin Efficiency

One of the theoretical idealizations of the transient technique utilized by the shuttle rig method of evaluation is that the flow entering the matrix is steady and uniform in velocity and temperature. A flow imbalance can occur within the matrix test sample when fin geometry variance exists. Consequently, this condition can substantially alter the heat transfer characteristics and, to a lesser extent, the pressure drop characteristics (Reference 10). Hence, the shuttle rig provides a true evaluation of the performance characteristics for a particular matrix geometry with respect to shape uniformity and dimensional tolerance limitations inherent in the applicable manufacturing process. Based on the existing matrix sample size, the corrugating, extrusion and calendering fabrication techniques can be evaluated.

Variations in roll pressure during forming, tension during wrapping, and shrinkage rate during firing can induce significant fin shape variance for both the corrugating and calendering processes as shown on Figure IV.B.2.1. In addition, a dispersal of circumferential delaminations (Figure IV.B.2.1) can occur due to variations in bond quality during the wrapping phase of the process.

Although the extrusion process is susceptible to variations in material thickness due to die wear, it has the best potential for fabricating uniform fin shape. Similar to the wrapped processes, the extrusion technique (which inherently eliminates delaminations due to bonding) is susceptible to variations in shrinkage during the firing cycle.

In addition, the condition of the flow passage perpendicular to the air flow can also influence the performance characteristics. As the surface becomes rougher, the flow friction and heat transfer characteristics are both likely to increase. It is difficult to ascertain which parameter will increase at a faster rate without an evaluation in a shuttle rig or equivalent test facility. Obviously, it would be desirable to increase the heat transfer characteristics at a faster rate which would increase the overall fin efficiency (J/F).

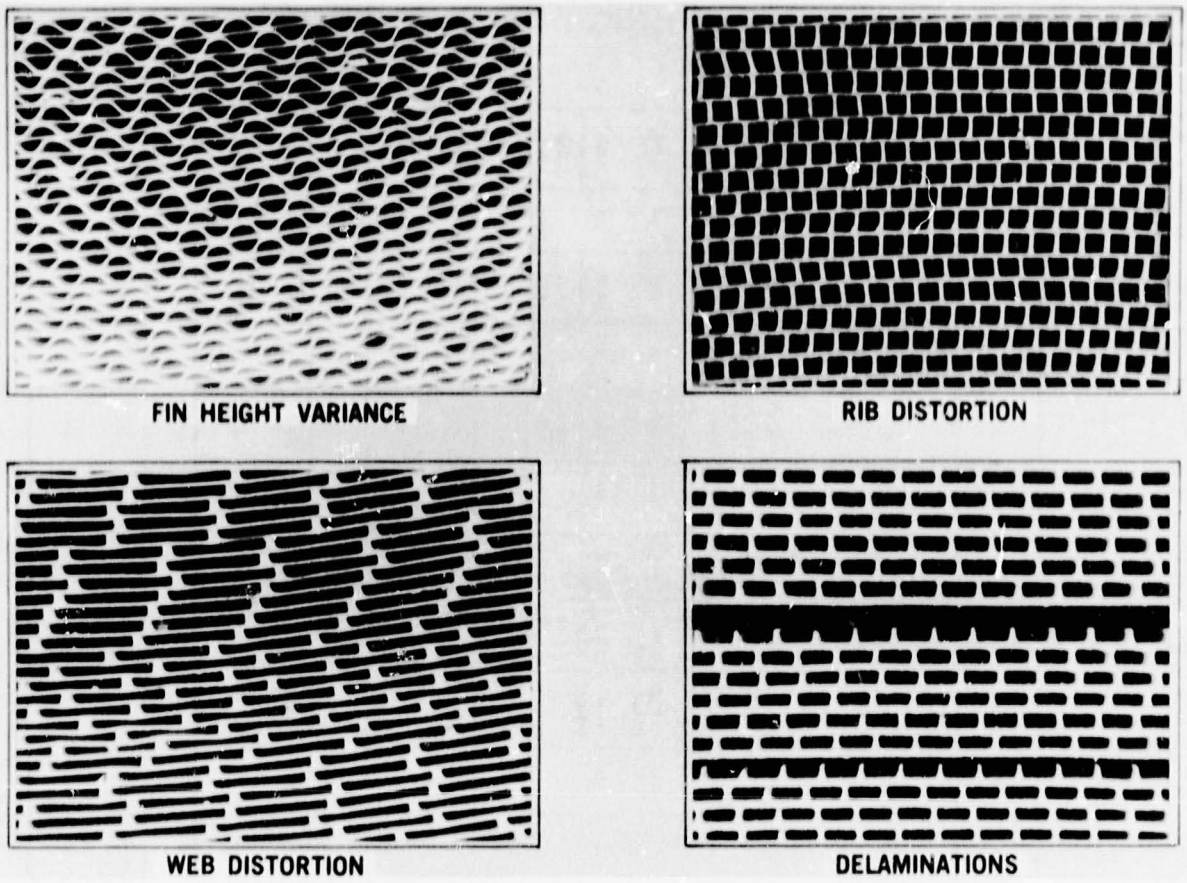

Figure IV.B.2.1 Photographs Illustrating Manufacturing Defects

In order to illustrate the importance of matrix sample quality, similar fin geometries with equivalent hydraulic diameters from the existing sample size (Tables IV.B.1.1 and IV.B.1.2) can be selected. These samples will be compared based on the standard heat transfer (J) and pressure drop (F) characteristics, which are based on the actual geometrical opening with the material wall thickness factored out. For optimum engine performance it is desirable to maximize the heat transfer efficiency and minimize the pressure loss associated with the heat exchanger. Therefore, the effect of matrix sample quality can be estimated by comparing the ratio of the heat transfer (J) to pressure drop (F) characteristics for similar fin geometries.

For the square fin matrix configuration, extruded matrices 12, 28 and 29 can be compared to equivalent embossed matrices 6 and 16 (Table IV.B.2.1). Based on the average performance characteristics for the two fabrication groups, the uniformity of the extruded structures indicates higher heat transfer characteristics (C_2) and lower pressure drop characteristics (C_1). The net result is an improvement of approximately 24% in overall fin efficiency, which is defined as the ratio of heat transfer (C_2) to pressure drop (C_1) characteristics.

To evaluate the effect of matrix sample quality for sinusoidal triangular structures, the pertinent fin parameters for three different examples are listed on Table IV.B.2.1. Matrices no. 10 and 19 were corrugated by Supplier A from the same tooling. Matrix No. 19, which had improved cell geometry uniformity, indicates a 20% improvement in the heat transfer characteristics ($J=C_2\ RE^{X2}$) with equivalent pressure drop characteristics ($F=C_1\ RE^{X1}$).

CODE
R — RECTANGULAR
I.T. — ISOSCELES TRIANGULAR
S.T. — SINUSOIDAL TRIANGULAR
H — HEXAGONAL

$$F = C_1 RE^{X_1} \qquad J = C_2 RE^{X_2}$$

$$\frac{\Delta P \cdot P}{L} = C \frac{WT}{AF}^{1.673} \qquad \frac{NTU}{L} = A\left[\frac{AFT}{W}^{0.673}\right]^{-X_2}$$

CORE NO	SUP-PLIER	TYPE OF FIN	X FINS/CM (FINS/IN)	Y ROWS/CM (ROWS/IN)	N HOLES/CM² (HOLES/IN.2)	S MM (IN.)	B MM (IN.)	H MM (IN.)	PH MM (IN.)	A.R. PH/H	ρ_w g/cc (LB/FT.3)	L/DH	σ	DH MM (IN.)	β M.2/M.3 (FT.2/FT.3)	C X 10⁶	A X 10³	C	X	C_1	X_1	J F @ RE = 100
12	A	R	7.0 (17.8)	7.1 (18)	49.6 (320)	.290 (.0114)	.290 (.0114)	1.123 (.0442)	1.427 (.0562)	1.27	1.67 (104.2)	62	.634	1.130 (.0445)	2244 (684)	46	1.75	16.5	-.1	5.0	-.1	.303
28	A	R	7.9 (20)	7.9 (20)	62 (400)	.165 (.0065)	.165 (.0065)	1.105 (.0435)	1.27 (.050)	1.15	1.68 (104.6)	64	.756	1.105 (.0435)	2736 (834)	37	1.85	15.1	-.1	4.25	-.1	.281
29	A	R	6.9 (17.5)	6.9 (17.5)	47.5 (306)	.279 (.011)	.279 (.011)	1.17 (.046)	1.45 (.057)	1.24	1.69 (105.6)	61	.653	1.17 .0462	2227 (679)	38	1.75	15.1	-.1	5.25	-.1	.348
																		15.6 AVE.		4.83 AVE.		.310 AVE.
6	D	R	6.9 (17.5)	7.5 (19)	51.5 (332)	.300 (.0118)	.300 (.0118)	1.036 (.0408)	1.450 (.0571)	1.40	1.47 (91.4)	67	.615	1.092 (.0430)	2254 (687)	.515	1.55	16.7	-.1	4.28	-.1	.256
16	D	R	6.6 (16.8)	6.7 (17.0)	44.2 (286)	.315 (.0124)	.315 (.0124)	1.179 (.0464)	1.511 (.0595)	1.28	1.51 (94.2)	60	.625	1.186 (.0467)	2106 (642)	.44	1.30	17.1	-.1	4.16	-.1	.243
																		16.9 AVE.		4.22 AVE.		.250 AVE.
10	A	S.T.	14.6 (37)	14.4 (36.5)	209.5 (1351)	.066 (.0026)	.066 (.0026)	.630 (.0248)	1.374 (.0541)	2.18	2.09 (130.4)	128	.767	.549 (.0216)	520 (1707)	1.60	5.9	16.3	-.1	3.29	-.1	.202
19	A	S.T.	15.0 (38)	13.6 (34.5)	203.9 (1311)	.061 (.0024)	.061 (.0024)	.676 (.0256)	1.336 (.0526)	1.98	2.10 (131.0)	122	.787	.579 (.0228)	504 (1653)	1.38	5.50	16.1		3.94	-.1	.245
1	A	S.T.	11.0 (28)	13.0 (33)	143 (924)	.109 (.0043)	.109 (.0043)	.660 (.0260)	1.813 (.0714)	2.75	2.20 (137.0)	121	.673	.589 (.0232)	424 (1392)	1.30	4.55	13.4	-.1	3.34	-.1	.208
20	A	S.T.	10.8 (27.5)	14.6 (37)	157.4 (1018)	.066 (.0026)	.066 (.0026)	.620 (.0244)	1.846 (.0727)	2.98	2.18 (136.3)	107	.780	.592 (.0233)	489 (1605)	1.36	5.00	15.4	-.1	3.19	-.1	.195
5	C	S.T.	9.9 (25)	15.4 (39)	151.1 (975)	.135 (.0053)	.135 (.0053)	.51 (.020)	2.0 (.080)	3.95	1.43 (89.0)	179	.569	.401 (.0158)	530 (1734)	2.25	10.2	9.1	-	.62	-.80	.171
25	C	S.T.	9.9 (25)	12.8 (32.5)	126 (813)	.183 (.0072)	.183 (.0072)	.61 (.024)	2.0 (.080)	3.39	2.33 (145.7)	153	.512	.417 (.0164)	457 (1496)	2.40	4.3	9.4	-.1	2.07	-.1	.220

Table IV.B.2.1 Effect of Matrix Sample Quality on Shuttle Rig Results

Matrix No. 20 was corrugated by Supplier A with a much thinner material using the same tooling that was designed for the thicker material of matrix no. 1. Consequently, the radius of curvature (R) for matrix 20 was increased during the forming process, which reduced the stiffness of the structure. With the reduced stiffness, the variation in fin height and shape was accentuated during the wrapping and firing stages of the process for matrix no. 20. The results indicate a significant increase in the pressure drop characteristics with a slight decrease in heat transfer characteristics. The net result produced an apparent reduction of 22% in overall fin efficiency (J/F) for matrix 20.

This example illustrates the difficulty in comparing performance characteristics of sinusoidal triangular fins with equivalent aspect ratios (PH/H) and hydraulic diameters (DH). Unless the radius of curvature (R) of the structures are also equivalent, the actual shape of the fin configurations can be significantly different. In order to illustrate this, figure IV.B.2.2 depicts sinusoidal triangular configurations with constant aspect ratio and three different radii. This figure clearly illustrates the extreme variance in fin shape that can occur, depending on the radius of curvature (R) induced from the corrugating, wrapping and firing processes. In addition, the degree of blockage in the corners from the bonding process can introduce another significant variable that can affect performance characteristics.

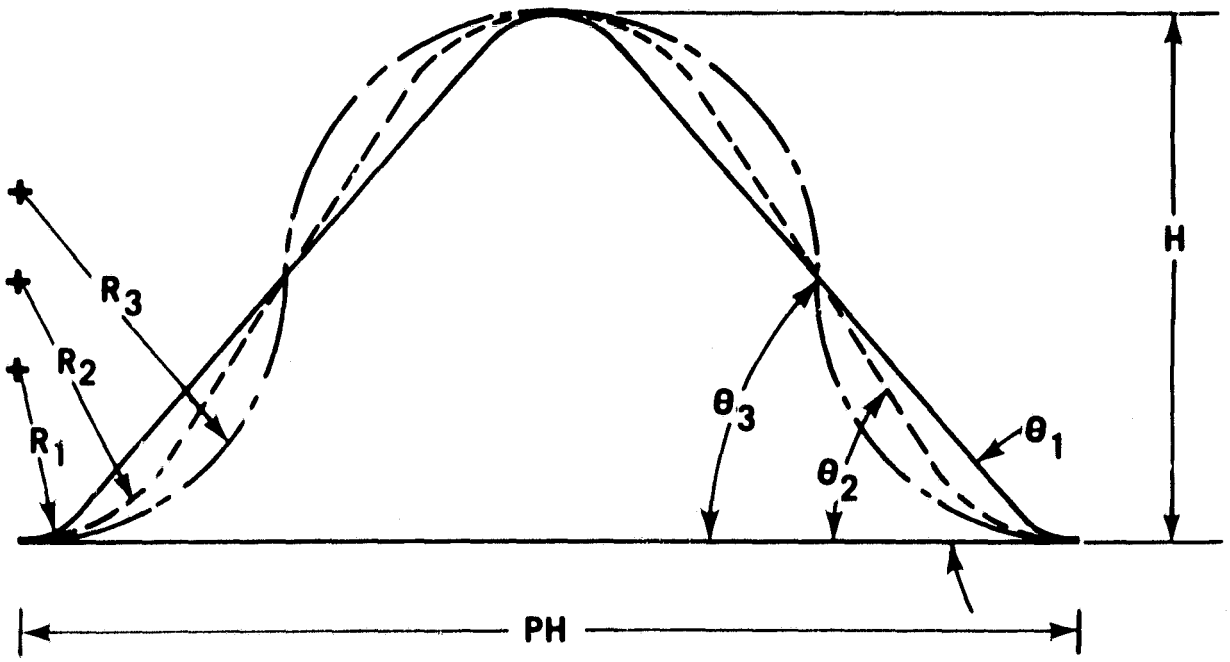

Figure IV.B.2.2 Schematic Illustrating Variation in Sinusoidal Triangular Fin Passage Shape with Respect to Radius of Curvature for a Constant Aspect Ratio

The third example for sinusoidal triangular fins compares matrices 5 and 25 (Table IV.B.2.1) from Supplier C. Matrix 25 was fabricated from a new set of tooling similar to the tooling utilized for matrix 5. The new tooling produced a more uniform structure, which resulted in a significant improvement in overall fin efficiency (J/F).

Based on the examples listed in Table IV.B.2.1, fin shape uniformity can result in a 20 to 25% improvement in overall fin efficiency (J/F) for square and sinusoidal structures with equivalent aspect ratio (PH/H) and hydraulic diameters (DH).

IV.B.3 The Effect of Matrix Fin Geometry on Performance

Based on the shuttle rig test data presented in Section IV.B.1, the effect of matrix fin shape on aerothermodynamic performance can be discussed. In order to evaluate the effect a change in matrix fin shape and/or package size will have on regenerator effectiveness and pressure drop, simplified parametric curves can be utilized. Regenerator pressure drop and effectiveness can be expressed in terms of flow conditions, package size and matrix fin parameters as follows (Reference 11):

$$U_0 \;\&\; (\Delta P/P) = \phi\,(\text{FLOW CONDITIONS}) \cdot (\text{PACKAGE SIZE}) \cdot (\text{FIN PARAMETERS})$$

$$U_0 = \left[\frac{2\mu}{W.PR^{2/3}}\right] \cdot \left[L\,(A_F)\right] \cdot \left[\frac{C_2\,\sigma}{DH^2}\right] \quad (\text{IF: } X_2 = -1)$$

$$\frac{\Delta P}{P} = \left[\frac{2\,\mu\,WRT}{g_C P^2}\right] \cdot \left[\frac{L}{A_F}\right] \cdot \left[\frac{C_1}{\sigma\,DH^2}\right]$$

$$\epsilon = \frac{U_0}{U_0 + 1} \quad (\text{IF: } X^* = 1)$$

Where:

X_2	=	Reynold's No. exponent for Colburn No. ($J = C_2\,RE^{X_2}$)
C_1	=	Fanning Friction Factor Constant for Laminar Flow ($F = C_1/RE$)
C_2	=	Colburn No. Constant for Laminar Flow
σ	=	Open Area Ratio
DH	=	Hydraulic Diameter
W	=	Air Flow Rate
μ	=	Viscosity
R	=	Universal Gas Constant
T	=	Average Temperature
g_C	=	Proportionality Factor in Newton's Second Law
L	=	Flow Length
A_F	=	Frontal Area
ΔP	=	Pressure Drop
P	=	Inlet Pressure
ϵ	=	Effectiveness = $\phi\,(U_0, X^*)$
X^*	=	Flow Capacity Rate Ratio
U_0	=	Number of Heat Transfer Units (NTU)
PR	=	Prandtl Number

Utilizing these expressions for a constant set of regenerator flow conditions, the parametric curves shown on Figure IV.B.3.1 were generated. In order to utilize these curves, the effectiveness and pressure drop must be determined for the refer-

ence or baseline regenerator size and fin geometry at a given set of flow conditions. Once the reference regenerator size and fin geometry have been selected, the following expressions must be determined for each change in fin geometry or package size:

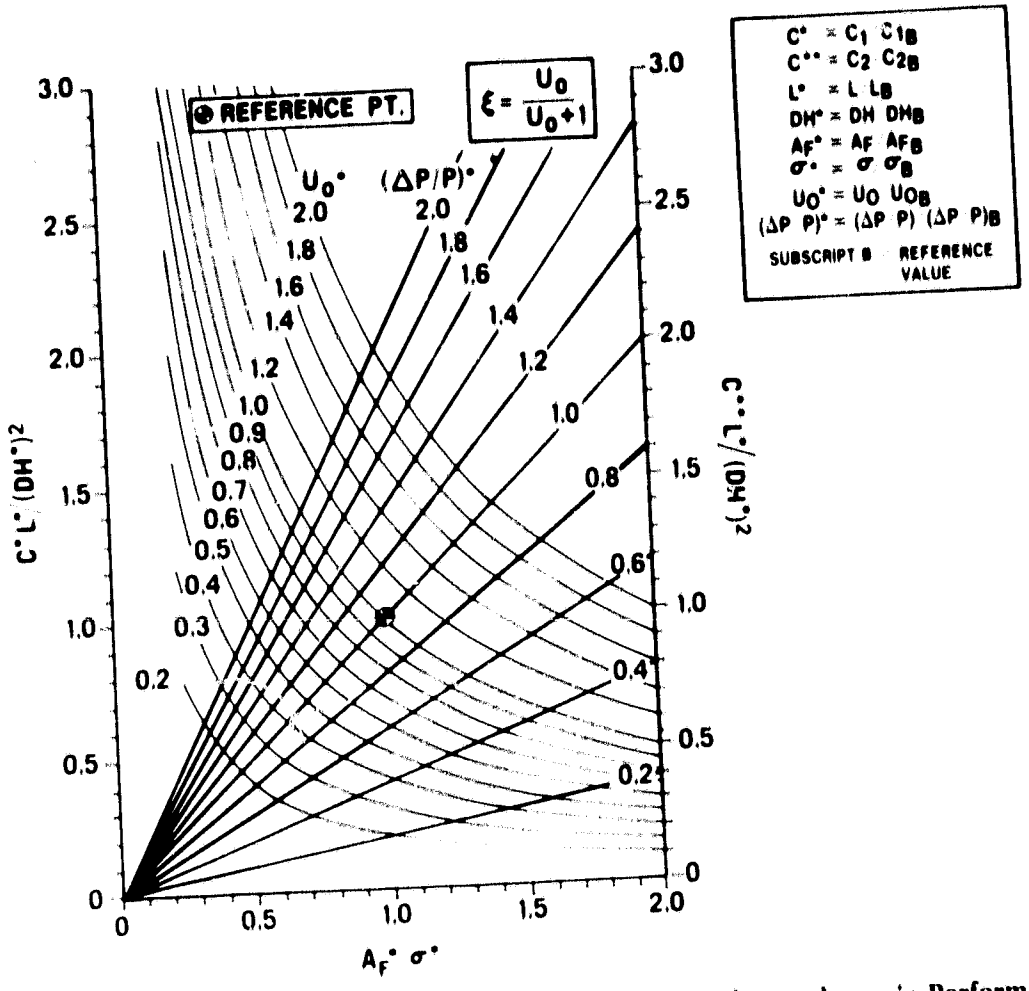

Figure IV.B.3.1 Parametric Curves for Heat Exchanger Thermodynamic Performance

C^* = Ratio of Fanning Friction Factor constant with respect to reference laminar flow Fanning Friction Factor constant, C_1/C_{1B}

C^{**} = Ratio of Colburn No. constant with respect to reference laminar flow Colburn No. constant, C_2/C_{2B}

L^* = Flow length or thickness ratio with respect to reference regenerator thickness, L/L_B

DH^* = Hydraulic diameter ratio with respect to reference fin hydraulic diameter, DH/DH_B

A_F^* = Frontal area ratio with respect to reference regenerator frontal area, A_F/A_{FB}

σ^* = Ratio of open area percentage with respect to reference fin open area ratio, σ/σ_B

U_o^* = Number of heat transfer units ratio with respect to reference regenerator number, U_o/U_{oB}

$\Delta P/P)^*$ = Pressure drop ratio with respect to reference regenerator pressure drop, $(\Delta P/P)/(\Delta P/P)_B$

After the above ratios are determined, the effect of alterations in fin geometry and/or package size can be estimated with respect to the reference or baseline configuration performance, provided the regenerator flow conditions are not altered.

Keeping in mind the considerations discussed for matrix sample quality, a comparison of performance characteristics between the rectangular, square, hexagonal, sinusoidal and isosceles triangular passages can be made. In order to compare matrix fin configurations on an equivalent basis, the hydraulic diameter, wall thickness and flow length should be approximately the same. The parametric curves (Figure IV.B.3.1) for performance were utilized to compare the effect of matrix fin shape.

From the present matrix sample size (Tables IV.B.1.1 and IV.B.1.2) matrices 1 (sinusoidal), 2 (square), 4 (isosceles) and 9 (rectangular) have approximately the same hydraulic diameter and flow length. The standard and alternate heat transfer and pressure drop characteristics for these matrices are repeated on Figures IV.B.3.2 and IV.B.3.3, respectively. Since matrix 1 represents the fin geometry that was utilized for the Ford 707 production turbine engine, it will be selected as the reference configuration. The performance for the production size regenerator at full power conditions is designated as Case A in Table IV.B.3.1. The predicted performance of matrices 2, 4 and 9 for the same size regenerator are listed as Case B, C and D respectively in Table IV.B.3.1.

As expected, the extruded isosceles triangular matrix (4), which had higher heat transfer and lower pressure drop characteristics (Figure IV.B.3.2), resulted in higher effectiveness and lower pressure drop compared to the wrapped corrugated triangular matrix (1). Conversely, the rectangular (9) and square (2) matrices resulted in lower effectiveness than the reference matrix (1) in spite of the superior heat transfer characteristics (Figure IV.3.2). This discrepancy illustrates the importance of material wall thickness.

The reason for this discrepancy is attributed to the severe penalty imposed on the rectangular and square configurations by the significantly greater material thickness (S and B) which creates a significantly lower open area ratio (σ). Consequently, the alternate heat transfer characteristics (Figure IV.B.3.3) allow a direct comparison of existing fin configurations for a fixed regenerator size at identical flow conditions with the material wall thickness factored in. The standard thermodynamic performance characteristics (Figure IV.3.2) are based on the actual opening of the fin configuration with the material wall thickness factored out.

A better comparison of the square, rectangular and sinusoidal configurations could be made if the material thickness were equivalent. To maintain the same F and J characteristics for the square and rectangular surfaces, assuming they could be fabricated with reduced material thickness, the geometrical opening (A Δ) is

kept constant to maintain the same hydraulic diameter by adjusting the cell density (N) proportionately to the material thickness change. Case E and F in Table IV.B.3.1 illustrates the improvement in performance of the square and rectangular passages if the material thickness could be equivalent to that of the sinusoidal.

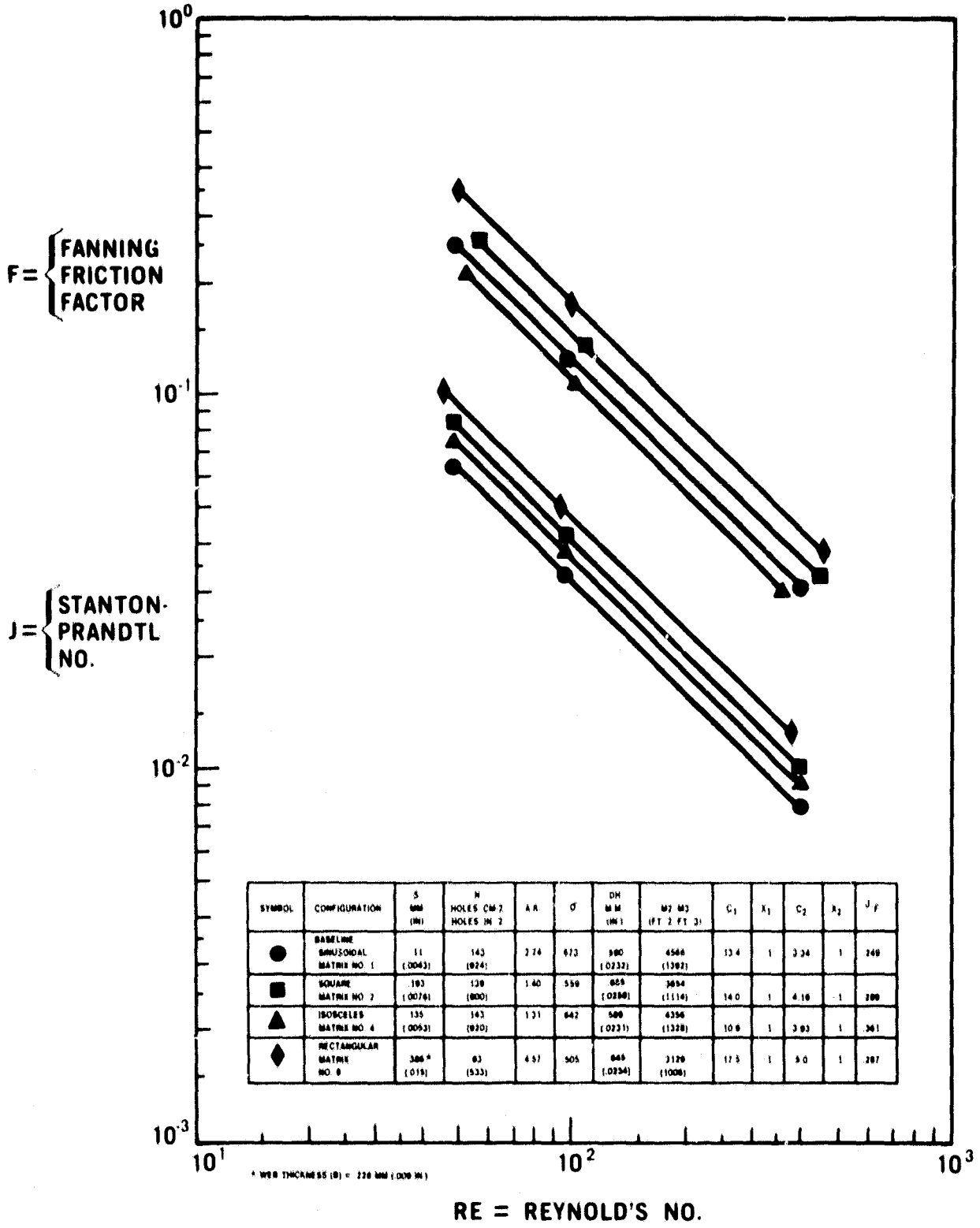

SYMBOL	CONFIGURATION	S MM (IN)	N HOLES CM-2 HOLES IN-2	A.R.	σ	DH MM (IN)	M2 M3 (FT 2 FT 3)	C_1	X_1	C_2	X_2	J_F
●	BASELINE SINUSOIDAL MATRIX NO. 1	11 (.0043)	143 (924)	2.74	673	590 (.0232)	4566 (1393)	13.4	1	3.34	1	249
■	SQUARE MATRIX NO. 2	193 (.0076)	139 (900)	1.40	559	865 (.0280)	3694 (1116)	14.0	1	4.16	1	280
▲	ISOSCELES MATRIX NO. 4	135 (.0053)	143 (920)	1.31	642	598 (.0231)	4356 (1328)	10.9	1	3.93	1	.361
♦	RECTANGULAR MATRIX NO. 9	386 * (.015)	93 (533)	4.57	505	846 (.0234)	3129 (1008)	17.5	1	5.0	1	.287

* WEB THICKNESS (B) = 226 MM (.009 IN.)

Figure IV.B.3.2 Standard Thermodynamic Performance Characteristics for Matrices 1, 2, 4 and 9

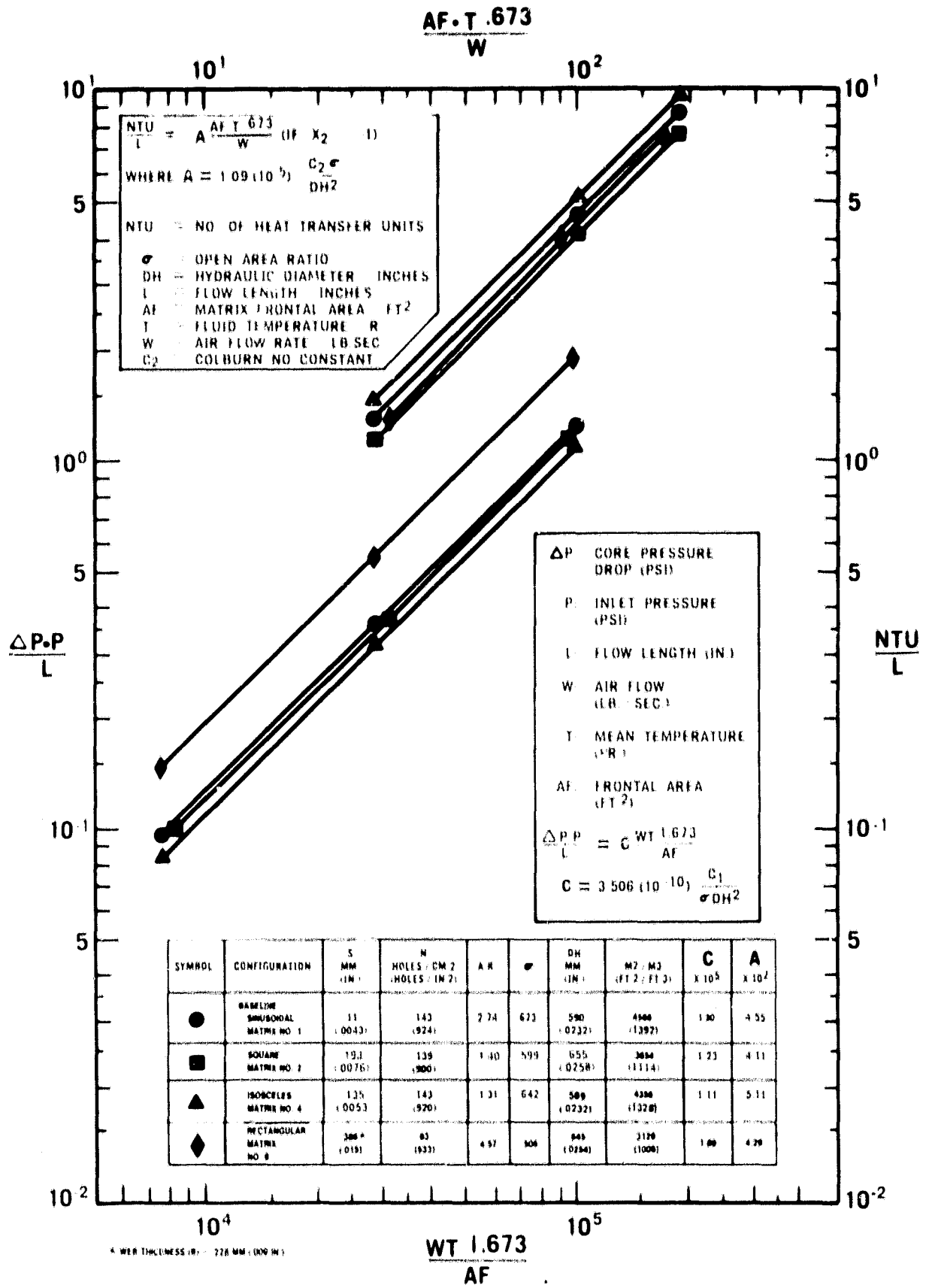

Figure IV.B.3.3 Alternate Thermodynamic Performance Characteristics for Matrices 1, 2, 4 and 9

CODE:
R — RECTANGULAR
SQ. — SQUARE
S.T. — SINUSOIDAL TRIANGULAR
I.T. — ISOSCELES TRIANGULAR

$F = C_1 RE^{-1}$

$J = C_2 RE^{-1}$

$\epsilon = \frac{U_o}{U_o + 1}$

CASE NO	MATRIX NO.	TYPE OF FIN	A_F FT²	L IN	VOL IN³	S IN.	B IN	ϵ	DH IN	AR	C_c	C_f	A_F/A_c	$\frac{C'U'}{(DH')^4}$	$\frac{C'L'}{(DH')^4}$	$(\Delta P/P)^2$	η_c^*	η_o	ϵ %	$(\Delta P/P)_T$ %
A	1	S.T.	3.58	2.82	1454	.0043	.0043	.673	.0232	2.75	13.4	3.34	1	1	1	1	1	6.70	87.0	3.93
B	2	SQ.				.0076	.0076	.599	.0258	1.40	14.0	4.19	.89	.84	1.01	.95	.88	5.90	85.5	3.73
C	4	I.T.				.0053	.0053	.642	.0232	1.31	10.9	3.83	.95	.81	1.18	.87	1.13	7.57	88.3	3.42
D	9	R				.0152	.0090	.505	.0254	4.57	17.5	5.0	.75	1.09	1.25	1.50	.93	6.23	86.2	5.90
E	2 $	SQ.				.0043	.0043	.735	.0258	1.27	14.0	4.19	1.09	.84	1.01	.75	1.10	7.37	88.1	2.95
F	9 $	R				.0043	.0043	.736	.0254	3.90	17.5	5.0	1.09	1.09	1.25	1.0	1.35	9.05	90.0	3.93
G	11	S.T.	3.58	2.82	1454	.0050	.0050	.720	.0305	3.73	14.5	2.79	1	1	1	1	1	3.52	77.9	2.45
H	8	R				.0112	.0084	.611	.0310	5.0	18.4	5.55	.85	1.23	1.91	1.45	1.60	5.63	84.9	3.55
I	24	R				.0164	.0110	.521	.0311	9.10	16.9	4.17	.72	1.12	1.44	1.58	1.00	3.52	77.9	3.87
J	8 $	R				.0050	.0050	.750	.0310	4.67	18.4	5.55	1.04	1.23	1.91	1.18	1.95	6.86	87.3	2 89
K	24 $	R				.0050	.0050	.746	.0311	3.54	16.9	4.17	1.04	1.12	1.44	1.08	1.45	5.10	83.6	2.65

$ — EXISTING MATRIX MODIFIED TO HAVE THE IDENTICAL OPENING WITH REDUCED MATERIAL THICKNESS (S AND B).

Table IV.B.3.1 Comparison of Effectiveness and Pressure Drop Characteristics

A similar comparison can be made between matrix 11 (sinusoidal) and rectangular matrices 8 and 24, since they have equivalent hydraulic diameters. For this example, matrix 11 will be selected as the reference fin with the predicted performance at full power in the Ford 707 production turbine engine listed as Case G in Table IV.B.3.1. Rectangular matrices 8 and 24 listed as Case H and I, respectively, show equal to or higher effectiveness combined with a significant increase in pressure drop compared to the sinusoidal matrix (Case G). Similar to the first example, rectangular matrices 8 and 24 were hypothetically modified to have material thickness equivalent to the reference sinusoidal matrix (11). The predicted performance for the modified rectangular matrices 8 and 24 are listed in Table IV.B.3.1 as Case J and K, respectively. As expected, the difference in effectiveness is even greater compared with the sinusoidal matrix (Case G) with only a slight penalty for pressure drop.

The primary reason for the improved performance of the square and rectangular geometries compared to a sinusoidal structure with equivalent material thickness is attributed to a reduction in boundary layer effects in the corners. In addition, the calendered rectangular fin does not have the double wall regions inherent in the wrapped corrugation process. Consequently, blockage is minimized and the available heat transfer surface area is utilized more effectively.

The relative merits of the hexagonal matrix 27 can be compared to rectangular matrices 17, 22 and 23 in addition to the square matrix 2, since they have approximately the same hydraulic diameter and flow length. The standard and alternate heat transfer and pressure drop characteristics for these matrices are repeated on Figures IV.B.4 and IV.B.5, respectively.

From the standard aerothermodynamic performance characteristics (Figure IV.B.3.4), which are based on the actual geometric opening with the wall material factored out, the hexagonal flow passage has lower heat transfer (J) and pressure drop (F) characteristics compared to the rectangular geometries. Based on the gross

measure of overall fin efficiency (J/F) the rectangular flow geometry appears to be more efficient, which substantiates theoretical predictions (Reference 12) for fully developed laminar flow (L/DH > 100).

The hexagonal flow passage has slightly higher pressure drop (F) characteristics with slightly lower heat transfer (J) characteristics compared to the square passage geometry. Consequently, the overall fin efficiency (J/F) for the square passage geometry appears to be better than the hexagon, for fully developed laminar flow.

The importance of the fin material thickness is illustrated by the alternate performance characteristics (Figure IV.B.5). The extremely thin wall material thickness of .058 mm (.0023 in.) of the hexagonal matrix more than compensates for the lower heat transfer characteristics to produce slightly better heat transfer effectiveness with significantly lower pressure drop compared to the existing square and rectangular matrices.

The examples in this section have served to illustrate the important factors that must be considered when selecting an optimum fin configuration for a given heat exchanger application. When selecting the best existing fin geometry for a given heat exchanger size and flow conditions, the passage geometry, material thickness and limitations of the method of fabrication must all be considered. Utilization of the alternate heat transfer (A) and pressure drop (C) characteristics accounts for all of these factors for matrices fabricated from existing tooling.

When selecting the most efficient fin shape for a new set of tooling, the standard heat transfer (J) and pressure drop (F) characteristics can be utilized, since the material thickness is factored out. Once the desired fin geometry is selected the fabrication technique must be capable of producing the required material thickness and sample quality. This explains how apparently less efficient fin shapes such as the sinusoidal (Case A thru D in Table IV.B.3.1) and the hexagonal (Figures IV.B.3.4 and IV.B.3.5) can yield improved performance for a specific regenerator application due to the ability of the fabrication method to produce a much thinner structure.

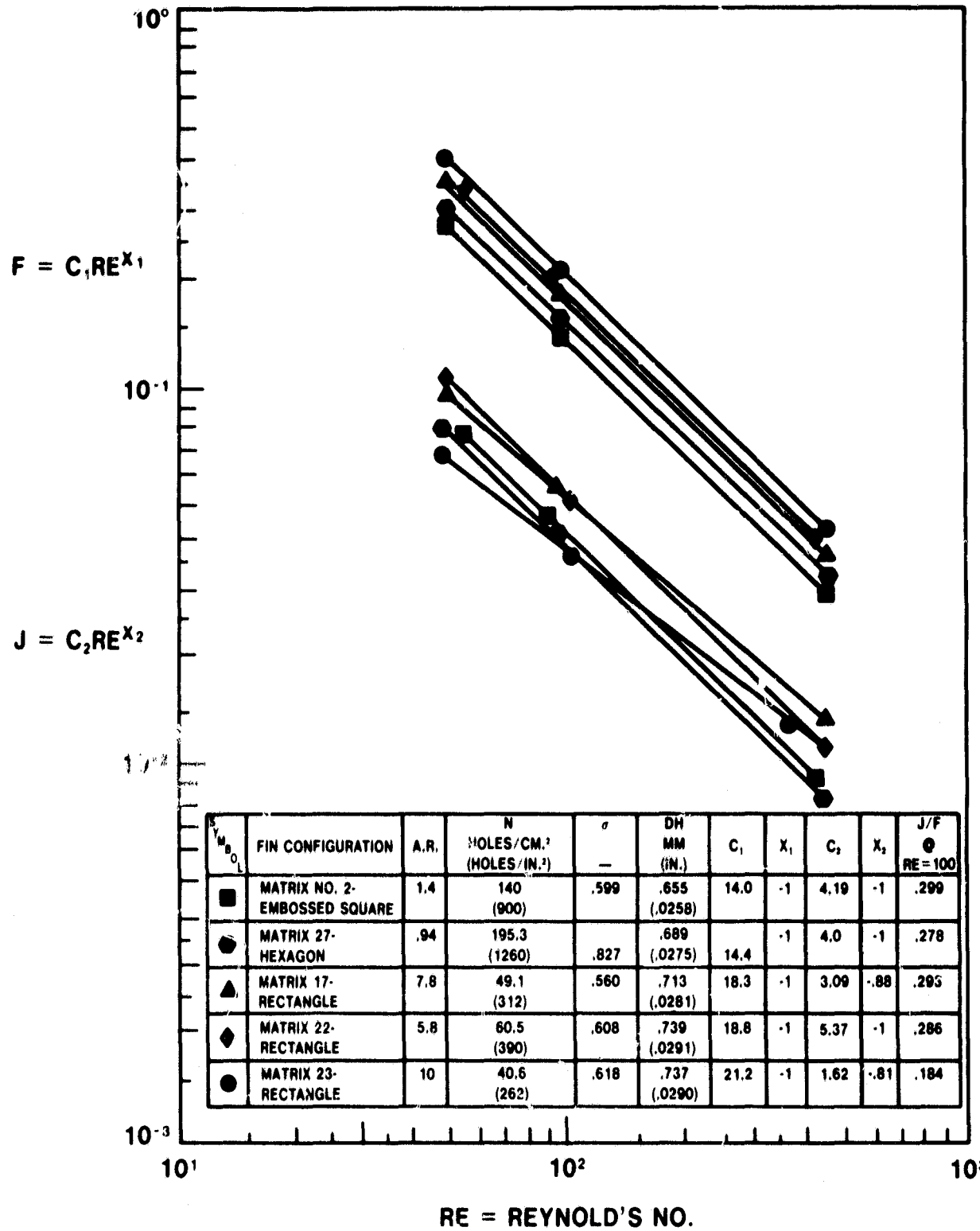

SYMBOL	FIN CONFIGURATION	A.R.	N HOLES/CM.² (HOLES/IN.²)	σ —	DH MM (IN.)	C_1	X_1	C_2	X_2	J/F @ RE=100
■	MATRIX NO. 2- EMBOSSED SQUARE	1.4	140 (900)	.599	.655 (.0258)	14.0	-1	4.19	-1	.299
●	MATRIX 27- HEXAGON	.94	195.3 (1260)	.827	.689 (.0275)	14.4	-1	4.0	-1	.278
▲	MATRIX 17- RECTANGLE	7.8	49.1 (312)	.560	.713 (.0281)	18.3	-1	3.09	-.88	.293
◆	MATRIX 22- RECTANGLE	5.8	60.5 (390)	.608	.739 (.0291)	18.8	-1	5.37	-1	.286
●	MATRIX 23- RECTANGLE	10	40.6 (262)	.618	.737 (.0290)	21.2	-1	1.62	-.81	.184

Figure IV.B.3.4 Standard Thermodynamic Performance Characteristics for Matrices 2, 17, 22, 23 and 27

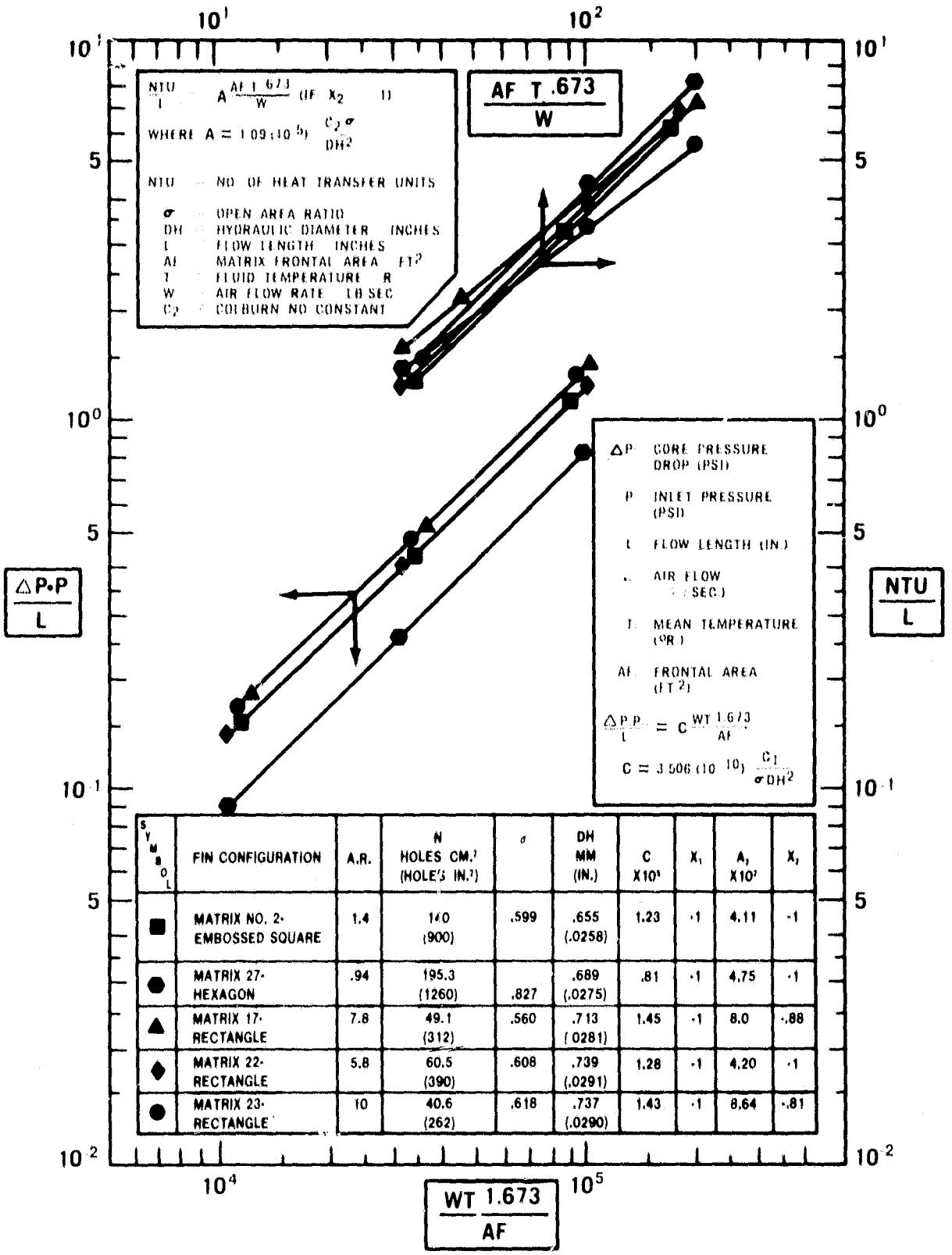

SYMBOL	FIN CONFIGURATION	A.R.	N HOLES CM.² (HOLES IN.²)	σ	DH MM (IN.)	C X10³	X_1	A_1 X10²	X_2
■	MATRIX NO. 2- EMBOSSED SQUARE	1.4	140 (900)	.599	.655 (.0258)	1.23	-1	4.11	-1
●	MATRIX 27- HEXAGON	.94	195.3 (1260)	.827	.689 (.0275)	.81	-1	4.75	-1
▲	MATRIX 17- RECTANGLE	7.8	49.1 (312)	.560	.713 (.0281)	1.45	-1	8.0	-.88
◆	MATRIX 22- RECTANGLE	5.8	60.5 (390)	.608	.739 (.0291)	1.28	-1	4.20	-1
●	MATRIX 23- RECTANGLE	10	40.6 (262)	.618	.737 (.0290)	1.43	-1	8.64	-.81

Figure IV.B.3.5 Alternate Aero-Thermodynamic Performance Comparison for Matrices 2, 17, 22, 23 and 27

IV.B.4 Influence of Aspect Ratio

Theoretical solutions for laminar flow, forced convection, heat transfer and flow friction available in the literature (Reference 12) are dependent on the accuracy of definition of the geometry and a limited number of boundary conditions that are not well duplicated in actual practice or even in the laboratory. In addition, the theoretical solutions apply only to fully developed laminar flow, which requires the length to hydraulic diameter ratio (L/DH) be greater than 100. Depending on the degree of variation in the matrix fin shape uniformity, length to hydraulic diameter ratio and actual thermal boundary condition imposed by the application environment, the disparity between computed and actual performance characteristics can be significant.

With the shuttle rig technique, limitations inherent in the applicable manufacturing process that influence matrix fin shape and uniformity are automatically accounted for. In addition, deviations from fully developed laminar flow can also be evaluated. Therefore, design predictions based on performance characteristics determined from shuttle rig test data will minimize the disparity between computed and actual heat exchanger performance.

Keeping in mind the matrix performance considerations discussed above and utilizing the test data accumulated at this time on rectangular and sinusoidal triangular surfaces, the effect of aspect ratio and length to hydraulic diameter on performance characteristics can be investigated.

For the rectangular fin configuration, aspect ratio (A.R.) is defined as the ratio of the distance between rib centerlines (PH) to the rib height (H), as shown on Figure IV.A.4. In effect this definition specifies the groove spacing and depth from the embossing roll after firing shrinkage has occurred. Theoretical predictions for performance characteristics are based on the aspect ratio of the actual opening (PH-S/H). In order to evaluate the rectangular configurations on an equivalent basis with theory, the effect of aspect ratio of the actual opening (PH-S/H) will be evaluated. For the present rectangular fin sample size (21 matrices) the modified aspect ratio (PH-S/H) variance is 1.0 to 9.1 while the length to hydraulic diameter ratio varies from 47 to 109. To evaluate the effect of aspect ratio on performance, only the matrices approaching fully developed laminar flow will be considered (L/DH > 90). Theoretically the slope (X_2) of the Colburn No. (J) characteristics should be -1 for fully developed laminar flow. Depending on matrix sample quality and actual laminar flow condition (L/DH), the slope of the heat transfer characteristic can be less than -1. Since 20% of the rectangular samples evaluated have a slope less than -1, a comparison of heat transfer characteristics will depend on the Reynold's No. range selected. Based on the predominant operating range for the Ford 707 gas turbine engine, the Reynold's No. range selected for discussion will be 100 to 200. The normal Colburn No. Constant (C_2) for laminar flow can be modified as follows:

$$J = C_2 \, RE^{X_2} \qquad \text{or} \qquad C_2 = \frac{J}{RE^{X_2}}$$

Let: $C_2' = J_{RE} \cdot RE$ Where: J_{RE} = value of Colburn No. at a given Reynold's No.

If: $X_2 = -1$; then $C_2' = C_2$

The effect of aspect ratio on performance characteristics for rectangular matrices approaching fully developed laminar flow is shown on Figure IV.B.4.1. The pressure drop characteristics agree very well with theoretical predictions. As expected, within the limits of sample quality, the heat transfer characteristics appear to improve with increasing aspect ratio up to a value of 7. When the aspect ratio exceeds a value of 7, the expected improvement appears to be offset by excessive cell geometry distortion. This is not surprising due to the susceptibility of the high aspect ratio rectangular fins to back web distortion (Figure IV.B.2.1). Since the heat transfer characteristics increase at a lower rate than the pressure drop characteristics, overall fin efficiency ($J/F = C_2'/C_1$) appears to decrease slightly with increasing aspect ratio.

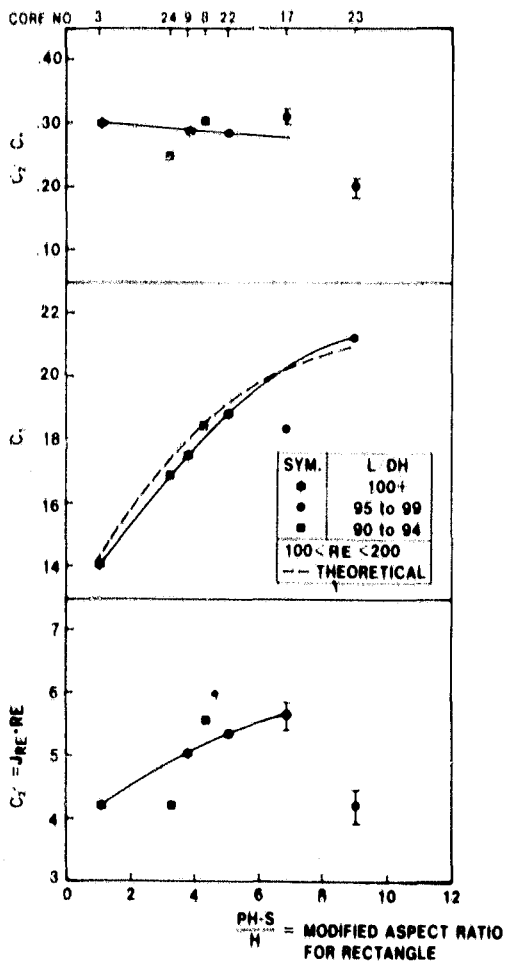

Figure IV.B.4.1 Performance Characteristics for Rectangular Fins vs. Aspect Ratio

To eliminate the influence of fin shape for the evaluation of the effect of L/DH on performance characteristics, rectangular configurations that are essentially square (modified aspect ratio, PH-S/H< 1.1) were selected (Figure IV.B.4.2). In ad-

dition, these matrices were segregated into the two different fabrication methods, embossed and extruded, to take into account matrix uniformity. The pressure drop characteristics for the entire sample appear to decrease approaching fully developed laminar flow (L/DH>90). The improved uniformity associated with the extruded structures appear to have higher heat transfer characteristics (C_2') compared to the embossed matrices, which remain essentially constant for the L/DH range evaluated. Consequently, the net effect appears to be a slight increase in overall fin efficiency (C_2'/C_1) approaching fully developed laminar flow.

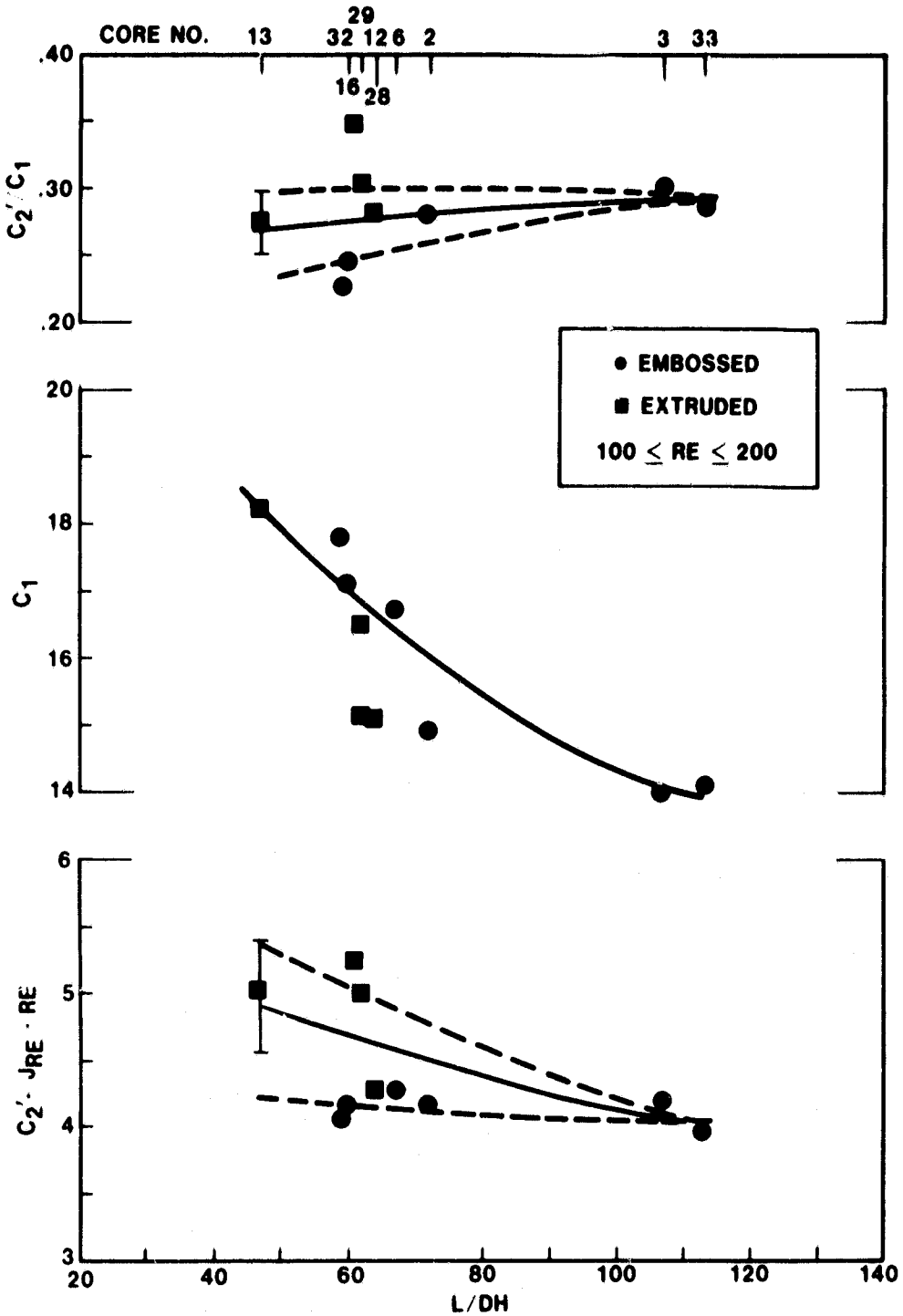

Figure IV.B.4.2 Effect of Length to Hydraulic Diameter Ratio for Square Fins

For a similar evaluation of sinusoidal triangular passages the aspect ratio must be modified in a different manner as shown on Figure IV.B.4.3 to attain an equivalent basis with theory for the actual opening. Performance characteristics of the sinusoidal matrices that approach fully developed laminar flow are shown on Figure IV.B.4.4 with respect to the modified aspect ratio [(PH-2K)/(H-S)]. Although the pressure drop characteristics exhibit the same general trend as the theory, the correlation is not good. Unlike the rectangular surfaces the heat transfer characteristics diminish with increasing aspect ratio. Similar to the rectangular passage, the net result is that overall fin efficiency appears to decrease with increasing aspect ratio.

The scatter in the pressure drop data substantiates the difficulty in comparing performance characteristics of sinusoidal configurations on the basis of aspect ratio, unless the radii of curvature (R) of the corrugations are equivalent. The significance of the radius of curvature was previously discussed in Section IV.B.2 and illustrated on Figure IV.B.2.2.

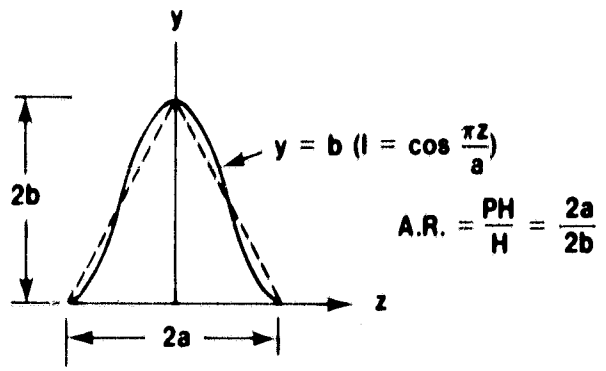

IDEALIZED SINUSOIDAL PASSAGE

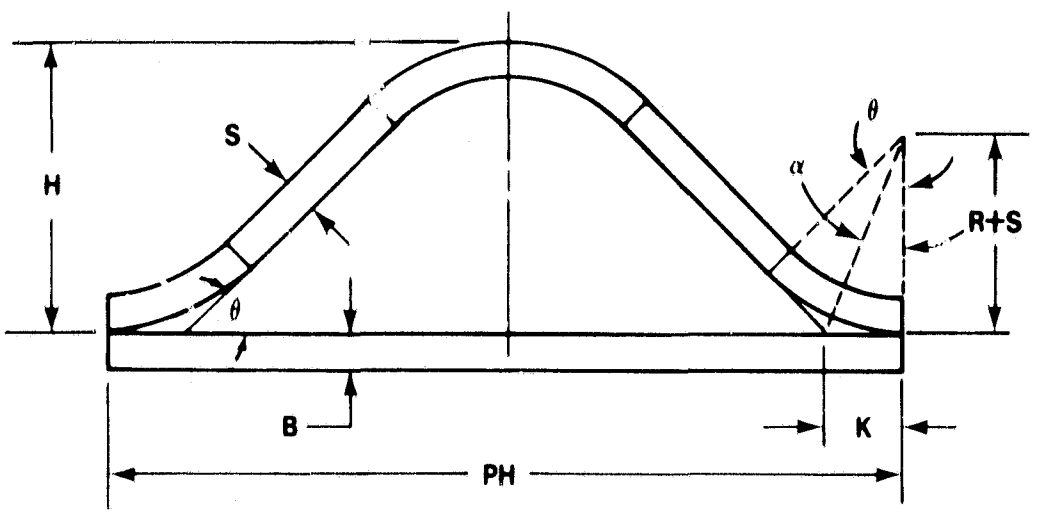

$$\text{TAN } \alpha = \text{TAN } \left(\frac{\theta}{2}\right) = \frac{K}{R+S} \quad \text{OR} \quad K = (R + S)\ \text{TAN } (\theta/2)$$

$$\text{A.R.}' = \text{MODIFIED ASPECT RATIO} = \frac{PH-2K}{H-S} = \frac{PH-2\ (R+S)\ \text{TAN } (\theta/2)}{H-S}$$

EQUIVALENT SINUSOIDAL PASSAGE

Figure IV.B.4.3 Illustration of Ideal and Equivalent Sinusoidal Passage

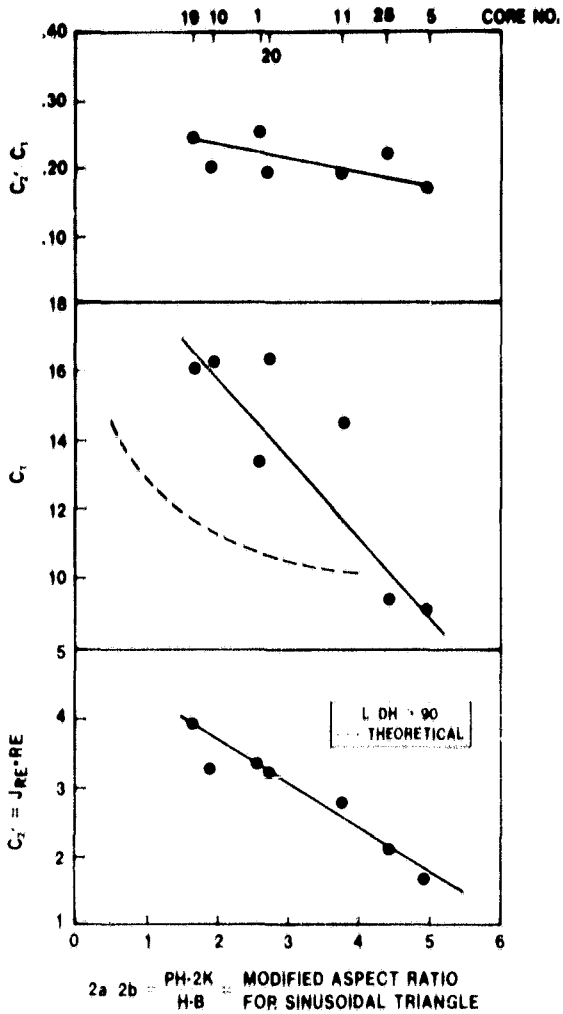

Figure IV.B.4.4 **Performance Characteristics for Sinusoidal Triangular Fins vs. Aspect Ratio**

Unlike the rectangular fin sample size, the present group of sinusoidal surfaces is devoid of a large group of samples for a given aspect ratio with a large variance for length to hydraulic diameter ratio. Consequently, the existing sample size must be subdivided into three sub-groups in an attempt to attain a preliminary estimate of the influence of L/DH on performance (Figure IV.B.4.5). Similar to the square passage, within the limits of the expected increased scatter in the data, both the heat transfer and pressure drop characteristics appear to decrease with increasing L/DH. The overall fin efficiency (J/F) does not appear to be influenced by the laminar flow regime. Additional samples are required before a firm conclusion can be made.

Matrices 30 (Figure IV.B.1.10) and 31 (Figure IV.B.1.11) represent the initial attempt to evaluate the effect of interrupting the flow in the axial direction with a wavy flow passage (Figure IV.B.1.12). These samples consist of layered stamped sheets bonded together. The stamping dies were machined to attain an equivalent rib height (H) and spacing (PH) for each structure.

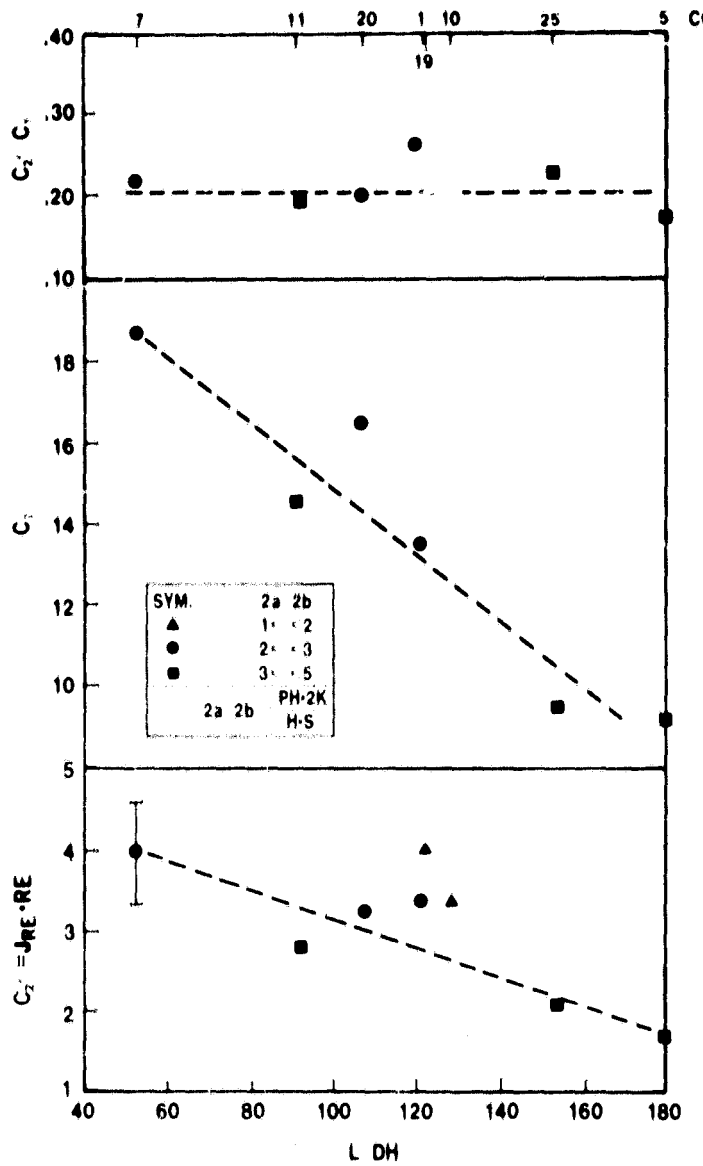

Figure IV.B.4.5 Effect of Length to Hydraulic Diameter Ratio for Sinusoidal Triangular Fins

The wavy flow passage incorporated in matrix 31 (Figure IV.B.1.12) resulted in an increase in L/DH of approximately 3%. The effect of interrupting the flow can be estimated by comparing the laminar flow pressure drop (C_1) and heat transfer (C_2) constants for matrices 30 and 31 from Table IV.B.1.2. Matrix 31 indicates an increase of 20% for the heat transfer constant (C_2) when compared to the straight-thru passage of matrix 30. Concurrently, the wavy flow passage increased the pressure drop constant (C_1) 17.5%. The net result is that the wavy flow passage increased the overall fin efficiency (C_2/C_1) by 2%.

The data presented in this section substantiated the importance of manufacturing process considerations with respect to matrix fin geometries that was discussed in Section IV.B.3. Two additional factors that must be considered have also been illustrated.

When selecting a matrix fin geometry for a fixed size heat exchanger the effect of length to hydraulic diameter should be considered. If the L/DH of the particular application is significantly different than the matrix test sample flow conditions, the performance characteristics of the matrix fin geometry should be adjusted accordingly.

Another factor to be considered in the selection of the optimum matrix fin geometry for a particular application is the trade-off in engine performance with respect to heat exchanger effectiveness and pressure drop. In general, engine specific fuel consumption (SFC) and horsepower (HP) are influenced by heat exchanger effectiveness (ϵ) and pressure drop (Δ P/P), respectively. If SFC is a more important factor for a given engine application, then overall fin efficiency (J/F) considerations are not adequate for proper matrix geometry selection. For example, the heat transfer characteristics for the rectangular matrix geometry increase significantly with increasing aspect ratio (Figure IV.B.4.1), provided the matrix non-uniformity is minimized. At the same time the overall fin efficiency (J/F) decreases with increasing aspect ratio. Therefore, a rectangular fin with a high aspect ratio might be a better fin selection even though the overall fin efficiency (J/F) is reduced.

C. TASK SUMMARY

Since the start of this program with NASA in October 1976 nineteen matrices were evaluated in the shuttle rig. This exceeds the twelve sample task objective. Together with the twenty matrices evaluated previously the existing matrix sample size is thirty-nine. Twenty-five rectangular, eight sinusoidal, four isosceles triangular, and two hexagonal configuration comprise the present matrix sample size.

In addition, the present sample size represents a good cross-section of the different manufacturing processes which are currently being evaluated as follows:

1. Supplier A	— Corrugating or extrusion
2. Supplier B	— Stacked extruded tubes
3. Supplier C	— Corrugating
4. Suppliers D and E	— Calendering
5. Supplier I	— Extrusion
6. Supplier J	— Embossing or stamped sheets

Several factors that merit design considerations in the utilization of this test data were illustrated as follows:

1. Matrix Quality
2. Fin Geometry
3. Aspect Ratio
4. Length to Hydraulic Diameter

Aerothermodynamic performance characteristics can be significantly altered by variations in fin shape uniformity, bond quality and surface roughness. Based on the present matrix sample size, up to 25% variation in overall fin efficiency can occur due to manufacturing process limitations.

Utilizing overall fin efficiency (J/F) as a basis for comparison, and considering matrix fin configurations with equivalent hydraulic diameter, material thickness, and flow length, the effect of fin geometry can be summarized as follows:

1. The sinusoidal triangular structure appears to be the least efficient fin configuration. An increase in heat transfer efficiency accompanied by an increase in pressure drop can be obtained by reducing the aspect ratio of this type of surface geometry to approach the extruded isosceles triangular structure.

2. For embossed rectangular structures, heat transfer and pressure drop characteristics appear to increase with increasing aspect ratio.

When selecting a matrix fin geometry for a fixed size heat exchanger the effect of length to hydraulic diameter should be considered. If the L/DH of the particular application is significantly different than the matrix test sample flow conditions, the performance characteristics of the matrix fin geometry should be adjusted accordingly.

The first attempt to evaluate the effect of a wavy flow passage was completed. The wavy flow passage increased the heat transfer and pressure drop characteristics 20% and 17.5% respectively for a 2% improvement in overall fin efficiency.

The examples in this section have served to illustrate the important factors that must be considered when selecting an optimum fin configuration for a given heat exchanger application. When selecting the best existing fin geometry for a given heat exchanger size and flow conditions, the passage geometry, material thickness and limitations of the method of fabrication must all be considered. Utilization of the alternate heat transfer (A) and pressure drop (C) characteristics accounts for all of these factors for matrices fabricated from existing tooling.

When selecting the most efficient fin shape for a new set of tooling, the standard heat transfer (J) and pressure drop (F) characteristics can be utilized, since the material thickness is factored out. Once the desired fin geometry is selected, the fabrication technique must be capable of producing the required material thickness and sample quality. This explains how an apparently less efficient fin shape (sinusoidal) can yield improved performance for a specific regenerator application due to the ability of the fabrication method to produce a much thinner structure.

TASK V. DESIGN STUDIES OF ADVANCED REGENERATOR SYSTEMS

V.A. INTRODUCTION

Since 1973, design studies of ceramic heat exchanger systems have been carried out in order to analytically evaluate the thermal and structural performance of the various supplier's matrices and to compare different drive, mounting, seal and stress relief schemes. Two types of rotary heat exchangers have been studied: a regenerator sized for the Ford 707 gas turbine engine and a preheater sized for the Ford Stirling engine. The regenerator has a 710mm (28.2 in) outside diameter and is 77mm (2.86 in) thick. The preheater has a 460mm (18.04 in) outside diameter, a 190mm (7.50 in) inside diameter, and is 41mm (1.6 in) thick. These ceramic heat exchanger systems have been analyzed for temperature inlet conditions of 800°C (1472°F) and 1000°C (1832°F) (Ref. 1,2). Task V of the NASA/Ford Ceramic Regenerator Program deals with design studies emphasizing regenerator system materials and configurations intended to improve aerothermodynamic performance, reduce thermal stress, and provide for higher temperature operation.

V.B. DISCUSSION

V.B.1 Material Properties

Material properties have been defined for the following matrix structures:

1. Thin-wall wrapped sinusoidal AS material from Supplier A.

2. Extruded isosceles triangular MAS material from Supplier I.

3. Embossed rectangular MAS material from Supplier D.

In order to more accurately predict the structural performance of thin-wall aluminum silicate regenerators, a study was undertaken to statistically characterize the physical properties of the thin-wall matrix. The radial and tangential strain tolerance and the radial compressive strength of several specimens cut from three Supplier A thin-wall aluminum silicate regenerator cores were determined.

The modulus of rupture and modulus of elasticity were measured using a four-point bend test. Specimen dimensions were 150mm x 25mm x 12.5mm (6.0 in x 1.0 in x 0.5 in). The loading spans were 100mm and 50mm (4.0 in and 2.0 in). The specimen faces were ground flat and parallel to ± .025mm (.001 in).

Compressive strength was measured using 50mm x 50mm x 50mm (2.0 in x 2.0 in x 2.0 in) specimens loaded to failure in a testing machine at a cross-head speed of 5mm/min (0.2 in/min). Upper and lower specimen surfaces were ground flat and parallel to ± .025mm (.001 in). In order to provide uniform loading, thin elastomer sheets were incorporated on the specimen loaded surfaces.

A Weibull failure distribution at a 90% confidence band was determined for each type of specimen from each of the three regenerator cores. The method em-

ployed uses a least squares approximation if a statistically significant difference existed between the Weibull distributions for the three different cores. This program uses a two-sided test for significance at the 0.1% level.

Significant differences in the Weibull distributions between cores would seem to be the result of processing variations rather than fundamental material property differences. In light of this, the Weibull distribution was determined for the aggregate data from the three cores to provide an estimate of the greatest variance that may be expected. This information is plotted in Figures V.B.1.1 through V.B.1.5 and the B_{10} and B_{50} values are listed in Table V.B.1.1.

A statistical evaluation of the radial and tangential flexure strength and modulus was carried out for the Supplier I extruded MAS matrix incorporating an isosceles triangular fin with a wall thickness of .135mm (.0053 in). Test specimens were cut from 51mm (2 in) square sample extrusions. For these samples, the radial direction was considered to be perpendicular to the matrix separator sheets. Specimen dimensions were 51mm x 13mm x 13mm (2.0 in x 0.5 in x 0.5 in) and the loading spans were 38mm and 13mm (1.5 in and 0.5 in). As always, the specimen faces were ground flat and parallel to ± .025mm (.001 in). Weibull plots of the strength and modulus data are presented in Figures V.B.1.6 through V.B.1.10.

Flexure strength and elastic modulus data, as well as radial compressive strength data were also generated from three matrices for the Supplier D embossed rectangular fin MAS-2 material incorporating a wall thickness of approximately 0.193mm (0.0076 in). Weibull plots of the strength and modulus data are presented in Figures V.B.1.11 through V.B.1.15. A summation of the physical properties for the three materials evaluated are listed in Table V.B.1.1.

As reported in Task I, the thin-wall AS structure has experienced separations in the elastomer-matrix bond area due to the significant reduction in strength associated with the thinner cross-section of the matrix walls. In order to characterize this structure more completely, the tangential shear strength of the matrix was investigated.

Four shear specimens cut from a Supplier A thin-wall regenerator were tested. The test results for the limited number of specimens (Figure V.B.1.16) indicate an average tangential shear strength of 393 KPa (57 psi).

For the purpose of calculating the shear stress imposed on a regenerator core by the drive system, a regenerator was assumed to be rigidly clamped at the seal midwidth, and subject to a torque equal to the seal drag torque, which is estimated to be 700 ft.-lb. during a cold start. The maximum shear stress is then estimated to be 131 KPa (19 psi).

This would indicate that the specimens tested provide a safety factor of 3 against shear failure. A general statement concerning the resistance of the thin-wall matrix to shear stress failure cannot be made, since the number of specimens tested was too small to provide a meaningful statistical evaluation of shear strength.

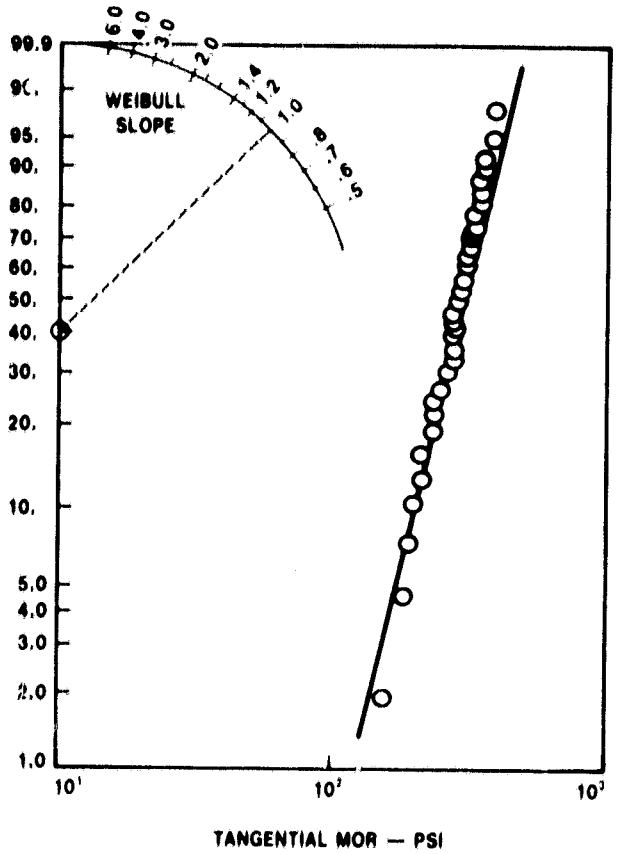

Figure V.B.1.1 Supplier A Thin-Wall AS Tangential MOR

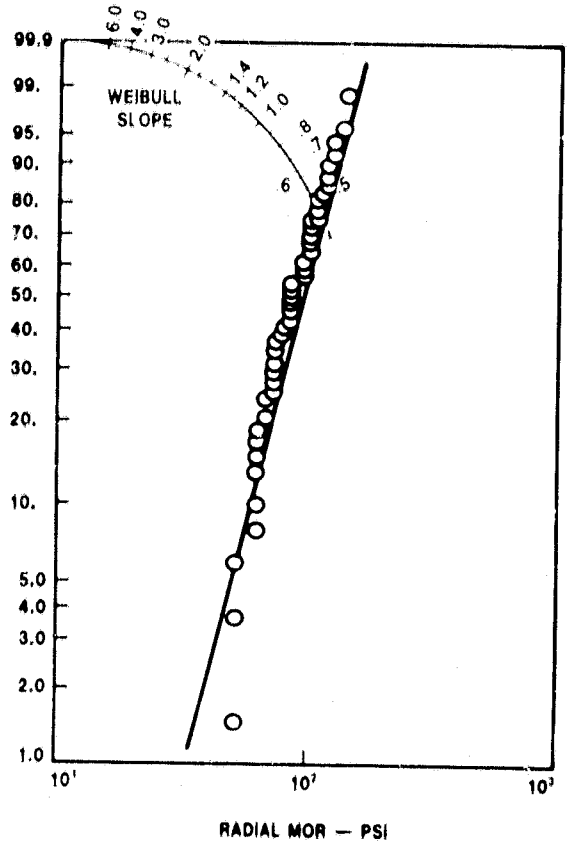

Figure V.B.1.2 Supplier A Thin-Wall AS Radial MOR

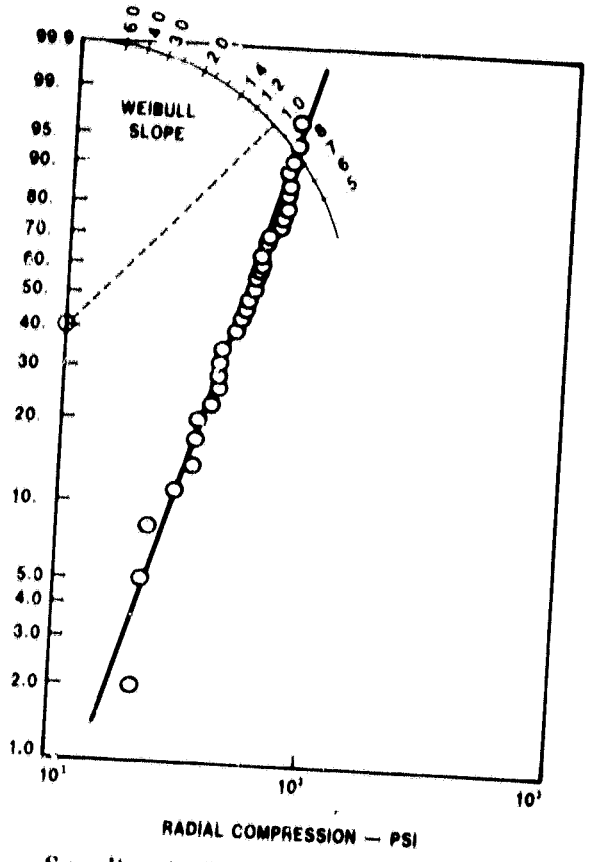

Figure V.B.1.3 Supplier A Thin-Wall AS Radial Compression Strength

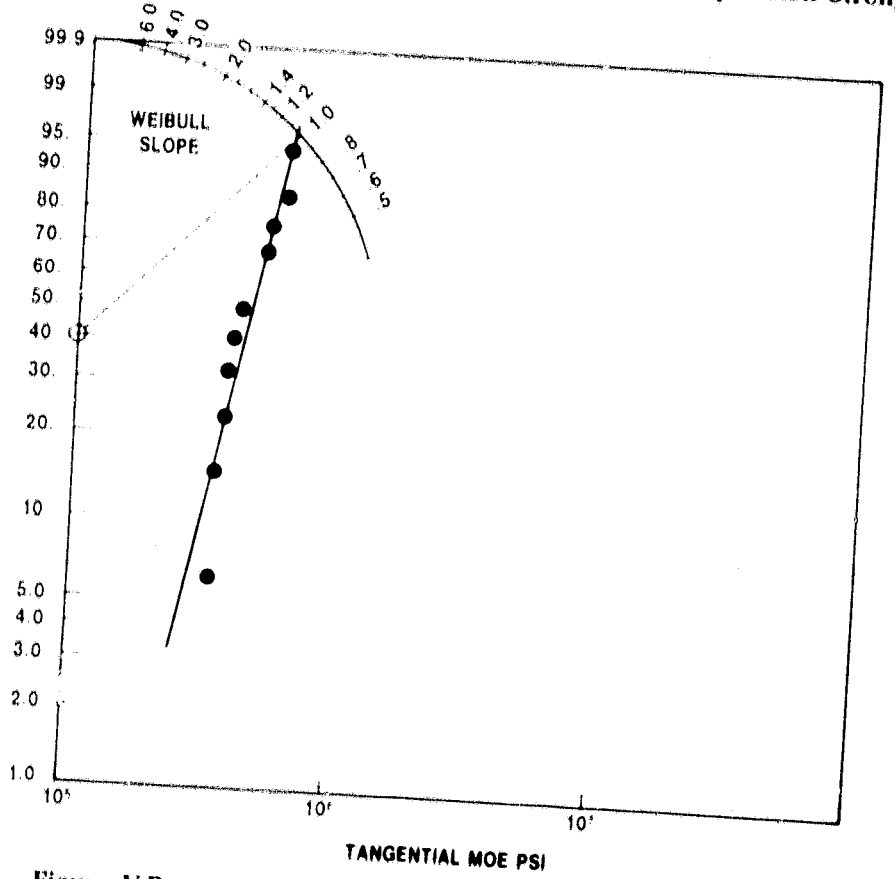

Figure V.B.1.4 Supplier A Thin-Wall AS Tangential MOE

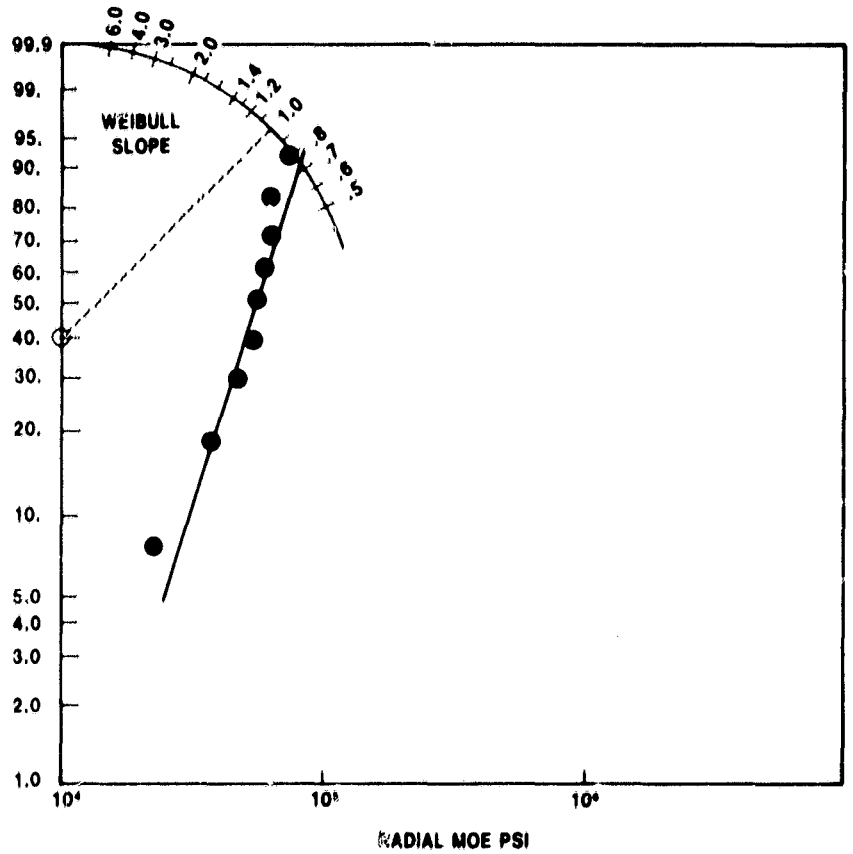

Figure V.B.1.5 Supplier A Thin-Wall AS Radial MOE

CODE:

R — RECTANGULAR
I.T. — ISOSCELES TRIANGULAR
S.T. — SINUSOIDAL TRIANGULAR
H — HEXAGONAL
W — WRAPPED
C — CORRUGATED
EX — EXTRUDED
EM — EMBOSSED

SUPPLIER	TYPE OF FIN	X FINS CM. (FINS/IN.)	Y ROWS CM. (ROWS/IN.)	N HOLES CM.² (HOLES/IN.²)	S MM. (IN.)	B MM. (IN.)	H MM. (IN.)	B_{50} MOR_T Kpa (PSI)	B_{10} MOR_T Kpa (PSI)	B_{50} MOE_T Kpa (PSI) (X10⁻⁶)	B_{10} MOE_T Kpa (PSI) (X10⁻⁶)	B_{50} MOR_R Kpa (PSI)	B_{10} MOR_R Kpa (PSI)	B_{50} MOE_R Kpa (PSI) (X10⁻⁶)	B_{10} MOE_R Kpa (PSI) (X10⁻⁶)	B_{50} $COMP_R$ Kpa (PSI)	B_{10} $COMP_R$ Kpa (PSI)	MIN. STRAIN TOL. (PPM)	MAT'L	MFG. PROCESS
A	S.T.	15.0 (38)	13.6 (34.5)	203.9 (1311)	.061 (.0024)	.061 (.0024)	.676 (.0266)	1998 (290)	1399 (203)	3.1 (.45)	2.14 (.31)	620 (90)	386 (56)	.379 (.055)	.193 (.028)	345 (50)	200 (29)	645	AS	W, C
I	I.T.	15.8 (40)	9.1 (23)	142.6 (920)	.135 (.0053)	.135 (.0053)	.970 (.0382)	2274 (330)	1240 (180)	4.13 (.60)	3.38 (.49)	2274 (330)	1516 (220)	4.31 (.625)	4.07 (.59)	1668 (245)	1226 (178)	528	MAS	EX
D	R	11.4 (29)	12.2 (31)	140 (903)	.193 (.0076)	.193 (.0076)	.627 (.0247)	2412 (350)	1654 (240)	6.75 (.98)	4.62 (.67)	1688 (245)	930 (135)	3.10 (.45)	2.34 (.34)	1309 (190)	944 (137)	357	MAS	W, EM

Table V.B.1.1 Matrix Mechanical Properties

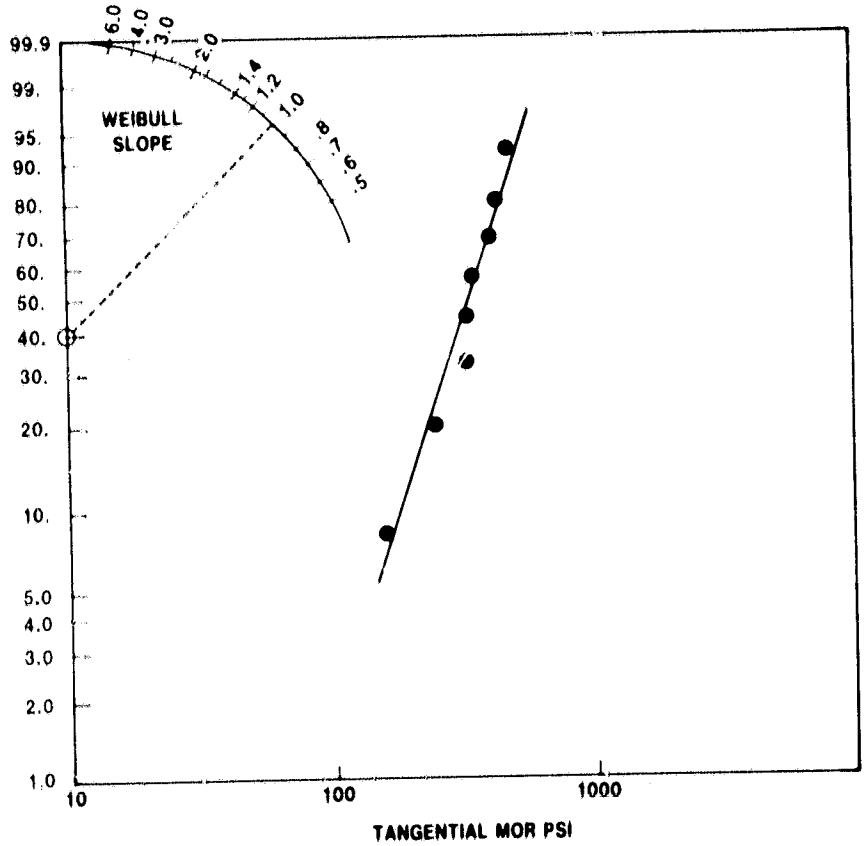

Figure V.B.1.6 **Supplier I MAS Tangential MOR**

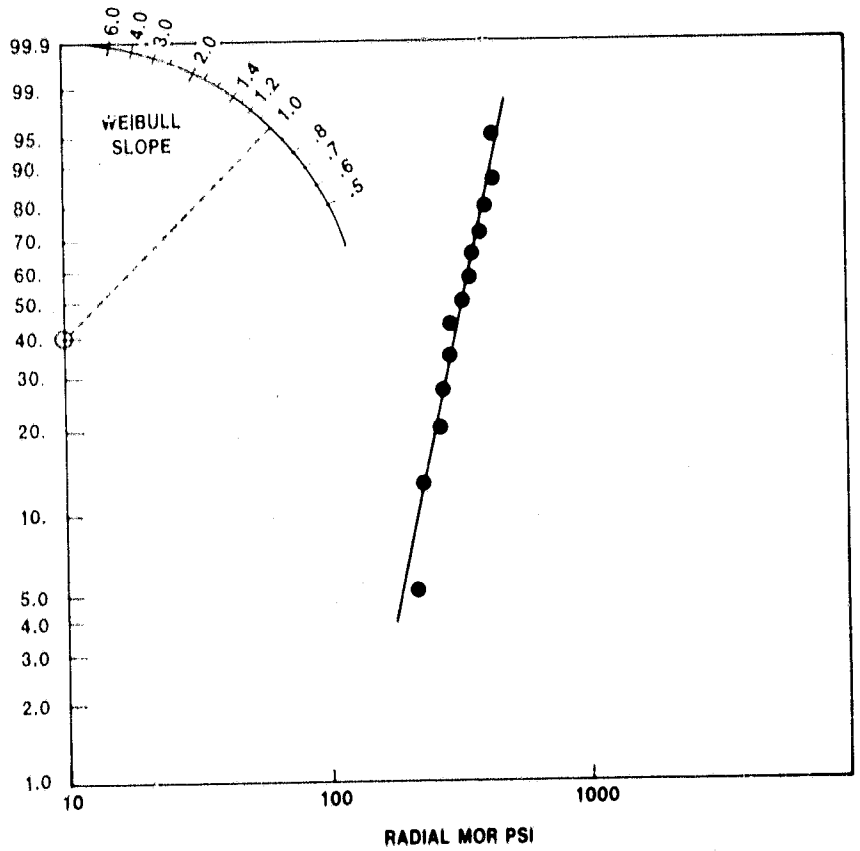

Figure V.B.1.7 **Supplier I MAS Radial MOR**

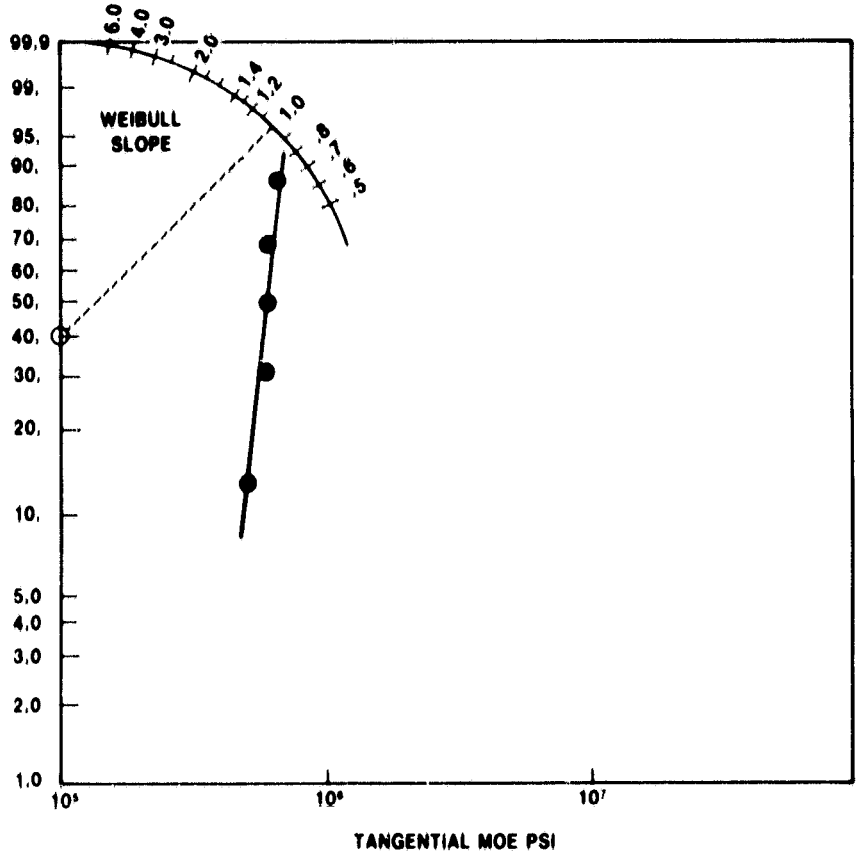

Figure V.B.1.8 Supplier I MAS Tangential MOE

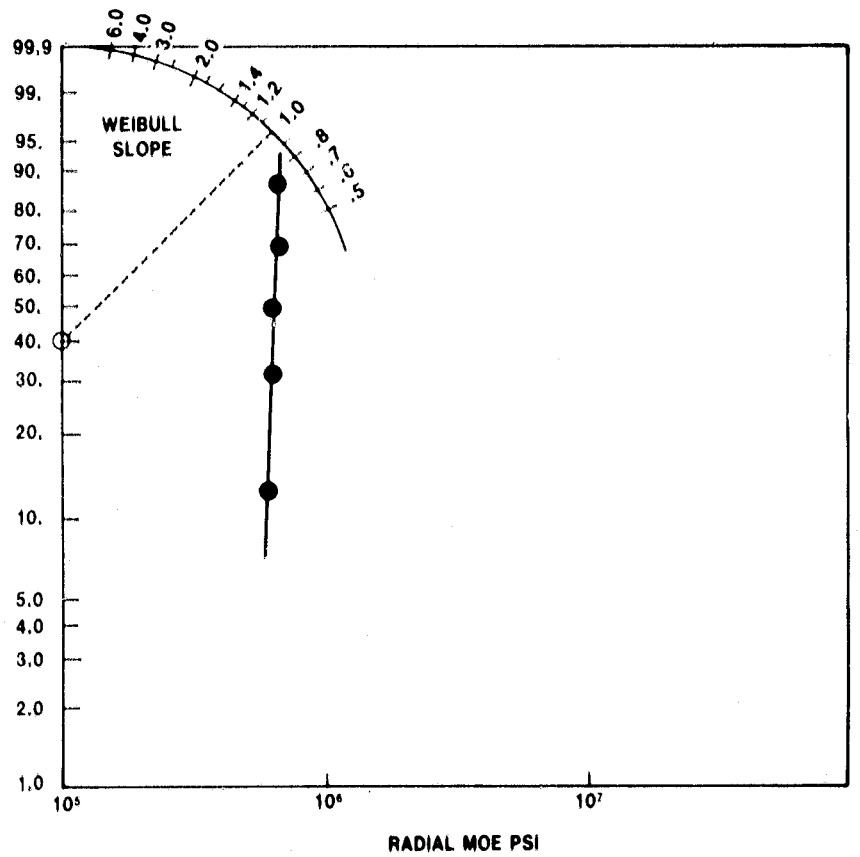

Figure V.B.1.9 Supplier I MAS Radial MOE

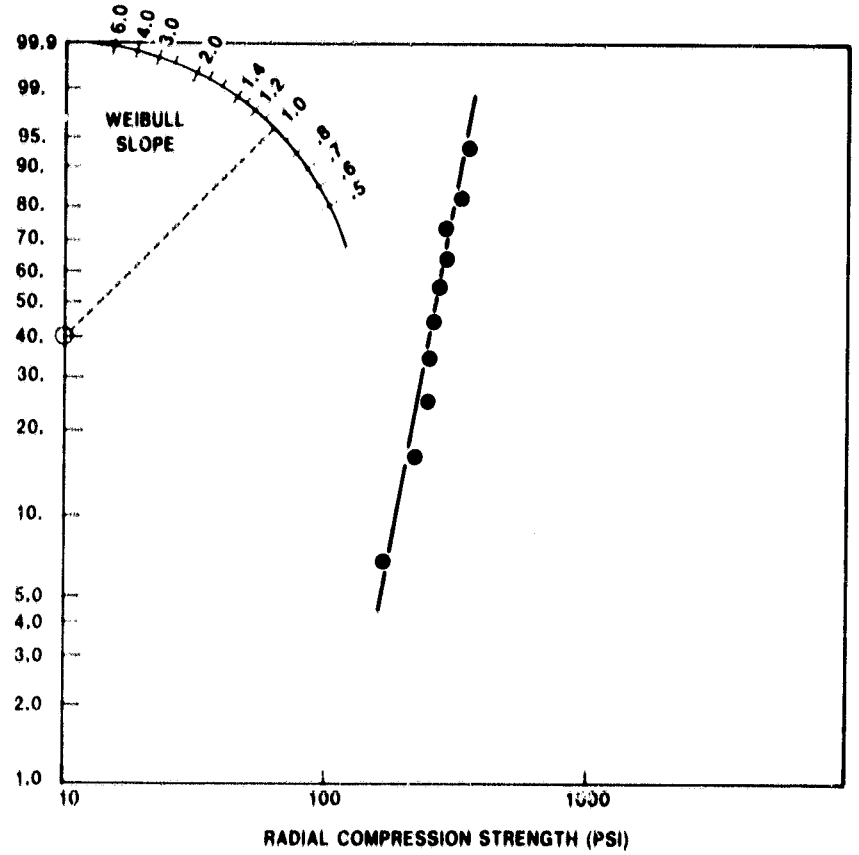

Figure V.B.1.10 Supplier I MAS Radial Compression Strength

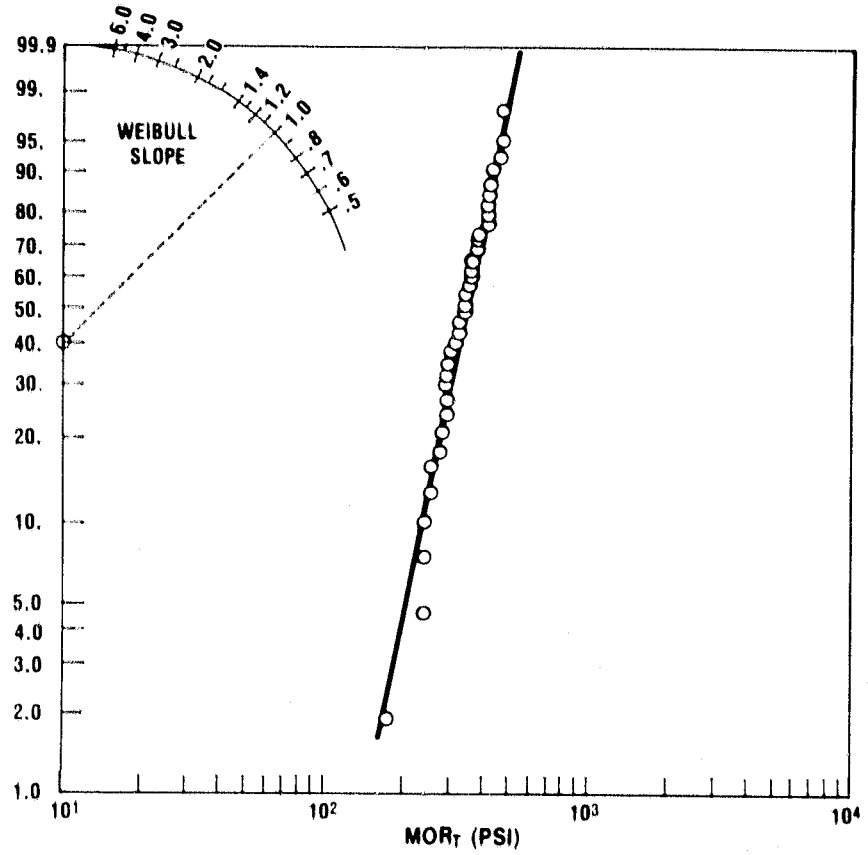

Figure V.B.1.11 Supplier D MAS-2 Tangential MOR

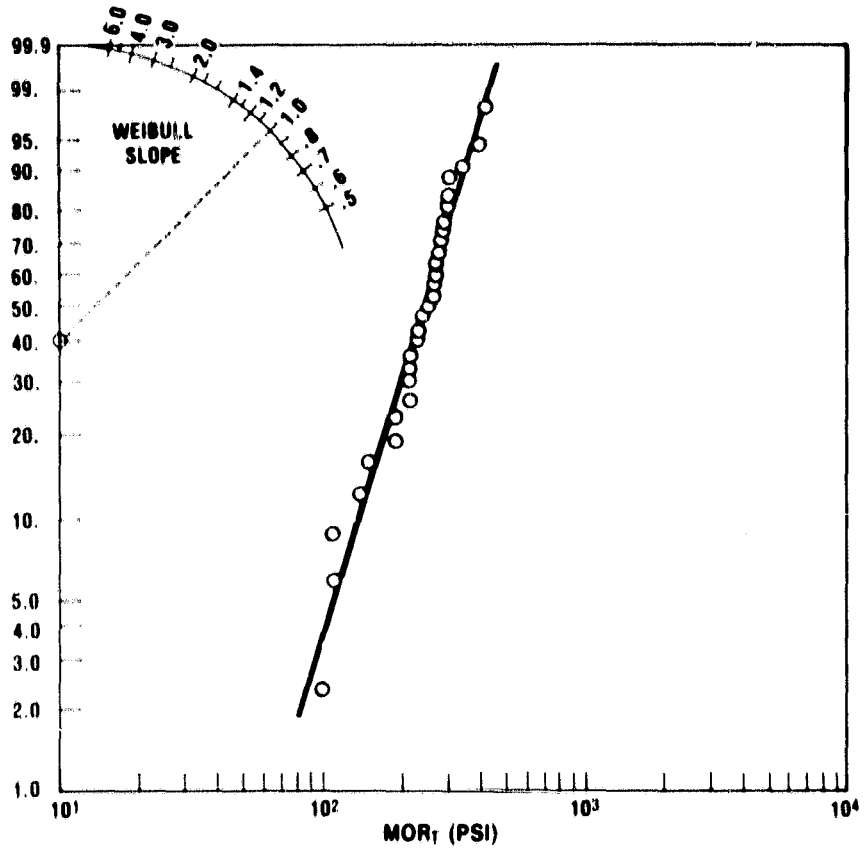

Figure V.B.1.12 Supplier D MAS-2 Radial MOR

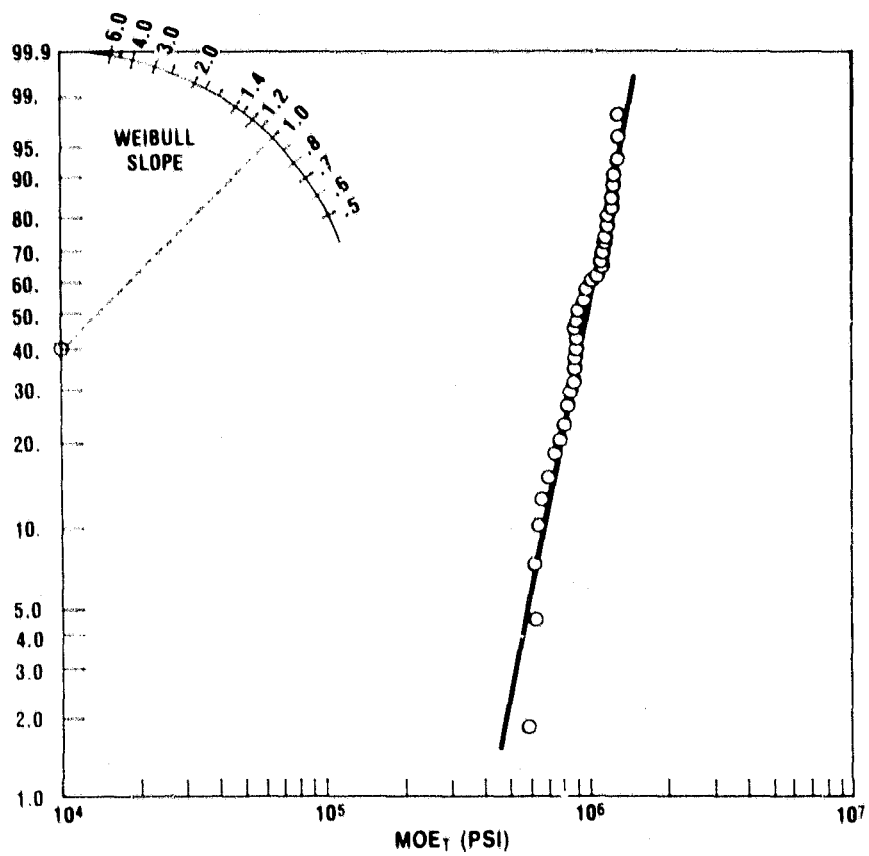

Figure V.B.1.13 Supplier D MAS-2 Tangential MOE

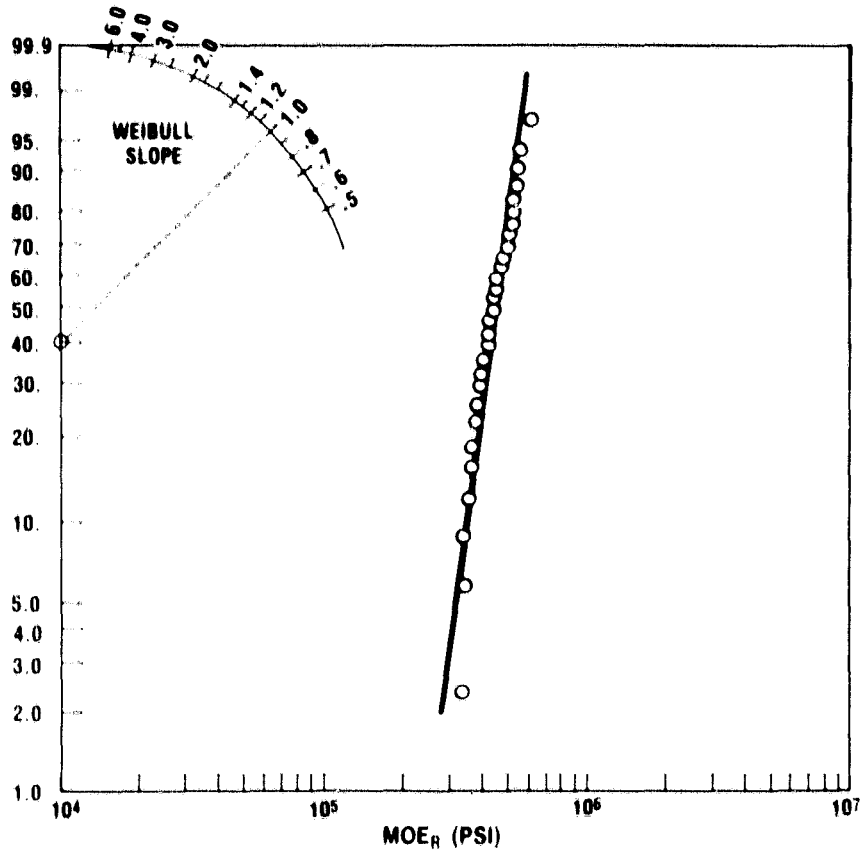

Figure V.B.1.14 Supplier D MAS-2 Radial MOE

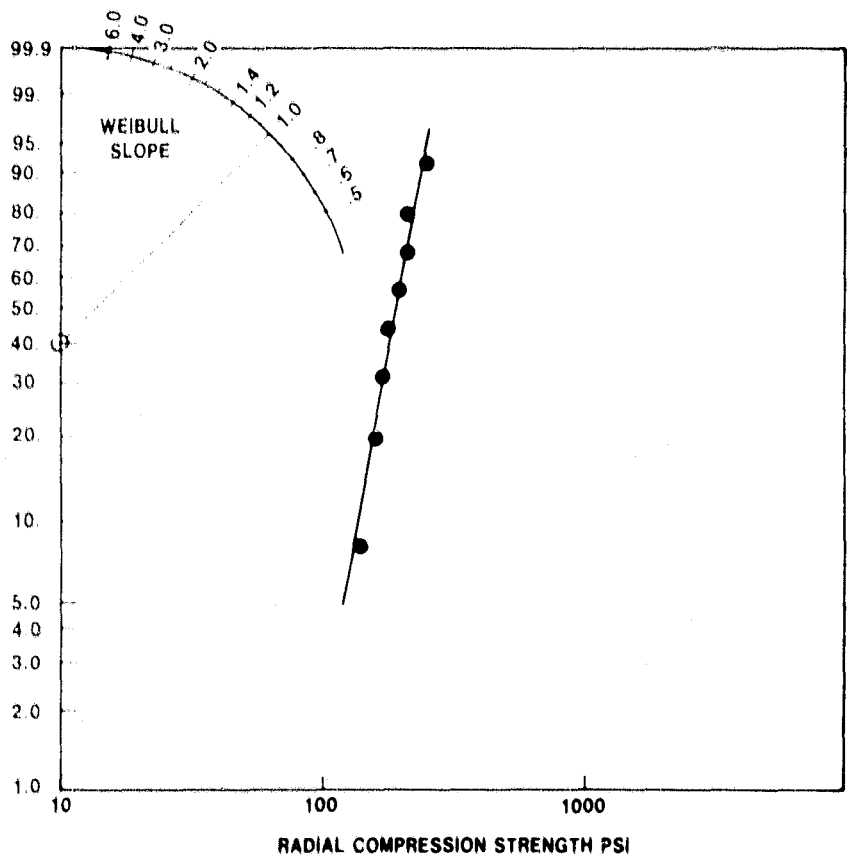

Figure V.B.1.15 Supplier D MAS-2 Radial Compression Strength

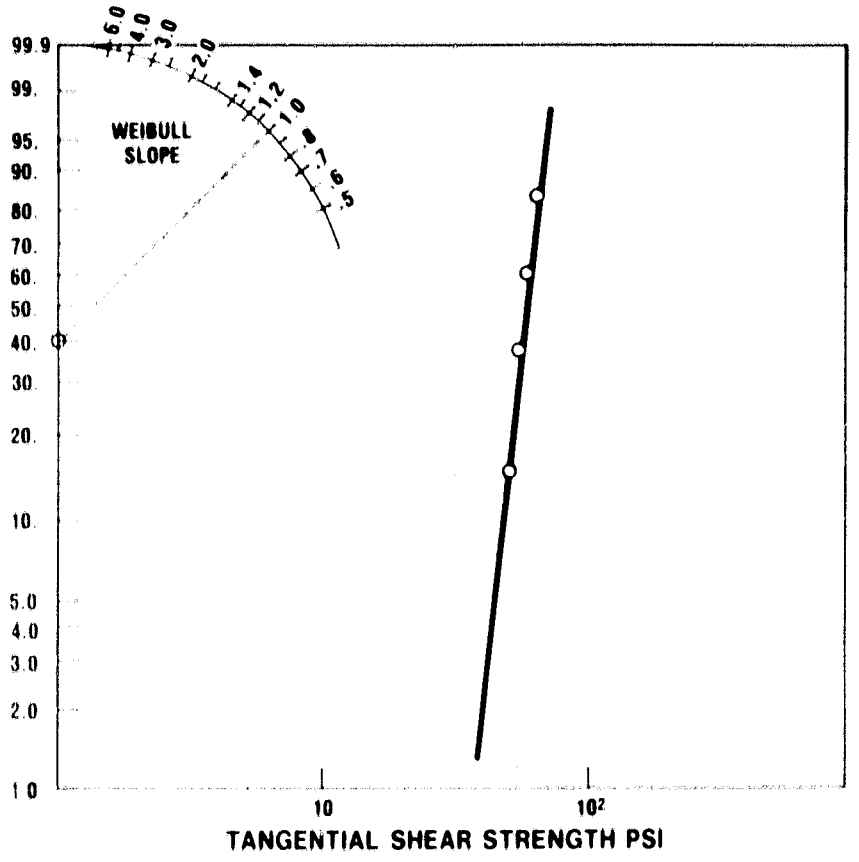

Figure V.B.1.16 Supplier A Thin-Wall AS Tangential Shear Strength

V.B.2 Stress Analysis

The critical thermal stress in a regenerator made from a high thermal expansion ceramic material is tangential tension at the hot face outside diameter. Engine operating experience (Task I) has shown that the addition of stress relief slots to the rim of a high expansion regenerator can substantially increase durability.

A simplified (axisymmetric model) finite element stress analysis was previously performed for three configurations of stress relieved LAS regenerators operating at an inlet temperature of 800°C (1472°F) (Reference 1). Each of the three slot configurations had a radial length at the hot face of 25mm (1.0 in). The slots were tapered axially from the hot face to the regenerator rim. Regenerators incorporating slots with axial lengths of 18mm (0.7 in), 36mm (1.4 in) and 71mm (2.8 in) were analyzed (Figure V.B.2.1). The maximum tangential stresses calculated for an unslotted regenerator and for regenerators incorporating the three stress relief schemes were 1980 KPa (288 psi), 1410 KPa (205 psi), 1040 KPa (141 psi), and 577 KPa (84 psi) with the highest stress occurring in the unslotted regenerator and diminishing with increasing slot depth.

Because the axisymmetric finite element model is essentially that of a regenerator incorporating an infinite number of slots and does not account for stress concentrations, a three-dimensional finite element model has been developed (Figure V.B.2.2). For comparison with the axisymmetric analysis, stress relieved LAS regenerators incorporating 21, 42 and 84 equally spaced 36mm x 25mm (1.4 in x 1.0) slots were analyzed at the 800°C (1472°F) operating condition.

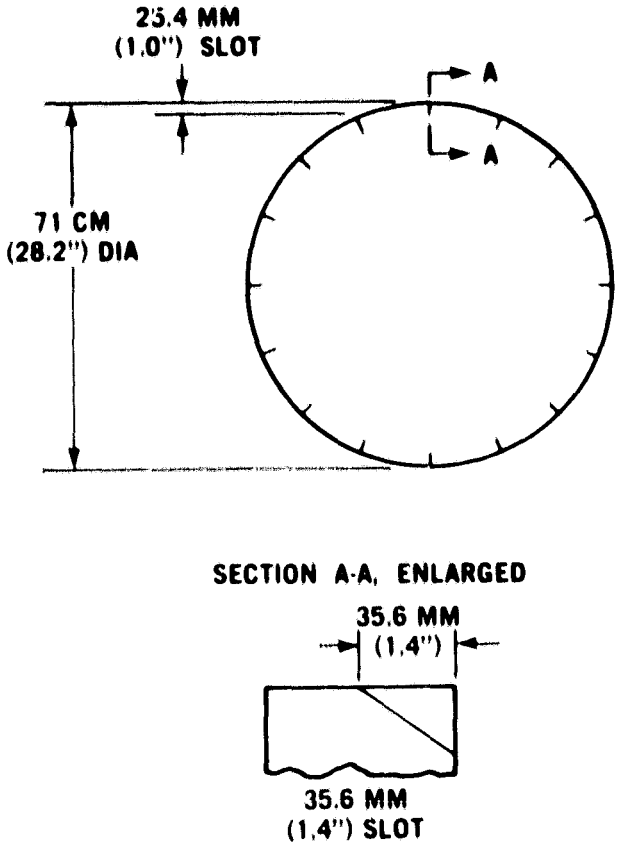

Figure V.B.2.1 Stress Relief Slot Configurations

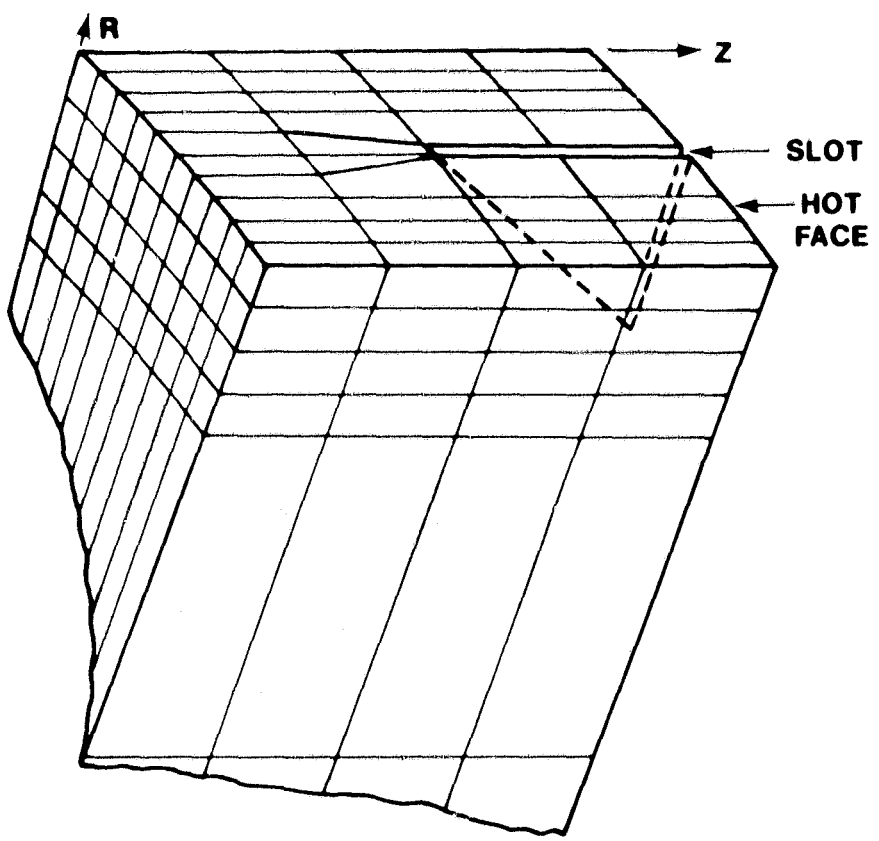

PARTIAL VIEW
— 3-D FINITE
ELEMENT MODEL

Figure V.B.2.2 Three-Dimensional Finite Element Model of Stress Relieved Regenerator

The material properties used in both the axisymmetric and three-dimensional analyses are given in Table V.B.2.1.

MODULUS OF ELASTICITY, MPa (PSI)	
RADIAL, E_R	1,344 (195,000)
AXIAL, E_Z	20,680 (3,000,000)
TANGENTIAL, E_θ	11,030 (1,600,000)
POISSON'S RATIO	
ν_{RZ}	.02
$\nu_{R\theta}$	.12
$\nu_{\theta Z}$	.11

COEFFICIENT OF THERMAL EXPANSION $X10^6\ °C^{-1}$ ($°F^{-1}$) @ °C(°F)			
−18°C	(0°F)	$-.49°C^{-1}$	($-.27°F^{-1}$)
204	(400)	−.27	(−.15)
371	(700)	−.11	(−.06)
538	(1000)	.11	(.06)
704	(1300)	.29	(.16)
871	(1600)	.49	(.27)
1038	(1900)	.67	(.37)

Table V.B.2.1 Supplier A-LAS Material Properties

The three-dimensional finite element analysis indicates that the effect of stress relief slots is to substantially reduce tangential stress in the rim between slots as compared to an unslotted regenerator. High stresses occur at the slots, but diminish rapidly with distance such that their effect is limited to very local areas of the rim in the vicinity of the slot (Figure B.V.2.3). This maximum stress is a function of the number of equally spaced slots around the rim: as the number of slots increases, the maximum stress decreases and approaches the value calculated using the axisymmetric model (Figure V.B.2.4). This indicates that the axisymmetric model can be used to estimate the maximum stress relief obtainable by the addition of slots. The maximum calculated tangential stresses in the rims of LAS regenerators incorporating twenty-one, forty-two and eighty-four slots using the three-dimensional model are 3838 KPa (557 psi), 2281 KPa (331 psi), and 1247 KPa (181 psi) respectively.

The next step in the analysis was to attempt to correlate three-dimensional results with the original stress relieved Supplier D MAS-1 regenerator engine operating experience described in Task I, and to evaluate the effect on thermal stress in the MAS core of various slot configurations.

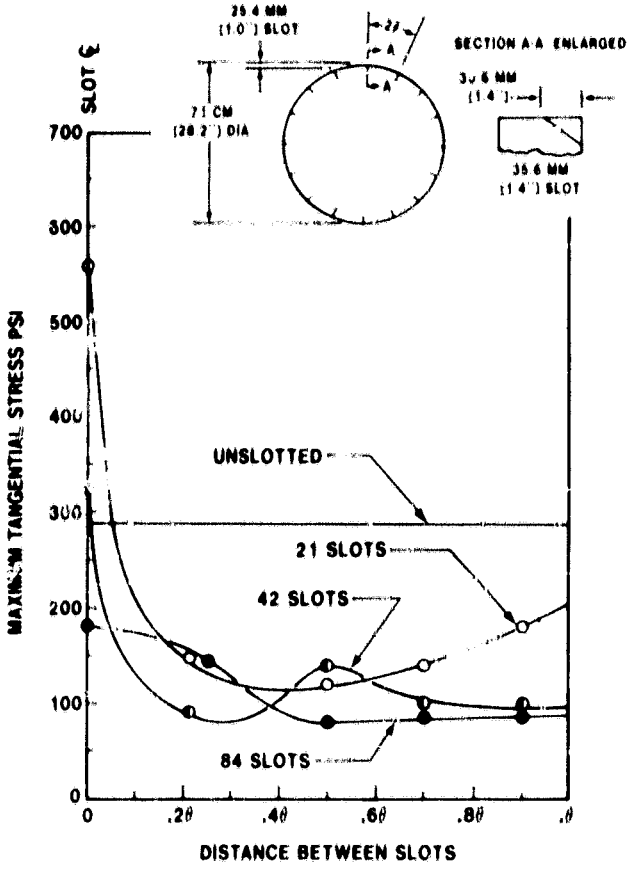

Figure V.B.2.3 Distribution of Tangential Stress in Slotted LAS Regenerator at 800°C (1472°F)

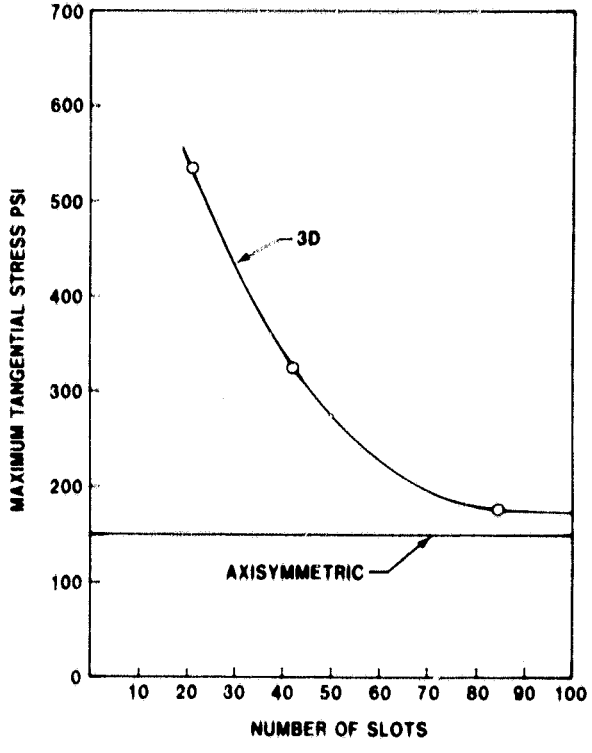

Figure V.B.2.4 Effect of the Number of 36 mm x 25 mm (1.4 inch x 1.0 inch) Stress Relief Slots on Maximum Tangential Stress In The Rim

Supplier D MAS-1 Regenerators were analyzed at the 800°C (1472°F) operating condition for two types of stress relief slots: The standard 36 mm x 25 mm (1.4 in x 1.0 in) slot incorporated in the regenerator undergoing engine test, and a slot extending axially 72mm (2.8 in), or the full width of the rim. These configurations were analyzed for regenerators incorporating 21, 42 and 84 equally spaced slots. The MAS material properties used in the analysis are given in Table V.B.2.2.

YOUNG'S MODULUS KPa X 10^{-6} (PSI X 10^{-6})	MAS-1	MAS-2
RADIAL, E_R	2.07 (.30)	3.1 (.45)
TANGENTIAL, E_T	3.03 (.44)	6.75 (.98)
AXIAL E_Z	11.37 (1.65)	34.11 (4.95)
SHEAR, G_{RZ}	.896 (.13)	.896 (.13)
POISSON'S RATIO		
NU_{RZ}	.17	.170
NU_{RT}	12	.120
NU_{TZ}	.08	.080
THERMAL EXPANSION PPM @		
100°C	55	25
200°C	150	70
300°C	280	150
400°C	460	290
500°C	690	475
600°C	940	680
700°C	1210	915
800°C	1500	1180
900°C	1810	1455
1000°C	2150	1750
STRENGTH KPa (PSI)		
TANGENTIAL		
MAXIMUM	1306 (190)	3100 (450)
MINIMUM	800 (115)	1653 (240)
AVERAGE	910 (130)	2411 (350)

Table V.B.2.2 Supplier D Magnesium Aluminum Silicate Material Properties

The maximum tangential stress in the rim of an unslotted MAS regenerator was previously calculated to be 3238 KPa (470 psi) (Reference 2.). As with the LAS matrix, the three-dimensional analysis showed that the effect of the addition of the slots is to reduce stress substantially (greater than 60%) for areas of the rim between slots (Figures V.B.2.5 and V.B.2.6).

For the 21-slot regenerator undergoing engine test, peak stresses of 4465 KPa (648 psi) and 2253 KPa (327 psi) were calculated at the slot location and midway between slots respectively, and thermal stress cracks would be expected at these locations. As described in Task I, cracks did occur between the slots and it is expected that cracks not evident from a non-destructive inspection were generated beneath the slots as well. Cracks generated beneath the slots would not be expected to propagate to the surface of the regenerator due to the state of stress of the core (tangential compression) which exists at the hot face in this region and which would act as a crack arrestor.

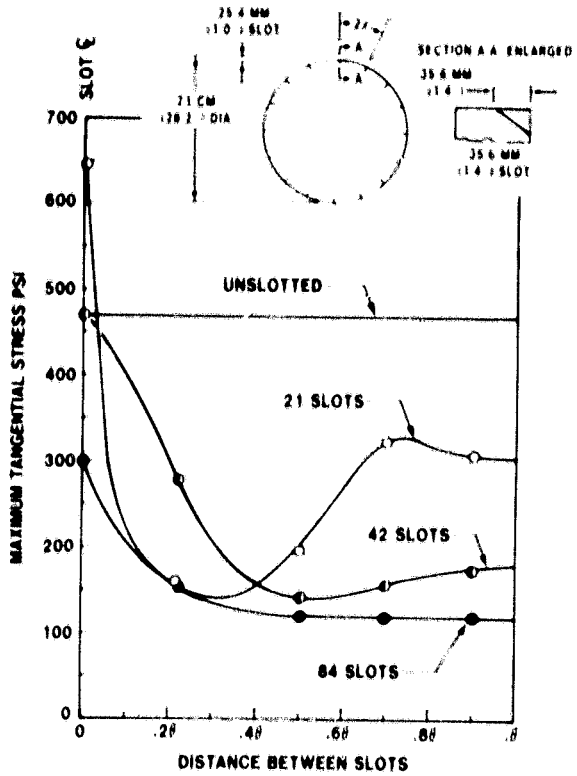

Figure V.B.2.5 **Distribution of Tangential Stress in Supplier D MAS-1 Regenerator Incorporating 36 mm x 25 mm (1.4 inch x 1.0 inch) Slots at 800°C (1472°F)**

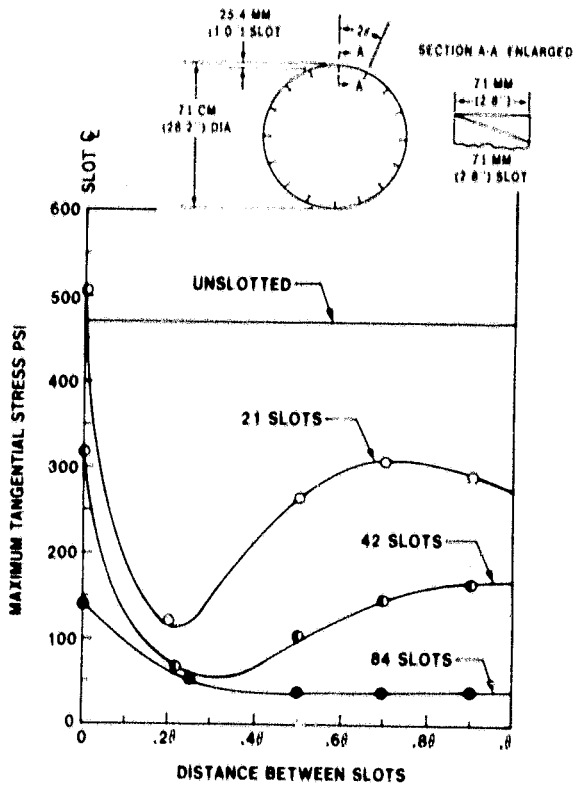

Figure V.B.2.6 **Distribution of Tangential Stress in Supplier D MAS-1 Regenerator Incorporating 72 mm x 25 mm (2.8 inch x 1.0 inch) Slots at 800°C (1472°F)**

The effect of increasing the number of slots is to reduce the maximum stress at the slot locations as well as reducing the level of tangential stress between slots. Regenerators incorporating forty-two and eighty-four 36 mm and 25 mm (1.4 in x 1.0 in) slots provide reductions in maximum stress of 27% and 54% respectively over the twenty-one slot configuration.

The analysis of the 72 mm x 25 mm (2.8 in x 1.0 in) slot indicates that a more effective method of reducing thermal stress than increasing the number of slots is to modify the slot geometry. Compared to the analytical results of the baseline 21-slot regenerator like the one operating in the engine, this configuration provides stress reductions of 22%, 51% and 78% for regenerators incorporating 21, 42 and 84 slots respectively.

More recently, Supplier D developed an improved MAS material (MAS-2) which exhibited reduced thermal expansion characteristics and increased strength (Table V.B.2.2).

A three-dimensional finite element analysis was undertaken to determine if the slotted MAS-2 regenerators (or similar ones) could withstand the thermal stresses imposed by operation at a regenerator inlet temperature of 1000°C (1832°F).

Three configurations of 42-slot regenerator consisting of (1) a constant depth slot extending the full width of the rim, (2) a tapered slot extending one-half the width of the rim, and (3) a tapered slot extending the full width of the rim were analyzed and are shown in Figure V.B.2.7 along with the results of the 1000°C (1832°F) analysis. As expected, the maximum stress in the rim decreases with increasing slot depth. Of particular interest is configuration 3, the configuration that ran at 800°C (1472°F) and 1000°C (1832°F). It can be seen that the tangential stress in the rim at 1000°C (1832°F) exceeds the average measured tangential modulus of rupture of the MAS-2 material at the slot locations and midway between slots. The thermal stress safety factors at these locations are .39 and .71 respectively. Thermal stress cracks would be expected to occur at these locations. Based on the analysis, and past experience with the MAS-1 regenerator, the cracks at the slot locations would not be expected to propagate to the surface of the hot face, and those between slots would not be expected to propagate below the seal I.D. where the core is subjected to tangential compressive stress. An estimate of the durability potential of this regenerator can be made by comparing the thermal stress safety factors with those calculated for the 21-slot MAS-1 regenerator at 800°C (1472°F) which accumulated over 5000 engine hours. Analysis of this early, high expansion, regenerator revealed a thermal stress safety factor of .17 to .29 at the slot locations and of .35 to .57 between slots for 800°C (1472°F) operation based on the range of MOR values measured for Supplier D MAS-1. At 1000°C (1832°F), the lower expansion MAS-2 material offers an improvement in minimum safety factor of about 30%.

As described in Tasks I & II, two full size regenerators from Supplier I consisting of 35 extruded segments bonded together (Figure I.B.5.5) accumulated limited durability at 800°C and 1000°C before termination of the program. Stress relief slots (2.8 in. x 1.0 in.) were incorporated at the mid-point of each of the 22 segments at the outer radius of the regenerator matrix. Since the cement bonding the 22 segments is

considerably weaker than the matrix, the bond areas can be considered equivalent to stress relief slots. Consequently, the full size matrix is equivalent to a 44-slot regenerator. This configuration was analyzed at the 1000°C (1832°F) operating condition utilizing the material properties listed in Table V.B.2.3. It can be seen that the tangential stress in the rim between the slots is equivalent to the average strength (Figure V.B.2.8). Localized stress at the slot below the hot face exceeds the average strength. Compared to the Supplier D-MAS-2 matrix at 1000°C the Supplier I MAS matrix would have a 35 to 60% improvement in tangential stress safety factor.

In order to place the tangential stress safety factors that have been determined, utilizing the three-dimensional analysis, for the various materials into proper perspective, a comparison with engine operating experience is desirable. Table V.B.2.4 summarizes the analytical results and engine operating experience for each of the materials evaluated.

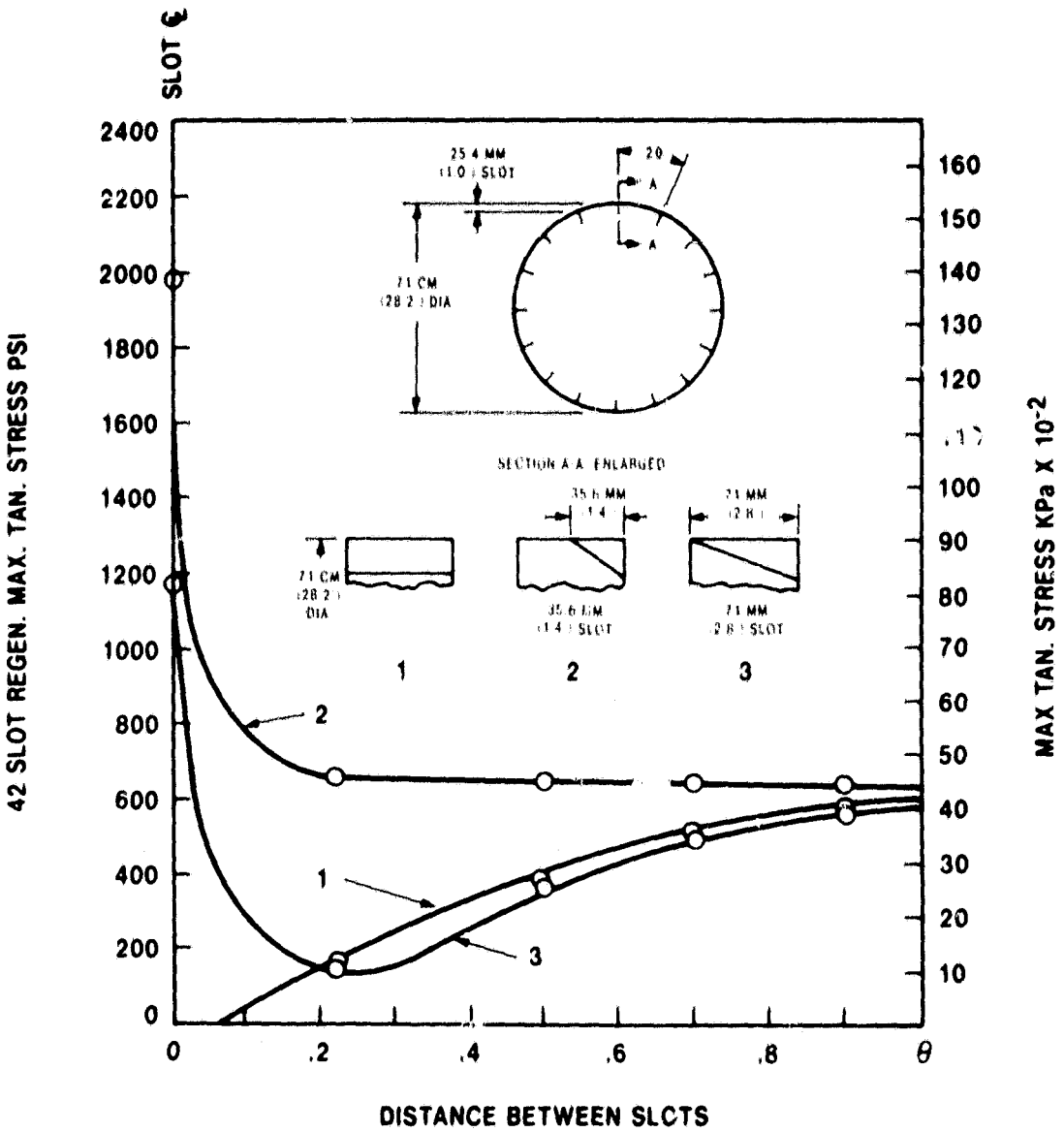

Figure V.B.2.7 Distribution of Tangential Stress in Supplier D MAS-2 Regenerator at 1000°C (1832°F)

YOUNG'S MODULUS KPa X 10 ^{6} (PSI X 10 ^{6})	SUPPLIER I-MAS
RADIAL, E_R	4.31 (.625)
TANGENTIAL, E_T	4.13 (.60)
AXIAL E_Z	34.11 (4.95)
SHEAR, G_{RZ}	.896 (.13)
POISSON'S RATIO	
NU_{RZ}	.17
NU_{RT}	.12
NU_{TZ}	.08
THERMAL EXPANSION PPM @	
100 C	20
200 C	0
300 C	60
400 C	170
500 C	300
600 C	515
700 C	710
800 C	960
900 C	1200
1000 C	1480
STRENGTH KPa (PSI)	
TANGENTIAL	2274 (330)
RADIAL	2274 (330)
MAXIMUM TANGENTIAL STRESS KPa (PSI)	
AT THE SLOT	3638 (528)
MIDWAY BETWEEN SLOTS	2343 (340)
TANGENTIAL SAFETY FACTOR	
AT THE SLOT	.97
MIDWAY BETWEEN SLOTS	.62

Table V.B.2.3 Supplier I-MAS Material Properties

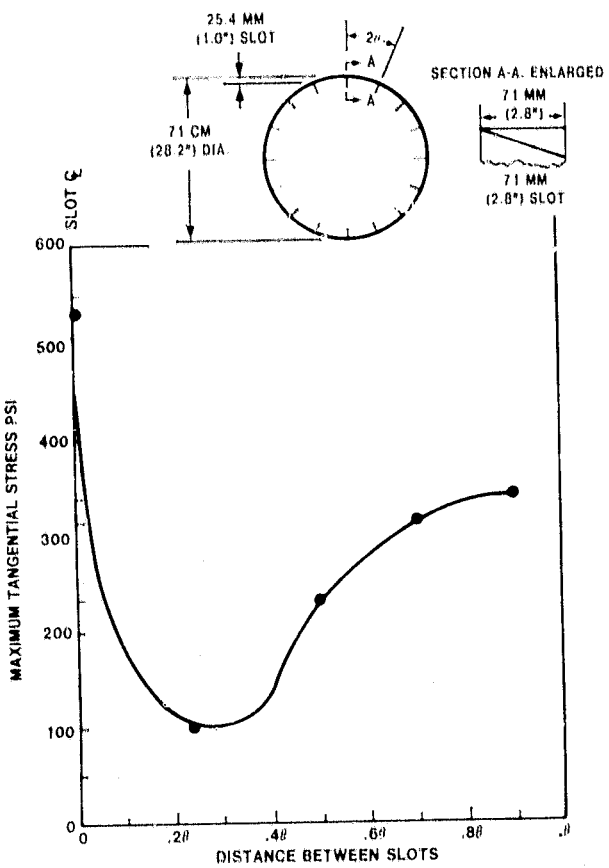

Figure V.B.2.8 Distribution of Tangential Stress in Supplier I MAS Regenerator at 1000°C (1832°F) Incorporating 44 - 72 mm x 25 mm (2.8 in. x 1.0 in.) slots

	SUPPLIER D MAS-1	SUPPLIER D MAS-2		SUPPLIER I MAS	
1. YOUNG'S MODULUS KPa X 10^{-6} (PSI X 10^{-6})					
A. RADIAL, E_R	2.07 (.30)	3.1 (.45)		4.31 (.625)	
B. TANGENTIAL, E_T	3.03 (.44)	6.75 (.98)		4.13 (.60)	
2. THERMAL EXPANSION — PPM @					
A. 200°C (392°F)	150	70		0	
B. 800°C (1472°F)	1500	1180		960	
C. 1000°C (1832°F)	2150	1750		1480	
3. INLET TEMPERATURE °C (°F)					
A. COLD SIDE	232°C (450°F)	232°C (450°F)	232°C (450°F)	232°C (450°F)	232°C (450°F)
B. HOT SIDE	800°C (1472°F)	800°C (1472°F)	1000°C (1832°F)	800°C (1472°F)	1000°C (1832°F)
4. TANGENTIAL STRENGTH — KPa (PSI)	910 (130)	2411 (350)		2272 (330)	
5. NUMBER OF SLOTS	21	42		44	
6. SLOT CONFIGURATION	2	3		3	
7. MAXIMUM TANGENTIAL STRESS — KPa (PSI)					
A. AT THE SLOT	4480 (650)	4100 (595)*	6200 (900)	2377 (345)*	3638 (528)
B. MIDWAY BETWEEN SLOTS	2240 (325)	2205 (320)*	3376 (490)	1516 (220)*	2343 (340)
8. TANGENTIAL SAFETY FACTOR					
A. AT THE SLOT	.20	.59	.39	.96	.62
B. MIDWAY BETWEEN SLOTS	.40	1.06	.71	1.5	.97
9. MAXIMUM DURABILITY HOURS AT PROGRAM TERMINATION	5381	3514	473	2474	236
*ESTIMATED VALUES					

Table V.B.2.4 Summation of Analytical and Experimental Results for MAS Regenerators

Based on these data several noteworthy observations can be stated as follows:

1. Due to the large variance in physical properties associated with cellular ceramic structures, there is an equally large variance in thermal stress safety factors. Since safety factor is based on a maximum localized stress, thermal stress for the majority of the regenerator rim is considerably less.

2. Based on engine operating experience, regenerator designs with safety factors considerably less than unity have achieved considerable durability hours. Consequently, safety factors for various designs should be compared on a relative basis to determine durability potential. As safety factor increases, the potential for the formation of rim cracks decreases.

3. Although formation of radial cracks in the rim are undesirable, they can be tolerated if crack propagation can be controlled. This explains how the Supplier D MAS-1 core accumulated over 5000 hours even though radial cracks in the rim between slots were evident after less than 200 hours of operation.

V.B.3 Drive and Mount Analysis

As described in Task I, there have been repeated instances of Supplier A thin-wall AS regenerator core compressive stress failures during the process of elas-

tomerically bonding the ring gear to the ceramic matrix. Cohesive failures of the matrix at the elastomer/core interface during engine operation have also been prevalent in this type of regenerator, and have happened occasionally with thick-wall AS cores. Recently, elastomer configurations providing a more compliant bond between the core and the gear have been incorporated, with some success, to inhibit such failures.

Analytical and experimental investigations were undertaken to determine the magnitude of the post-bond compressive stress in a regenerator incorporating the standard elastomer design, and to provide an estimate of the elastomer compliance required to successfully bond thin-wall cores.

The procedure for bonding a ring gear to a regenerator core consists of four steps.

(1) Locating the gear with respect to the core in an assembly fixture.

(2) Placing a thin foam rubber strip around the circumference of the core.

(3) Filling the gap between the core O.D. and the gear I.D. with elastomer.

(4) Induction heating the ring gear to a temperature of 232°C (450°F) to allow the elastomer to partially cure.

The assembled regenerator is allowed to cool to room temperature in the fixture prior to post-curing in an oven. As mentioned previously, this elevated temperature bonding procedure allows the elastomer to cure (to a stress-free state) at a temperature approximating its engine operating temperature. Although LAS, MAS, and thick-wall AS cores have all been successfully assembled and operated using this method, the weaker thin-wall AS cores have exhibited a propensity for radial compressive stress failure in the assembly fixture during cool-down.

An axisymmetric, finite element computer program was used to calculate the stresses imposed on the regenerator core by the elastomer and ring gear thermal contraction during this cool-down portion of the assembly operation. Because the qualities of the semi-cured elastomer as it exists during this segment of the bonding procedure were unknown, the analysis was carried out for both the thick and thin-wall cores for various values of elastomer modulus of elasticity.

The experimental part of the investigation consisted of strain-gaging the rim of a thick-wall AS core and measuring the room temperature compressive strain induced by the bonding of the ring gear. By combining the analytical and experimental results, the room temperature stress in the thin-wall core was estimated.

In order to experimentally evaluate the stress in the thick-wall regenerator core, strain gages were attached to the face of the regenerator at the rim to measure radial and tangential strain, and to the O.D. of the core at the center of the rim to measure tangential and axial strain. The gages on the core O.D. were protected from the radial pressure of the contracting elastomer and gear during the bonding procedure. The strain gage locations are illustrated in Figure V.B.3.1. By comparing

measured strain to analytically determined strain for various assumed values of elastomer modulus of elasticity, an estimate of the actual elastomer modulus was made, and thus the state of stress of the thick and thin-wall cores were determined. The results of this analysis are shown graphically in Figure V.B.3.2.

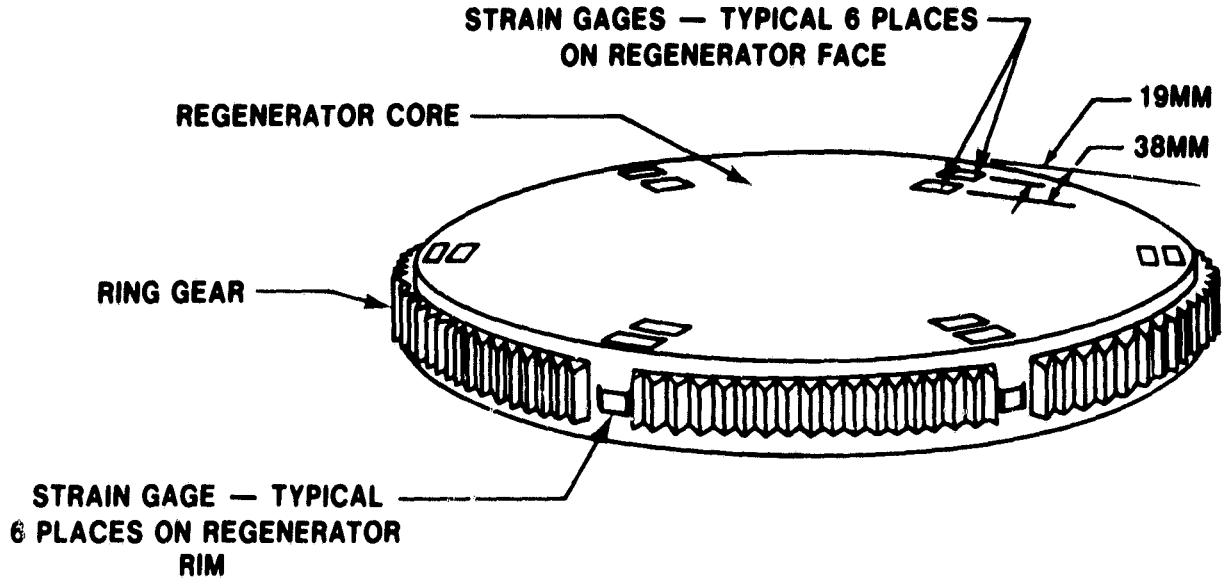

Figure V.B.3.1 Location of Strain Gages on Instrumented Core

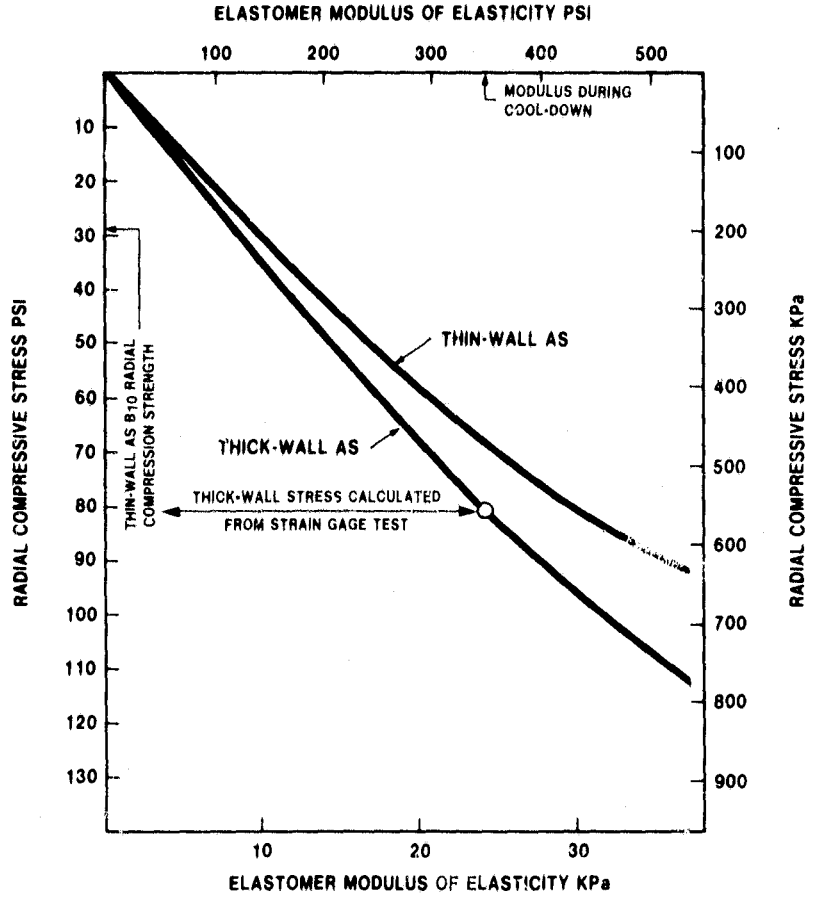

Figure V.B.3.2 Radial Compressive Stress Vs. Apparent Elastomer Modulus of Elasticity During Bonding

The calculated maximum radial compressive stress from the strain gage test of the thick-wall core is 558 KPa (81 psi). There is very little radial compressive strength data available for the thick-wall AS matrix. Three radial compression specimens from a single core have been tested with resulting strengths varying from 434 KPa to 1123 KPa (63 psi to 163 psi) with an average of 882 KPa (128 psi). Bearing in mind that no thick-wall cores have been known to fail in the bonding fixture, it would appear that the induced compressive stresses are acceptable. In the future, however, a reduced modulus elastomer scheme will most likely be incorporated for this type of regenerator simply to increase the margin of safety.

Referring to Figure V.B.3.2, the radial compressive stress imposed on a thin-wall core is 469 KPa (68 psi) if the same modulus is assumed. Based on radial compressive strength data from samples taken from three thin-wall cores, the B_{10} radial compressive strength of this material is 200 KPa (29 psi) and the B_{50} radial compressive strength is 345 KPa (50 psi). From Figure V.B.3.2, a reduction in elastomer modulus of 70% must be effected in order for the B_{10} strength not to be exceeded during the assembly.

The operating experience of regenerators incorporating compliant elastomer schemes is described in Task I. These schemes are intended to preclude compressive stress failures in the bonding fixture and to isolate the core from stress imposed during operation by the drive and support system. One such scheme, which provided mixed durability results, provided compliance by introducing 300+ equally spaced axial holes in the elastomer (Figure IV.B.3.3).

To determine the reduction in apparent modulus realized by this system, 94mm x 44mm x 5mm (3.75 in x 1.77 in x .190) specimens of the two elastomer configurations were tested to provide compressive stress-strain data. The specimens were tested at room temperature using a testing machine at a cross-head speed of .5 mm/min (.02 in/min). The results of these tests are shown in Figure V.B.3.4. It can be seen that the reduction in apparent elastomer modulus realized by incorporating the 300+ axial holes is about 50%. As mentioned above, a minimum reduction in modulus of 70% is required.

A more compliant scheme similar to the slotted elastomer configuration (Figure IV.B.3.3) is required to avoid rim damage and eventual matrix/elastomer separation. It can be seen from Figure IV.B.3.4. the slotted elastomer configuration provides a decrease in apparent modulus of about 90% compared to the standard scheme.

In addition to the compression testing of the three elastomer configurations, three 707 engine regenerators, each incorporating a different elastomer scheme, have been subjected to a static torque of about twice that encountered during engine operation, and the ring gear radial deflection for each case was measured. The following core/elastomer combinations were tested to a static torque of 1356 Nm (1000 ft-lbs):

1. A thick-wall AS core incorporating the standard elastomer configuration.

2. A thick-wall AS core incorporating a compliant elastomer scheme consisting of 180 equally-spaced axial holes through the elastomer.

3. A thin-wall AS regenerator incorporating the interrupted elastomer scheme. None of the cores tested sustained any damage due to the torsion load.

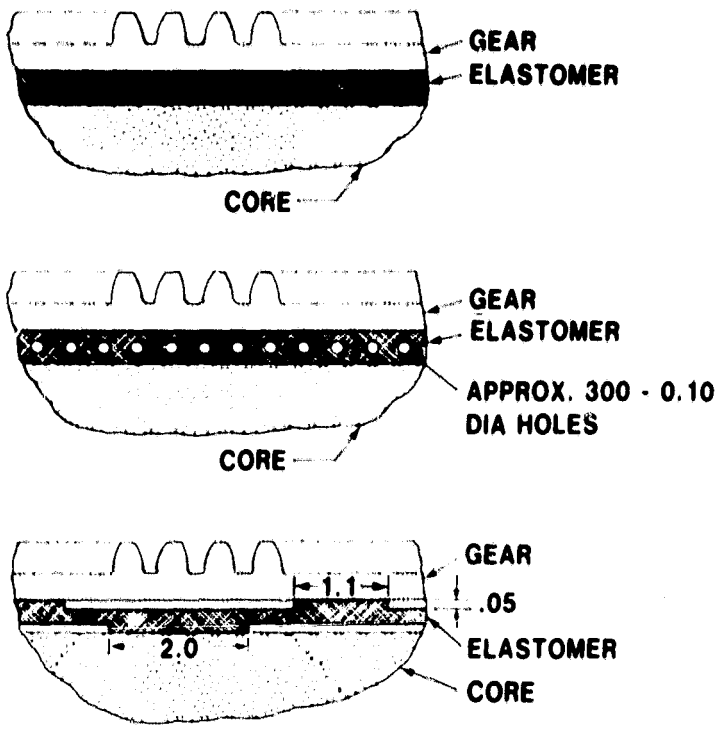

Figure V.B.3.3 Compliant Elastomer Schemes

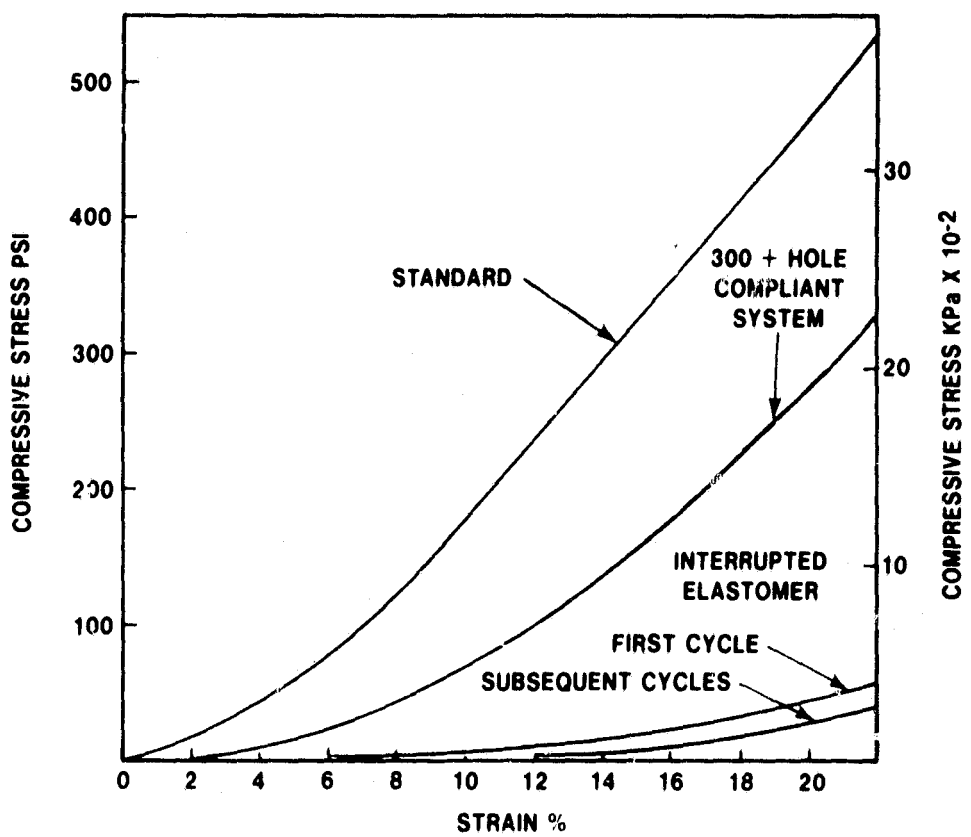

Figure V.B.3.4 Compressive Stress Vs. Strain for Compliant Elastomer Systems

The static torque test consisted of clamping the regenerator to a back-plate on which were mounted the fixed and spring support rollers located in their respective engine positions. Torque was applied through a pinion attached to a lever arm. The ring gear deflection was measured using dial indicators located strategically around the regenerator periphery. The test results are shown in Figure V.B.3.5. The maximum deflection of the ring gear occurs between the fixed roller and the pinion. For the standard elastomer scheme at a torsion load of 1356 Nm (1000 ft-lbs), this deflection is .813mm (0.032 in). For the 180-hole scheme and for the interrupted scheme, the maximum ring gear deflections at this load are .33mm (0.013 in) and .419mm (0.0165 in) respectively.

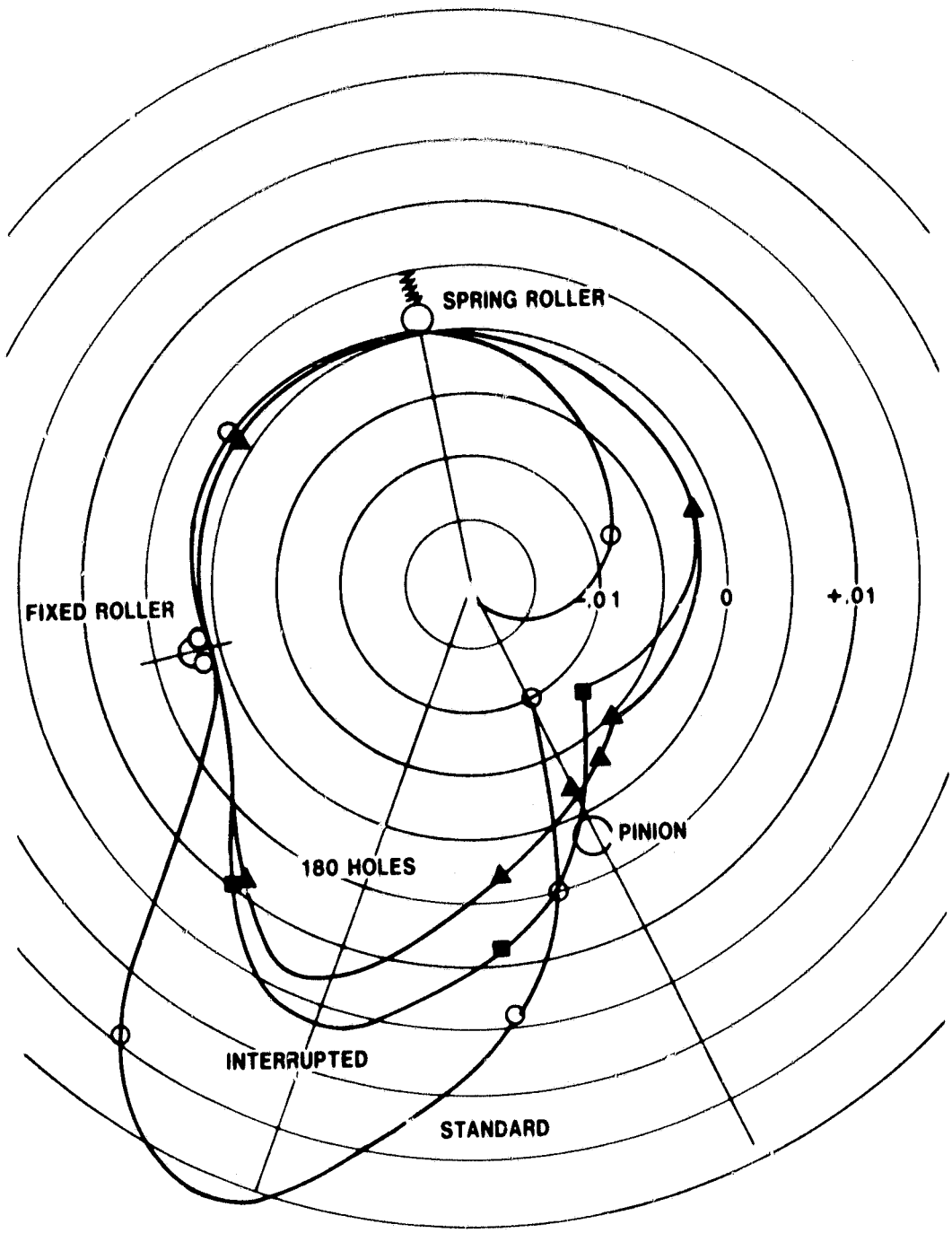

Figure V.B.3.5 Regenerator Ring Gear Deflection

V.B.4 Seal Requirements

Due to the current interest in increasing the regenerator inlet temperature requirement to 1200°C (2192°F) for future engine applications, the projected requirements for the regenerator seal system must be assessed. In order to project future temperature requirements for the regenerator seal coatings, a preliminary test evaluation of the existing Ford 707 production engine seal system has been completed.

For test evaluation purposes, thermocouples were attached to the edge of the coated substrate (Figure V.B.4.1) at selected locations to a production inner and outer seal assembly. A schematic of the thermocouple locations is shown on Figure V.B.4.2 with the actual inner and outer seal assemblies shown on Figures V.B.4.3 and V.B.4.4, respectively.

The assemblies were then installed in the modified Ford 707 production engine described in Task II, which allows a maximum regenerator inlet temperature of 982°C (1800°F). In the absence of a gas turbine or test rig facility capable of providing higher regenerator inlet temperatures, the measured test data were extrapolated to the desired 1200°C (2192°F) condition. Regenerator seal temperatures were recorded for regenerator inlet temperatures of 871°C (1600°F) to 982°C (1800°F) in 28°C (50°F) increments at a compressor discharge air temperature of 104°C (220°F).

The projected seal component temperatures for a 1200°C (2192°F) regenerator inlet gas temperature with 104°C (220°F) and 232°C (450°F) compressor discharge air temperatures are listed on Table V.B.4.1. Based on these preliminary projected temperatures the status of the existing 707 production engine seal coatings is shown on Table V.B.4.1.

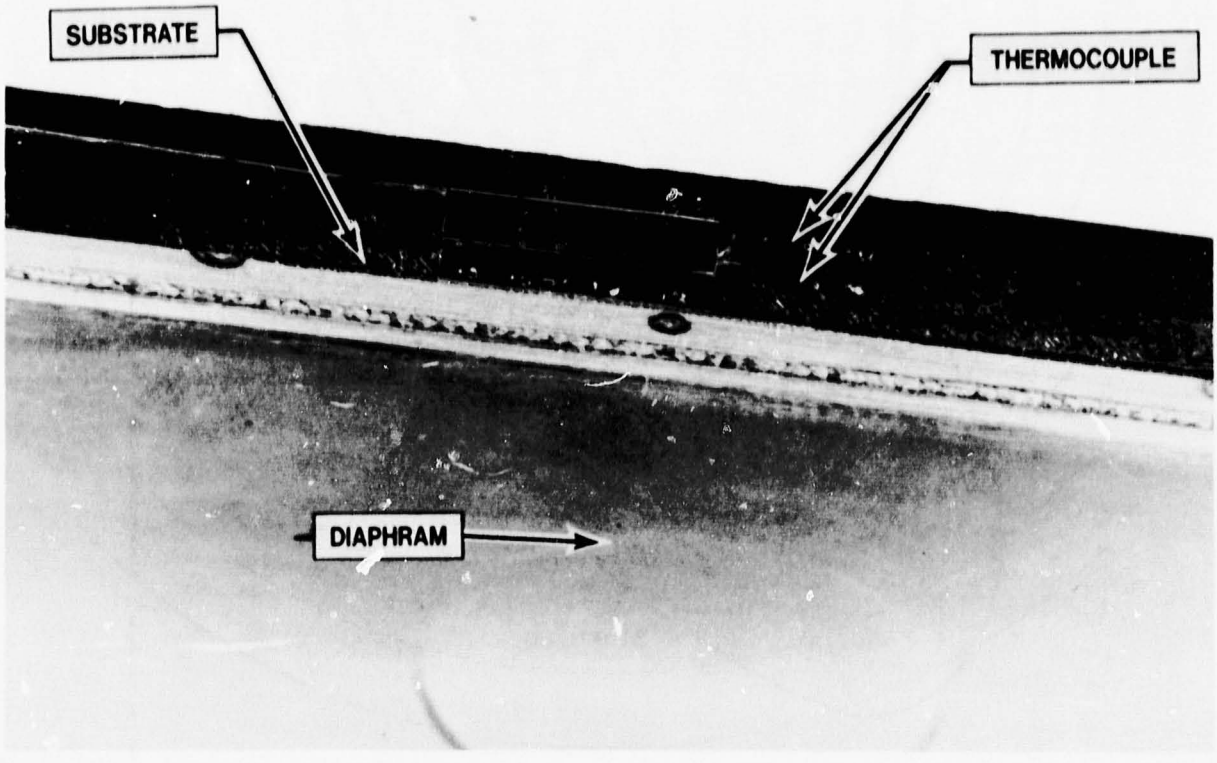

Figure V.B.4.1 Crossarm Seal Probe Mounting Location

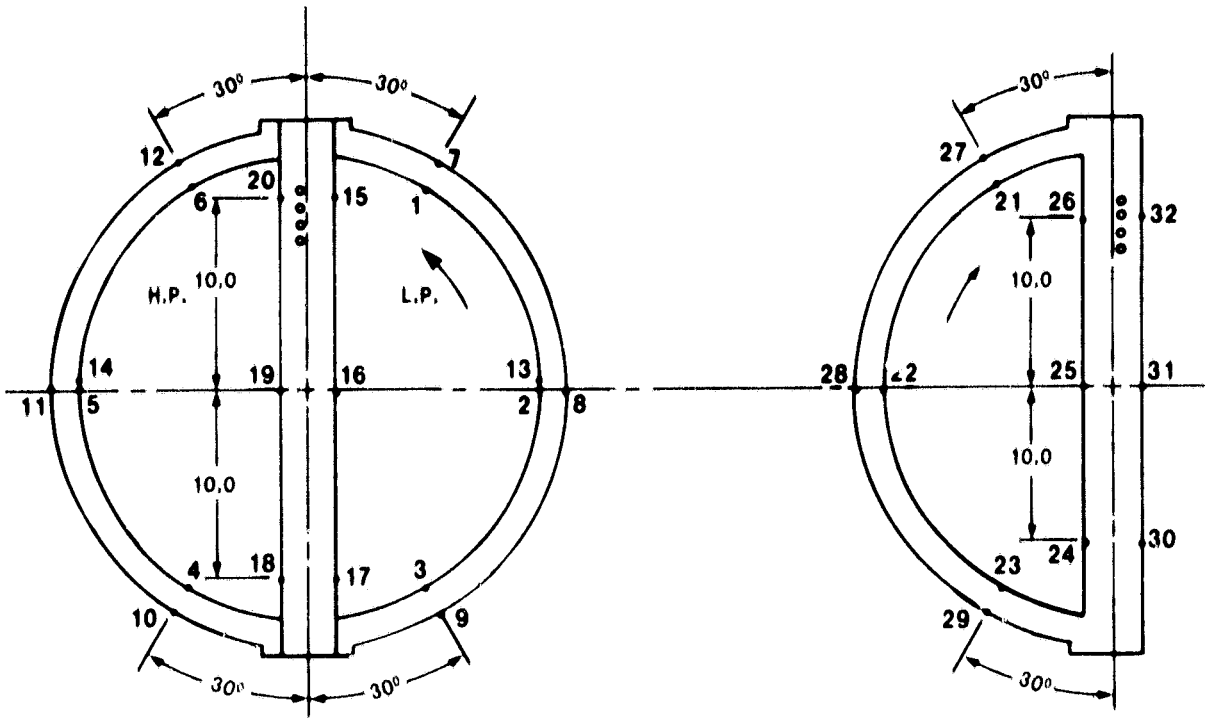

Figure V.B.4.2 Outer Seal Probe Mounting Location

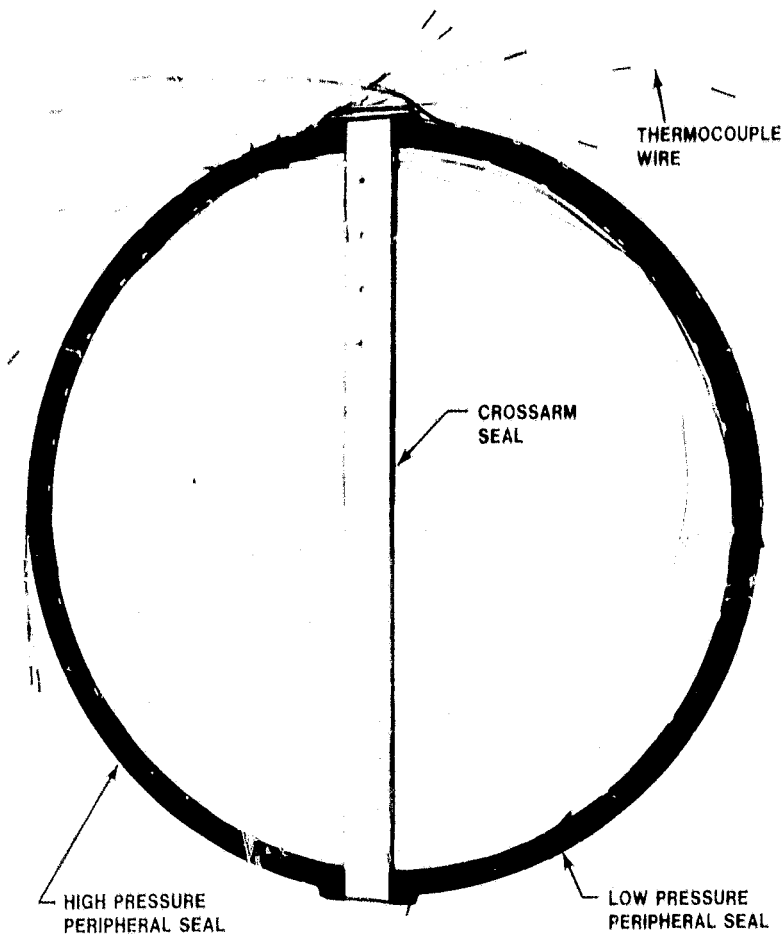

Figure V.B.4.3 Instrumented Inner Seal Assembly

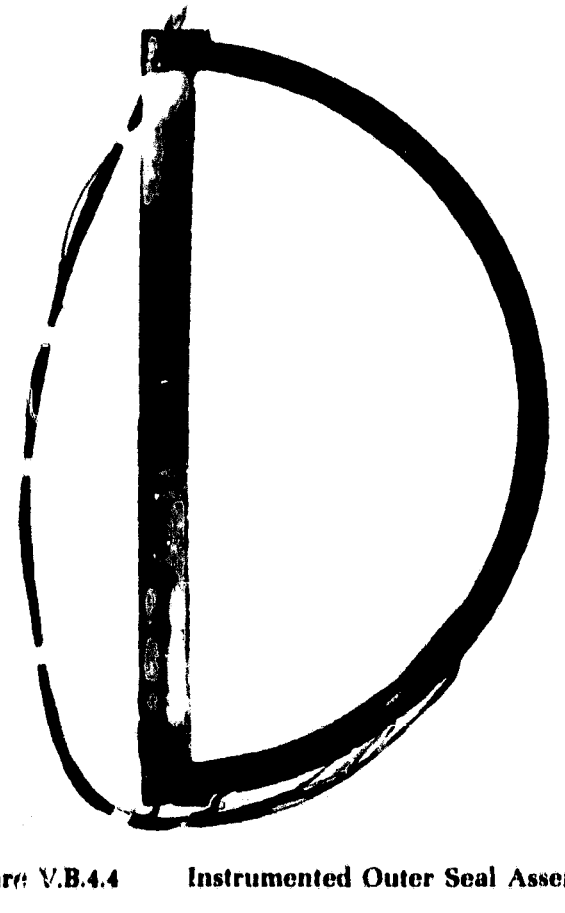

Figure V.B.4.4 Instrumented Outer Seal Assembly

SEAL COMPONENT	CURRENT FORD COATING	L.P. GAS INLET = 1200°C (2192°F.) H.P. AIR INLET TEMP. 104°C. (220°F.)	232°C. (450°F.)	ESTIMATED COATING REQUIREMENTS FOR 1200°C APPLICATION
		°C (°F)	°C (°F)	
1. INNER SEAL				
A. HIGH PRESSURE "C" SHOE	A	125-195 (257-383)	265-330 (509-626)	COATING A IS MARGINAL AT THIS TEMP. REPLACE WITH COATING B
B. LOW PRESSURE "C" SHOW	A	145-335 (293-635)	280-475 (536-887)	COATING A MUST BE REPLACED WITH B AT THESE TEMPERATURES
C. CROSS-ARM	B			
1. H.P. CARRY-OVER		730-955 (1346-1751)	865-1090 (1589-1994)	COATING B MAY BE MARGINAL AT THIS TEMP. A NEW COATING MAY HAVE TO BE DEVELOPED
2. L.P. CARRY-OVER		600-705 (1112-1301)	735-845 (1355-1553)	
2. OUTER SEAL				
A. PERIPHERY	C	115-150 (239-302)	255-290 (491-554)	REPLACE WITH COATING A
B. CROSS-ARM				
1. H.P. CARRY-OVER	C	110-125 (230-257)	250-260 (492-500)	REPLACE WITH COATING A
2. L.P. CARRY-OVER	A	125-420 (257-788)	260-560 (500-1040)	REPLACE WITH COATING B OR DEVELOP NEW COATING

Table V.B.4.1 Seal Temperatures for 1200°C (2192°F) Regenerator Inlet Temperature

With the exception of the inner seal crossarm location, it appears the current state of the art seal coatings can be substituted at various seal component locations to satisfy projected temperature requirements. More testing is required before the upper temperature limitation of the current inner seal crossarm coating can be defined.

V.C. TASK SUMMARY

Three matrix types have been characterized in terms of radial and tangential MOR and MOE and radial compressive strength: the Supplier A wrapped, sinusoidal passage AS; the Supplier D wrapped, rectangular passage MAS-2; and the Supplier I extruded triangular passage MAS. Weibull distribution of these data indicates the variation in properties are the result of processing variations between cores rather than fundamental material property differences.

Three-dimensional finite element stress anaylsis of the above matrix configurations indicated stress relief slots substantially reduce tangential stress in the rim of a regenerator, compared to an unslotted regenerator. Localized high stress regions do occur at the slot below the hot face, but they diminish rapidly with distance. Consequently, they usually do not propagate to the hot surface of the core.

The maximum stress is a function of the number of equally spaced slots and the slot geometry. The slot geometries evaluated consist of a one inch radial depth at the hot face which is tapered axially to 25%, 50% or 100% of the core thickness.

Tangential stress safety factors are defined as the ratio of maximum stress to average strength. Due to the large variance in physical properties of cellular ceramic structures, there is an equally large variance in thermal stress safety factors. Consequently these values should be compared on a relative basis to determine durability potential for various designs.

An axisymmetric finite element analysis indicates that in order to successfully bond a ring gear to a thin-wall AS core, a minimum reduction of 70% in apparent modulus is required. The interrupted elastomer configuration, which has operated successfully in the engine, has been shown to provide a 90% reduction in apparent modulus compared to the standard configuration.

A preliminary test evaluation indicates that with the exception of the inner seal crossarm, current state of the art seal coatings appear to be acceptable for 1200°C (2192°F) regenerator inlet temperature operation. Additional testing is required to establish the upper temperature limitation of the crossarm coating. A more refractory material, such as silicon nitride, may be required for regenerators where the inlet temperature exceeds 1100°C (2012°F) or 1200°C (2192°F).

TASK VI. THERMAL STABILITY TESTS OF CERAMICS

VI. A. INTRODUCTION

The ongoing development work on the continuous combustion engines places a major emphasis on increasingly higher operating temperatures to realize improved efficiencies. As a consequence the exhaust gas energy recovery systems face a constant demand for higher temperature operating capability. It is, therefore, the purpose of this task to evaluate candidate heat exchanger materials at high temperature in presence of appropriate corrosive agents to define their operating temperature limits in the regenerator application.

The laboratory testing program developed and pursued in this task, which is based on the experience gained in Task III, had the dual purpose of determining the upper service temperature limit for the state-of-the-art regenerator matrix material (e.g. leached LAS and MAS) and to evaluate new materials with potential for temperature capability well above the service temperature of the regenerator in the 707 gas turbine engine (800°C-1472°F). The test program involved the evaluation of the thermal stability of various candidate materials at 1000°C (1832°F), 1100°C (2012°F) and 1200°C (2192°F) in air alone and in presence of sodium salt.

The thermal stability of the materials in air was evaluated by the measurement of dimensional change following periodic exposure to test temperature, and by studying the change in thermal expansion behavior of the material after the test. For the evaluation of the thermal stability in sodium salt the specimens were soaked in a 3.5% sodium chloride solution before exposing to the test temperature. All the length measurements of the specimens were made by means of a Sheffield Visual Comparator with 5000:1 magnification. The lengths were measured to within 2.5 x 10^{-5} mm (one millionth of an inch), with an accuracyof ± 1.30 x 10^{-4} mm (± 5 millionths of an inch). The thermal expansion of the material was determined by means of Theta differential dilatometer from room temperature to test temperature with the specimen in the as received condition and after the high temperature test.

The materials evaluated are listed in Table III.B.1.1 and the same specimen machining and cleaning procedures described in task III were used in this program. Duplicate samples of each material have been prepared for each temperature and were evaluated with 9455 LAS Standard. When a material failed at one of the higher temperatures the test was repeated at a temperature 50°C below the failure temperature.

VI.B. DISCUSSION

VI.B.1. 1000°C (1832°F) Test Temperature

Sixteen experimental materials (2-LAS/MAS, 8-MAS, 3-leached LAS, 1-LAS, 1-ZR/MAS and 1-siC) along with 9455 LAS Standard have been evaluated in this program. Ten of these materials were tested during the earlier part of the program and the other six (3-MAS, 1-LAS/MAS, 1-AS and 1-ZR/MAS identified with (⊙), (▼), (▽), (⊡), (▲), and (◯) in Table III.B.1.1) were evaluated towards the end of the program. These last six materials represented an improvement in both material and

processing technology and can be considered to be the state-of-the-art materials. The thermal stability data for all of these materials at 1000°C (1832°F) in air are presented in Figure VI.B.1.1. A discussion of the data for the ten materials evaluated during the early part of the program is presented first followed by the discussion of the last six materials.

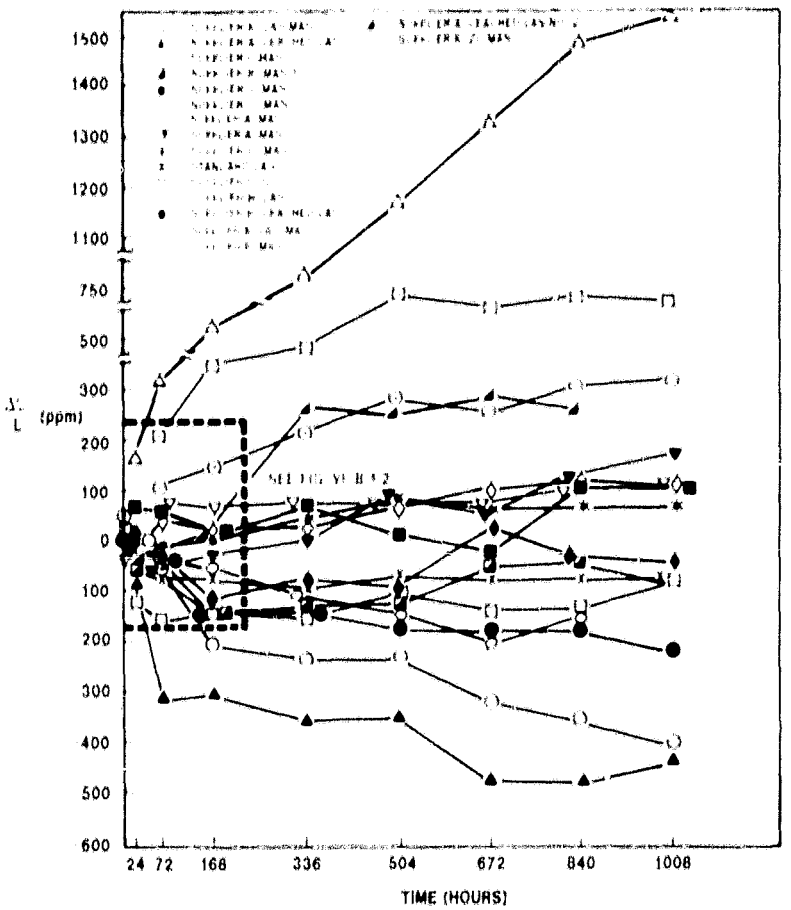

Figure VI.B.1.1 Physical Stability of Various Materials at 1000°C (1832°F)

The area shown in the dotted section in Figure VI.B.1.1 is expanded and presented in Figure VI.B.1.2 to clearly show the trends of behavior of these materials during the initial 72 hours of the test. The thermal stability data at 1000°C in air presented in Figure VI.B.1.1 and VI.B.1.2 show the following trends: (1) the thermal instability of Supplier K-LAS/MAS (Δ) continues to increase with increasing exposure to 1000°C, (2) the leached LAS materials of Supplier A (▲) and Supplier B (●) after sharp early shrinkage continues to shrink at a much reduced rate. This is understandable from the fact that this material has a collapsed skeletal structure due to the Li ion removal from the lattice and will consolidate on heating. Since the magnitude of this shrinkage is a function of temperature, the Supplier B leached LAS structure (●) is apparently more stable than the Supplier A leached LAS structure, (3) the MAS materials are generally quite stable and (4) the Supplier L. Silicon carbide (*) showed no thermal instability. These trends showed little change as the testing continued towards the completion of 1000 hours. It is interesting to note that most of the materials showed less than 100 ppm change during the last 900 hours test, and particularly, the MAS materials showed little dimensional change during this period.

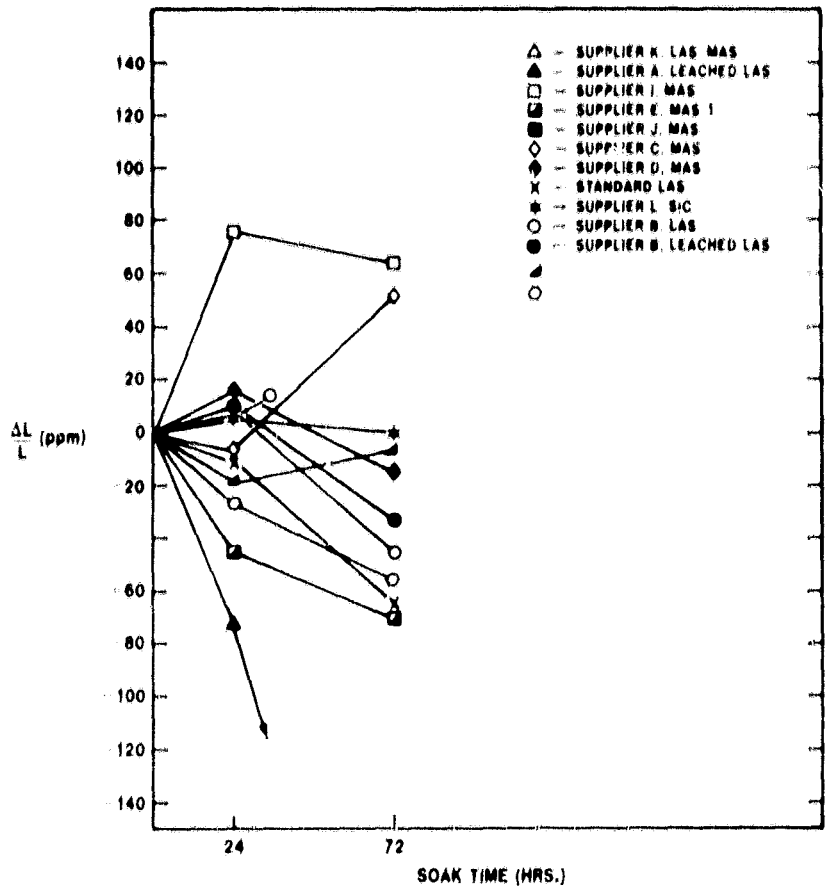

Figure VI.B.1.2 Enlargement of Area of Figure VI.B.1.1; 1000°C (1832°F)

The later and presumed to be improved LAS/MAS composition (⊡) from Supplier K showed a slightly improved instability but it is significantly higher than the standard 9455 LAS composition (X). As is the case with the earlier composition (Δ) this new composition showed a continuing increase in instability with increasing test time, indicating that this material is inherently unstable. All of the new MAS materials, i.e. Supplier E-MAS (▽), A-MAS extruded (⊙) and A-MAS wrapped (▼), showed very small dimensional change indicating excellent thermal stability. Of these the Supplier A-MAS extruded matrix, however, showed the largest dimensional change, indicating that this material is less stable than the other MAS materials evaluated.

The second generation leached LAS (◢) material (Figure VI.B.1.1) from Supplier A exhibits a reduced level of instability in the opposite direction when compared to the first generation as material (▲).

The Supplier K-ZR/MAS (◯) material exhibits a significant improvement in stability when compared to their LAS/MAS materials (Δ and ⊡).

The thermal expansion behavior of these materials before and after testing generally confirm these observations based on thermal stability data. The thermal expansion of these materials from room temperature to 1000°C (RT — 1832°F) before and after the 1900°C (1832°F) thermal instability test are presented in Figs. VI.B.1.3 through VI.B.1.17.

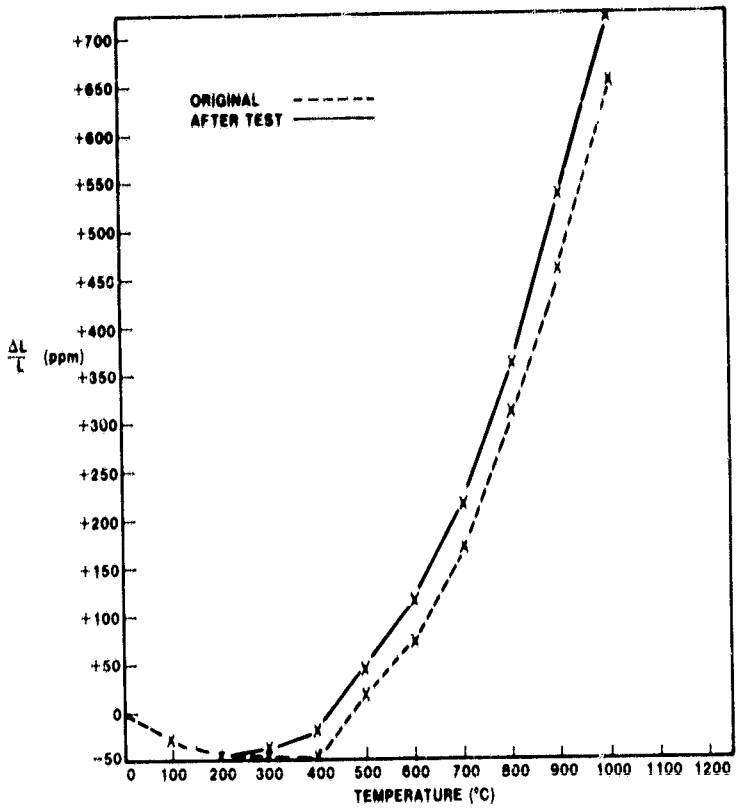

Figure VI.B.1.3 **9455 LAS Standard; Thermal Expansion Before and After 1000°C (1832°F) Thermal Stability Testing**

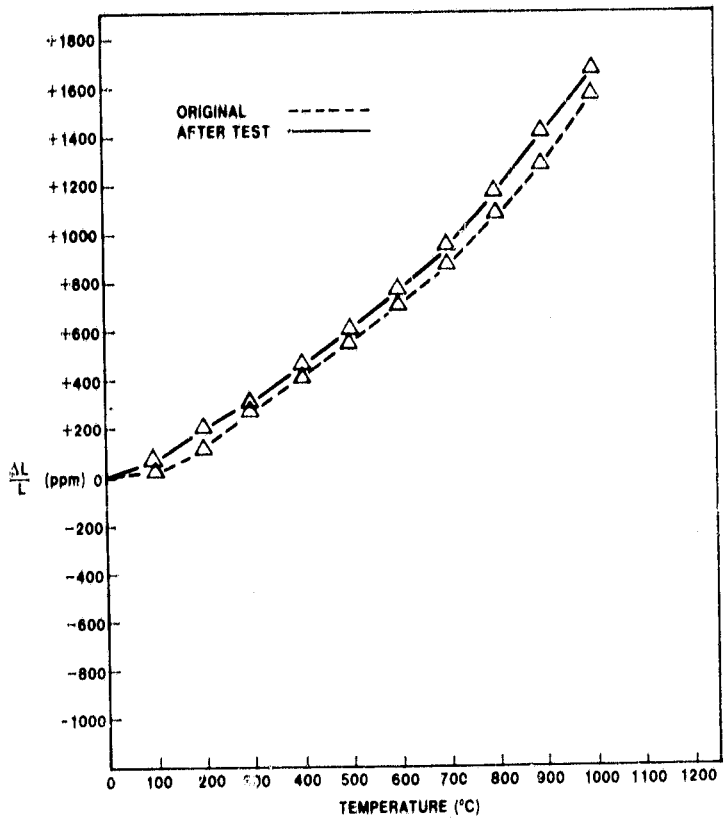

Figure VI.B.1.4 **Supplier K LAS/MAS; Thermal Expansion Before and After 1000°C (1832°F) Thermal Stability Testing.**

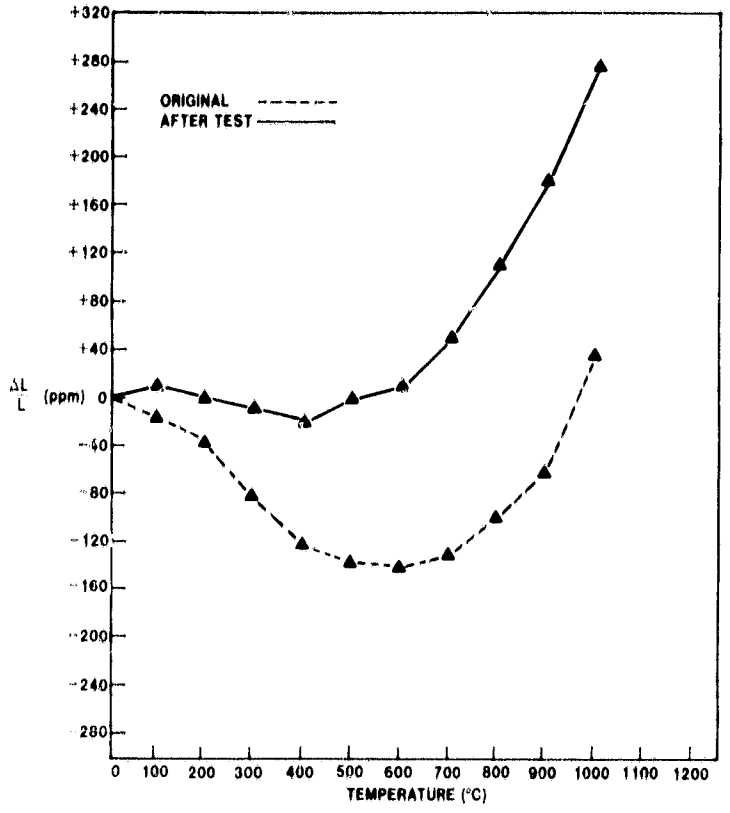

Figure VI.B.1.5 Supplier A Leached LAS; Thermal Expansion Before and After 1000°C (1832°F) Thermal Stability Testing

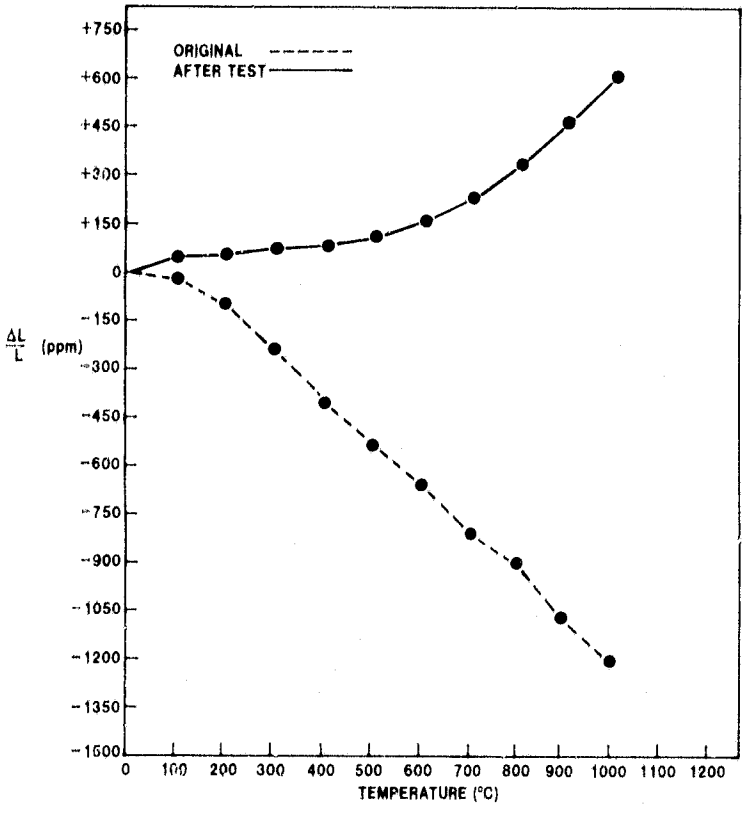

Figure VI.B.1.6 Supplier B Leached LAS; Thermal Expansion Before and After 1000°C (1832°F) Thermal Stability Testing

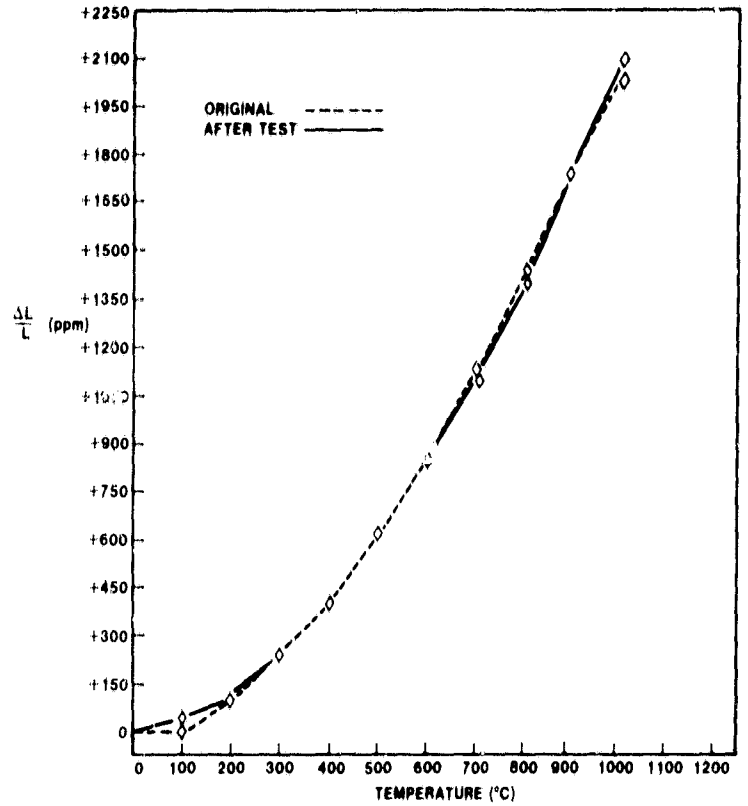

Figure VI.B.1.7 Supplier C MAS; Thermal Expansion Before and After 1000°C (1832°F) Thermal Stability Testing

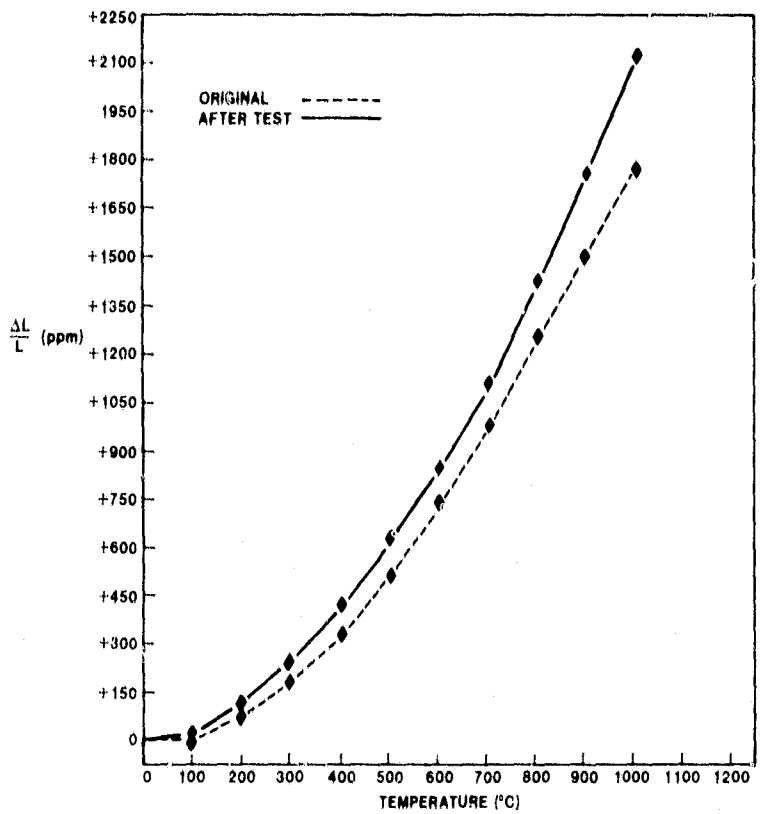

Figure VI.B.1.8 Supplier D MAS; Thermal Expansion Before and After 1000°C (1832°F) Thermal Stability Testing

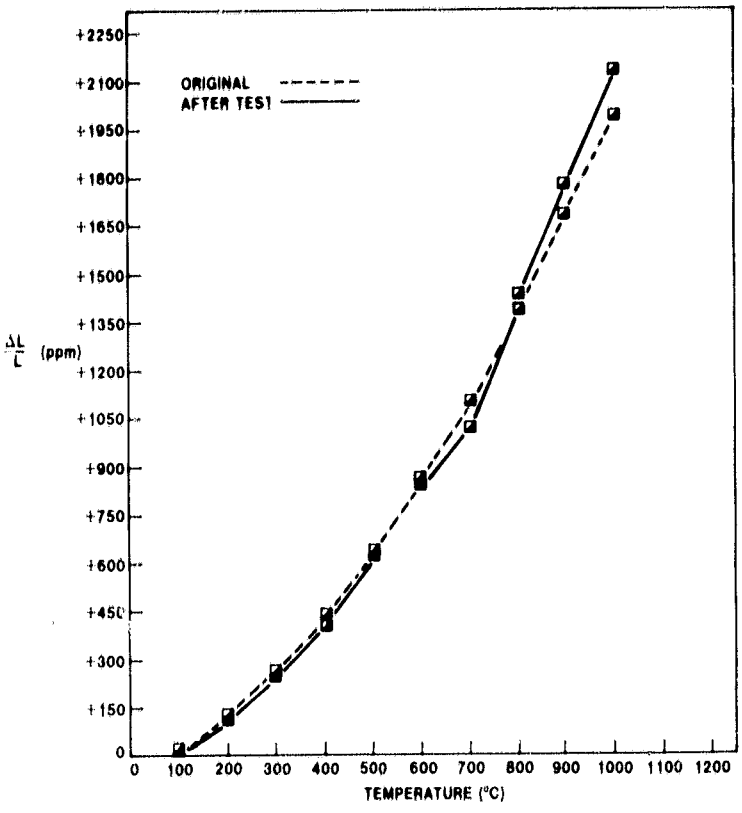

Figure VI.B.1.9 Supplier E MAS; Thermal Expansion Before and After 1000°C (1832°F) Thermal Stability Testing

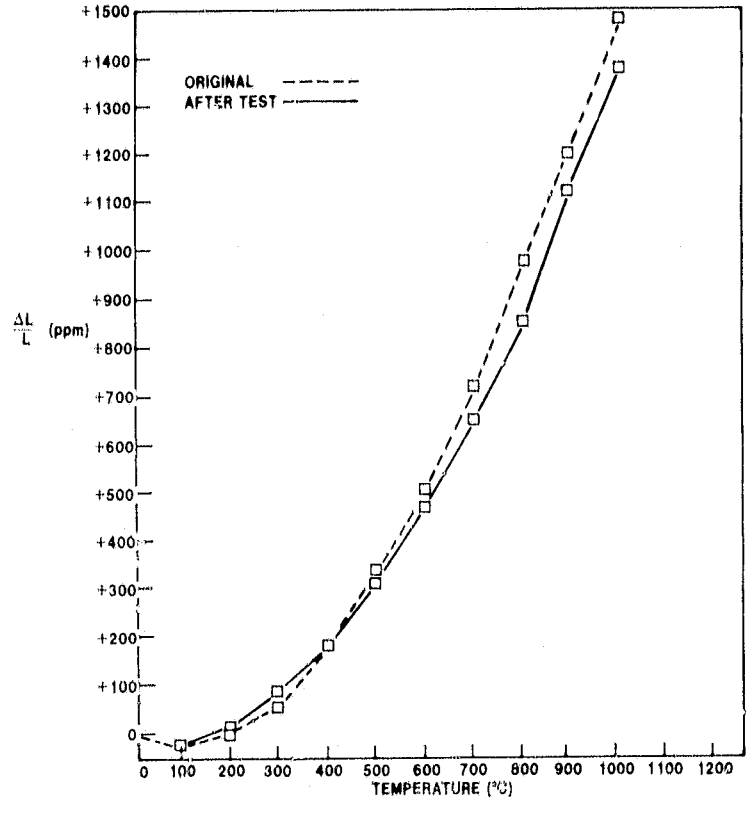

Figure VI.B.1.10 Supplier I MAS; Thermal Expansion Before and After 1000°C (1832°F) Thermal Stability Testing

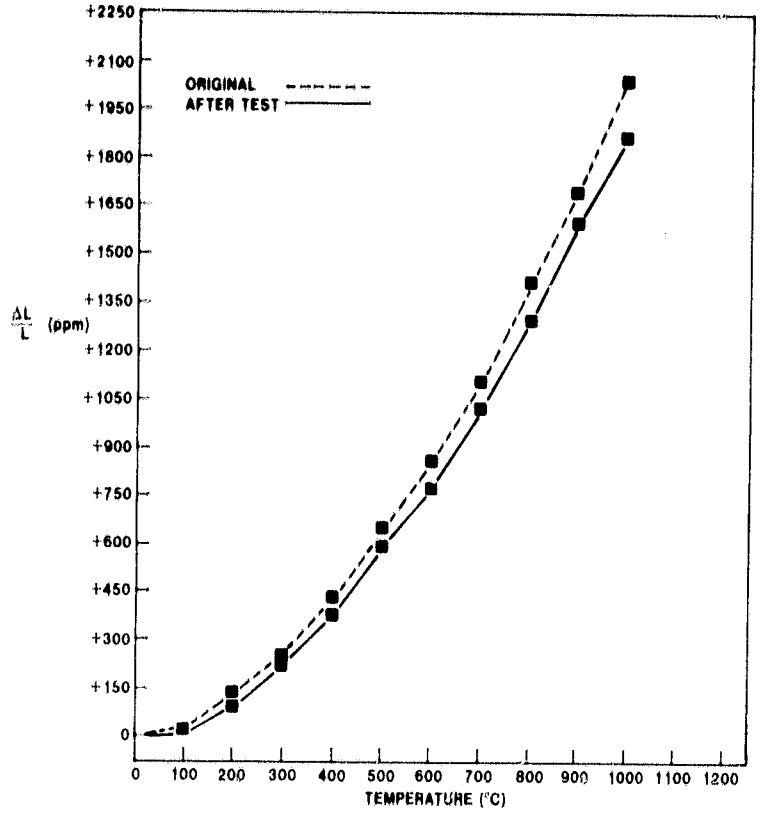

Figure VI.B.1.11 Supplier J MAS; Thermal Expansion Before and After 1000°C (1832°F) Thermal Stability Testing

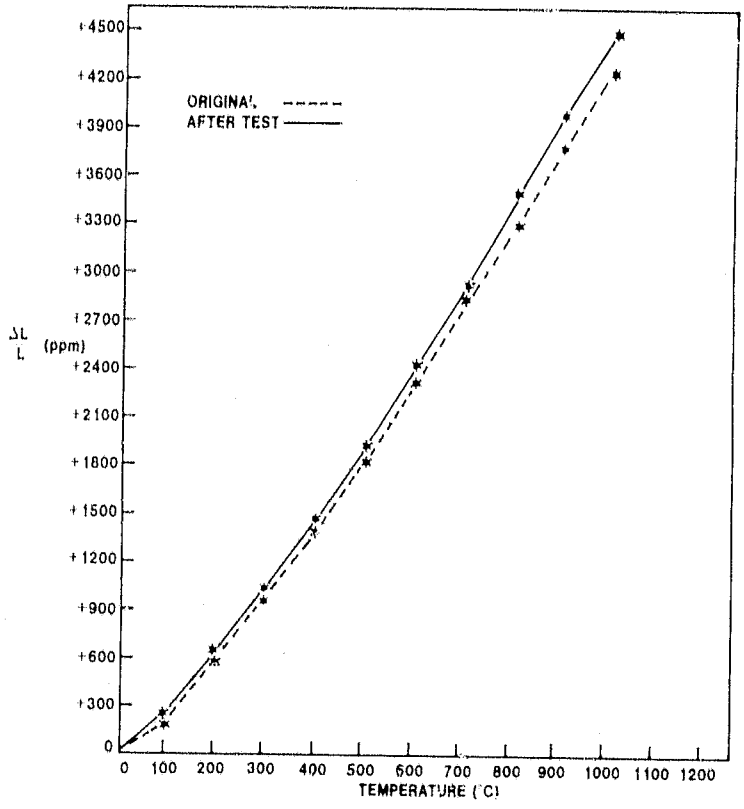

Figure VI.B.1.12 Supplier L SiC; Thermal Expansion Before and After 1000°C (1832°F) Thermal Stability Testing

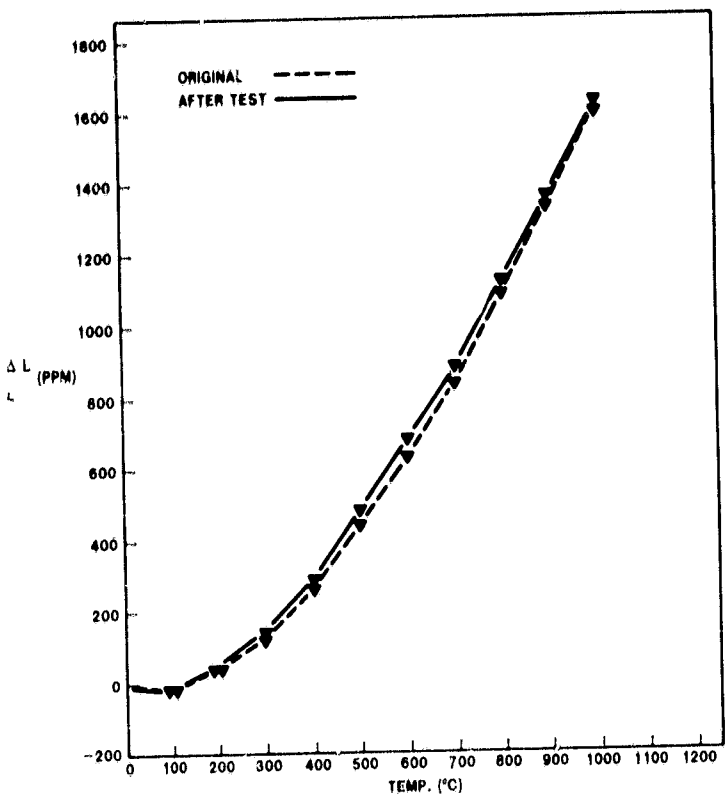

Figure VI.B.1.13 Supplier A, MAS (Wrapped); Thermal Expansion Before and After 1000°C (1832°F) Thermal Stability Testing

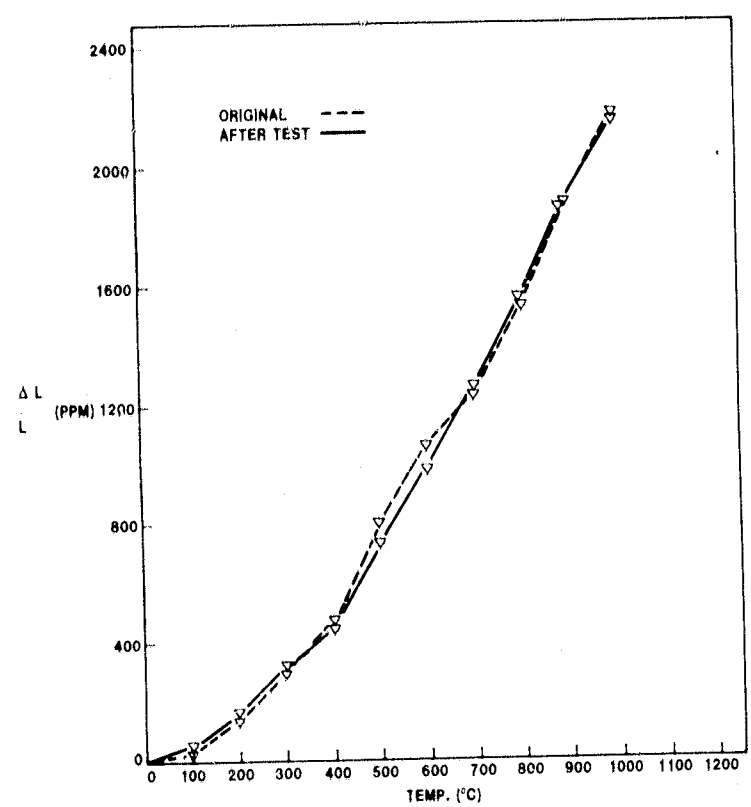

Figure VI.B.1.14 Supplier E. MAS; Thermal Expansion Before and After 1000°C (1832°F) Thermal Stability Testing

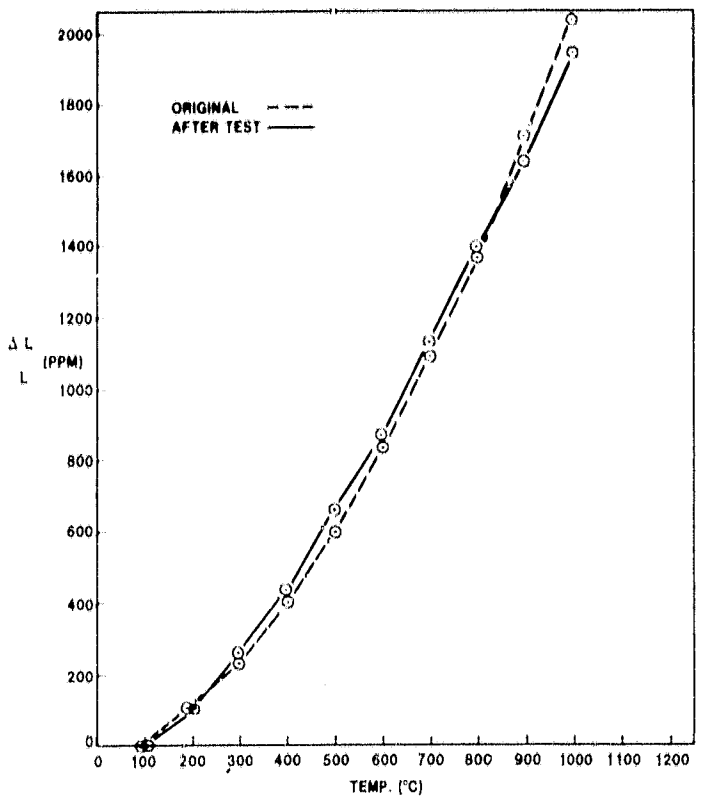

Figure VI.B.1.15 Supplier A, MAS (Extruded); Thermal Expansion Before and After 1000°C (1832°F) Thermal Stability Testing

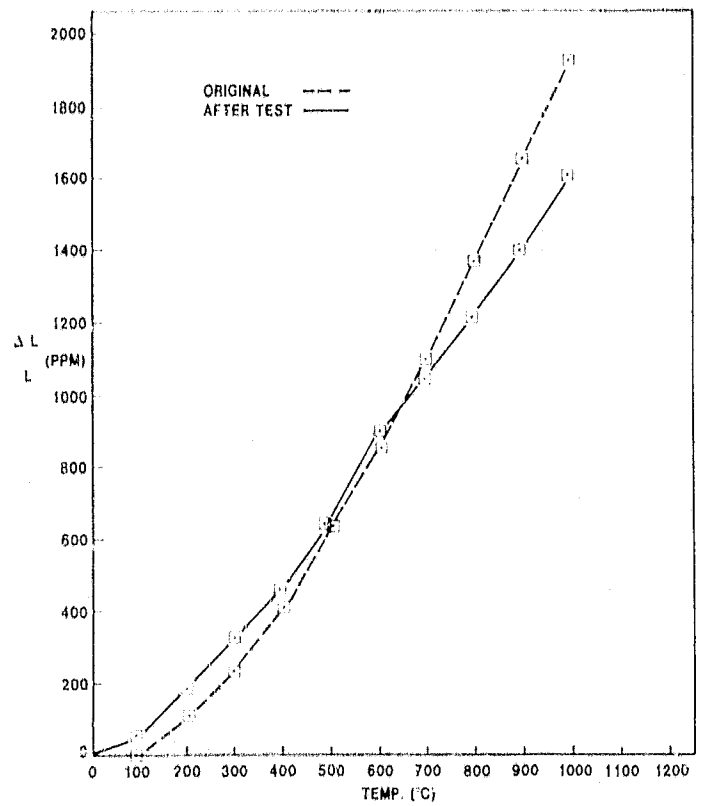

Figure VI.B.1.16 Supplier K, LAS/MAS; Thermal Expansion Before and After 1000°C (1832°F) Thermal Stability Testing

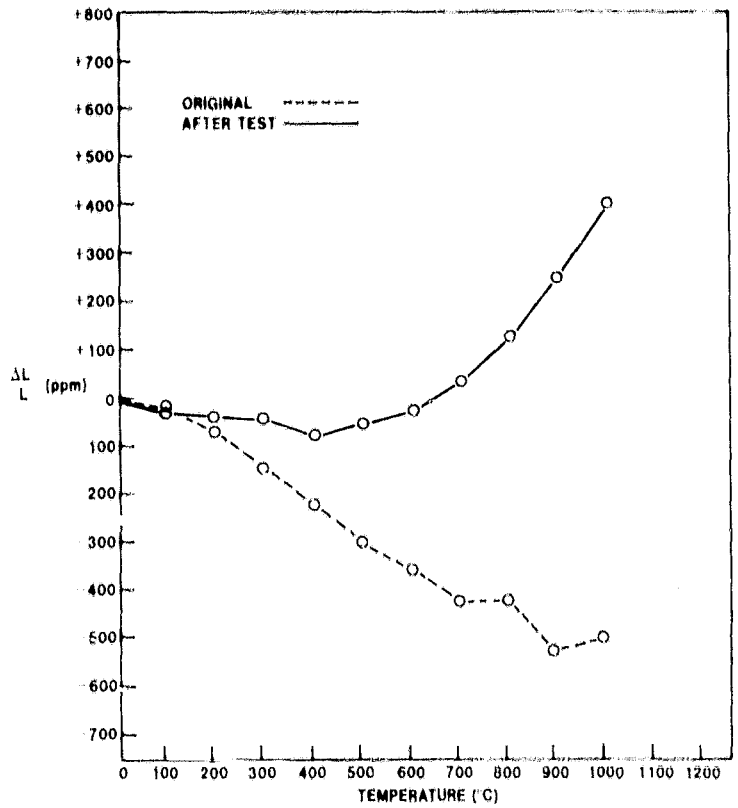

Figure VI.B.1.17 Supplier B LAS; Thermal Expansion Before and After 1000°C (1832°F) Thermal Stability Testing

The thermal expansion data for the 9455 LAS standard shown in Figure VI.B.1.3 is consistent with the data obtained during earlier tests and the magnitude in the observed change is well within the reproducibility of the dilatometer. The Supplier B-LAS (o) which exhibited a large instability (Figure VI.B.1.1 and VI.B.1.2) showed a significant change in thermal expansion (VI.B.1.17), moving from negative expansion to positive expansion, after 1000 hour exposure to the 1000°C. This behavior indicates that this material is unstable and may not be suitable for the regenerator application.

Figures VI.B.1.4 and VI.B.1.16 illustrate the thermal expansion characteristics of the Supplier K-LAS/MAS first generation (Δ) and second generation (⊡) materials, respectively. In contrast to the large growth observed in instability test, the thermal expansion behavior indicates relatively little change. This behavior is somewhat surprising and leads one to conclude that the phase transformations at 1000°C (1832°F) which caused the observed dimensional changes do not affect the thermal expansion behavior of this material.

Figures VI.B.1.5 and VI.B.1.6 show the thermal expansion behavior of the leached LAS materials before and after the 1000°C (1832°F) thermal instability test. While both materials exhibited similar thermal instability behavior (Figure VI.B.1.1), their thermal expansion behavior following the thermal instability test is markedly different. The Supplier A-leached LAS (▲, Figure VI.B.1.5) has undergone an increase in thermal expansion. The basic response pattern, initially contractive followed by air expansion, has been preserved. In contrast, the leached LAS of Supplier B, (●, Figure VI.B.1.6) has undergone a complete change in both

the magnitude and the character of the thermal expansion response. Before the 1000°C (1832°F) thermal instability test, the material was strongly contractive, while it became slightly expansive following the test.

Figures VI.B.1.7 through VI.B.1.11 compare the thermal expansion behavior of the 1st generation MAS materials discussed earlier, before and after the 1000°C thermal instability test. They show very little change in the thermal expansion behavior after 1000 hour exposure to 1000°C (1832°F), confirming the excellent stability of these materials indicated by data in Figure VI.B.1.1

The thermal expansion behavior of the Supplier L silicon carbide before and after the 1000°C thermal instability test is shown in Figure VI.B.1.12. There is no change in the thermal expansion plots, indicating that the silicon nitride is unaffected by the 1000-hour exposure to 1000°C (1832°F), confirming the excellent thermal stability indicated by the dimensional change data shown in Figure VI.B.1.1.

The new generation MAS materials, whose thermal expansion behavior before and after 1000°C (1832°F) thermal stability test in air is shown in Figures VI.B.1.13 (▼), VI.B.1.14 (▽) and VI.B.1.15 (⊙), appear to be highly stable and are unaffected by the high temperature exposure. As can be seen in the Figures VI.B.1.1 and VI.B.1.13 through VI.B.1.15 there is practically no change in the thermal expansion of these materials, and, with the exception of the Supplier A-extruded MAS matrix (⊙) there is no dimensional change after 1000°C (1832°F) thermal stability test.

The 1000°C (1832°F) thermal stability in presence of sodium test data for these materials is presented in Figure VI.B.1.18.

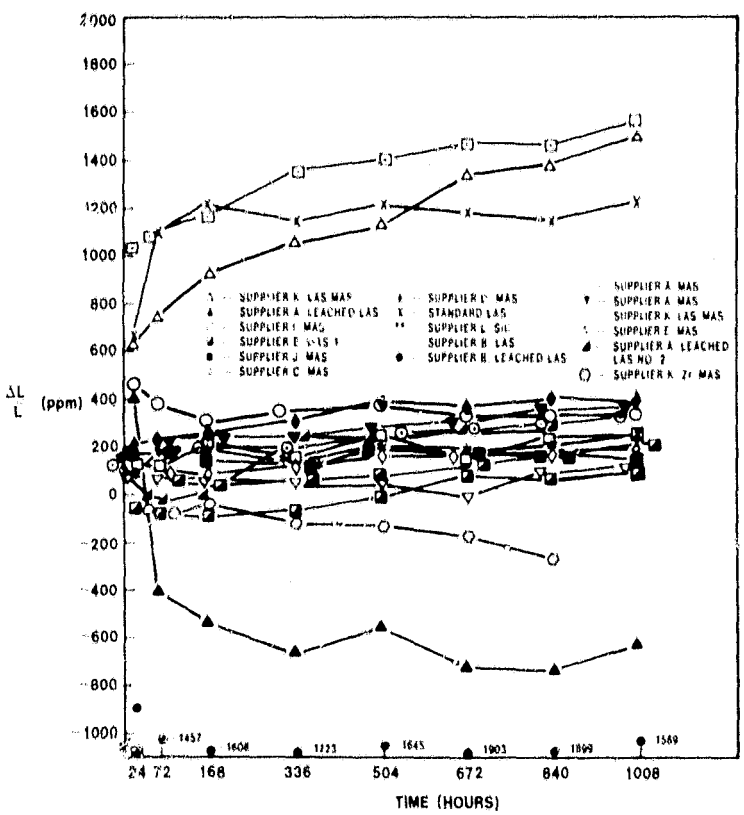

Figure VI.B.1.18 Physical Stability of Various Materials at 1000°C (1832°F) with Sodium Present

The MAS materials and the ZR/MAS material all exhibit good thermal stability in presence of sodium salt at 1000°C (1832°F). The LAS/MAS mixture exhibits a progressive growth in this environment similar to its previous exposure without sodium present. This suggests that the material may be thermally unstable, rather than susceptible to sodium attack.

The Supplier A (▲) and B (●) leached LAS (referred to as AS hereafter) materials react contractively to the sodium stability test. The contraction of the material of Supplier B (●) was so dramatic as to fall off scale, and the numbers to the immediate right of each symbol are the normalized length changes, in parts per million, measured at each time interval. The second generation as material from Supplier A (▲) exhibits reduced instability in the presence of sodium.

A comparison of these data with the corresponding test set without sodium present (Figure VI.B.1.1) points out a most interesting observation. The LAS material of Supplier B appears to be more stable (in a dimensional sense) in the sodium-enriched environment. This observation, without further investigation of the change in material behavior as a result of stability testing, may be misleading as can be seen from thermal expansion comparisons offered for each tested material in Figures VI.B.1.19 through VI.B.1.33. (Note scale differences among the figures). A comparison between these figures and the corresponding figures for similar testing without sodium present just discussed, together with the dimensional stability data, enable one to draw more meaningful conclusions.

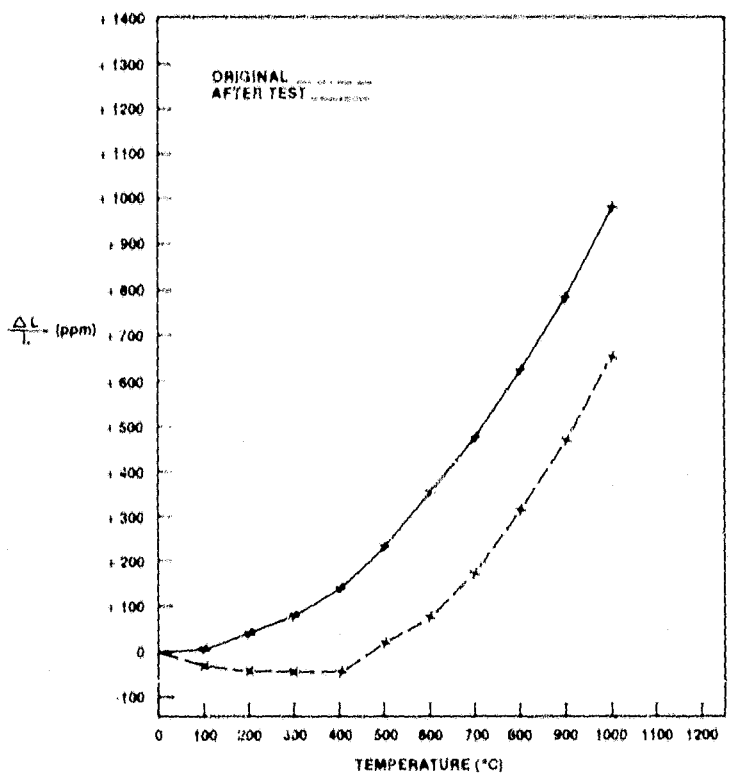

Figure VI.B.1.19 **9455 LAS Standard; Thermal Expansion Before and After 1000°C (1832°F) Thermal Stability Testing with Sodium Present**

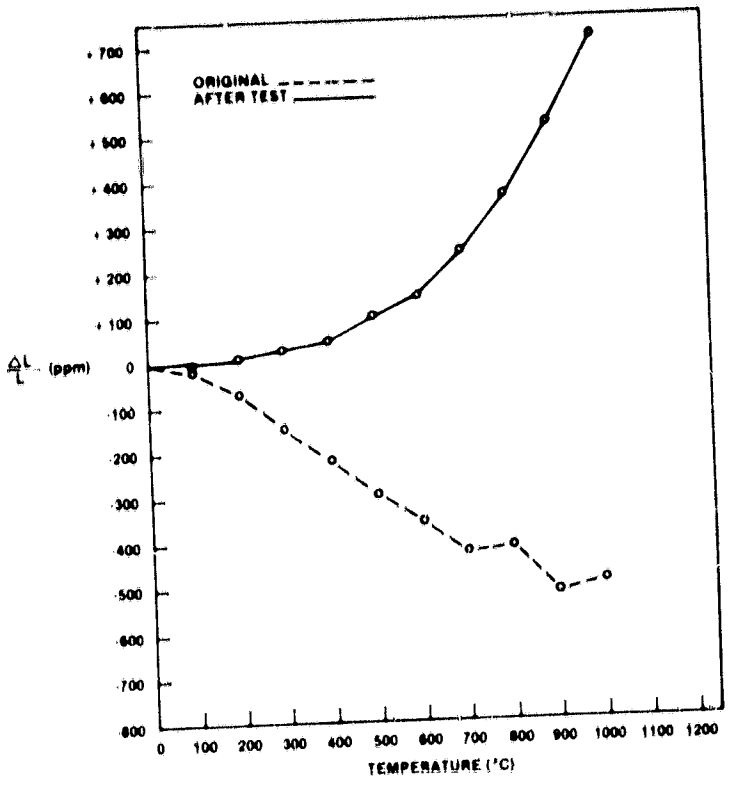

Figure VI.B.1.20 Supplier B LAS; Thermal Expansion Before and After 1000°C (1832°F) Thermal Stability Testing with Sodium Present

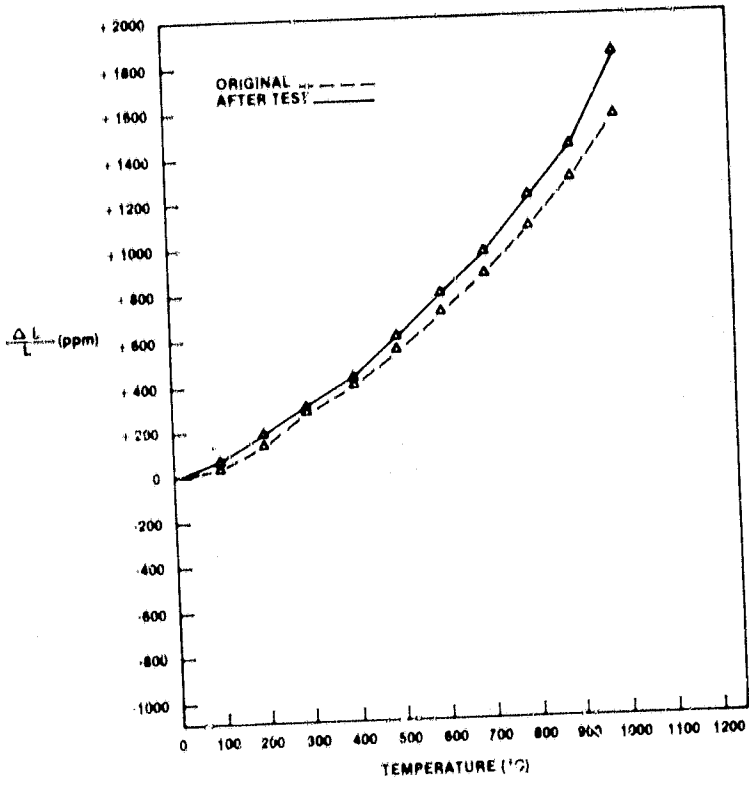

Figure VI.B.1.21 Supplier K LAS/MAS; Thermal Expansion Before and After 1000°C (1832°F) Thermal Stability Testing with Sodium Present

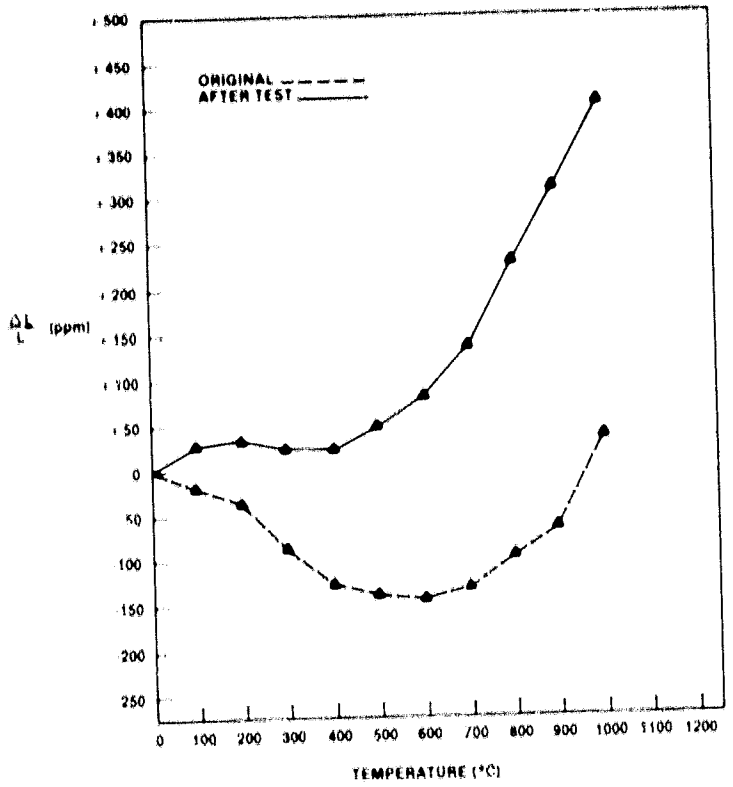

Figure VI.B.1.22 **Supplier A AS; Thermal Expansion Before and After 1000°C (1832°F) Thermal Stability Testing with Sodium Present**

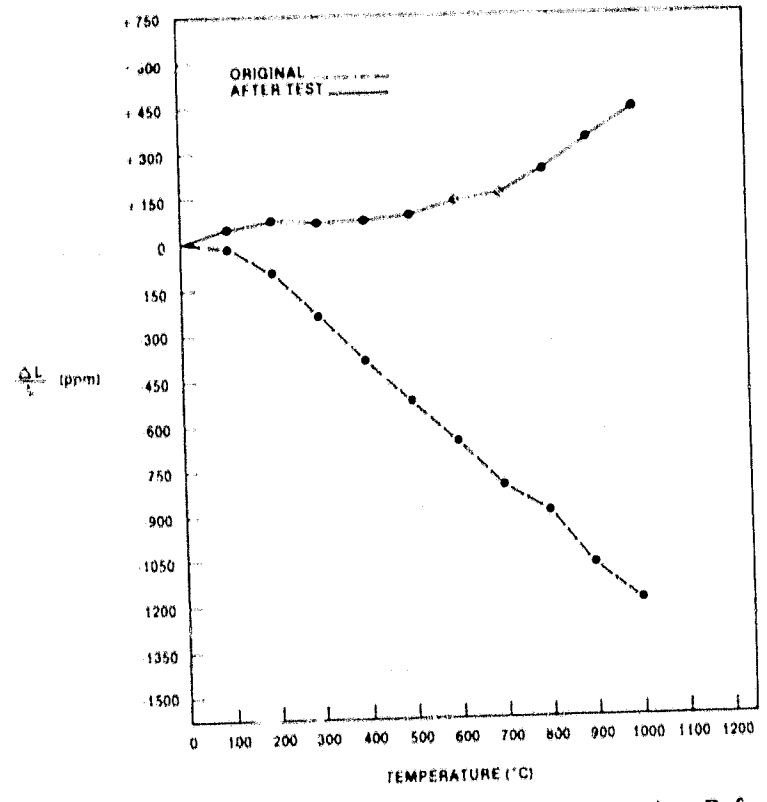

Figure VI.B.1.23 **Supplier B AS, Thermal Expansion Before and After 1000°C (1832°F) Thermal Stability Testing with Sodium Present**

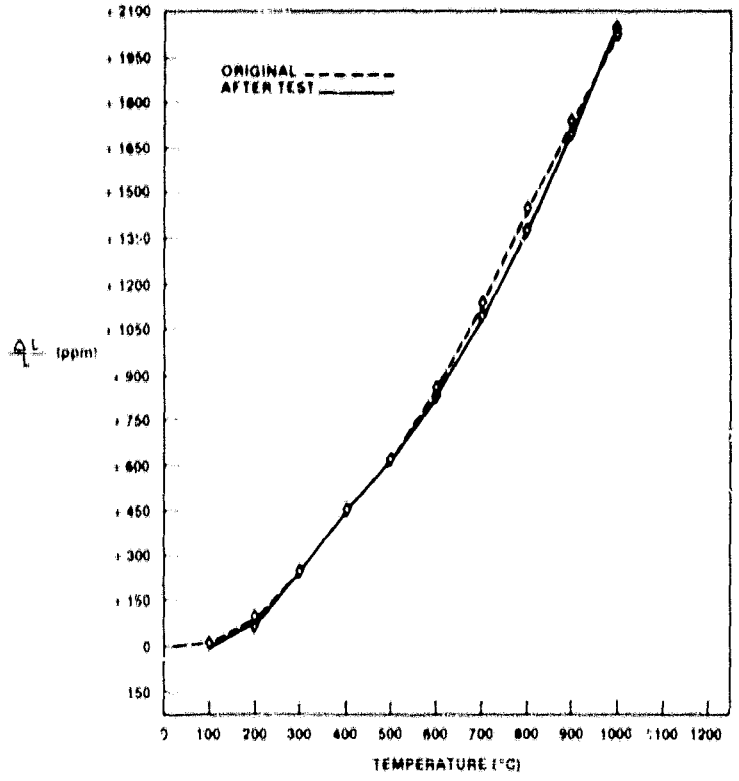

Figure VI.B.1.24 **Supplier C MAS; Thermal Expansion Before and After 1000°C (1832°F) Thermal Stability Testing with Sodium Present**

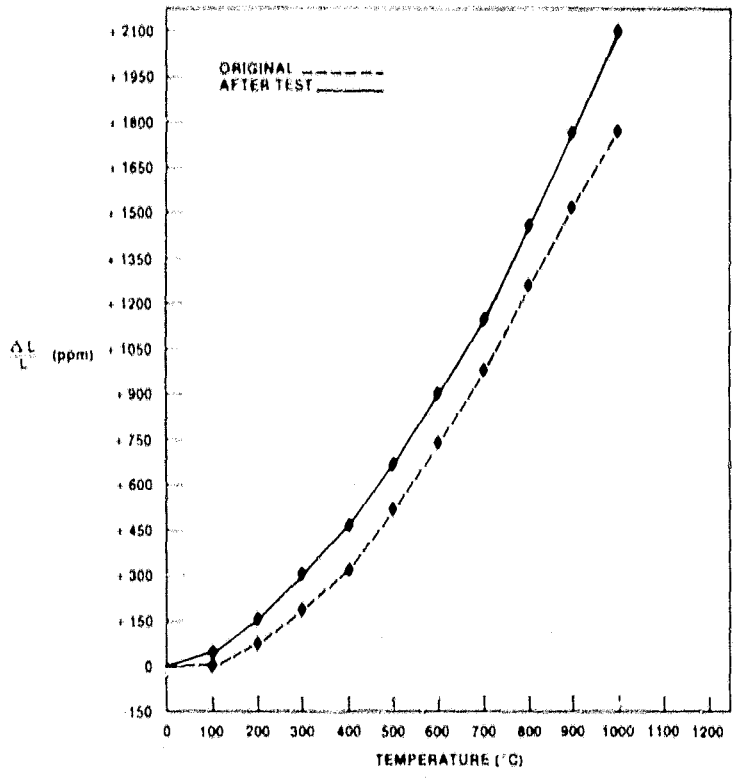

Figure VI.B.1.25 **Supplier D MAS; Thermal Expansion Before and After 1000°C (1832°F) Thermal Stability Testing with Sodium Present**

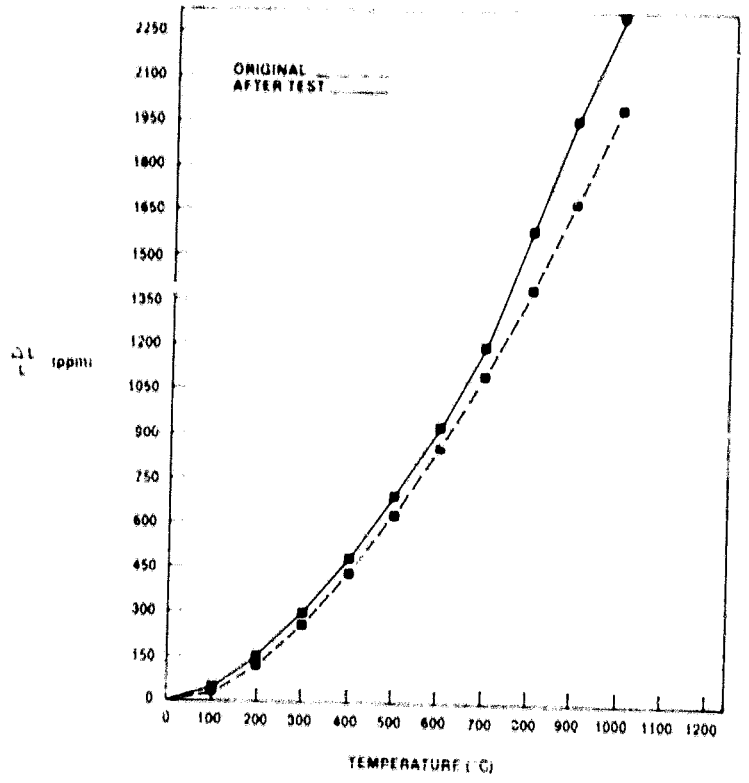

Figure VI.B.1.26 **Supplier E MAS #1; Thermal Expansion Before and After 1000°C (1832°F) Thermal Stability Testing with Sodium Present**

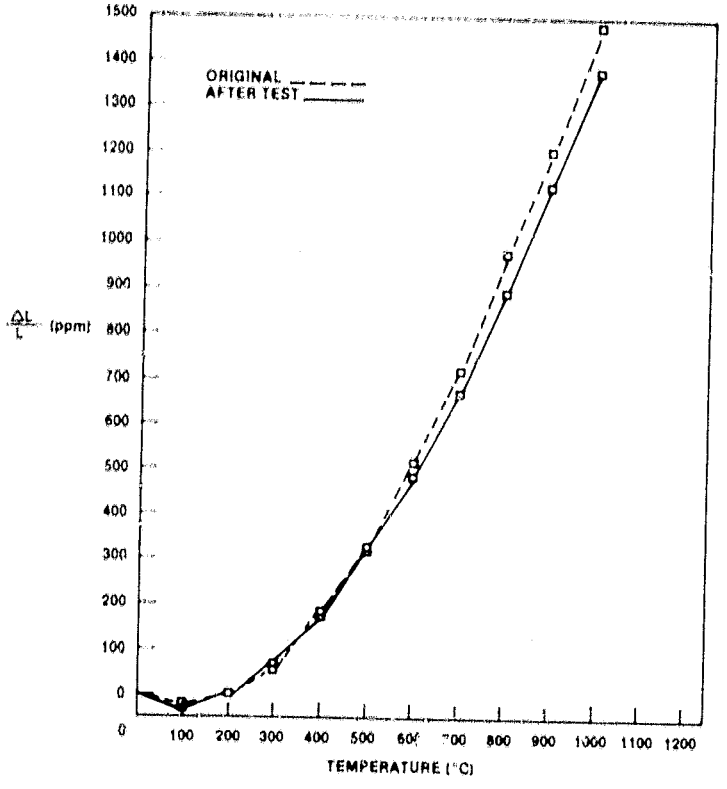

Figure VI.B.1.27 **Supplier I MAS; Thermal Expansion Before and After 1000°C (1832°F) Thermal Stability Testing with Sodium Present**

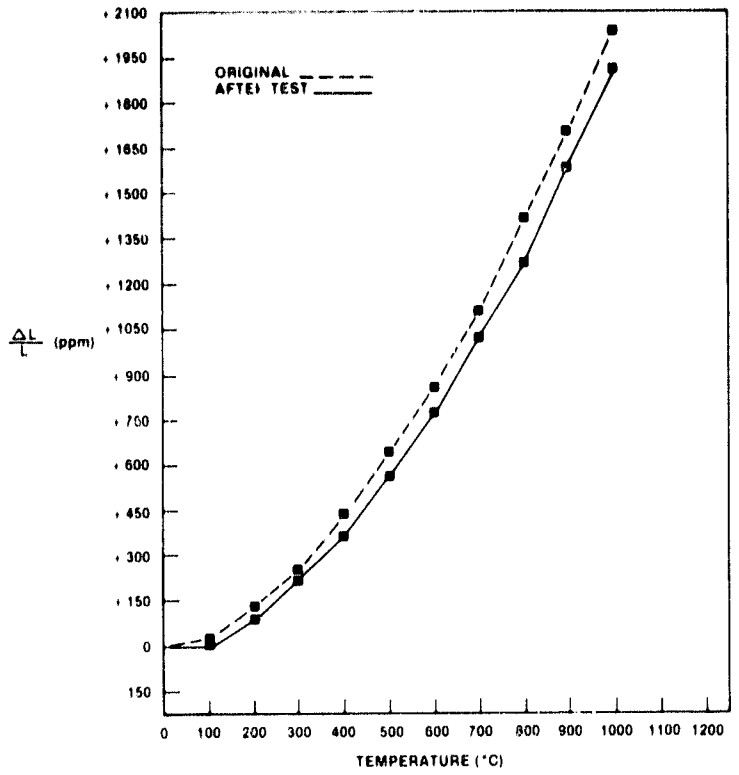

Figure VI.B.1.28 **Supplier J MAS; Thermal Expansion Before and After 1000°C (1832°F) Thermal Stability Testing with Sodium Present**

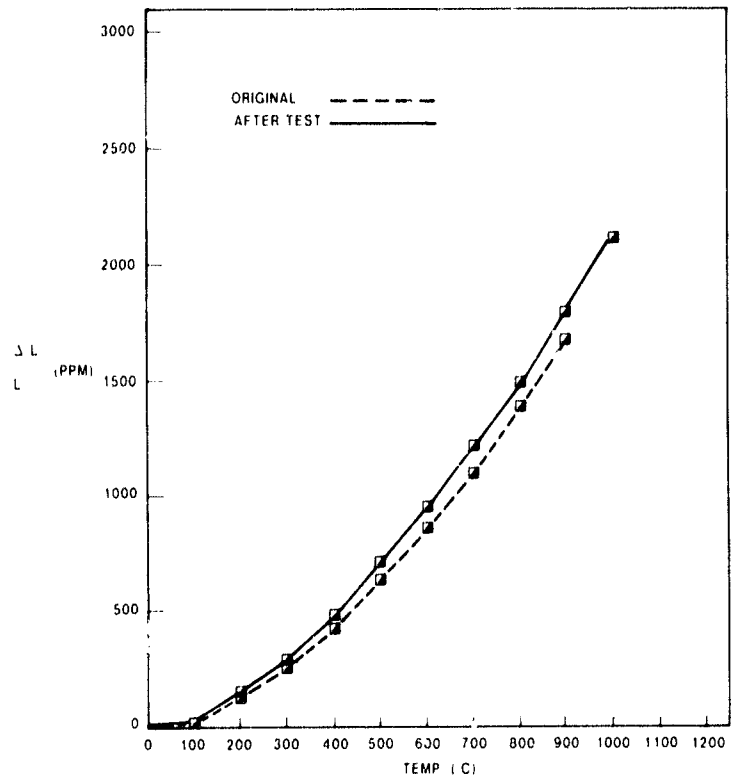

Figure VI.B.1.29 **Supplier E, MAS; Thermal Expansion Before and After 1000°C (1832°F) Thermal Stability Testing with Sodium Present: Duplicate Specimen of Fig. VI.B.1.26**

C-3

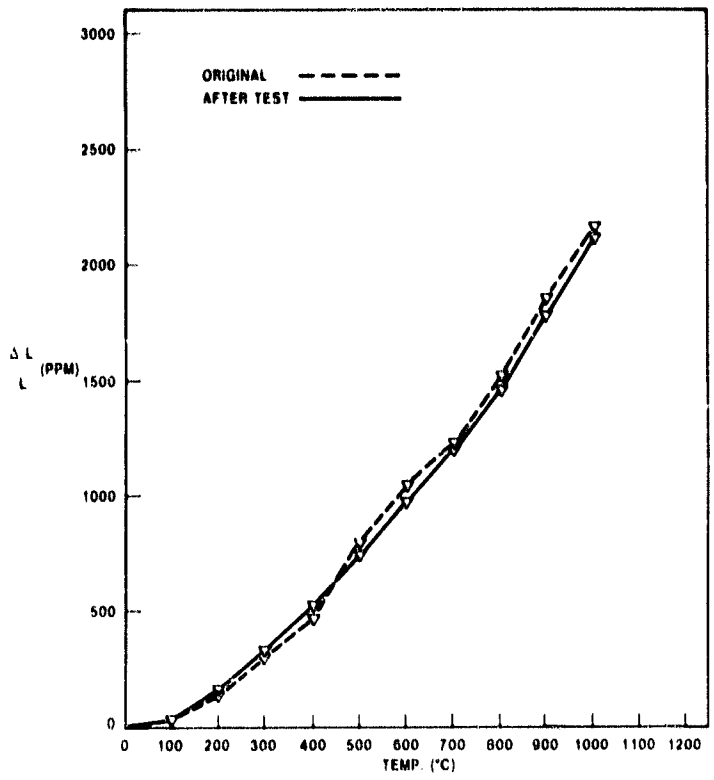

Figure VI.B.1.30 Supplier E, MAS; Thermal Expansion Before and After 1000°C (1832°F) Thermal Stability Testing with Sodium Present

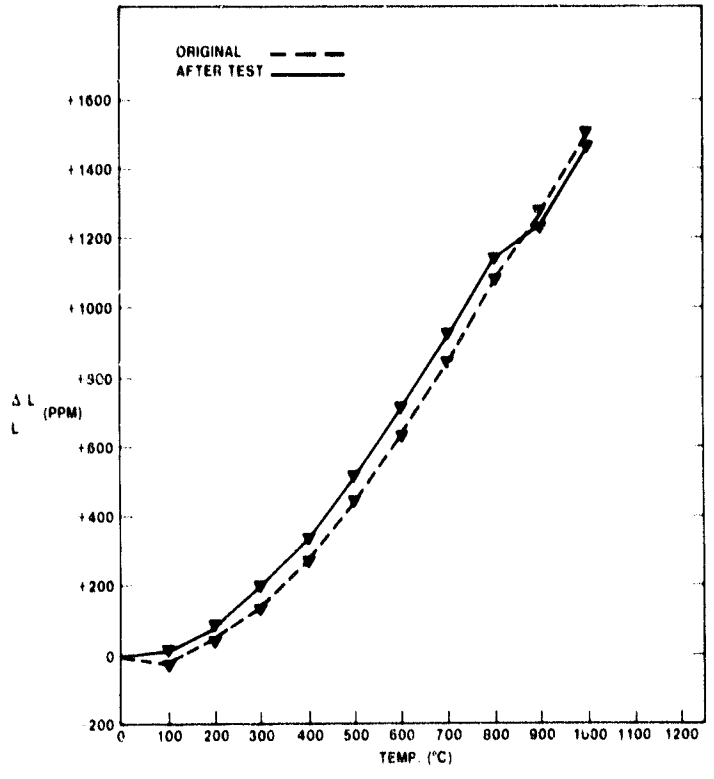

Figure VI.B.1.31 Supplier A, MAS (Wrapped); Thermal Expansion Before and After 1000°C (1832°F) Thermal Stability Testing with Sodium Present

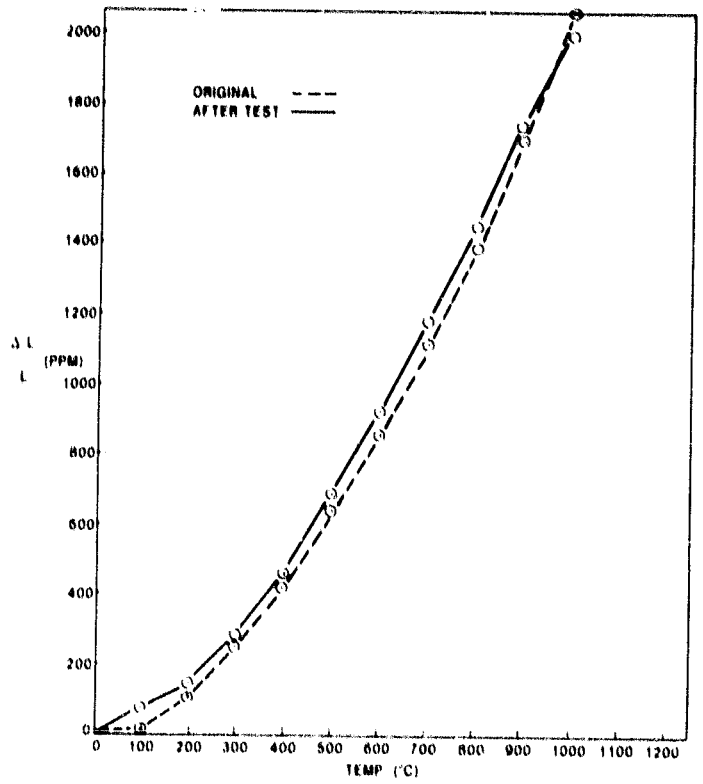

Figure VI.B.1.32 Supplier A, MAS (Extruded); Thermal Expansion Before and After 1000°C (1832°F) Thermal Stability Testing with Sodium Present

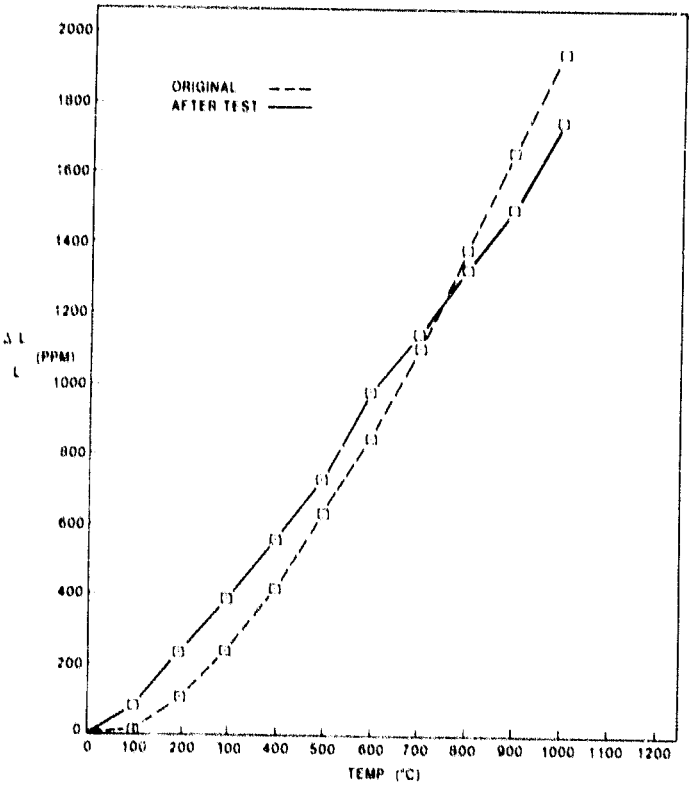

Figure VI.B.1.33 Supplier K, LAS/MAS; Thermal Expansion Before and After 1000°C (1832°F) Thermal Stability Testing with Sodium Present

The change in thermal expansion behavior (Figure VI.B.1.19) indicates a significant material change in the standard 9455 LAS (X). The point made earlier concerning the physical stability of the LAS material of Supplier B can be reinforced by comparing the thermal expansion plots for this material tested with sodium present (Figure VI.B.1.20) and without sodium present (Figure VI.B.1.17). Contrary to the impression created by the dimensional stability data alone, (Figures VI.B.1.1 and VI.B.1.18) this material has obviously suffered more damage as the result of the presence of sodium. In some manner, most likely sodium-for-lithium ion exchange, the sodium has mitigated the contractive nature of this material. This effect is the same as that observed in the accelerated corrosion testing of this material as a matrix insert and detailed in Task III.B.2 of this report.

The LAS/MAS (Δ) mixture of the first generation, while obviously unstable in this thermal environment with or without sodium present, does not suffer a significant change in thermal expansion behavior (Figure VI.B.1.21). The new generation material (□) exhibited a similar behavior (Figure VI.B.1.33).

The AS materials of Supplier A (▲) (Figure VI.B.1.22) and Supplier B (●) (Figure VI.B.1.23) have both experienced a change in their thermal expansion behavior, rendering these originally contractive materials now expansive. Both of these materials underwent a dimensional contraction during testing (Figure VI.B.1.18). The reaction of the Supplier B material (●) was a great deal larger in magnitude than the reaction of the material of Supplier A (▲). This difference is also noted in the degree of change in thermal expansion behavior of the two materials. While the material of Supplier A has become more expansive (Figure VI.B.1.22), the nature of the thermal expansion response before and after testing bear a similarity to each other. The change noted for the AS material of Supplier B (Figure VI.B.1.23) is not only severe, but the nature of the material's response to changes in temperature has been altered. This observation, coupled with the greater dimensional instability observed, indicates that the AS of Supplier A is more resistant to sodium corrosion at 1000°C (1832°F) than the AS material of Supplier B.

All of the MAS materials exhibited good dimensional stability under these test conditions. An examination of each material's thermal expansion behavior before and after testing (Figures VI.B.1.24 through VI.B.1.32) points out that these materials incur little, if any, change as a result of exposure to sodium at 1000°C (1832°F). It is concluded that any of these materials should prove to be satisfactory for service in a regenerator application at 1000°C (1832°F).

Figure VI.B.1.34 indicates the thermal expansion behavior of SiC before and after testing at 1000°C (1832°F) with sodium present. The stability of this material in the corrosive environment at this temperature is excellent; however, its high thermal expansion, high thermal conductivity, and the difficulty of processing will limit its use in regenerator applications.

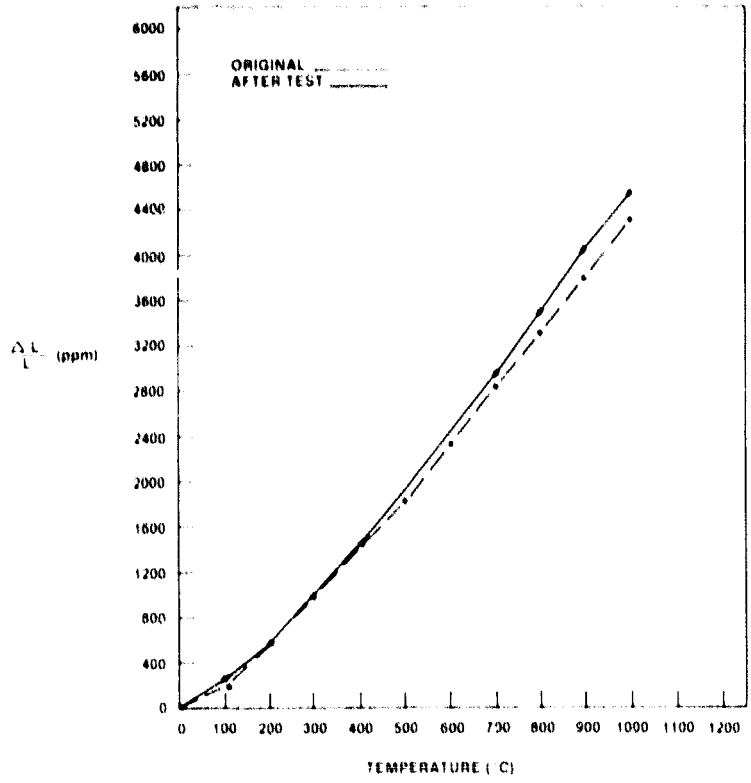

Figure VI.B.1.34 Supplier I. SiC; Thermal Expansion Before and After 1000°C (1832°F) Thermal Stability Testing with Sodium Present

VI.B.2 1050°C (1922°F) Test Temperature

While the initial testing plan defined a program of evaluation at 1000°C (1832°F), 1100°C (2012°F), and 1200°C (2192°F), it is the intent of this contract task to place an upper operating limit on the ceramic regenerator materials. Therefore, tests of three materials, (Supplier A-AS (▲), Supplier B-leached LAS and Supplier B-LAS, 2-AS, 1-LAS), which evidenced a loss of physical integrity at 1100°C (2012°F) and 1200°C (2192°F) (refer to following sections) were placed on test at this midpoint temperature (1050°C).

The thermal stability of these three materials at 1050°C in air is shown in Figure VI.B.2.1. The behavior of these materials at 1050°C is quite similar to that at 1000°C; however, the magnitude of the dimensional change is slightly higher for the first generation Supplier A AS material. A maximum contraction of 750 ppm occurred at 1050°C during 500-800 hour exposure vs. 500 ppm at 1000°C for the same period for this material. For the other two materials no significant increase in instability occurred at 1050°C. The 1050°C thermal stability in presence of sodium salt of these materials is shown in Figure VI.B.2.2 along with the data for the standard LAS matrix. Both the LAS standard and the LAS matrix from Supplier B showed very little dimensional change during this test. This result is very much similar to that of the 1000°C test.

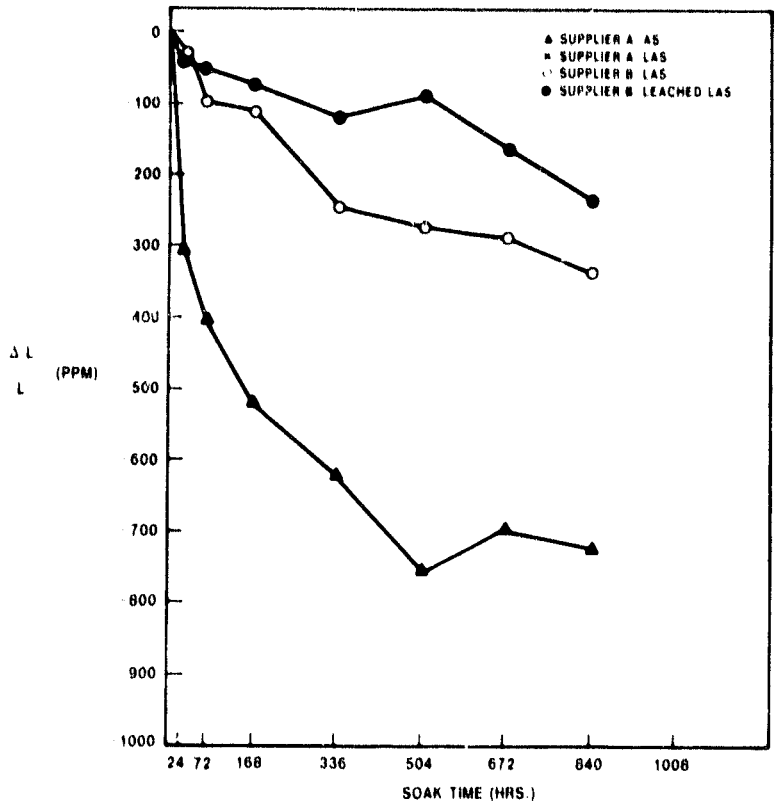

Figure VI.B.2.1 **Physical Stability of Various Materials at 1050°C (1922°F)**

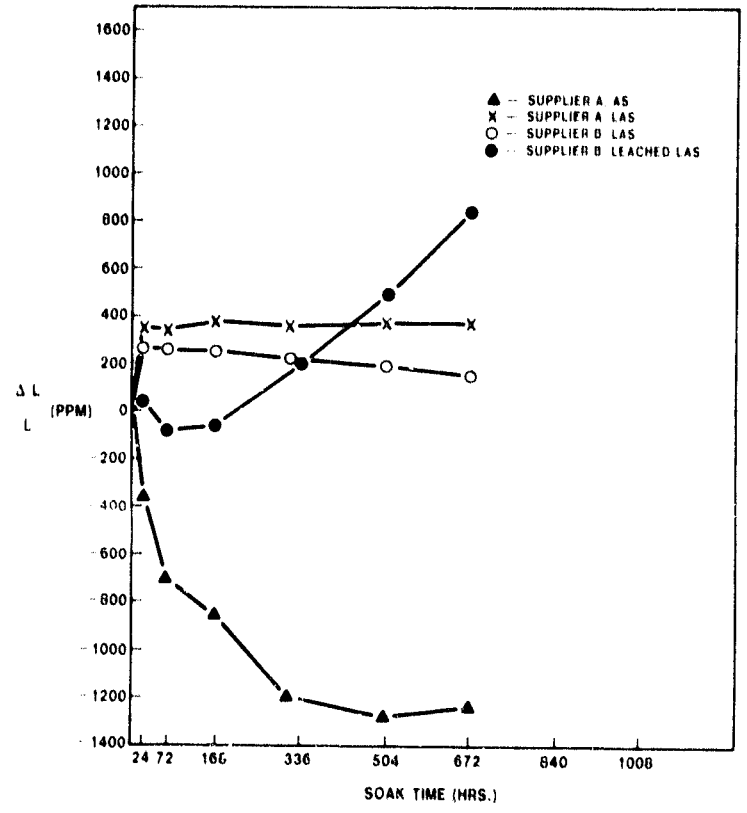

Figure VI.B.2.2 **Physical Stability of Various Materials at 1050°C (1922°F) with Sodium Present**

The thermal stability of the first generation Supplier A AS material at 1050°C in presence of sodium is very much similar to that at 1000°C and 1100°C. The magnitude of the dimensional change at 1050°C (1300 ppm) is approximately halfway between that at 1000°C and 1100°C (Ref. 5, Figures VI.B.1.18 and VI.B.3.10). On the basis of these results, it appears that the operating temperature limit for the first generation Supplier A AS material is expected to be no higher than 1000°C. Even at this temperature this material suffers at least 700 ppm dimensional change (Figure VI.B.1.18) and a drastic change in thermal expansion behavior (Figures VI.B.1.5, VI.B.1.22).

The AS matrix from supplier B showed an unexpectedly low dimensional change at 1050°C in presence of sodium when compared to the data 1000°C (refer to previous section) and 1100°C (refer to following section). Considering the fact that the thermal expansion behavior of both AS materials, i.e. from Suppliers A and B, is very much alike (ref. Figures VI.B.1.22 and VI.B.1.23) this result is unexpected.

In view of the high instability the first generation AS materials (both Supplier A and B) are not considered suitable for application above 1000°C.

It is interesting to note that the behavior of these materials in the 1000°C (1832°F) thermal stability test in presence of sodium salt is very much similar to that observed in case of the hot face test conditions (refer to Section III.B.). The magnitude of the observed changes, particularly for the AS materials and the LAS/MAS, is greater in the 1000°C test compared to the hot face test, i.e., at 800°C (1472°F).

VI.B.3. 1100°C (2012°F) Test Temperature

Seven of the ten 1st generation experimental materials (4-MAS, 2-AS, 1-LAS) and six second generation (3-MAS, 1-LAS/MAS, 1-AS, 1-ZR/MAS) experimental materials (refer to Section VI.B.1) were evaluated at 1100°C for thermal stability in air and in presence of sodium salt. The thermal stability data at 1100°C in air for all these materials are presented in Figure VI.B.3.1. Most of the MAS materials and the ZR/MAS and 9455 LAS standard exhibit good thermal stability. The Supplier B LAS material has experienced some degree of growth as a result of this high temperature exposure. The two first generation AS materials (▲), (●) have contracted to the point where physical deterioration was obvious, necessitating termination after 672 test hours. The numbers immediately adjacent to the graphing symbols for these materials indicate a degree of dimensional change too great to include in the graphing scale. The second generation as material from Supplier A (▲) exhibits a significant improvement in stability compared to the first generation materials.

Figures VI.B.3.2 through VI.B.3.11 are comparisons of each individual material's change in thermal expansion behavior as a result of the 1100°C (2012°F) thermal stability testing. These data, combined with the dimensional stability measurements, afford one an insight into the effect of the test environment on each specific material.

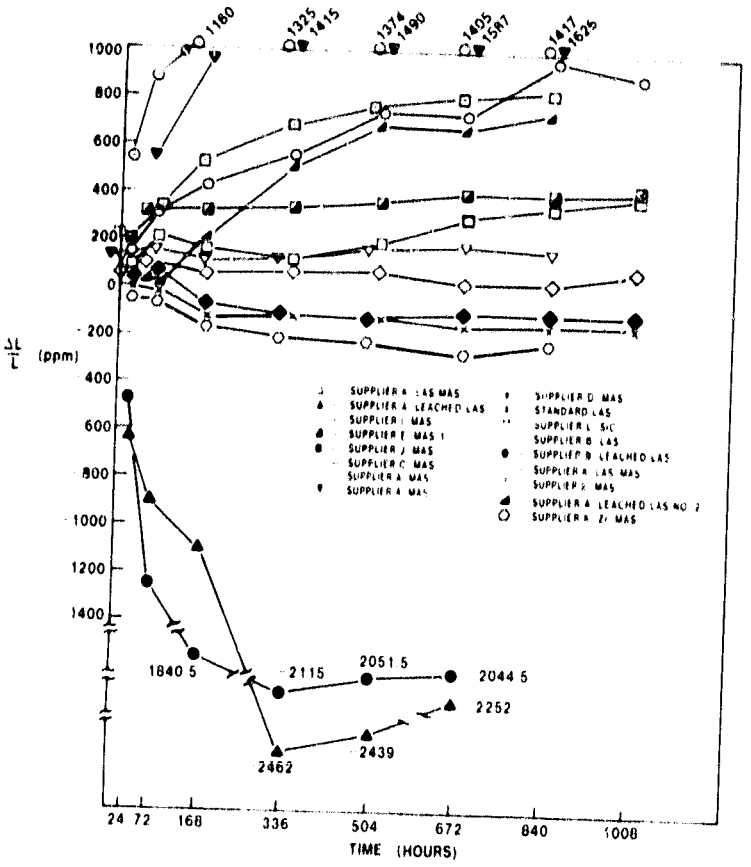

Figure VI.B.3.1 **Physical Stability of Various Materials at 1100°C (2012°F)**

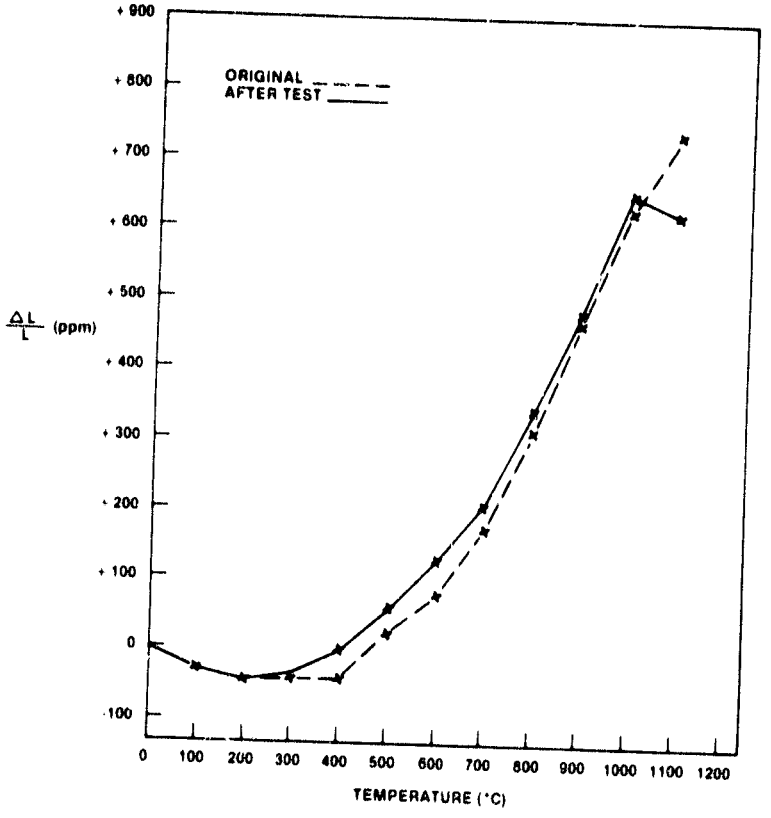

Figure VI.B.3.2 **9455 LAS Standard; Thermal Expansion Before and After 1100°C (2012°F) Thermal Stability Testing**

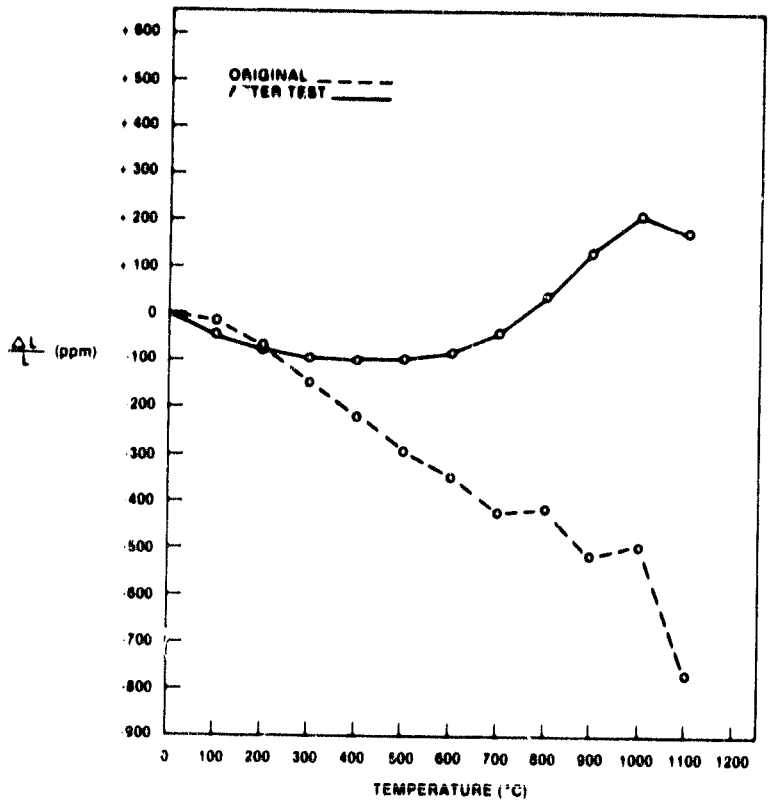

Figure VI.B.3.3 **Supplier B LAS; Thermal Expansion Before and After 1100°C (2012°F) Thermal Stability Testing**

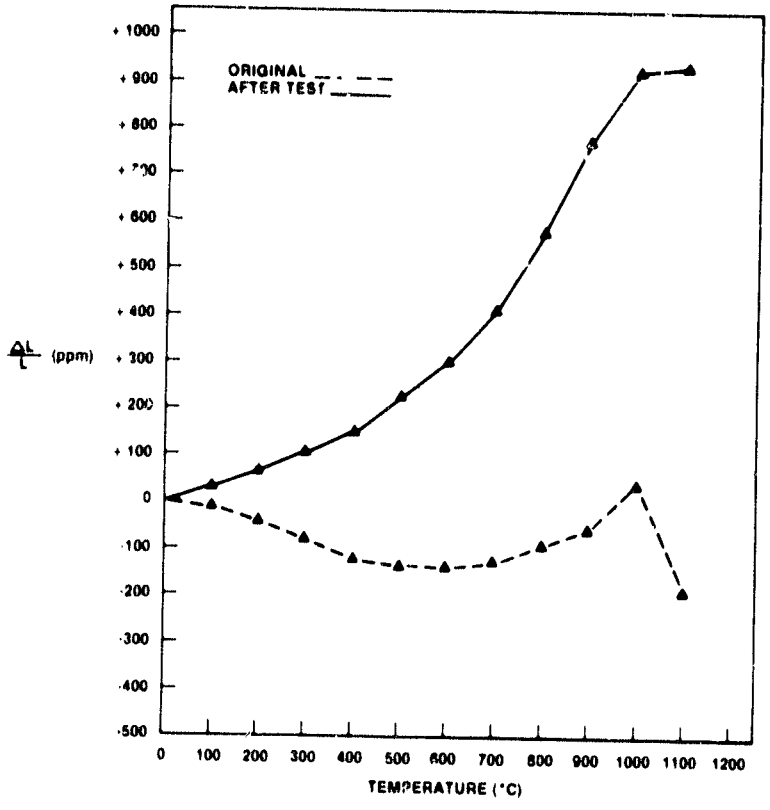

Figure VI.B.3.4 **Supplier A AS; Thermal Expansion Before and After 1100°C (2012°F) Thermal Stability Testing**

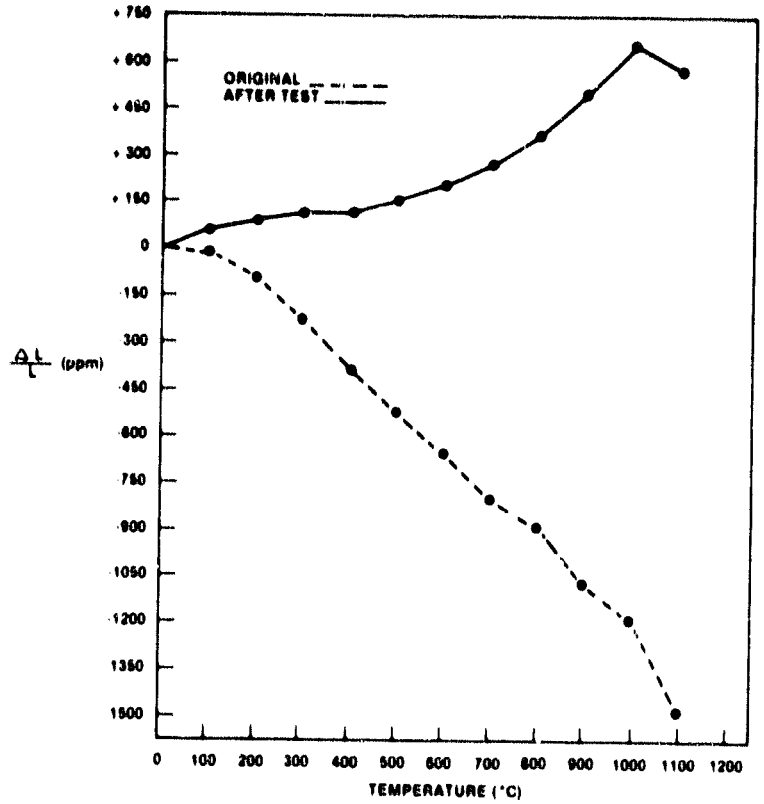

Figure VI.B.3.5 **Supplier B AS; Thermal Expansion Before and After 1100°C (2012°F) Thermal Stability Testing**

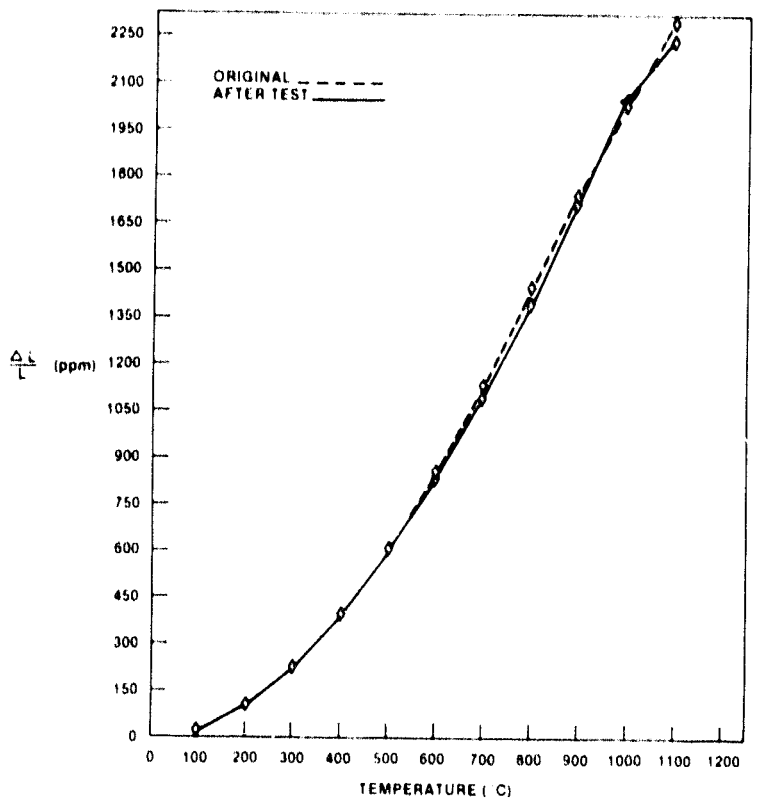

Figure VI.B.3.6 **Supplier C MAS; Thermal Expansion Before and After 1100°C (2012°F) Thermal Stability Testing**

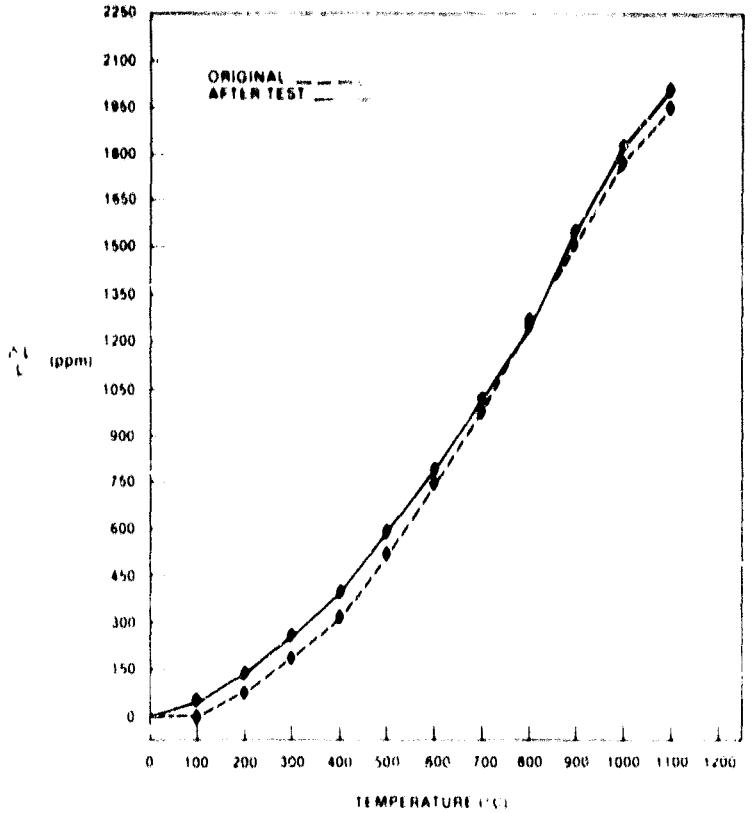

Figure VI.B.3.7 **Supplier D MAS; Thermal Expansion Before and After 1100°C (2012°F) Thermal Stability Testing**

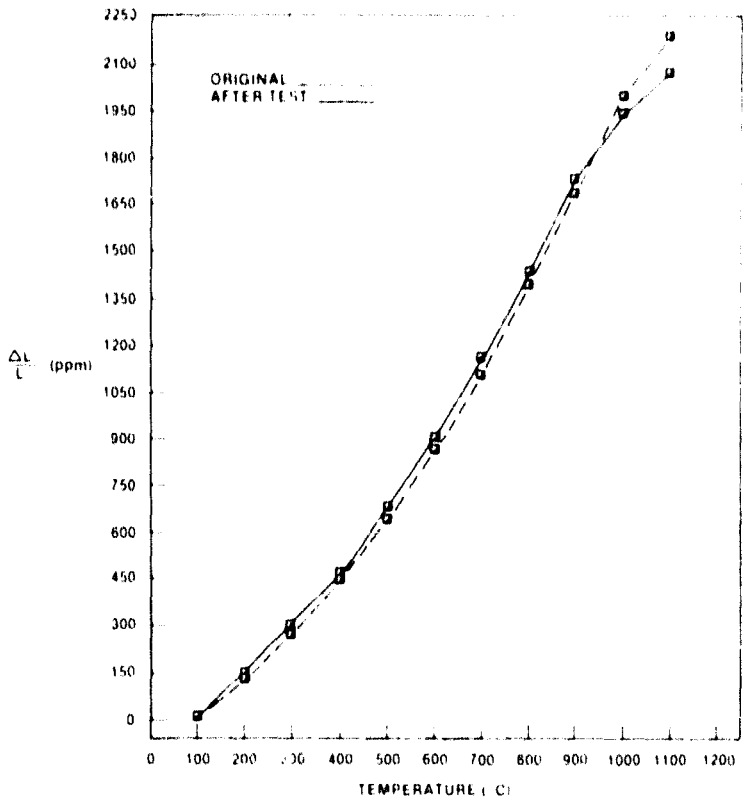

Figure VI.B.3.8 **Supplier E MAS #1; Thermal Expansion Before and After 1100°C (2012°F) Thermal Stability Testing**

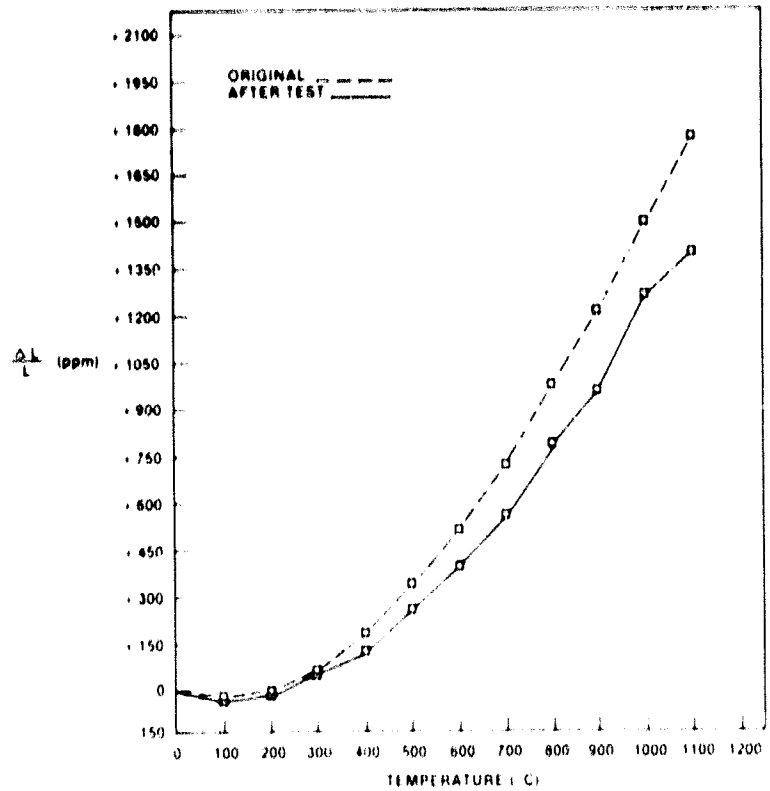

Figure VI.B.3.9 **Supplier I MAS; Thermal Expansion Before and After 1100°C (2012°F) Thermal Stability Testing**

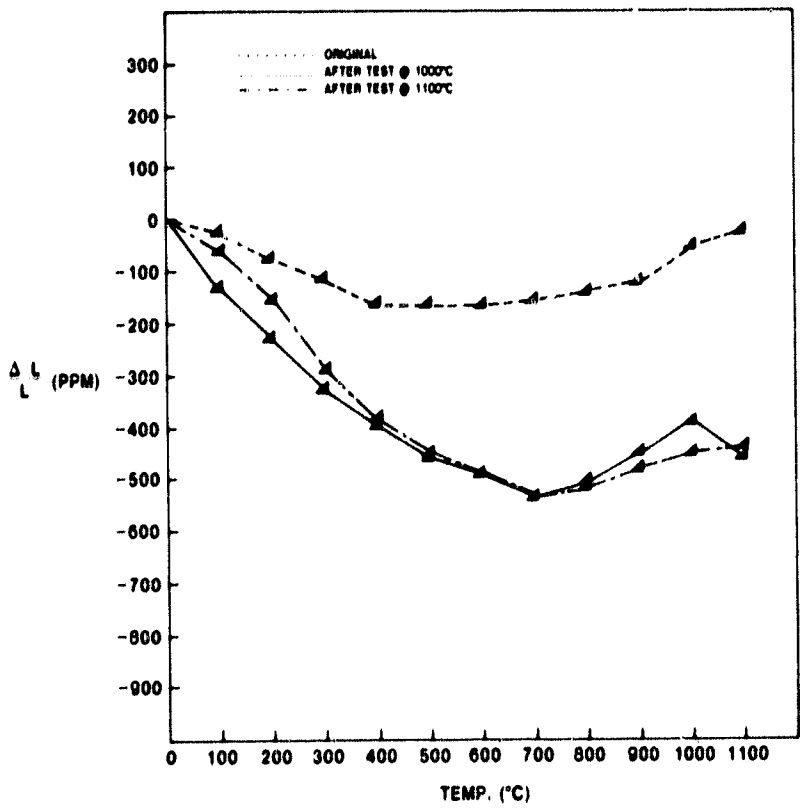

Figure VI.B.3.10 **Supplier A Leached LAS (AS-2) — 2nd Generation; Thermal Expansion Before and After Thermal Stability Testing at 1000°C and 1100°C**

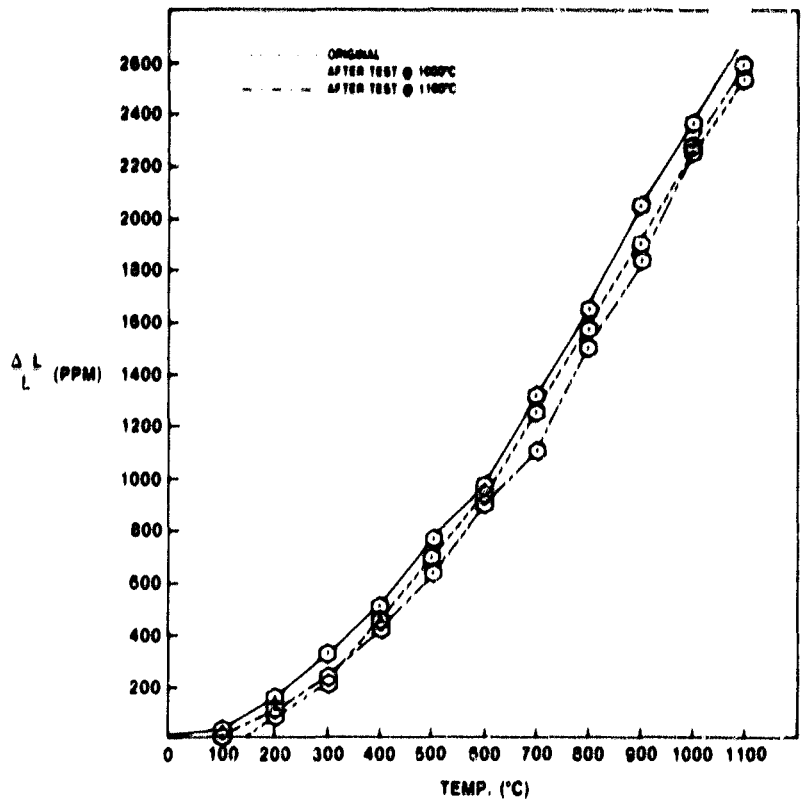

Figure VI.B.3.11 Supplier K — Zr/MAS; Thermal Expansion Before and After 1000°C and 1100°C Thermal Stability Testing

Figures VI.B.3.2 and VI.B.3.3 represent the thermal expansion characteristics of the 9455 LAS standard and the LAS composition of Supplier B, respectively. The standard material (Figure VI.B.3.2) remains relatively unchanged as a result of the 1100°C (2012°F) thermal stability testing, although this material does exhibit a tendency to slump at a lower temperature after going through the test. In contrast, the LAS of Supplier B (Figure VI.B.3.3) has undergone a rather large change in thermal expansion behavior as a result of the 1008 cumulative hour exposure to a temperature of 1100°C (2012°F). This material, while originally contractive between room temperature and 1100°C (2012°F), has become expansive over this same temperature interval subsequent to the test. This observation corroborates the dimensional instability observed in this material during the course of the thermal stability testing at 1000°C.

Figures VI.B.3.4 and VI.B.3.5 dramatically illustrate the pronounced changes in thermal expansion behavior of the first generation AS materials of Suppliers A and B respectively, as a result of the 1100°C (2012°F) thermal stability testing. Both of these materials were very unstable under the conditions of this test (they were dropped from testing after a cumulative exposure of 672 hours). Both had suffered visible physical degradation. As can be seen in their thermal expansion plots, both materials have become quite expansive, with the material of Supplier A (Figure VI.B.3.4) undergoing the greater change. This observation correlates well with the thermal instability data (Figure VI.B.3.1). In this case the difference in the severity of attack is not important since both materials are quite unstable at 1100°C (2012°F).

At this test temperature, the MAS materials of the first generation seem to be diverging into two groups representing different levels of stability (Figure VI.B.3.1). Figures VI.B.3.6 and VI.B.3.7 indicate the essentially identical thermal expansion response of the very stable MAS materials of Suppliers C (◊) and D (♦), respectively. Figures VI.B.3.8 and VI.B.3.9 illustrate the more marked change in thermal expansion experienced by the somewhat less stable MAS materials of Suppliers E (◪, material #1) and I (□), respectively. While these measured differences do exist, the data would suggest that all of the MAS materials appear to be viable candidates for regenerator service at 1100°C (2012°F). Of the second generation MAS materials (Supplier A wrapped MAS (▼) extruded MAS (ø) and Supplier E MAS #2, wrapped ∇) both the Supplier A materials (extruded MAS (o) and wrapped MAS ▼) showed a very large dimensional change (1200 to 1600 ppm) during the initial 72 hours and remained relatively unchanged (less than 100 ppm) during the subsequent 900+ hours at the 1100°C (2012°F) test temperature in air. These materials exhibited nearly identical behavior during the 1100°C (2012°F) thermal stability test in presence of sodium salt (refer Figures VI.B.3.1 and VI.B.3.12). This initial large dimensional change may be due to the transformation of the residual glass phase to crystalline cordierite structure. The Supplier E MAS #2 matrix (∇) showed very little dimensional change indicating an excellent thermal stability.

The results of the 1100°C (2012°F) thermal stability testing with sodium present illustrated graphically in Figure VI.B.3.12, indicate that the introduction of sodium into the test environment at this temperature tends to accentuate the material responses noted in the thermal stability testing at this temperature without sodium present (Figure VI.B.3.1). The MAS materials, while all relatively stable under these test conditions, tend to divide more dramatically into the same two groups of differing stability. The Supplier B LAS and the two first generation AS materials exhibited a marked physical deterioration early in the test sequence, and these materials were terminated after 160 cumulative hours of test time. Of curious interest is the lack of continuous growth beyond the 24 hour test interval, of the 9455 LAS standard. The second generation as material (▲) from Supplier A and ZR/MAS (◯) material from Supplier K appear to be unaffected by sodium at this temperature.

The effects of the 1100°C (2012°F) thermal stability testing with sodium on each material's thermal expansion behavior are presented in Figures VI.B.3.13 through VI.B.3.22. Figures VI.B.3.13 and VI.B.3.14 represent the original and final thermal expansions of the 9455 LAS standard and the LAS of Supplier B, respectively. As previously noted, the curious lack of long-term response by the standard material to the test environment is underscored by the significant change in thermal expansion behavior reported in Figure VI.B.3.13, especially when compared to the lack of change (Figure VI.B.3.2) resulting from the 1100°C (2012°F) thermal stability testing without sodium present. The LAS of Supplier B is clearly changed by the high-temperature and sodium-rich environment of the test, and has become so strongly expansive (Figure VI.B.3.14) as to become self-destructive.

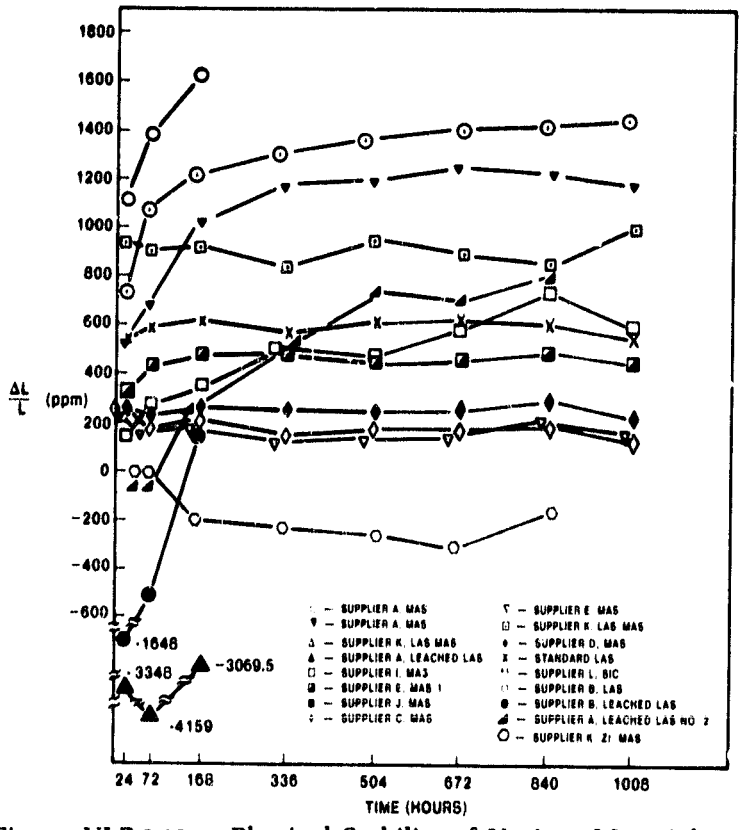

Figure VI.B.3.12 Physical Stability of Various Materials at 1100°C (2012°F), with Sodium Present

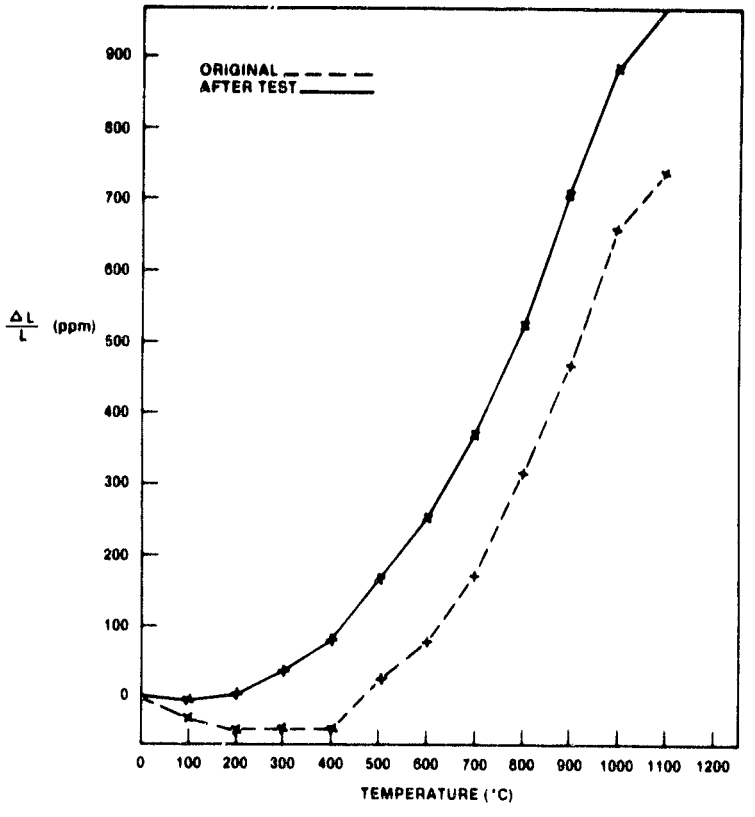

Figure VI.B.3.13 9455 LAS Standard; Thermal Expansion Before and After 1100°C (2012°F) Thermal Stability Testing with Sodium Present

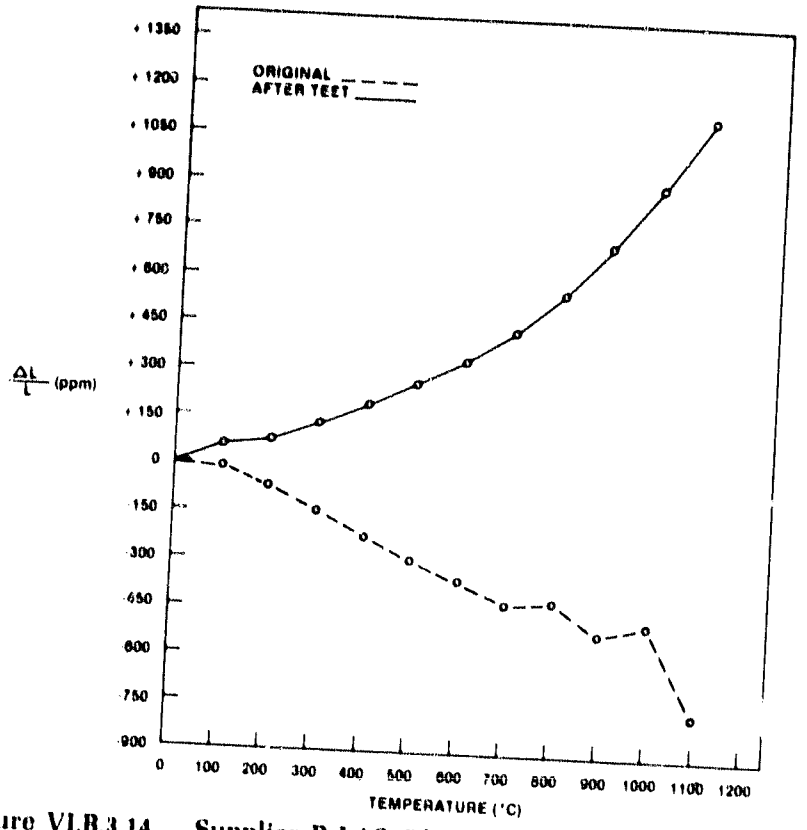

Figure VI.B.3.14 Supplier B LAS; Thermal Expansion Before and After 1100°C (2012°F) Thermal Stability Testing with Sodium Present

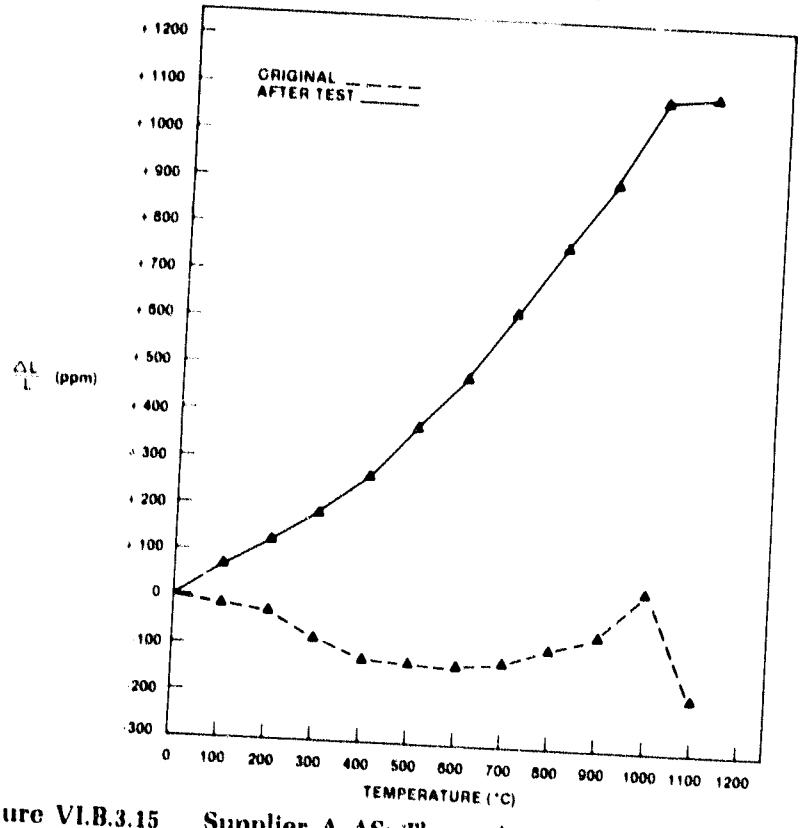

Figure VI.B.3.15 Supplier A AS; Thermal Expansion Before and After 1100°C (2012°F) Thermal Stability Testing with Sodium Present

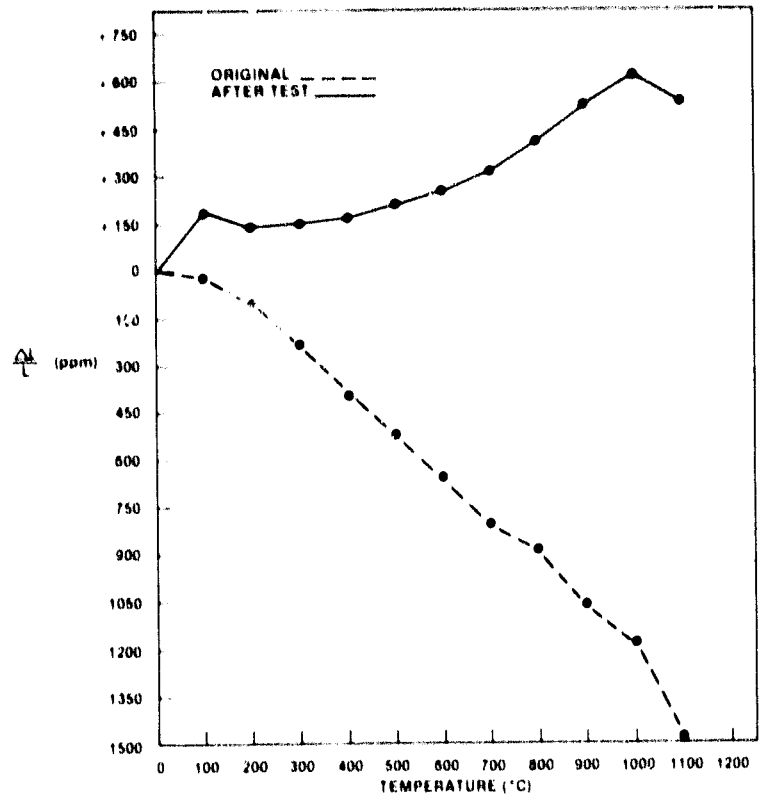

Figure VI.B.3.16 **Supplier B AS; Thermal Expansion Before and After 1100°C (2012°F) Thermal Stability Testing with Sodium Present**

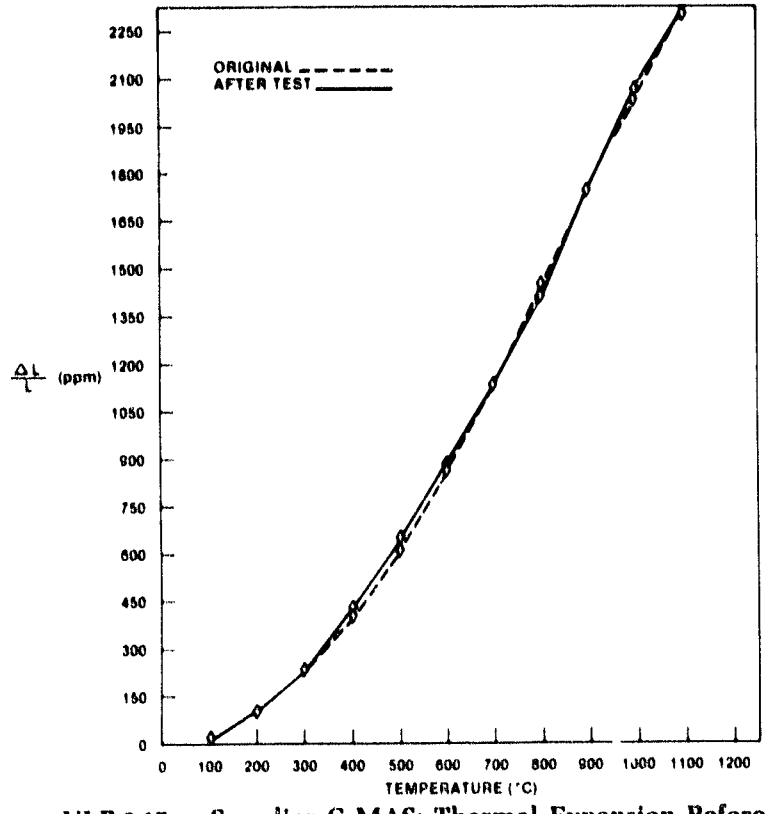

Figure VI.B.3.17 **Supplier C MAS; Thermal Expansion Before and After 1100°C (2012°F) Thermal Stability Testing with Sodium Present**

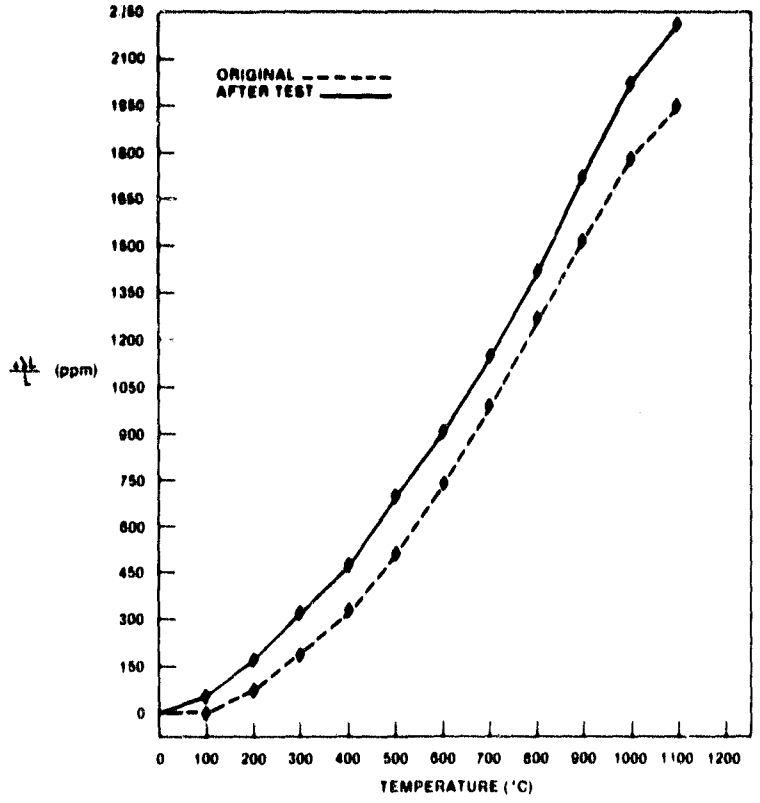

Figure VI.B.3.18 **Supplier D MAS; Thermal Expansion Before and After 1100°C (2012°F) Thermal Stability Testing with Sodium Present**

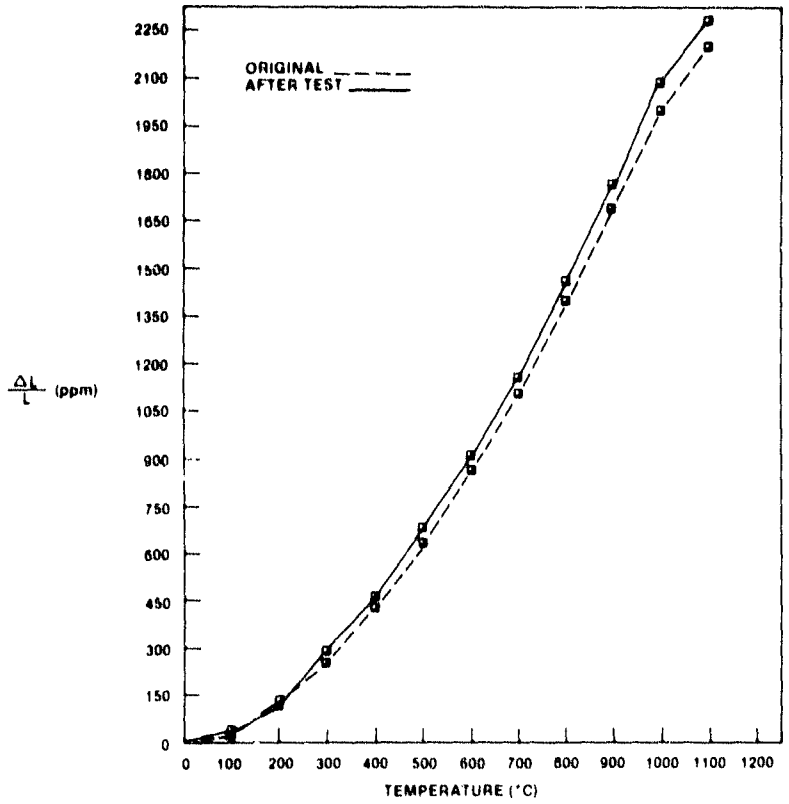

Figure VI.B.3.19 **Supplier E MAS #1; Thermal Expansion Before and After 1100°C (2012°F) Thermal Stability Testing with Sodium Present**

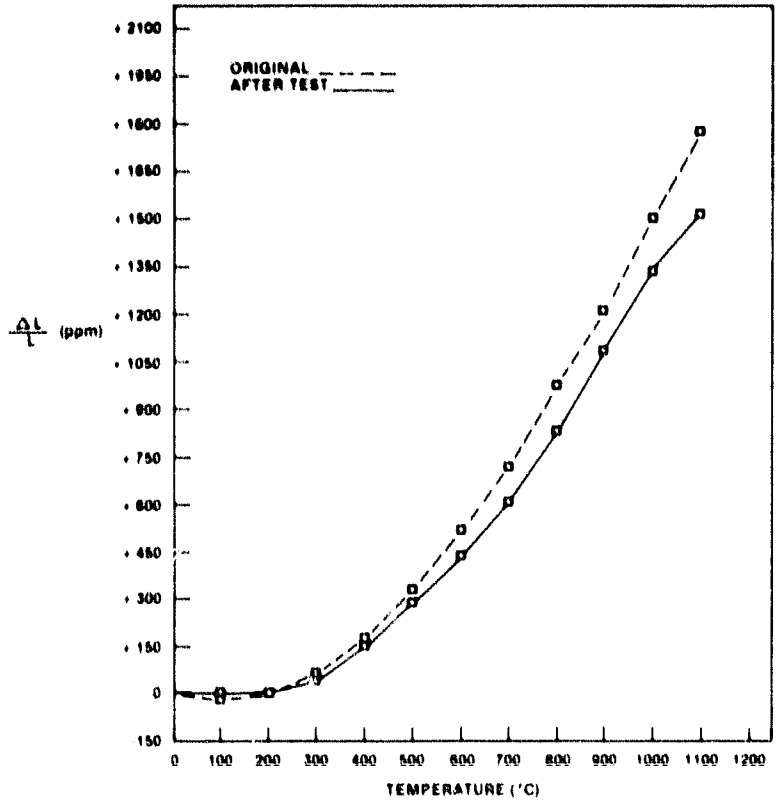

Figure VI.B.3.20 **Supplier I MAS; Thermal Expansion Before and After 1100°C (2012°F) Thermal Stability Testing with Sodium Present**

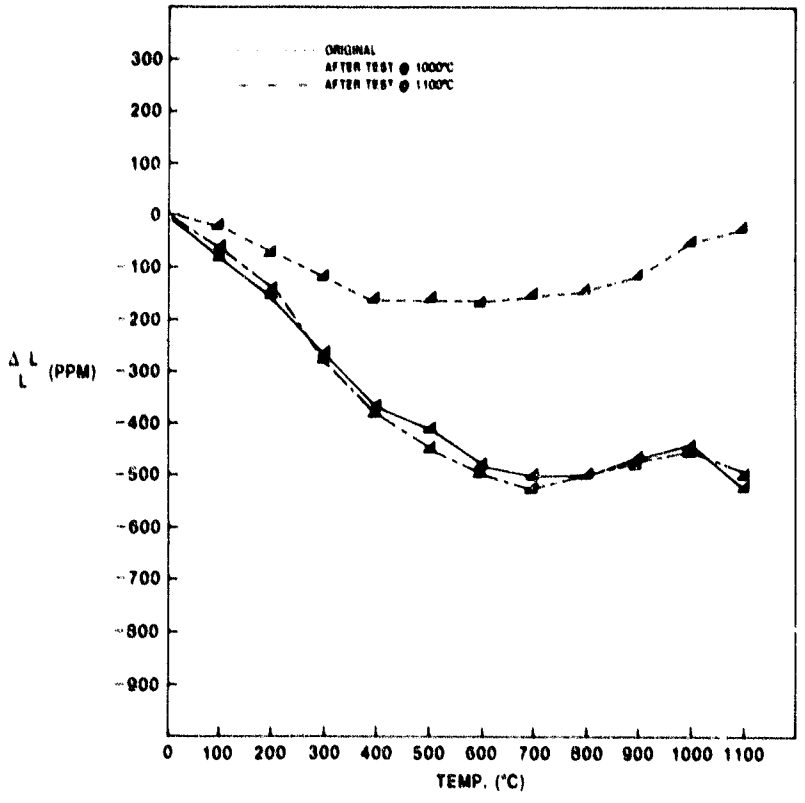

Figure VI.B.3.21 **Supplier A Leached LAS — 2nd Generation; Thermal Expansion Before and After 1000°C and 1100°C Thermal Stability Testing**

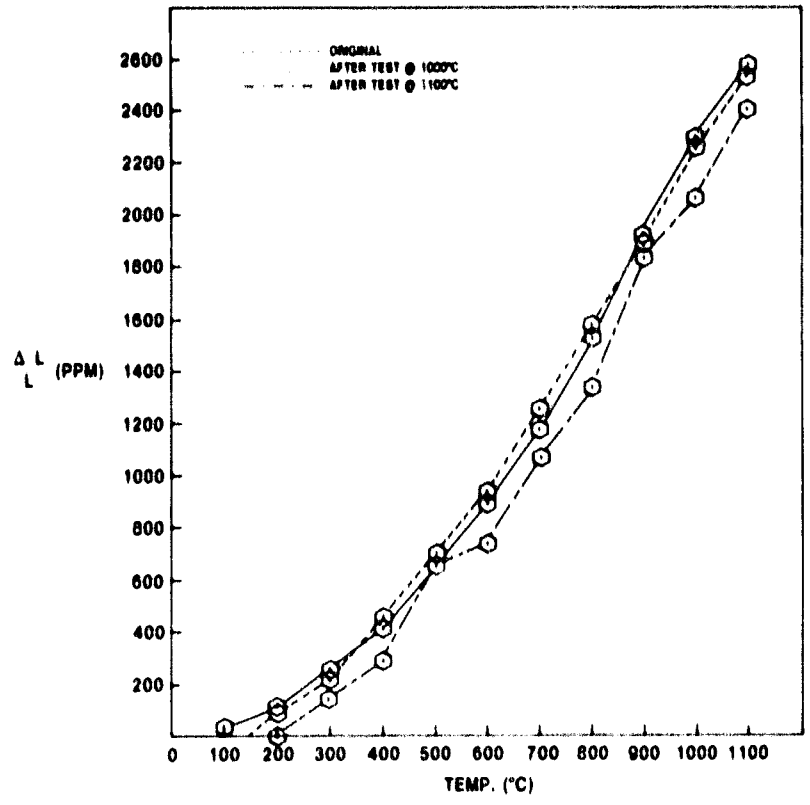

Figure VI.B.3.22 Supplier K, Zγ-MAS; Thermal Expansion Behavior Before and After 1000°C (1832°F) and 1100°C (2012°F) Thermal Stability Testing with Sodium Present

Figures VI.B.3.15 and VI.B.3.16 illustrate the change in thermal expansion response for the first generation AS materials of Suppliers A and B, respectively. The same relative effects are observed for both materials tested with sodium as were reported for the purely thermal tests: the AS of Supplier A (Figure VI.B.3.15) evidences more physical instability and a greater change in thermal expansion than does the AS of Supplier B (Figure VI.B.3.16).

The MAS materials evidence the best resistance to corrosion at 1100°C (2012°F) of the three basic materials groups tested. Figures VI.B.3.17 through VI.B.3.20 indicate quite similar thermal expansion behaviors for these materials before and after the testing sequence. As was observed in the testing without sodium present (Figure VI.B.3.1) the MAS materials divide into two stability groups during testing with sodium present (Figure VI.B.3.12). The MAS materials of Suppliers C (◊) and D (♦) appear to be slightly more stable than those of Supplier E (◪, Material #1) and Supplier I (□). This observation is not so dramatically supported by the thermal expansion data, as was the case in the 1100°C (2012°F) thermal stability testing without sodium present; but the conclusion to which one is drawn remains the same: all of these MAS materials would seem to be candidates for regenerator service at 1100°C (2012°F).

The Supplier K LAS/MAS matrix (□) at 1100°C in air showed a gradually decreasing growth, with an initial rate of 300 ppm/100 hrs. which dropped to 50 ppm/100 hrs. after 800 hrs. In presence of sodium, however, there is a very rapid

initial growth, nearly 800 ppm within 24 hours, followed by a gradual decrease in growth rate in a manner similar to that observed at 1100°C in air. The growth rate after 500 hours in presence of sodium salt is essentially the same as that in air. This gradually decreasing but sustained growth, as opposed to sharp initial growth followed by relative dimensional stability observed with MAS matrices, indicates a progressive deterioration of the LAS/MAS matrix.

VI.B.4 1200°C (2192°F) Test Temperature

Four MAS materials and one AS (leached LAS) material from the first generation matrix samples were selected for the 1200°C temperature evaluation. In view of the failure of the first generation AS material during the 1100°C test, the inclusion of this material is only to observe its behavior and not intended for regenerator application at such high temperature. All the second generation materials, i.e., in three MAS materials and one LAS/MAS material, have also been evaluated.

The thermal stability data for these materials at 1200°C (2192°F) in air are presented in Figures VI.B.4.1 and VI.B.4.2. The thermal expansion behavior of these materials before and after the 1200°C thermal stability test is shown in Figures VI.B.4.3 through VI.B.4.11.

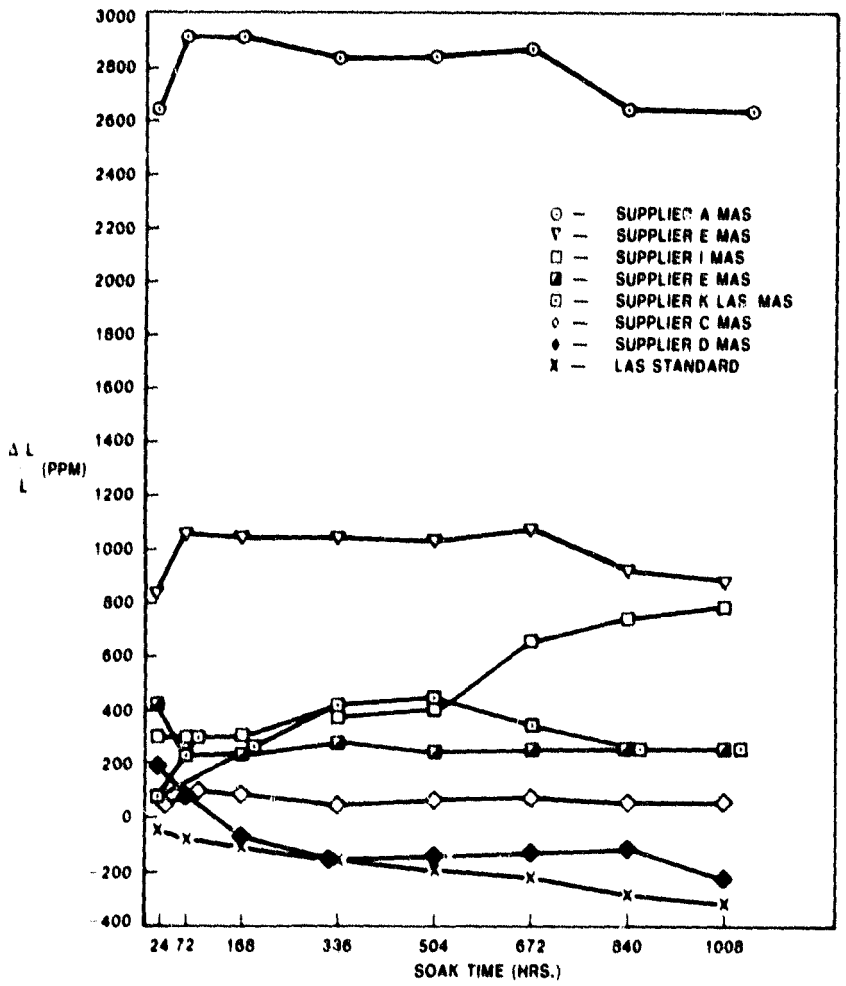

Figure VI.B.4.1 Physical Stability of Various Materials at 1200°C (2192°F)

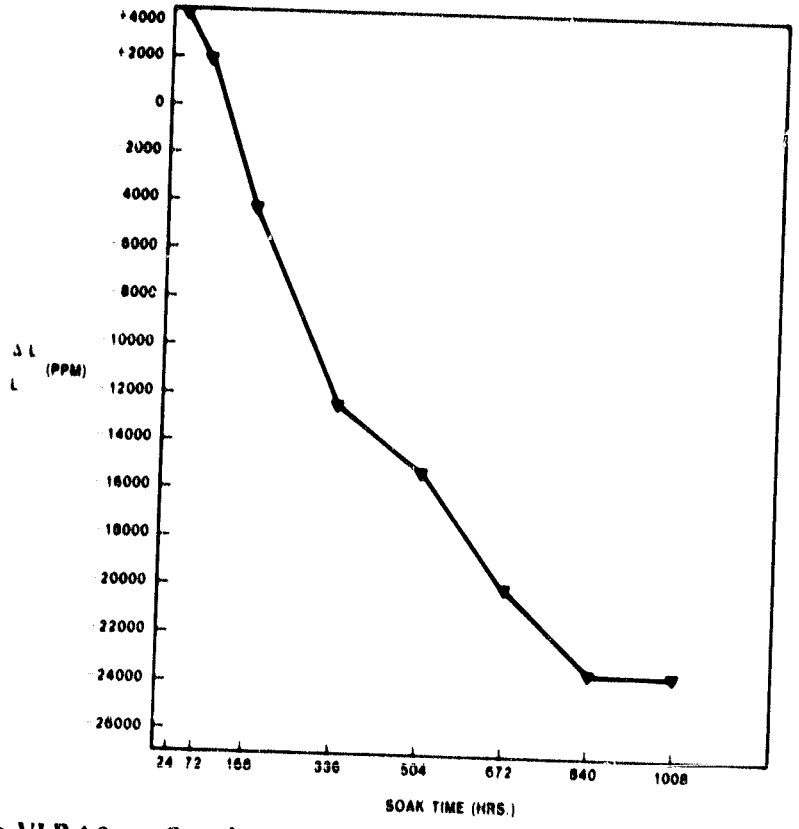

Figure VI.B.4.2 Supplier A, MAS; Physical Stability at 1200°C (2192°F)

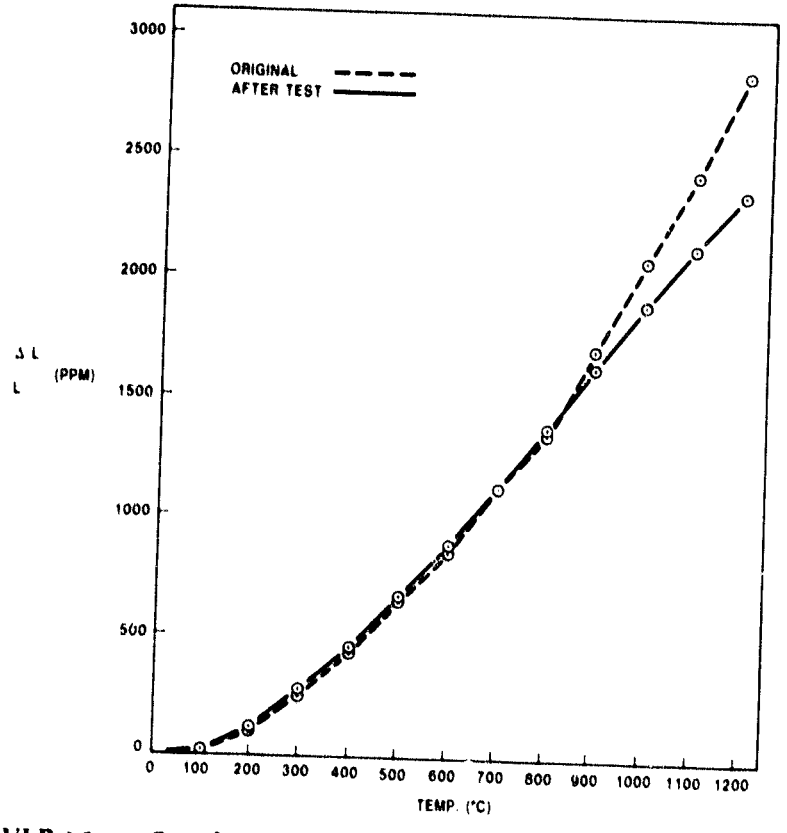

Figure VI.B.4.3 Supplier A, MAS (Extruded); Thermal Expansion Before and After 1200°C (2192°F) Thermal Stability Testing

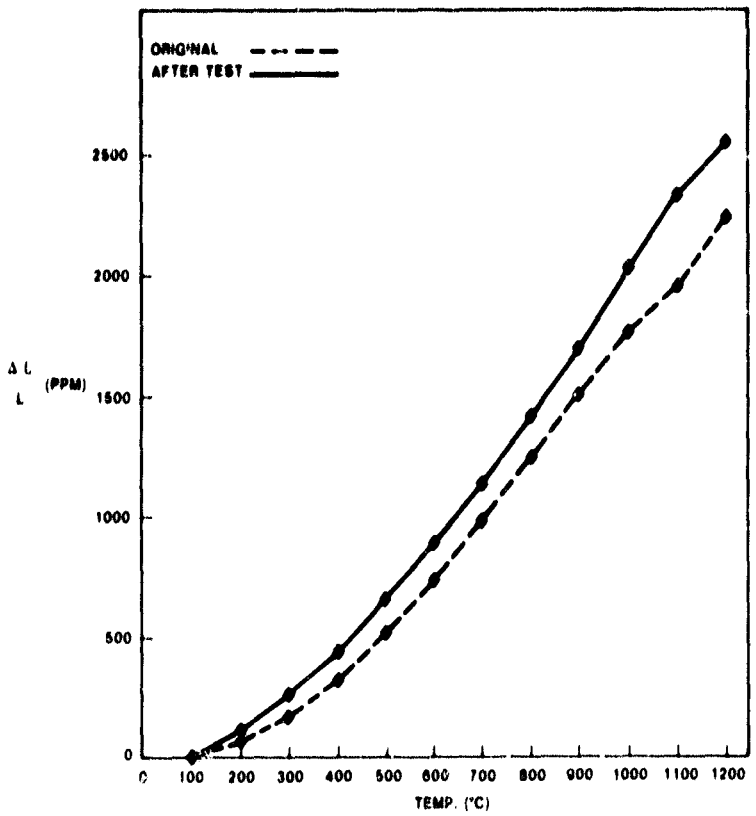

Figure VI.B.4.4 **Supplier D, MAS; Thermal Expansion Before and After 1200°C (2192°F) Thermal Stability Testing**

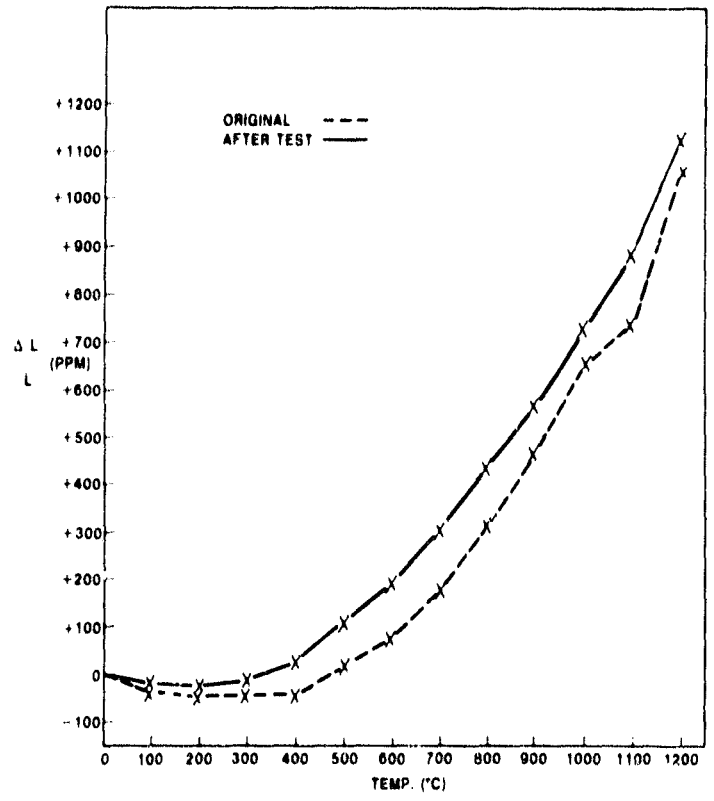

Figure VI.B.4.5 **Supplier A, LAS; Thermal Expansion Before and After 1200°C (2192°F) Thermal Stability Testing**

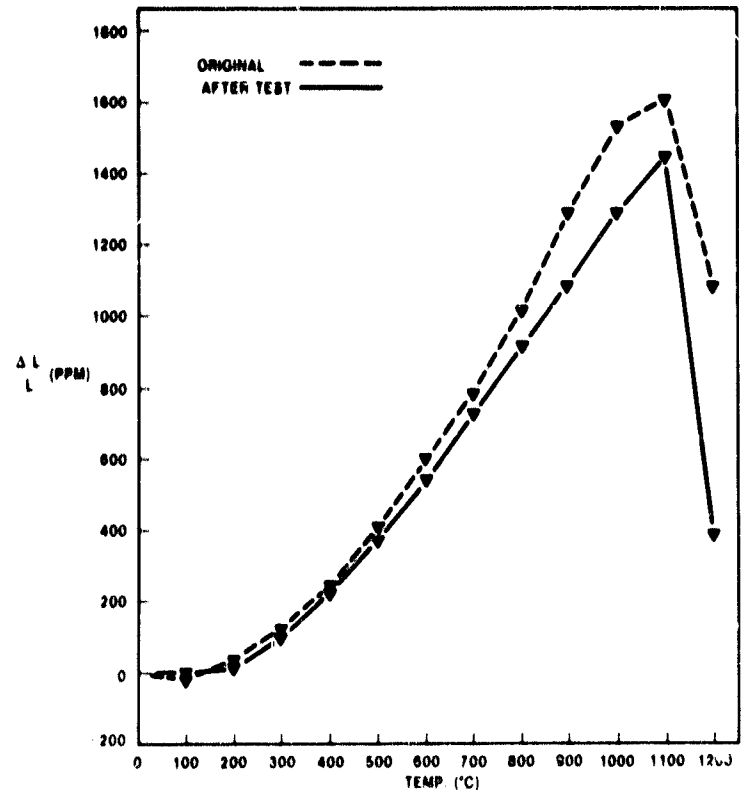

Figure VI.B.4.6 **Supplier A, MAS; Thermal Expansion Before and After 1200°C (2192°F) Thermal Stability Testing**

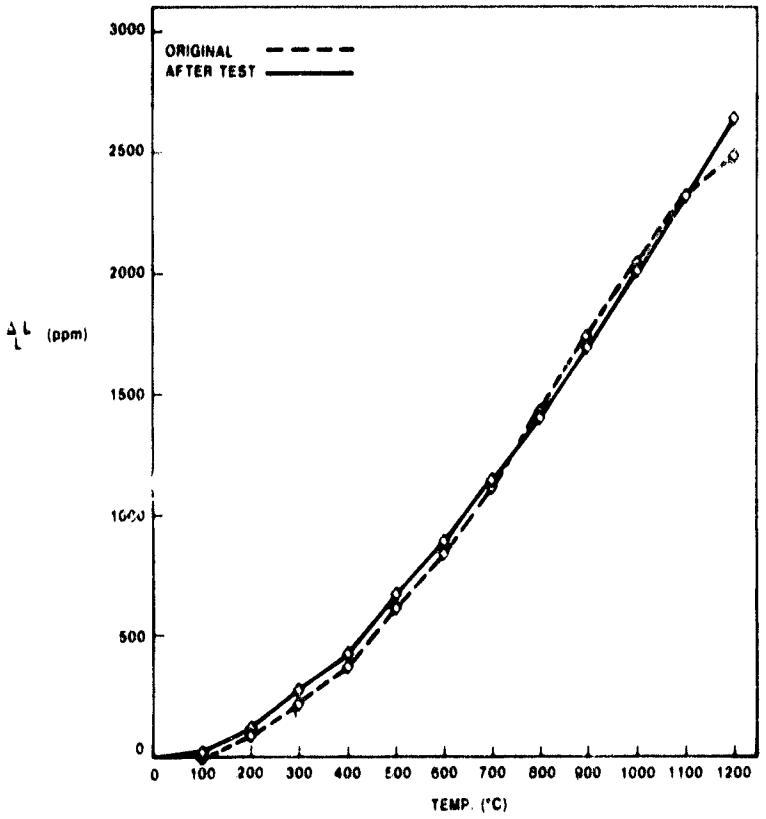

Figure VI.B.4.7 **Supplier C, MAS; Thermal Expansion Before and After 1200°C (2192°F) Thermal Stability Testing**

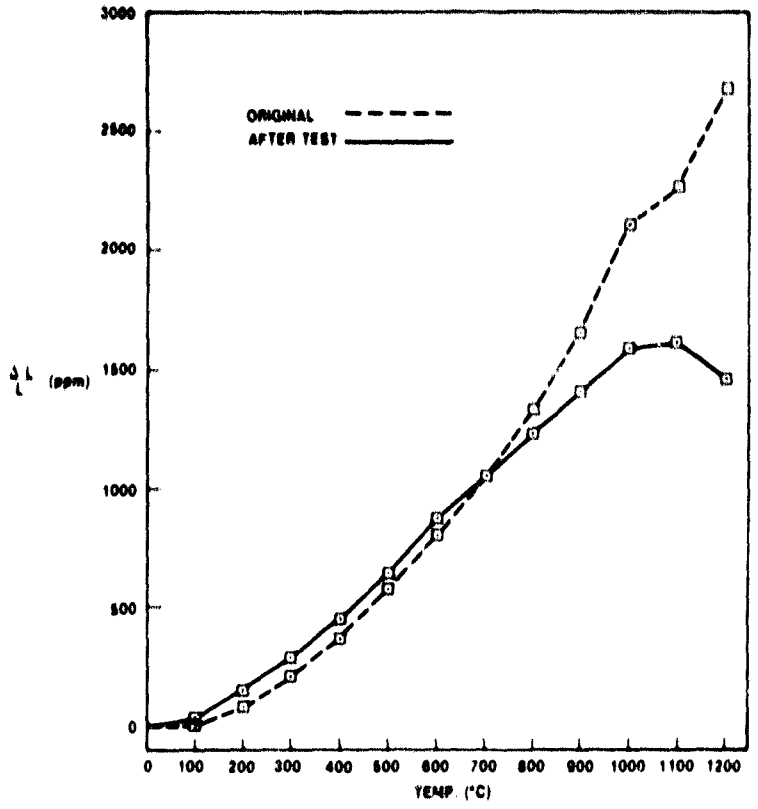

Figure VI.B.4.8 **Supplier K, LAS/MAS; Thermal Expansion Before and After 1200°C (2192°F) Thermal Stability Testing**

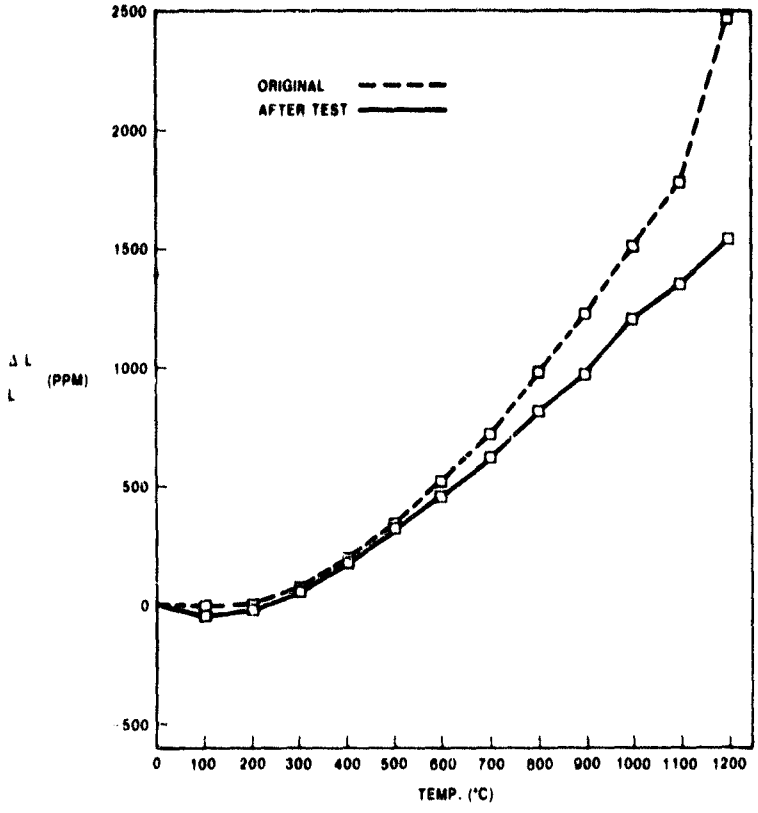

Figure VI.B.4.9 **Supplier I, MAS; Thermal Expansion Before and After 1200°C (2192°F) Thermal Stability Testing**

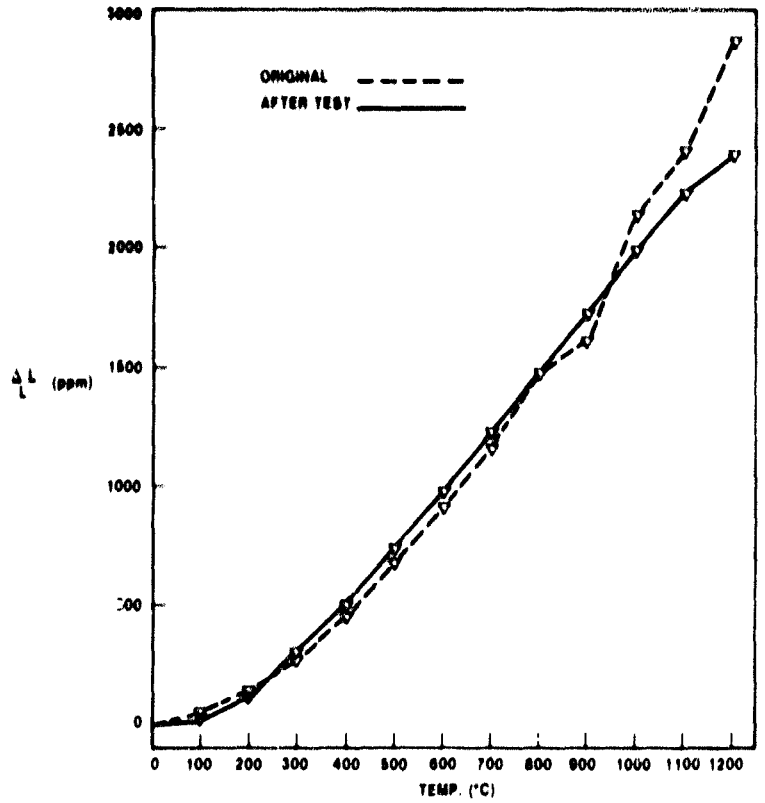

Figure VI.B.4.10 Supplier E, MAS; Thermal Expansion Before and After 1200°C (2192°F) Thermal Stability Testing

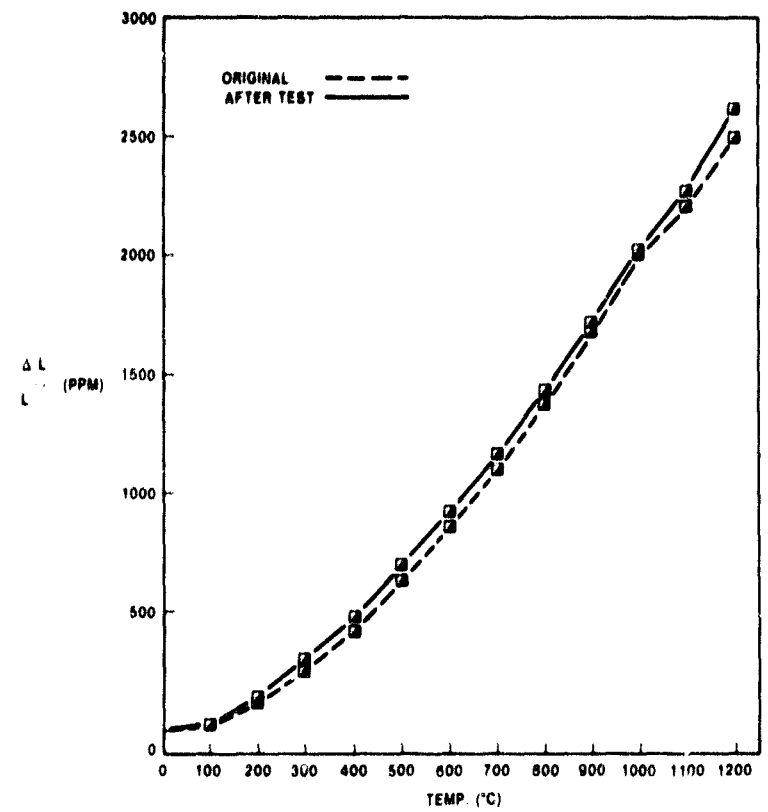

Figure VI.B.4.11 Supplier E, MAS; Thermal Expansion Before and After 1200°C (2192°F) Thermal Stability Testing

All the MAS matrices, with the exception of the Supplier A wrapped structure and Supplier I extruded specimen showed very little dimensional change after the initial 24 to 72 hour period. The supplier A extruded (⊙) and Supplier E wrapped (▽) matrices showed a very large initial growth (2700 ppm and 1100 ppm respectively), while others showed comparatively small growth or contraction (less than 300 ppm). As observed earlier this large initial dimensional change could be due to the conversion of the residual phases such as glass to stable MAS cordierite phase. This is borne out by the shape of the thermal expansion curves for these two materials. The thermal expansion showed a marked drop at 1200°C after the 1200°C thermal stability test as compared to the original (untested) matrices (Figures VI.B.4.3 and VI.B.4.9) and virtually retraced the curves for the original matrix for temperatures below 800°C. For the other MAS matrices that showed little instability, the thermal expansion curves after the thermal stability test in air followed very closely those of the original matrices indicating the absence of any phase changes in the material.

The Supplier A wrapped (▼) matrix and the Supplier I extruded (□) matrix which showed continuous instability also showed significant change in thermal expansion (Figures VI.B.4.6 and VI.B.4.9) after the 1200°C thermal stability test. The Supplier A matrix showed a marked drop in length change above 1100°C. This phenomenon is observed in this material after the 1200°C thermal instability test as well as the original matrix. This marked drop may actually be due to the softening and densification of the porous matrix causing the dilatometer push rod to recede, rather than the thermal contraction of the specimen. This softening or densification appears to start at 1000°C in case of the untested matrix as indicated by the discontinuity in the thermal expansion curve (VI.B.4.6). While in case of the specimen exposed to 1200°C thermal stability test, softening occurs above 1100°C. There is a significant reduction in the thermal expansion of the matrix after the 1200°C test which further strengthens the observation that the initial thermal instability is a result of the transformation of residual glass phase to crystalline cordierite.

In case of the Supplier I MAS matrix, no softening is observed, however, a marked drop in thermal expansion has been observed after the 1200°C test as compared to the original matrix (Figure VI.B.4.9). The thermal expansion of the matrix after the 1200°C thermal stability test is smooth and is more uniform than that of the original matrix indicating that the reduction of inhomogenieties has occurred during the test. The thermal instability curve for Supplier I matrix in Figure VI.B.4.1 shows a flattening out after 900 hours, which supports this observation. It should be noted that the thermal expansion curves up to 1100°C for these two materials (Supplier A and I MAS) after the 1200°C thermal stability test are remarkably similar.

The thermal stability test data for these materials at 1200°C (2192°F) in presence of sodium are presented in Figure VI.4.12.

Figures VI.B.4.13 through VI.B.4.18 illustrate the effect of the test environment on the thermal expansion behavior of each material between room temperature and the test temperature. The 9455 LAS standard does not exhibit a very marked change in thermal expansion (Figure VI.B.4.13) although the dimensional changes observed during testing (Figure VI.B.4.12) are quite uncharacteristic. Clearly, the AS of Supplier A is not the same material after having gone through the test, as the thermal expansion (Figure VI.B.4.14) is completely uncharacteristic of that of the original material.

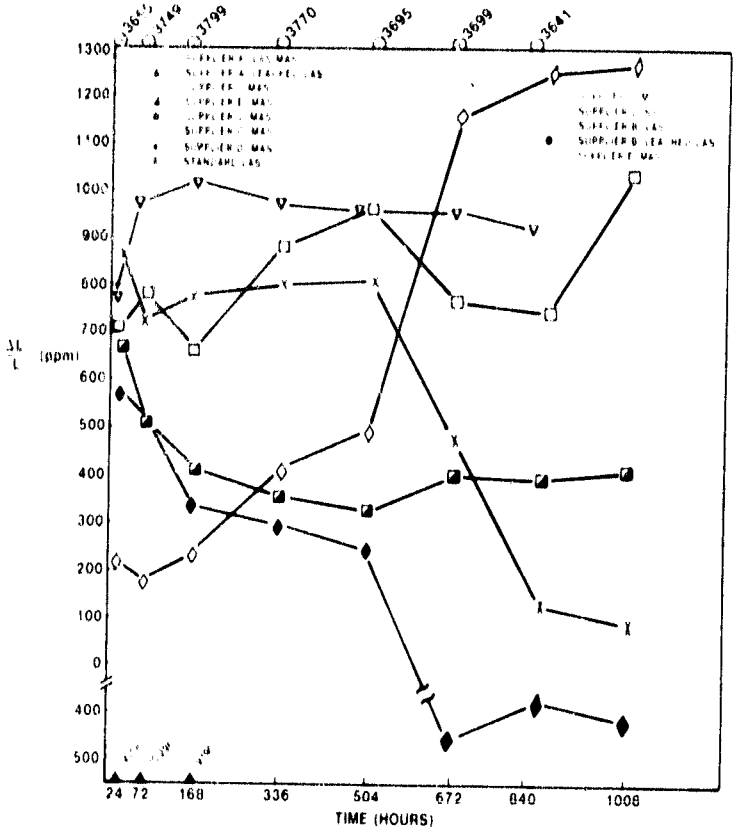

Figure VI.B.4.12 **Physical Stability of Various Materials at 1200°C (2192°F) with Sodium Present**

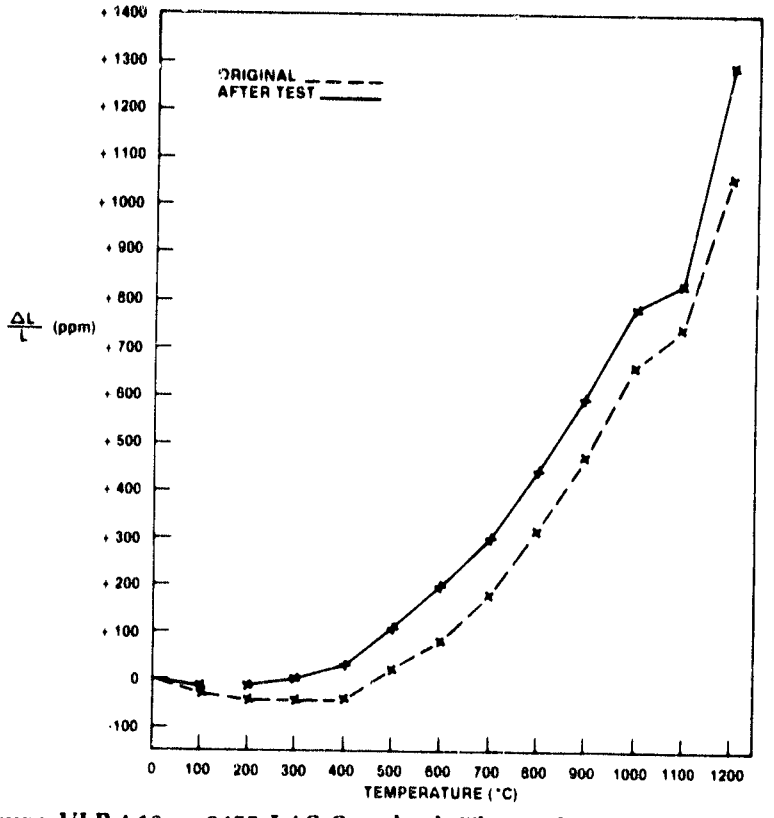

Figure VI.B.4.13 **9455 LAS Standard; Thermal Expansion Before and After 1200°C (2192°F) Thermal Stability Testing with Sodium Present**

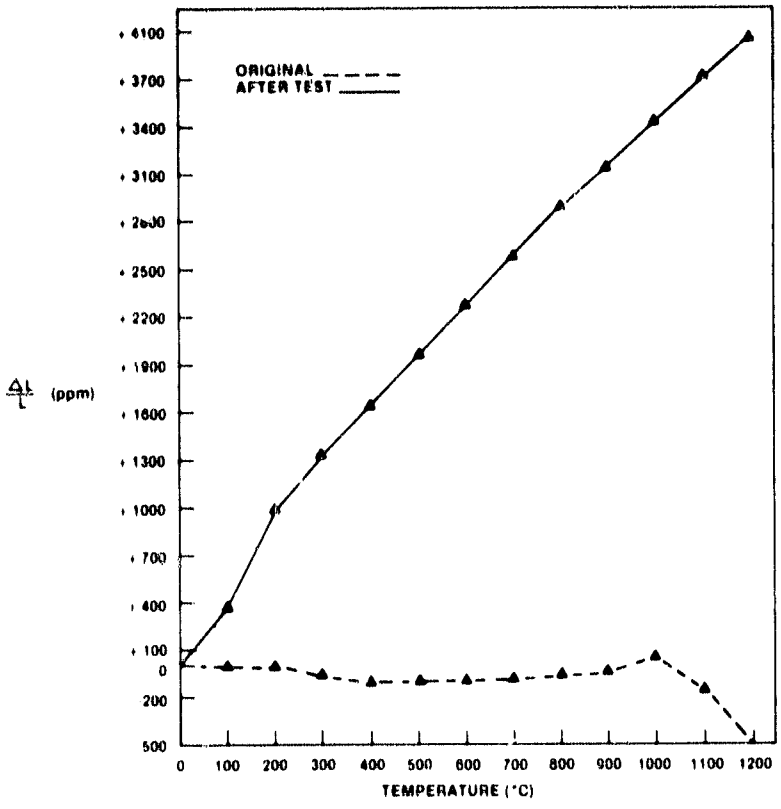

Figure VI.B.4.14 Supplier A AS; Thermal Expansion Before and After 1200°C (2192°F) Thermal Stability Testing with Sodium Present

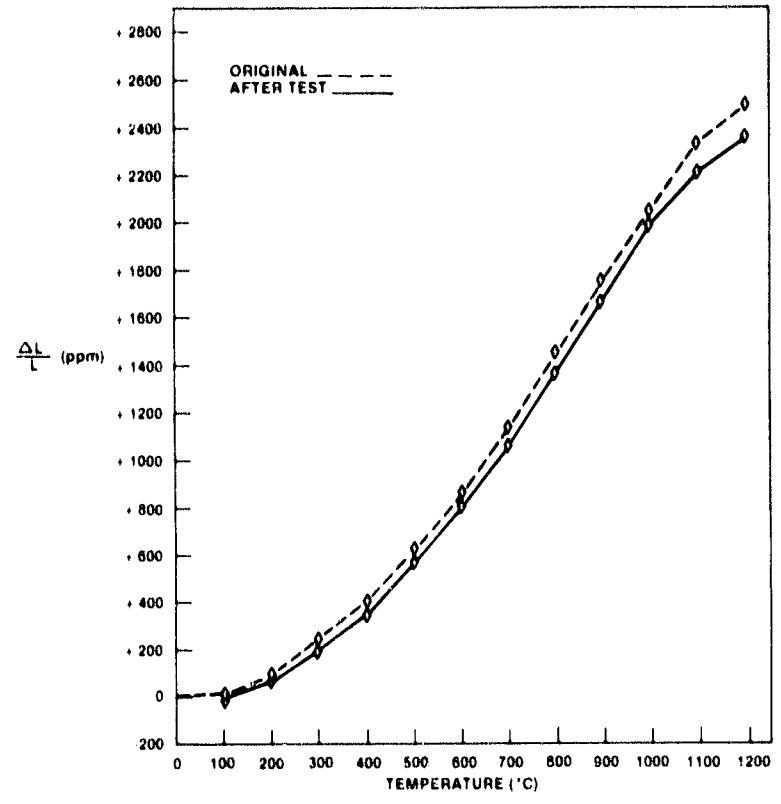

Figure VI.B.4.15 Supplier C MAS; Thermal Expansion Before and After 1200°C (2192°F) Thermal Stability Testing with Sodium Present

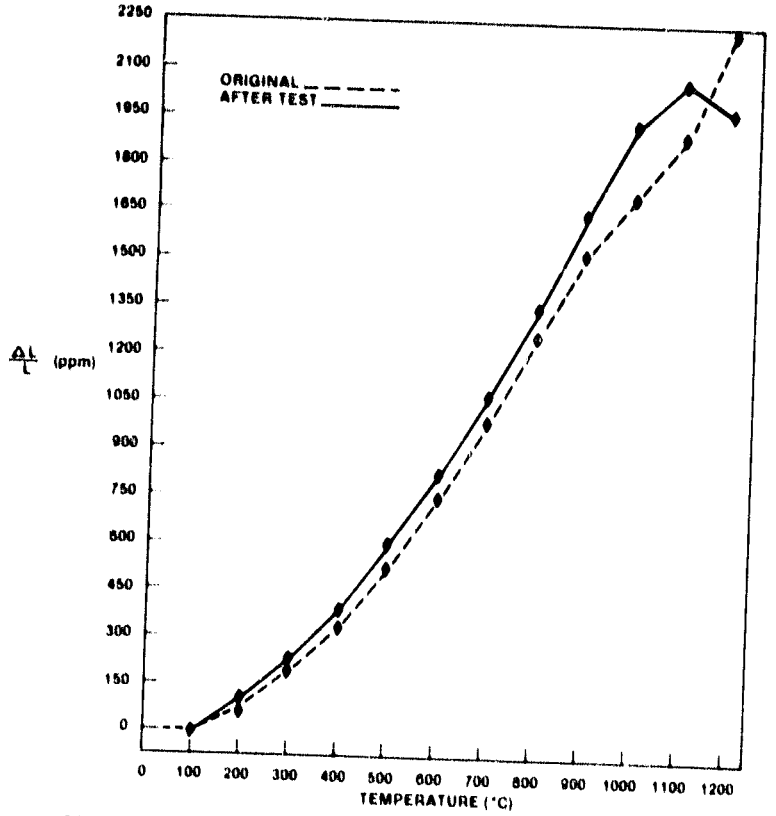

Figure VI.B.4.16 Supplier D MAS; Thermal Expansion Before and After 1200°C (2192°F) Thermal Stability Testing with Sodium Present

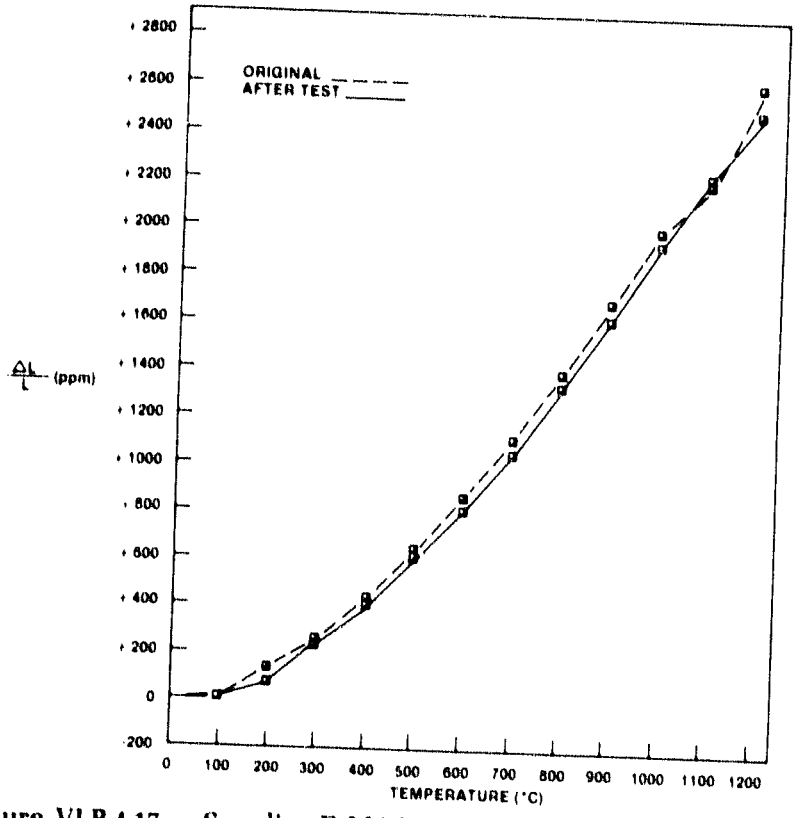

Figure VI.B.4.17 Supplier E MAS #1; Thermal Expansion Before and After 1200°C (2192°F) Thermal Stability Testing with Sodium Present

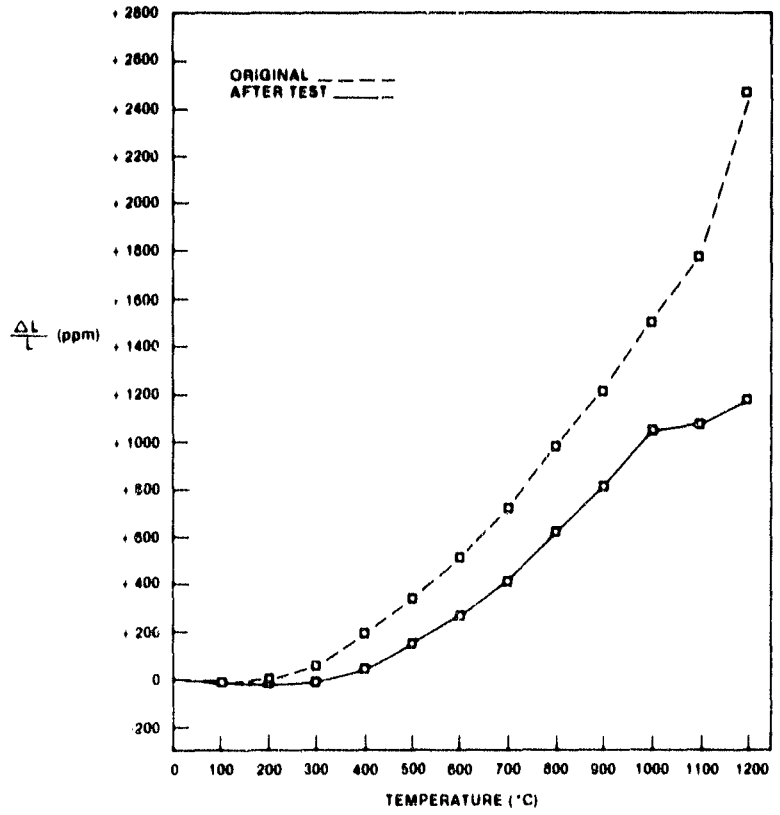

Figure VI.B.4.18 **Supplier I MAS; Thermal Expansion Before and After 1200°C (2192°F) Thermal Stability Testing with Sodium Present**

The MAS materials, while all displaying a good deal of dimensional change during the course of the test (Figure VI.B.4.12), do not reflect, with the exception of that material from Supplier I (Figure VI.B.4.18) much change in their thermal expansion behaviors (Figures VI.B.4.14 through VI.B.4.17). The data accumulated to date at 1200°C (2192°F) are not as consistent and therefore, not as open to interpretation as those data gathered at the lower test temperatures.

The new matrix materials, i.e. the Supplier A extruded and wrapped MAS matrices, Supplier E wrapped MAS matrix and the Supplier K LAS/MAS matrix, have also been evaluated at 1200°C thermal stability test in presence of sodium salt. The Supplier A wrapped MAS matrix and the Supplier K LAS/MAS matrix fluxed within the first 24 hours. The test data for the remaining two materials (extruded MAS ○ and wrapped MAS ▽), are presented in Figure VI.B.4.12 along with the data for the other materials. Comparing the 1200°C thermal stability data for these two materials in air and in presence of sodium salt (Figures VI.B.4.1 and VI.B.4.12) it is apparent that these two materials are relatively unaffected by the presence of sodium salt. This is remarkable since all other materials exhibited a certain degree of instability in presence of sodium salt at 1200°C as can be seen in Figure VI.B.4.12. All the evidence points to the fact that a fully stabilized, either by prior heat treatment or an appropriate fabrication process, cordierite type MAS material matrices offer the potential for 1200°C regenerator application.

In view of the 1200°C thermal stability (in air) data and the behavior of these materials at 1100°C and 1000°C it appears that only the MAS material have the service potential in applications where the regenerator temperatures reach 1200°C.

C. Summary

As a result of this test program sufficient engine test data are now available with respect to the behavior of the AS (leached LAS), MAS and the standard LAS materials in the regenerator application in the 707 engine. It can be concluded that while the standard LAS regenerators are vulnerable to chemical attack in the standard 707 engine exhaust gas environment (i.e. 800°C maximum temperature), the AS and the MAS materials are generally impervious to chemical attack up to 1000°C (the maximum regenerator test temperature capability of the 707 engine).

The laboratory test data generated in Task III and Task VI provide a basis for the determination of the potential service temperature capability of the various materials available for the regenerator application. Pertinent test data from these two tasks are summarized in Figures VI.C.1, VI.C.2 and VI.C.3 to provide a thermal stability comparison for the two most promising (AS and MAS) materials.

The laboratory tests on the first generation AS matrix specimens at temperatures up to 1200°C revealed some serious limitations with respect to the thermal stability and resistance to sodium attack at temperatures above 1000°C. At 1000°C, the thermal stability as well as the resistance to sodium attack (Figure VI.C.1) appear marginal.

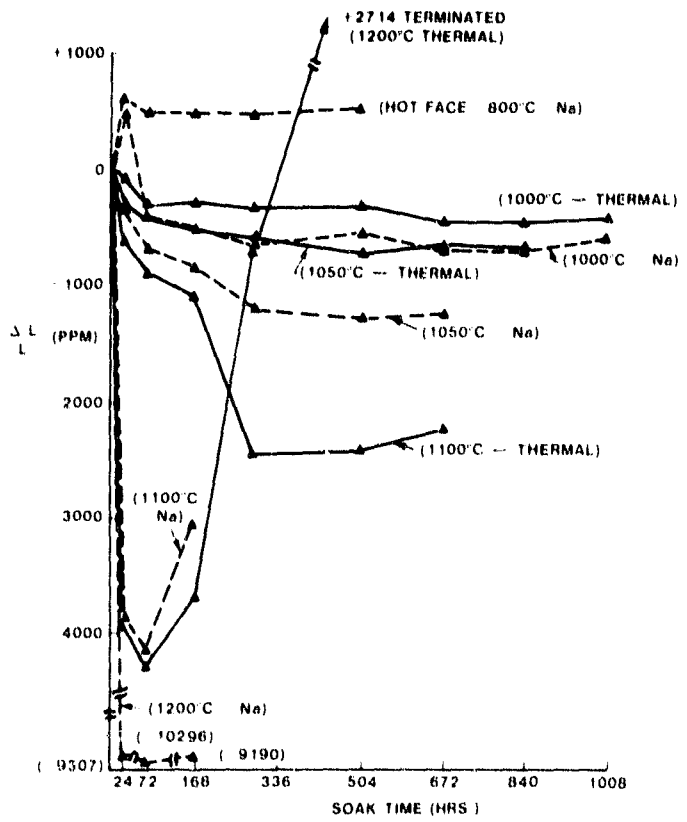

Figure VI.C.1 **Supplier A, First Generation AS; Thermal Stability With and Without Sodium at 800°C to 1200°C.**

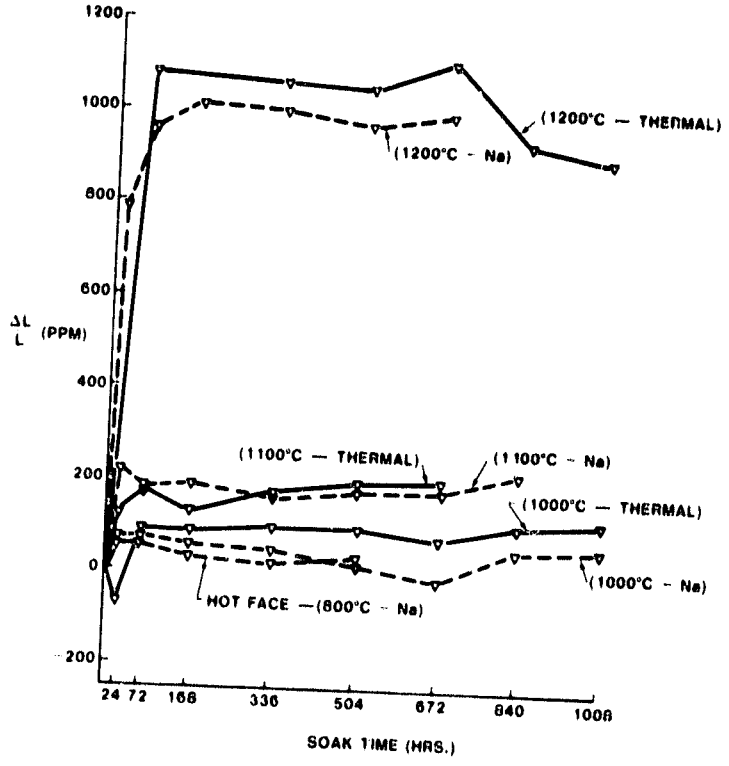

Figure VI.C.2 Supplier E, MAS Glass Frit; Thermal Stability With and Without Sodium at 800°C to 1200°C.

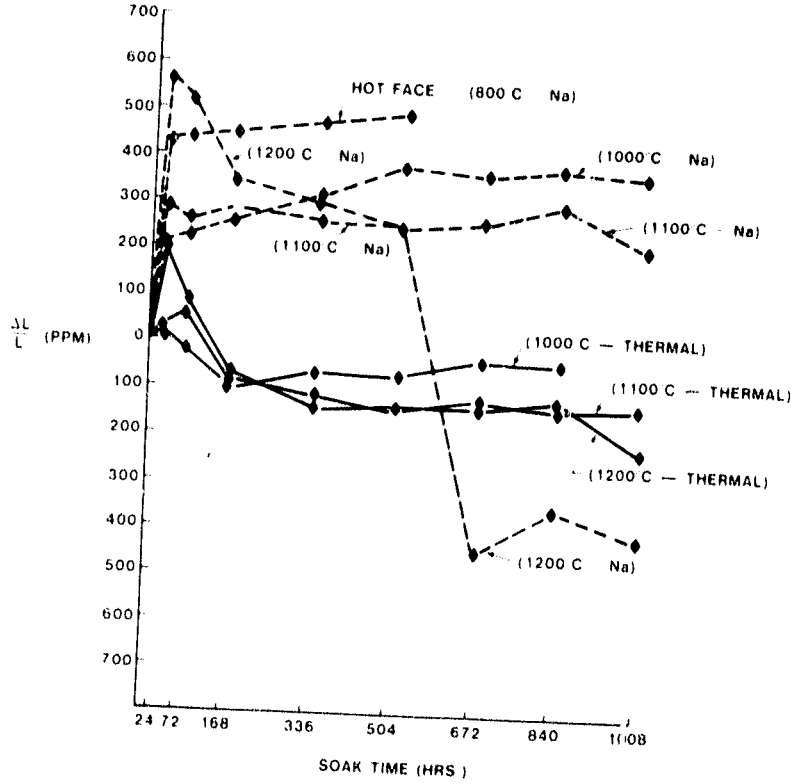

Figure VI.C.3 Supplier D, MAS Mineral Base; Thermal Stability With and Without Sodium at 800°C to 1200°C.

At 1050°C, 1100°C and 1200°C they are very poor (Figure VI.C.1). The current AS regenerators are made from the LAS matrix by leaching out all the lithium and subsequently heat treating the skeletal β spodumene structure to partially sinter and strengthen the matrix. This structure is inherently unstable and will ultimately convert to AS keatite/mullite structure. The rate of this transformation is a function of temperature and can occur very rapidly at temperatures 1000°C and above. This phase transformation results in a change in cell dimensions, as has been observed in the 1100°C and 1200°C thermal instability test, as well as a change in thermal expansion. Although no sodium ion attack is observed below 1000°C, above this temperature the sodium appears to diffuse rapidly into the lattice forming low melting silicate compounds. At temperatures above 1100°C, these reactions are so rapid that severe fluxing of the first generation AS matrix occurred in a very short time.

The second generation AS material with potential for improved thermal stability up to 1100°C was received at the end of the program for evaluation in the laboratory as well as engine testing. Based on limited engine and laboratory testing this material appears to have 1100°C (2012°F) temperature capability in the regenerator application. Limited laboratory testing of the ZR/MAS material indicates potential at this temperature also.

The current MAS matrix materials, being of the cordierite type with the Mg ions tightly bonded to the silicate structure, are highly stable and are more resistant to ion exchange. Properly fired MAS matrices have demonstrated thermal stability and excellent resistance to sodium ion attack at temperatures up to 1200°C (Figures VI.C.1, VI.C.2, VI.C.3). The MAS matrices tested are made by two different processes from two types of raw materials, namely mineral base and glass frit base. For the mineral base MAS the starting materials are primarily clay and talc, with the composition adjusted to yield cordierite ($MgO:Al_2O_3$: SiO_2—2:2:5) in the fired structure by the addition of alumina and silica. This type of matrix is usually porous but of lower thermal expansion. For the glass-ceramic, the starting material is a glass-frit powder of primarily MAS-2:2:5 composition with minor amounts of nucleating agents. The firing cycle is such that glass sinters and crystallizes more or less completely during firing. Very high wall density and high strengths are achieved with this material, however, the thermal expansion is usually slightly higher than the mineral base MAS matrix. The source of thermal instability in both types is usually the transformation of the residual glass phase in the fired matrix. This can, however, be removed by appropriate heat treatment prior to service installation. The glass frit base matrix demonstrated excellent resistance to chemical attack (Figure VI.C.2). The mineral base matrix (Figure VI.C.3), though not as good as that of the glass frit base, is still adequate up to 1200°C.

At the present time test data that can systematically evaluate the influence of oxides and/or sulphates of Fe, Zn, Mg, Na, Cu, etc., which can form low melting compounds capable of severe fluxing action, on these matrix materials at temperatures up to 1200°C is non-existent. Any future programs should include the evaluation of the resistance of the regenerator materials to these compounds.

In summary, it appears that the current AS and MAS ceramic materials can perform adequately in the regenerator application of the "state-of-the-art" gas turbine

engines (up to 1000°C). For higher temperature applications, the first generation AS material, which has desirable low thermal expansion characteristics, must demonstrate improved thermal stability and resistance to chemical attack at temperatures up to 1100°C. The second generation AS material, appears to satisfy this requirement. Further development of this material may be required for 1200°C applications.

Based on laboratory testing up to 1200°C, the current MAS materials offer the potential for adequate thermal stability and resistance to chemical attack up to 1200°C application. For applications involving still higher temperatures, materials such as silicon carbide and silicon nitride appear to be the only materials with potential. Any future programs should include the evaluation of these materials.

TASK VII. MANUFACTURING COST STUDIES

VII.A INTRODUCTION

A heat exchanger cost study was initiated at Ford during the last quarter of 1975. Several ceramic companies which had experience in ceramic matrix fabrication contributed to the study. An air preheater, about 46 cm. (18 in) in diameter, fabricated of ceramic material and designed for 1000°C (1832°F) operation in the 170 horsepower Stirling engine, was used as the subject for this study. An annual production volume of 500,000 units was used in the cost analysis. This study concluded with a lowest predicted manufacturing cost range of $25-$30 per core. This cost presumed technological developments not now in general practice in the various core production schemes.

The purpose of this task was to update the initial study and to apply the present cost study factors to new configurations of potential interest.

VII.B DISCUSSION

The initial area of effort was originally felt to be a purely financial updating of the initial report, including the effects of inflation and rising energy costs. Upon further study, it became clear that the lack of a suitable range of heat exchanger models upon which to base cost studies was a more pressing concern. Therefore, two additional regenerators applicable to an automotive application were evaluated.

A thorough evaluation of the initial cost study (Reference 2) was completed by updating the most detailed cost information applicable to the production of Stirling preheater cores. It was assumed that MAS material, tunnel kiln firing, and belt grinding were utilized to attain the high production rate. All costs were updated economically, assuming 2 years of 7% inflation. Table VII.B.1 collates the results of this study. The first configuration is that of the original study, and this updated cost was the base from which the new configurations were analyzed. Configuration (2) is for a single-core automotive gas turbine engine, and configuration (3) is intended for service in a dual core automotive gas turbine engine, where the combined performance of both smaller cores equals that of the single larger core configuration. The unit costs listed in Table VI.B.1 do not include costs associated with ring gear and elastomer assembly, product launching, research development, and profit.

The new core costs were arrived at by projecting the machinery and process line requirements for each manufacturing step based on the amount of material used in each core configuration and the production rate. Plant floor space was then adjusted to these new line and equipment requirements. Investment capital for equipment and plant facilities were recalculated based on the above adjustments. New variable labor allocations were established based upon the equipment requirements for each core size. The manufacturing burden (including premium pay, supplies, expenses, gas and power) was calculated for each production step based on allocations of material, manpower, and equipment for each core size. Finally, an economic adjustment, to compensate for inflation, was made to each cost.

CONFIGURATION	CORE SIZE (FINISHED)	PROJECTED COST/UNIT
1	457.2 MM (18") O.D. X 190.5 MM (7.5") I.D. X 39.9 MM (1.6") THICK	$29-34 (BASE)
2	368.3 MM (14.5") O.D. X 190.5 MM (7.5") I.D. X 88.9 MM (3.5") THICK	$33-39
2A	368.3 MM (14.5") O.D. X 25.4 MM (1.0") I.D. X 88.9 MM (3.5") THICK	$38-46
3	266.7 MM (10.5") O.D. X 190.5 MM (7.5") I.D. X 88.9 MM (3.5") THICK	$23-27
3A	266.7 MM (10.5") O.D. X 25.4 MM (1.0") I.D. X 88.9 MM (3.5") THICK	$29-34

Table VII.B.1 Projected Cost for Various Core Configurations

In addition, an evaluation of the extra cost associated with a zero-diameter (nominally 1 in. or 25.4mm) wind fabrication process was completed (configurations 2A and 3A in Table VII.B.1). A switch to zero wind fabrication process would increase unit costs approximately 15-18% for configuration 2 and 26% for configuration 3.

VII.C. TASK SUMMARY

The initial cost study was updated to include more recent process developments and to account for inflation and rising energy costs. In addition two additional heat exchanger sizes applicable to automotive gas turbine engines were also evaluated.

A comparison of conventional and zero-wind fabrication costs was completed. Data for two regenerator core configurations indicate a production cost increase ranging from 15% to 26%, depending on the core outer diameter.

VIII. CORE MATERIAL AND DESIGN SPECIFICATION

VIII.A. INTRODUCTION

Quality control of vendor-supplied hardware is a crucial step in the fabrication of an automotive gas turbine regenerator. Therefore, it is important that the proposed heat exchanger system for alternate engines be well-defined prior to large production efforts. From this perspective, a rather complete regenerator core specification for 800°C (1472°F) operation was drawn up and published (Reference 1). This specification was based on a considerable amount of experience with a regenerator matrix fabricated by one method (wrapped sinusoidal corrugations) with one material (LAS). Since the ceramic regenerator systems development program consists of several materials fabricated by a variety of methods, a modification of the original specification was required.

As engine and materials technology improve, proposed regenerator operating temperatures increase. In anticipation of predicted engine demands, a preliminary attempt to define a 1000°C (1832°F) specification is desirable.

The effort directed toward this contractual task had two objectives. The primary task was perceived to be a general updating of the existing specification, as new design understanding, better materials, and additional test experience have evolved since the original specification was written. A second goal was the drafting of a knowledgeable framework on which a 1000°C (1832°F) material and design specification can be constructed.

VIII.B CERAMIC REGENERATOR PROCUREMENT SPECIFICATION FOR 800°C AND 1000°C APPLICATION

VIII.B.O. INTRODUCTION

This procurement specification for ceramic regenerator cores has evolved from a data base established over a thirteen year period of activity in laboratory and engine testing of ceramic materials proposed for service as regenerator cores in the Ford 707 gas turbine engine. An active manufacturing development program has complemented these test data. The specification is written in a general sense and is intended to include a wide variety of ceramic materials fabricated into high-open-area cellular structures by any one of a number of viable processes including extrusion, wrapped paper, calendaring, embossing, glass tube bundling, and others.

By far the most test experience at Ford has been accumulated on regenerator cores manufactured by the wrapped paper process. This process entails the concurrent wrapping of flat and corrugated paper sheets which have been coated with a ceramic binder slurry. The cellular structure so formed is converted into a useful product by a high-temperature densification treatment. During the heating cycle, the organic binder (added to the ceramic slurry to impart sufficient mechanical strength for handling in the unfired state) and the paper are decomposed and driven from the structure. During the time spent at elevated temperature, the densifying product develops interparticle bonding and a crystal structure which determines the physical and chemical properties of the regenerator core.

For cores other than those wrapped from zero diameter, a hub must be cemented into the matrix to complete the regenerator assembly. This hub assembly may be a matrix, a solid, or a composite. The solid components are slip cast (or green formed in any suitable manner) of ceramic compositions such that their insertion into the regenerator core would not introduce deleterious residual stresses. The goal is to match solid and matrix components sufficiently well, producing a composite assembly with stress levels so low over the temperature range of application as to not limit the lifetime of the core. The solid components are cemented into the regenerator matrix, and much experience with a foaming cement has been gathered. A detailed description of a foam cement operation is available (Reference 13). In essence, this method entails control of the size and distribution of gas bubbles trapped in a glass at elevated temperatures, the bubbles expand the viscous cement, establishing an intimate contact between the cement and surfaces to be joined, thereby promoting good chemical bonding.

These specifications, coupled with the present regenerator rim, drive, and mounting system design, should enable the regular procurement, from a variety of manufacturers, of a regenerator which will meet the DOE/NASA objectives for an automotive gas turbine heat exchanger. These objectives are:

1) Operation at regenerator inlet temperatures up to 1000°C (1832°F).
2) A B_{10} life of 3500 hours in a typical passenger car duty cycle.
3) Operation on No. 1 and No. 2 diesel fuel and non-leaded gasoline.

VIII.B.1 MATRIX SPECIFICATION

VIII.B.1.0

This specification applies to core dimensions, engineering requirements, and visual inspections for each core shipped to the procurer. Sampling inspection procedures can be applied to all the characteristics inspected. The characteristics that require 100 percent inspection in low volume development or production operations are indicated. The VIII.B.1 specification data must accompany each core shipped to the procurer.

VIII.B.1.1

The matrix cell density (cells/cm^2) will be measured over a 6.45 cm^2 (1 inch square) area at a 180mm (7 in) disc radius. The cell density will be within ±5% of the nominal value specified by the procurer.

VIII.B.1.2

The matrix open frontal area (σ) will be calculated from the fire bulk density (ρ B) and the wall density (ρ W) measured from the firing shrinkage and bulk density of the matrix as follows:

$$\sigma = 1 - \rho B / \rho W$$

The matrix open frontal area will be within ±5% of the nominal value specified by the procurer.

VIII.B.1.3*

The matrix material will have a maximum thru-wall circumferential leakage of .063 $\frac{kg}{sec \cdot m^2}$ ($9x10^{-5}$lb/sec−in^2) at 138 KPa (20 psi) air pressure across a 38.1mm (1.5 in) wide rubber seal through 3.2mm (1/8 in) wide by 152.4mm (6 in) long slot radially oriented. Figure VIII.B.1.1 is a schematic drawing of the test apparatus.

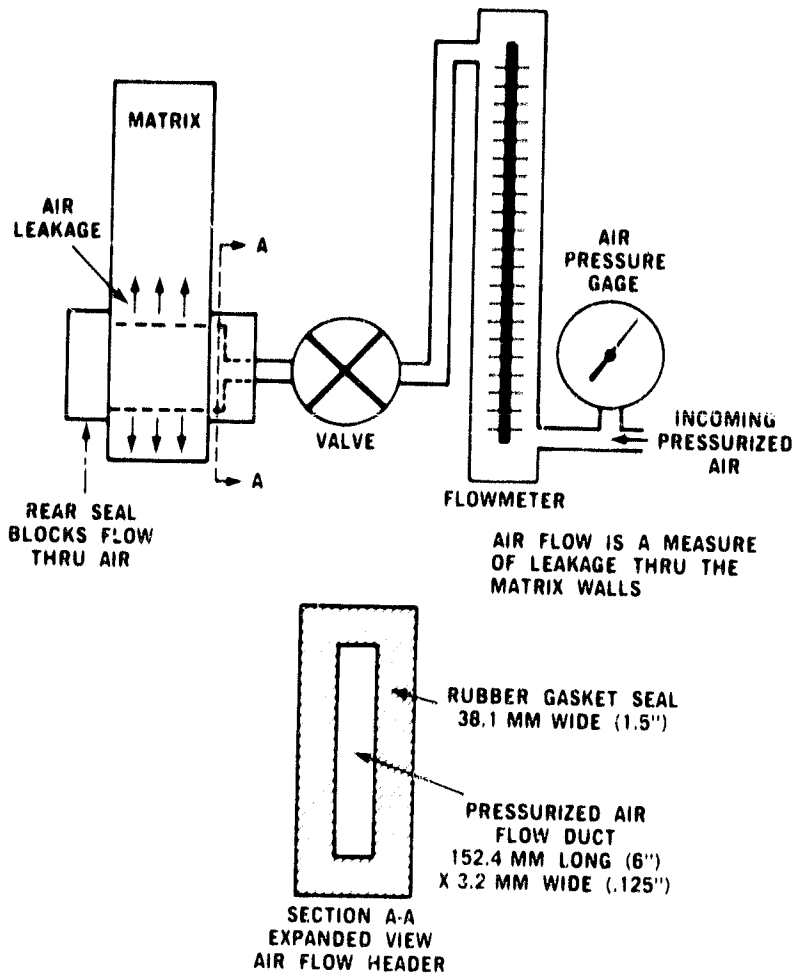

Figure VIII.B.1.1 Schematic of Matrix Wall Leakage Measurement Device

VIII.B.1.4

The matrix passage geometry and wall thickness result in values of C and A which define the thermal and pressure loss performance of that matrix through the following relationships:

$$\frac{(\Delta P)P}{L} = C \left(\frac{W(T)}{A_F}\right)^{1.673} \qquad \frac{NTU}{L} = A \left(\frac{A_F T}{W}\right)^{.673}$$

where

ΔP = pressure KPa
P = inlet pressure, KPa
L = core thickness, mm
W = air flow, kg/sec
T = Avg. temperature of inlet air — °K
AF = matrix frontal area, m^2

* Indicates 100% inspection for low volume development or production operations.

$$C = \frac{3.56x10{-}9C_1}{\sigma DH^2} \; , \; \frac{(KPa)^2 sec.m.^2}{kg\ cm\ °K}$$

$$A = \frac{3.11\ (10{-}5)C_2\sigma}{DH^2} \; , \; \frac{kg}{sec.\ cm\ m_2 °K;} \; ;IF:\ X_2 = -1$$

C_1 = Fanning Friction Factor constant for laminar flow, $F = \frac{C1}{RE}$

C_2 = Colburn No. constant for laminar flow, $J = C_2 REx2$

σ = open area ratio

DH = hydraulic diameter, cm

X_2 = Reynolds No. (RE) exponent from the Colburn No., $J = C_2 REx2$

Using the pressure drop rig shown schematically in Figure VIII.B.1.2, the maximum allowable value for C will be 2.1 (10−5). Using a matrix shuttle rig or equivalent the minimum allowable value for A will be 2.0 (10−2).

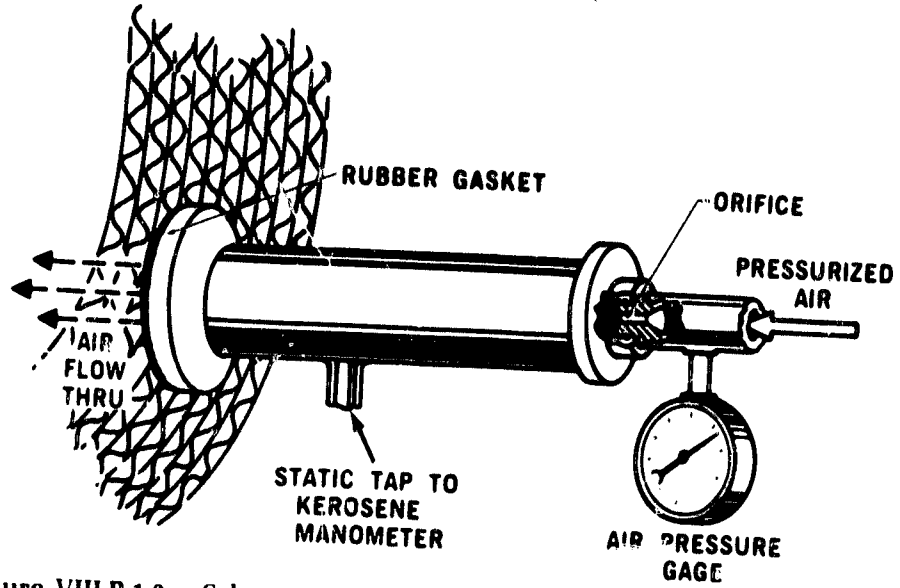

Figure VIII.B.1.2 Schematic of Matrix Pressure Drop Measurement Device

VIII.B.1.5 Dimension Requirements

VIII.B.1.5.2* Thickness

The matrix must be inspected at three places approximately 120° apart. The average reading must be within 71.51±0.08mm, (2.815±0.003 in).

VIII.B.1.5.3 Parallel

Faces of the matrix must be parallel within 0.08mm, (0.003 in).

VIII.B.1.5.4 Flatness

Each face of the matrix must be flat within 0.08mm, (0.003 in).

VIII.B.1.5.5 The Matrix Fill in the Core Face in Contact With Peripheral Seal

The fill inside radius must be within 336.5-335.79mm (13.250-13.220 in), and the fill extends to the core outer diameter with a depth (reference only) of from 5.1 to 15mm (0.20-0.60 in). The material and fill procedure are given in Section VIII.B.6.

VIII.B.1.6* Visual Verification

VIII.B.1.6.1 Delaminations

There are points on the matrix where the corrugated sheets have not bonded to the adjacent flat sheet resulting in a visually detectable gap and are shown in Figure VIII.B.1.3. Delaminations are generally not a serious occurrence. Periodic splicing of the paper carrier used in the winding process result in a much larger delamination as shown in Figure VIII.B.1.4.

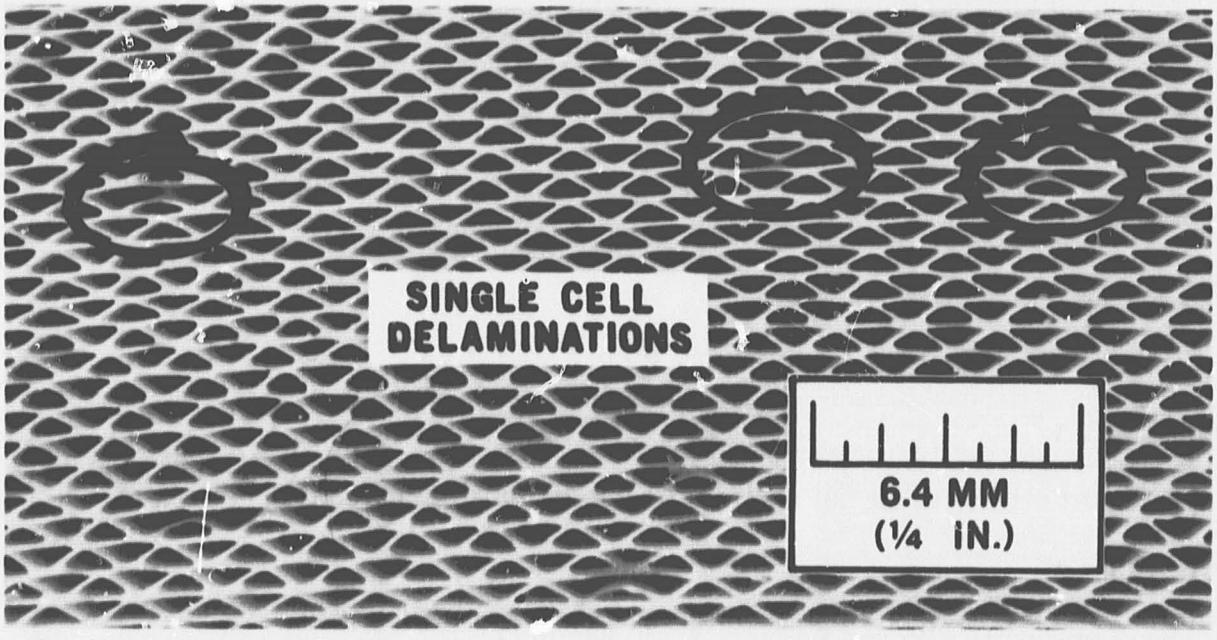

Figure VIII.B.1.3 Matrix Photograph Showing Single Cell Delaminations

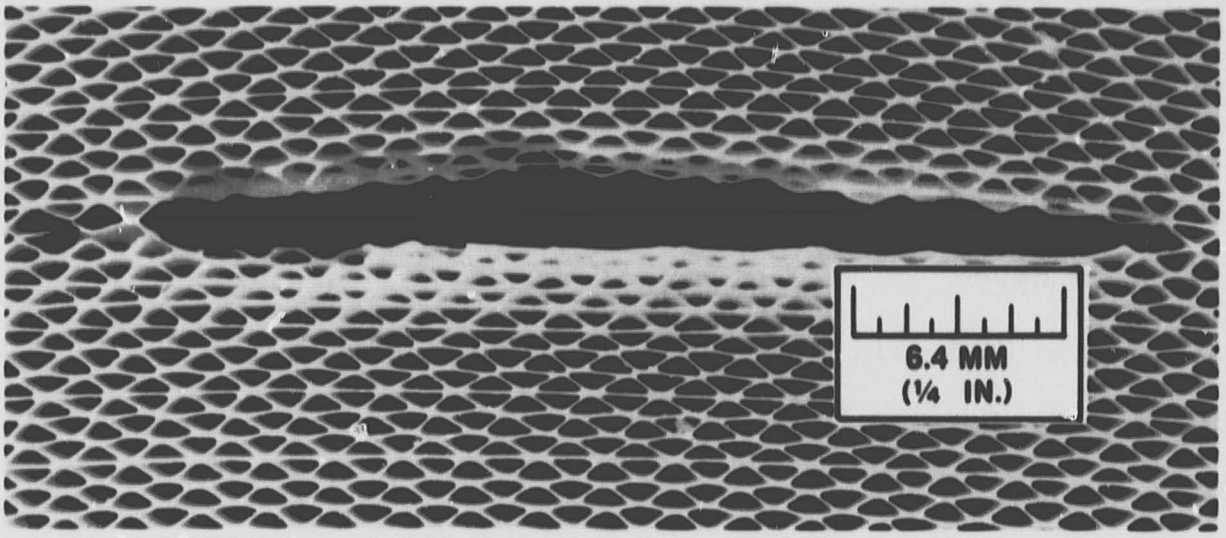

Figure VIII.B.1.4 Matrix Photograph Showing a Splice Delamination

VIII.B.1.6.1.1

Maximum unbonded junction (each cell) delaminations allowed are 5 per square cm ($30/in^2$). A 1.2x5.0 cm (0.5x2.0 in) template is to be used for inspection purposes applying the 5.0 cm (2 in) length of the template circumferentially on the matrix.

VIII.B.1.6.1.2

Only six delaminations per face are allowed between 19 and 38mm (3/4-1-1/2 in) long and no more than two within ±1.5mm (±.060 in) radially at any location.

VIII.B.1.6.1.3

The maximum length delamination allowed is 38mm long x 2.5mm (1-1/2x.10 in) wide inspected at the surface with the unaided eye.

VIII.B.1.6.1.4

Due to measuring errors, readings within 5mm (.20 in) of specifications are acceptable.

VIII.B.1.6.2

Scuff: Surface abrasion as shown in Figure VIII.B.1.5.

VIII.B.1.6.2.1

Disregard scuffs under 13mm (1/2 in) maximum dimension.

VIII.B.1.6.2.2

Three scuffs are allowed per face up to 38mm (1.5 in). Maximum dimension with a maximum depth of 64mm (1/4 in) allowable.

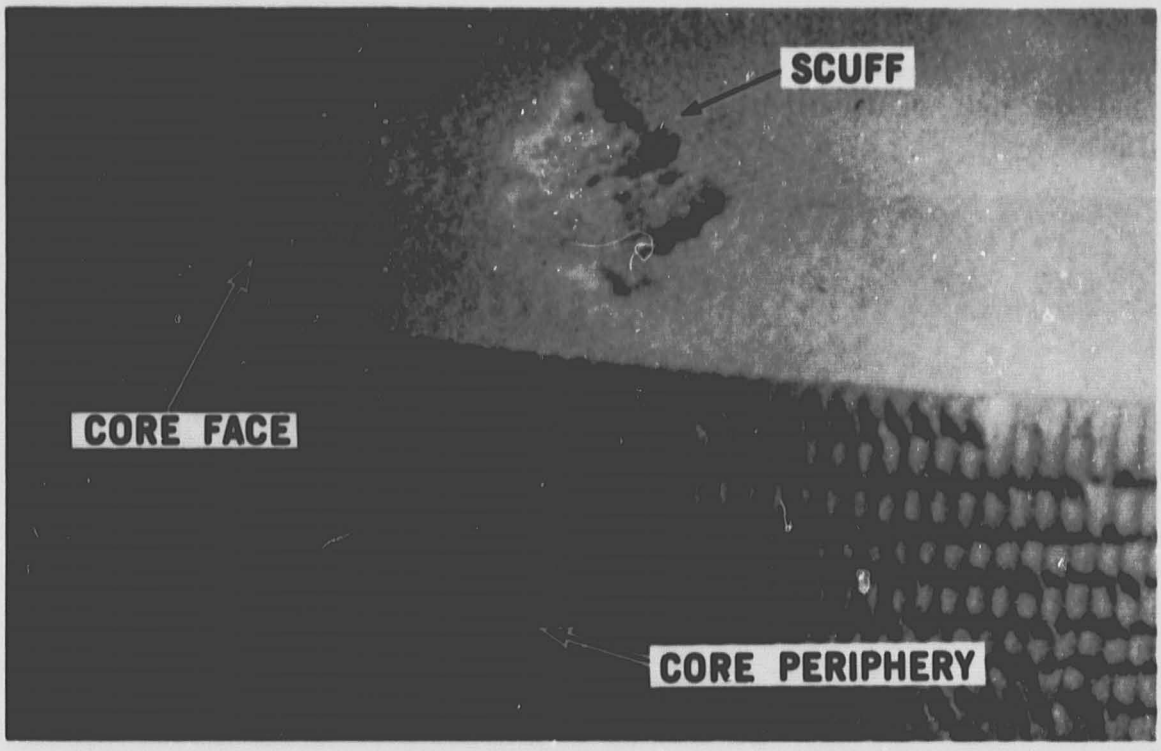

Figure VIII.B.1.5 Matrix Photograph Showing a Scuff on the Matrix Face near the Core O.D.

VIII.B.1.6.2.3

No scuff allowed greater than 13mm (1/2 in) maximum dimension between the 339mm (13.350 in) radius and the core outer diameter.

VIII.B.1.6.3

Radial Cracks: Disregard continuous radial cracks under .25mm (.10 in) long (radial cracks in two successive flat sheets). The matrix material shall be free of any other length of radial cracks. See Figure VIII.B.1.6.

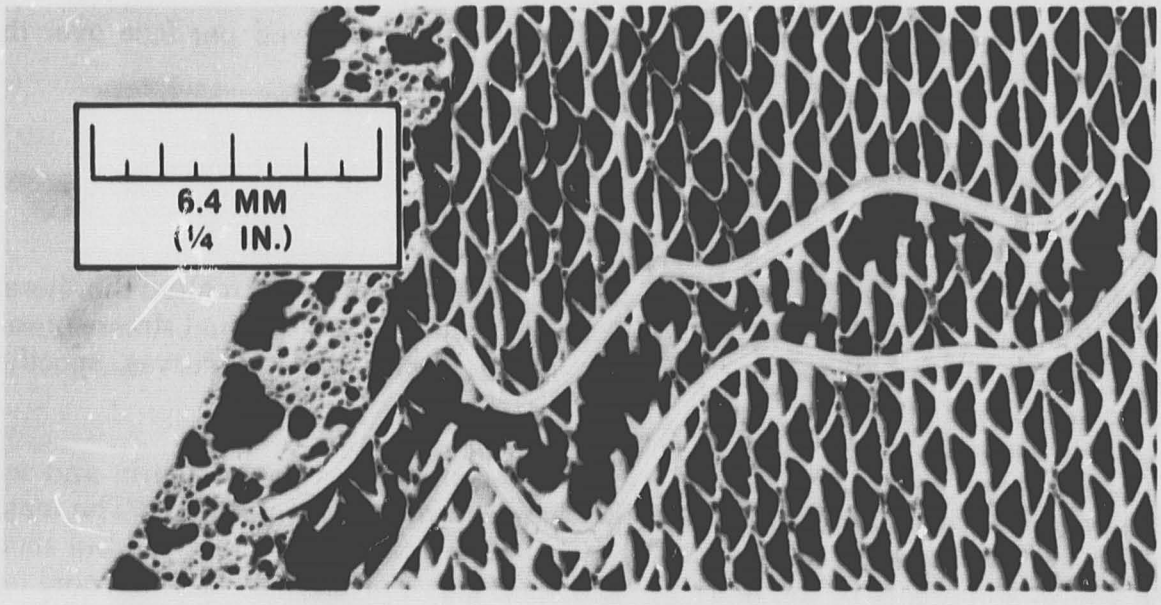

Figure VIII.B.1.6 Matrix Photograph Showing a Long Radial Crack near the Solid Hub

VIII.B.1.6.4

Cement Spill Around Hub: The maximum cement spill-over into the matrix around the hub shall not exceed 9.5mm (.375 in) on both faces. See Figure VIII.B.1.7.

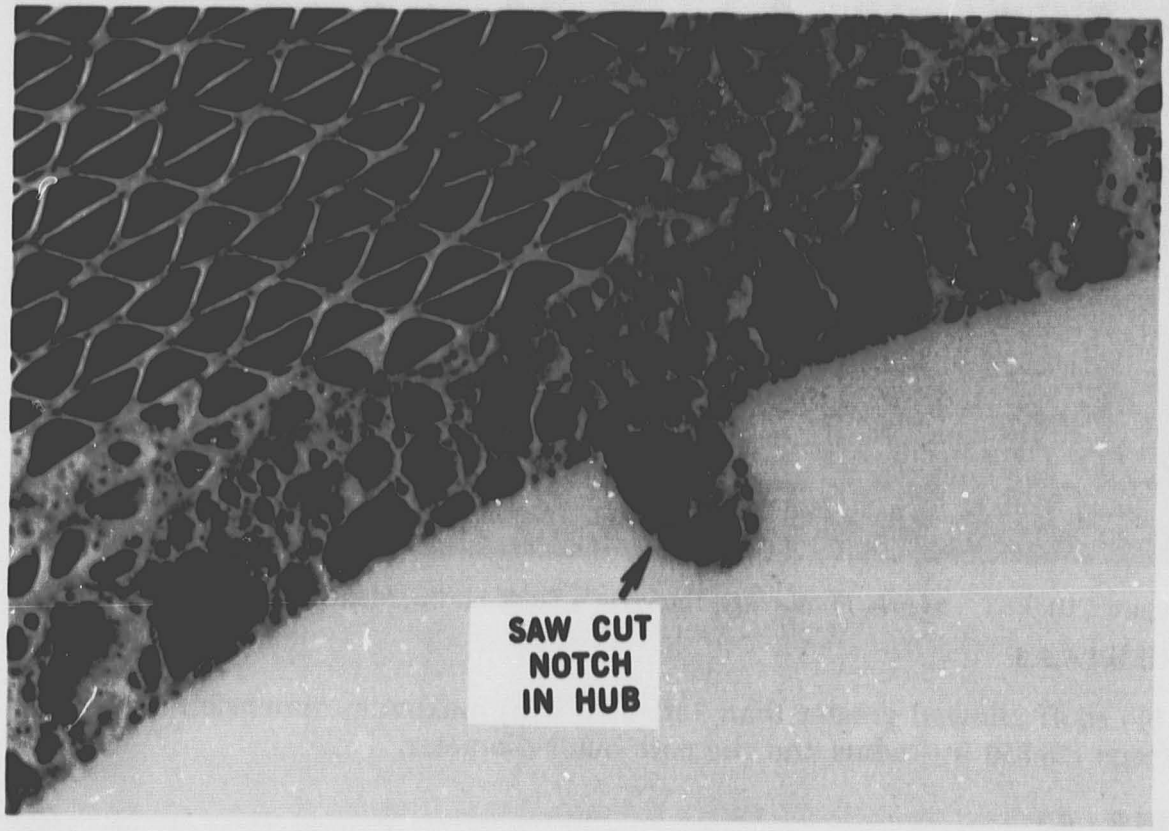

Figure VIII.B.1.7 Matrix Photograph Showing Foam Cement Spillover in the Hub Area. Also shown is the Sawcut Notch (See 2.3.4)

VIII.B.1.6.5

A total of 1290mm^2 (2 in^2) of any cement spill-over allowed per face over that specified in VIII.B.1.5.5 and VIII.B.1.6.4.

VIII.B.2 HUB SPECIFICATION

VIII.B.2.0 Solid Hub

Since the solid components are processed differently than the matrix, the thermal expansion may differ slightly. To prevent unacceptable core residual stresses resulting from excessive mismatch of component thermal expansion curves, specifications were established.

The ceramic foam cement similar in thermal properties to the matrix and solid components is used as the bonding agent between the solid and matrix. The matching of the cement expansion to that of the solid and matrix is not critical but should be within 25 percent of the thermal expansion curve of the matrix from room temperature to 1000°C (1832°F).

As the regenerator assembly cools down from the foam cement maturing temperature, the glassy phase portion of the foam cement is viscous and any solid-matrix expansion mismatch is taken up by viscous flow. As the temperature decreases, the foam cement strain point is reached and from this point to room temperature any expansion mismatch results in matrix and cement residual stresses. The solid component residual stresses being negligible.

In Figure VIII.B.2.1 the magnitude of the mismatch value is determined by measuring the differential solid-matrix contraction starting at the foam cement strain point and ending at 100°C (212°F). Positive mismatch is defined by a greater contraction of the solid relative to the matrix (curve A) and negative mismatch is the reverse (curve B).

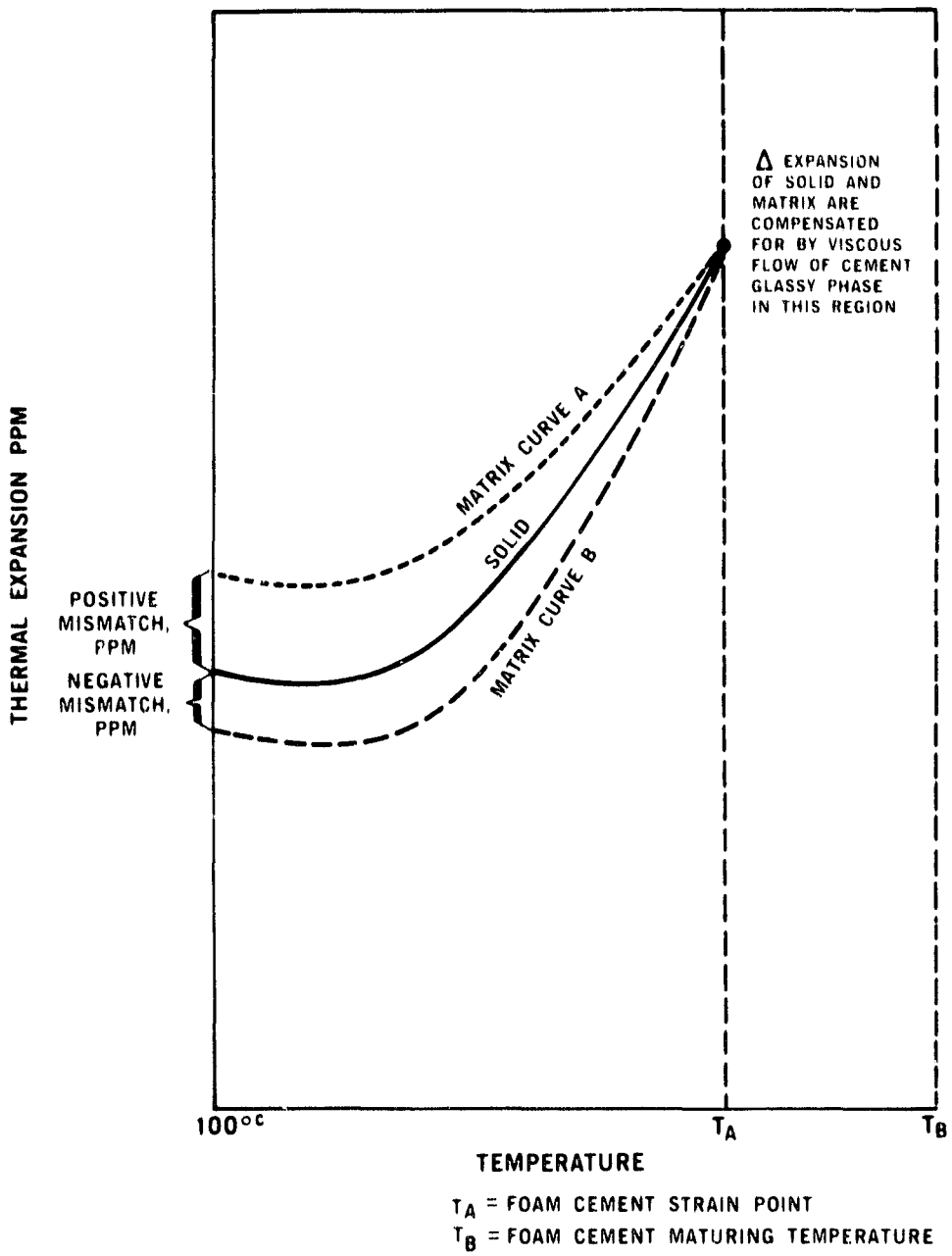

Figure VIII.B.2.1 Schematic Thermal Expansion Plot Showing Negative and Positive Mismatch

VIII.B.2.0.1* Thermal Expansion Mismatch

The hubs must be matched with the matrix for expansion, the matrix sample is taken at the inner most diameter and hub samples can be taken anywhere on the hub. Mismatch must be within +70 ppm and −50 ppm.

VIII.B.2.0.2 Dimensional Requirements

VIII.B.2.0.2.1 Outside Diameter

The outside diameter shall not exceed 102mm (4.0 in).

VIII.B.2.0.2.2* Thickness

The hub must have a thickness of 71.51 ± 0.08mm (2.815 ± 0.003 in).

VIII.B.2.0.2.3

Overall Surface Finish: Must be within 30 micrometers.

VIII.B.2.0.3 Visual Verification

VIII.B.2.0.3.1 Voids

VIII.B.2.0.3.1.1

Disregard voids under 1.6mm (1/16 in).

VIII.B.2.0.3.1.2

Only four voids are allowed per hub face up to 4mm (0.15 in).

VIII.B.2.0.3.2

Fissures: Fissures are long, narrow, slit-like openings which were not filled in the slip casting operation. See Figure VIII.B.2.2.

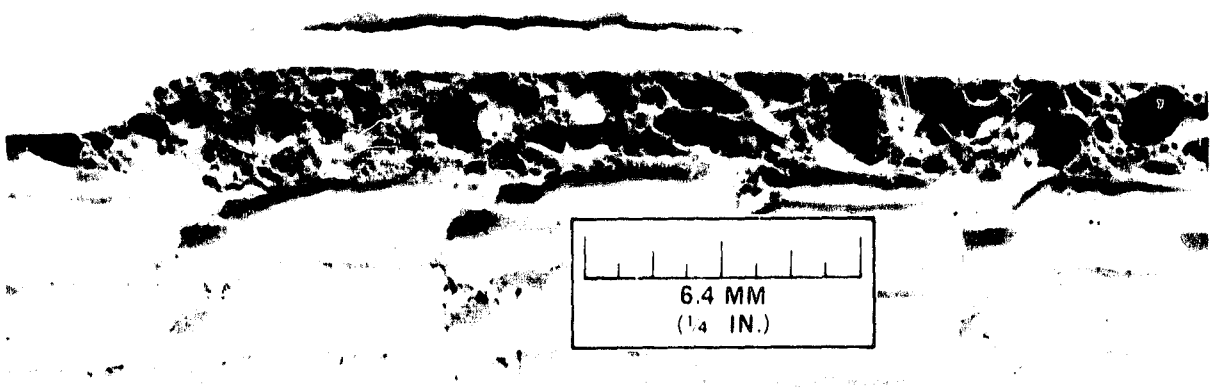

Figure VIII.B.2.2 Hub Photograph Showing a Fissure

VIII.B.2.0.3.2.1

Disregard fissures under 3.2mm (1/8 in).

VIII.B.2.0.3.2.2

Only two fissures, up to 25.4mm (1.0 in) in length are allowed per hub face.

VIII.B.2.3.3

Chips: Breakage of material caused by damage to the edges of the part. See Figure VIII.B.2.3.

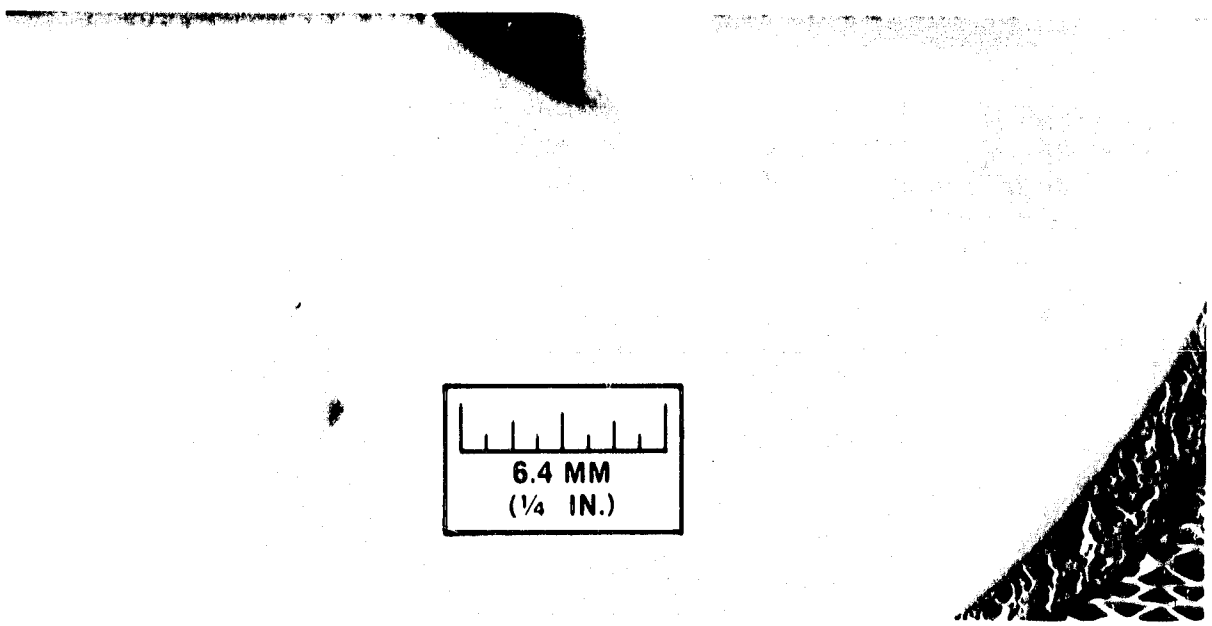

Figure VIII.B.2.3 Hub Photograph Showing a Chip

VIII.B.2.0.3.3.1

Disregard chips under 3.2 x 3.2mm (1/8 x 1/8 in).

VIII.B.2.0.3.3.2

Only two chips allowed per face up to 12.7 x 6.4mm (1/2 x 1/4 in) long. Break sharp edges.

VIII.B.2.0.3.4 Identification Requirements:

The matrix "up-face" or the exposed surface during firing is mechanically stronger than the "down-face" and this face is the hot side of the core during operation. This face is identified as follows:

VIII.B.2.0.3.4.1

The hub shall have an approximate 5mm long x 2.5mm wide (.2 x .1 in) saw cut notch at the O.D. edge visible when viewing the up-face, see Figure VIII.B.1.7.

VIII.B.2.0.3.4.2

The same face is ink stamped "Hot Side H".

VIII.B.2.1 MATRIX HUB

The use of a matrix hub is necessarily bounded by the same constraints as were applied to the use of a solid hub. The regenerator core, the hub, and the cement used to bond the components together must be closely matched so no deleterious residual stress levels exist in the regenerator assembly. The foaming cement requirements have been described in Section VIII.B.2.0 and presented graphically in Figure VIII.B.2.1.

VIII.B.2.1.1* Thermal Expansion Match:

The thermal expansion of the matrix hub must be within 50 ppm of the thermal expansion of the regenerator core as measured from room temperature to 1000°C (1832°F). The regenerator sample shall be selected adjacent to the inner diameter, and the hub sample may be selected at random.

VIII.B.2.1.2 Dimensional Requirements

VIII.B.2.1.2.1 Outside Diameter:

The outside diameter of the matrix hub shall not exceed 102mm (4.0 in).

VIII.B.2.1.2.2* Thickness:

The hub must have a thickness of 71.51 ± 0.08mm (2.815 ± 0.003 in).

VIII.B.2.1.3 Visual Verification:

The matrix hub shall be subject to the regenerator matrix criteria outlined in specification section VIII.B.1.6.

VIII.B.3 CEMENT JOINT SPECIFICATION

VIII.B.3.0 Dimensional Requirements:

VIII.B.3.0.1 Width:

The joint width at the hub must be within 1.3-4.3mm (0.050-0.170 in) with an allowable deviation of up to 9.5mm (0.375 in) maximum, but the total length of the joint deviation must be less than 38mm (1.5 in).

VIII.B.3.1 Visual Verification

VIII.B.3.1.1

Foam bubble size for proper cement firing condition.

VIII.B.3.1.1.1

Lower bubble size limit: There must be at least 10 bubbles .25 (.010 in) or larger per linear inch of cement.

VIII.B.3.1.1.2

Large bubble size limit: No bubbles greater than 12.7mm (1/2 in) are allowed.

VIII.B.3.1.2 Cracks

See Figure VIII.B.3.1.

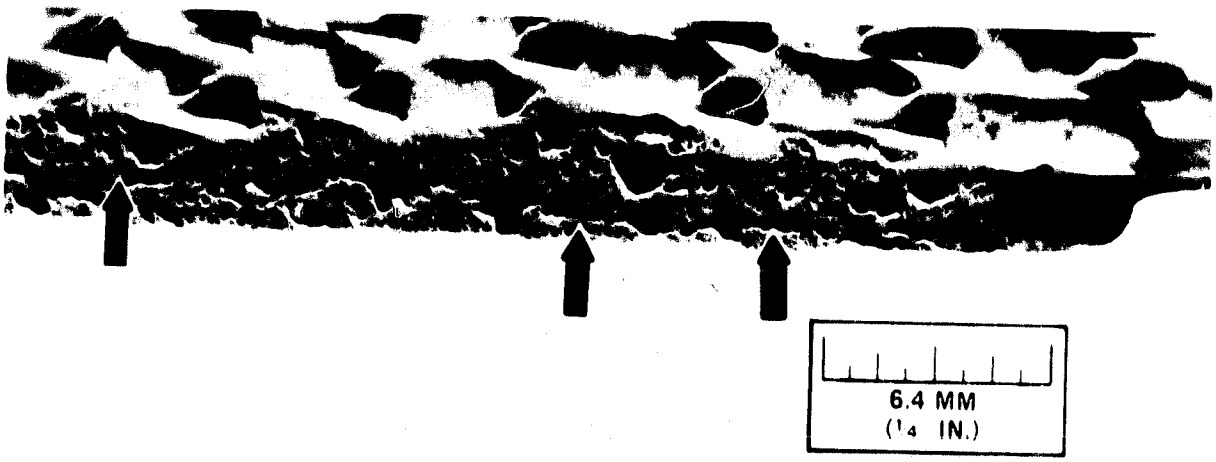

Figure VIII.B.3.1 Photograph of Regenerator Core O.D. Showing a Foam Cement Crack

VIII.B.3.1.2.1

Disregard cracks under 3.2mm (1/8 in) long.

VIII.B.3.1.3

Cement unfilled areas: See Figure VIII.B.3.2.

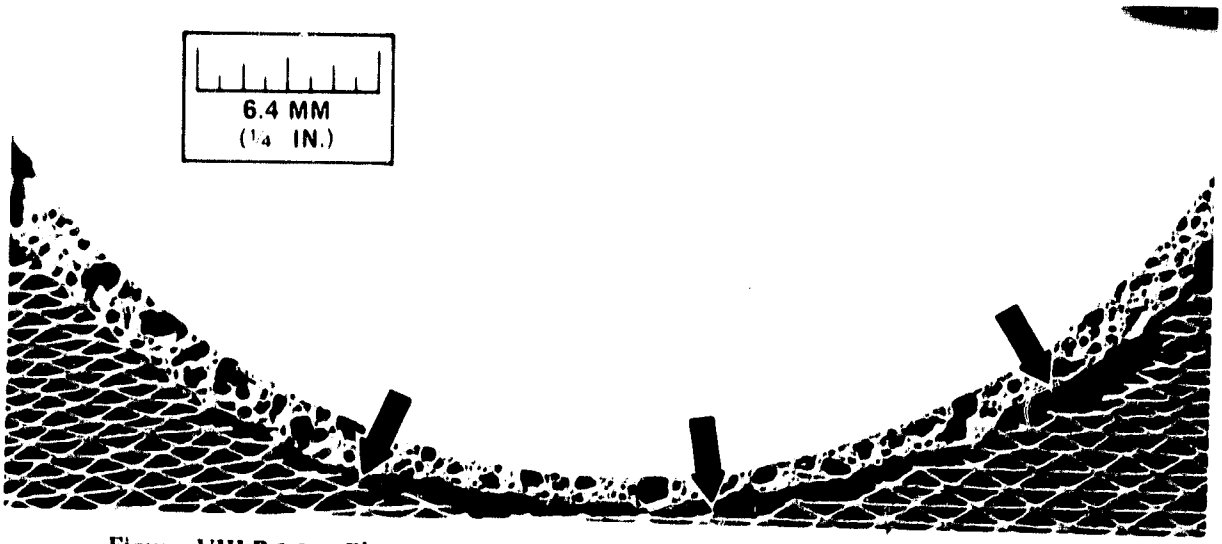

Figure VIII.B.3.2 Photograph Showing a Cement Unfilled Region at the Hub

VIII.B.3.1.3.1

Hub cement: Unfilled areas are allowed up to 9.5mm (3/8 in) deep for a total of one linear inch per face.

VIII.B.4 REGENERATOR TESTING SPECIFICATION

This section describes destructive and longer term testing that is required to ensure that processing parameters corresponding to high quality regenerators with high mechanical and thermal integrity are maintained.

VIII.B.4.0 Selection of Samples:

Regenerator matrix samples representative of the material and process or processes used for fabricating regenerator cores will be tested by the supplier for thermal and mechanical properties at intervals of core manufacture corresponding to the rate of cores produced, process reliability, degree of process development, etc. In addition, representative samples will be tested before and after a major process change.

VIII.B.4.1 Routing of Samples:

The regenerator shall be cut in half; one half will be shipped to the procurer for testing, and the other half will be retained by the supplier. Included with the matrix half retained by the supplier will be:

VIII.B.4.1.1

A representative samples of the hub component used for the fabrication of regenerator cores during the manufacturing period. Samples shall be cut to the dimensions of the thermal expansion samples.

VIII.B.4.1.2

Two thermal expansion samples will be taken and put through the assembly firing schedule.

VIII.B.4.2

For every third set of samples selected for testing, there shall also be selected a full size core for strain testing.

VIII.B.4.3

Periodic retention of cores: The supplier is to periodically retain a full size core rejected from the manufacturing process to be used for future analysis and supplementation of process records.

The frequency of selection and the length of the retention period corresponds to the status of the supplier production process and also to some established average period of time that the supplier production cores will be in field use.

VIII.B.4.4 Reporting

Unless otherwise specified, copies of the test reports will be forwarded to the procurer no later than the scheduled dates below:

VIII.B.4.4.1 Thermal Instability	2 months after matrix firing date
VIII.B.4.4.2 Thermal Expansion	
VIII.B.4.4.2.1 Test 1	1 month after matrix firing date
VIII.B.4.4.2.2 Test 2	1 month after matrix firing date
VIII.B.4.4.2.3 Test 3	2 months after matrix firing date
VIII.B.4.4.3 Modulus of Rupture & Elastic Modulus	1 month after matrix firing date
VIII.B.4.4.4 Open Frontal Area	1 month after matrix firing date
VIII.B.4.4.5 Assembly Strain	1 month after matrix firing date

VIII.B.4.5 Test Requirements

VIII.B.4.5.1 Thermal Instability

Matrix and solid

VIII.B.4.5.1.1 Specification:

The dimensional change upon exposure of 1000 hours at 1000°C (1832°F) must not exceed ±400 ppm from the original size.

VIII.B.4.5.1.2 Sample and Procedure:

The suggested sample size is 76.2 x 12.7 x 12.7mm (3 x 1/2 x 1/2 in) with the long dimension parallel to the matrix axial direction.

VIII.B.4.5.1.3 Matrix Sample Selection:

At least two (2) samples should be taken near the core outer diameter and at least two (2) samples should be taken near the core inner diameter. Data should be generated at intervals of 1, 2, 4 days, 1 week and weekly thereafter for a total of 6 weeks using a Pratt and Whitney supermicrometer or the equivalent.

VIII.B.4.5.2 Thermal Expansion

VIII.B.4.5.2.1 Specification:

The total excursion in thermal expansion allowable between room temperature and 1000°C (1832°F) is dependent on matrix tangential strain tolerance and the regenerator rim design.

Upon mutual procurer-supplier agreement on a standard material expansion curve between 20°C (68°F) and 1000°C (1832°F) the thermal expansion curve of any material produced shall not vary from the standard more than ±100 ppm measured at temperature intervals of 100, 200, 300, 400, 600, 800, and 1000°C (1832°F).

VIII.B.4.5.2.2

Sample and procedure: The suggested sample size is 51 x 6.4 x 6.4mm (2 x 1/4 x 1/4 in) sectioned with the long dimension parallel to the axial direction of the matrix. Orientation is arbitrary in the solid material.

VIII.B.4.5.2.3

Testings

VIII.B.4.5.2.3.1

Test I: Matrix and hub material matrix sample selection should include at least one sample taken near the O.D. and at least one taken near the I.D. Data should be generated between 1000°C (1832°F) and room temperature.

VIII.B.4.5.2.3.2

Test II: After assembly firing (matrix only: ref. VIII.B.4.1.2), matrix sample selection should include at least one sample taken near the O.D. and at least one taken near the I.D. Data should be generated between 1000°C (1832°F) and room temperature.

VIII.B.4.5.2.3.3

Test III: Thermal Expansion Stability (Matrix only). A matrix O.D. thermal expansion sample will be soaked at 1000°C (1832°F) for 1000 hours. Data should be generated between 1000°C (1832°F) and room temperature.

VIII.B.4.5.4 Modulus of Rupture and Elastic Modulus Specification

VIII.B.4.5.3.1

The allowable average strain tolerance (Modulus of Rupture/Elastic Modulus) based on eight (8) separate determinations is dependent on the matrix material thermal expansion characteristics and the regenerator rim design.

VIII.B.4.5.3.2

Sampling and Procedure: The effect of specimen orientation, sheet radius of curvature and size is important in obtaining good mechanical property data and, therefore, the following requirements must be met.

VIII.B.4.5.3.2.1

Specimen Size Radial Specimen — 114 mm long x 19 mm tan. direction x 12.7 mm axial direction (4-1/2 x 3/4 x 1/2 in)

Tangential Specimen — 152 mm long x 25.4 mm radial direction x 12.7 mm axial direction (6 x 1 x 1/2 in)

VIII.B.4.5.3.2.2

Sample location, Cutting and Finishing: The location of the tangential (T) and radial (R) samples relative to the core radius and flat sheet radius of curvature is shown in Figure VIII.B.4.1. Tangential specimens must be in true chordal orientation and radial specimens must have the lon, axis truly radial.

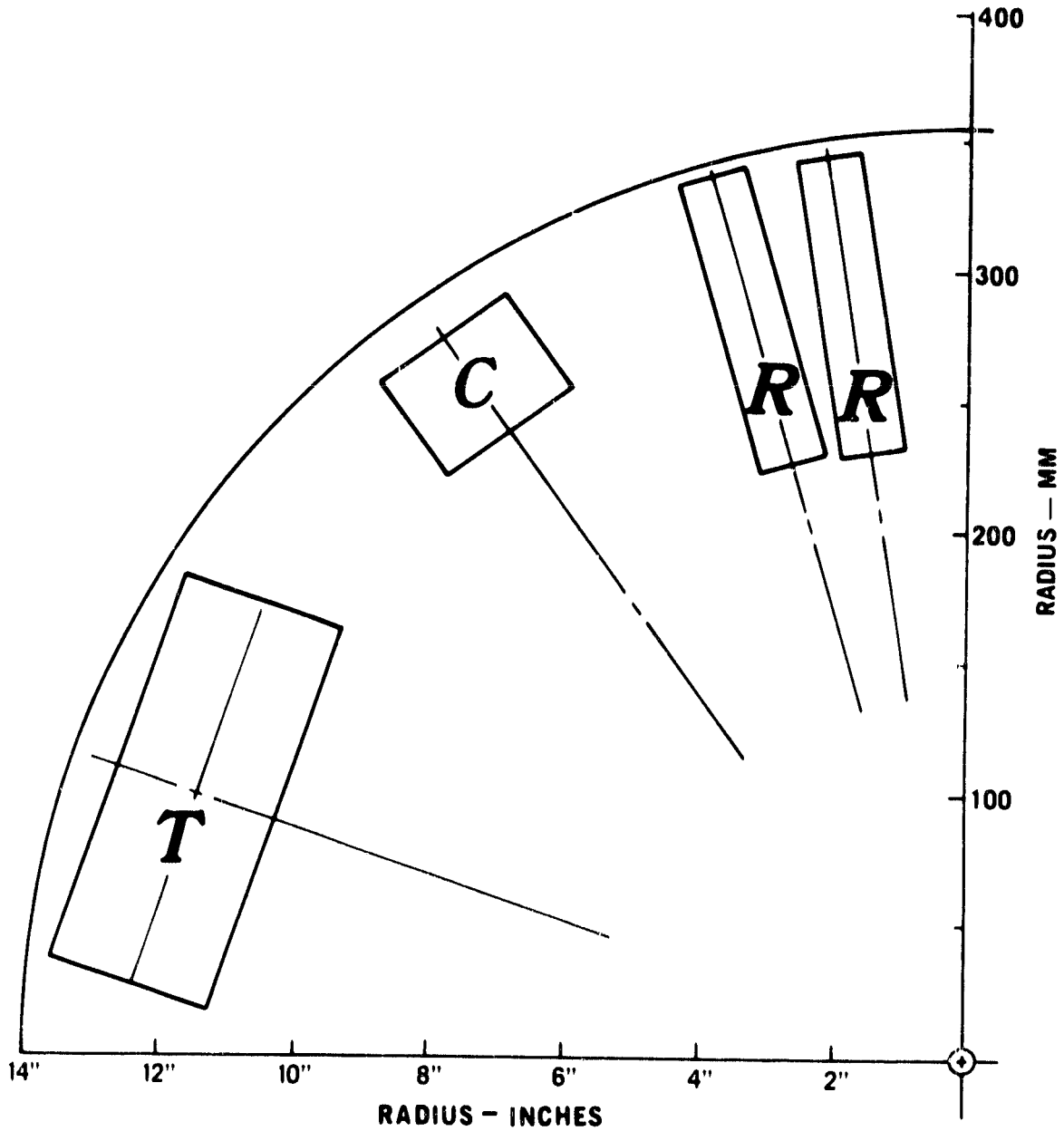

Figure VIII.B.4.1 Location of Mechanical Test Specimens on Regenerator Core

The specimens are outlined and saw cut from the full size matrix; the tangential matrix block will yield eight (8) specimens and each radial block yields four (4) specimens for a total of eight (8).

The planar surface of each specimen is ground flat and parallel to within ±.03 mm (±.001 in). The planar surfaces are the two longer dimensions in both orientations.

VIII.B.4.5.3.2.3 Modulus of Elasticity Test

VIII.B.4.5.3.2.3.1

Strain gauge (static test): Strain gauges between 12.7mm and 19mm (1/2 x 3/4 in) long are applied to the tensile surface of the 4-point bend specimen, and stress versus strain recorded until specimen failure occurs.

VIII.B.4.5.3.2.3.2

Sonic Resonance Method: Use ASTM Standard C623-69T, "Tentative Method of Test for Young's Modulus, Shear Modulus and Poisson's Ratio for Glass and Glass Ceramics by Resonance."

VIII.B.4.5.3.2.4

Modulus of Rupture Test: Room temperature 4-point bend test with a 88.9mm (3-1/2 in) outside span and a 19mm (3/4 in) inside span. The stress application rate should be approximately 689 KPa/min (100 psi/min) for tangential specimens and approximately 1378 KPa/min (200 psi/min) for radial samples. See Figure VIII.B.4.2.

VIII.B.4.5.4 Thermal Stress Factor

The thermal stress factor (θ) is a parameter that relates mechanical properties to thermal properties by the following expression:

$$\theta = \frac{S.T.}{\Delta PPM} = \frac{MOR/MOE}{\Delta PPM} = \text{Thermal Stress Factor}$$

where

MOR = Modulus of rupture from a 4-point bend test (VIII.B.4.5.3.2.4), psi

MOE = Modulus of elasticity (VIII.B.4.5.3.2.3), psi

S.T. = Strain tolerance (VIII.B.4.5.3.1), ppm

ΔPPM = Maximum thermal strain differences between 1000°C (1832°F) and room temperature (VIII.B.4.5.2.1), ppm

The allowable thermal stress factor for a given application is heavily dependent on the regenerator rim design. For a regenerator with an all matrix rim, the minimum value should be 0.75. If the regenerator rim contains solid ceramic pins, the minimum value will approach 1.0. Incorporating rim stress relieve slots as discussed in Section V can lower the minimum thermal stress factor considerably. Consequently, the minimum thermal stress factor must be determined by the procurer based on the regenerator rim design selected.

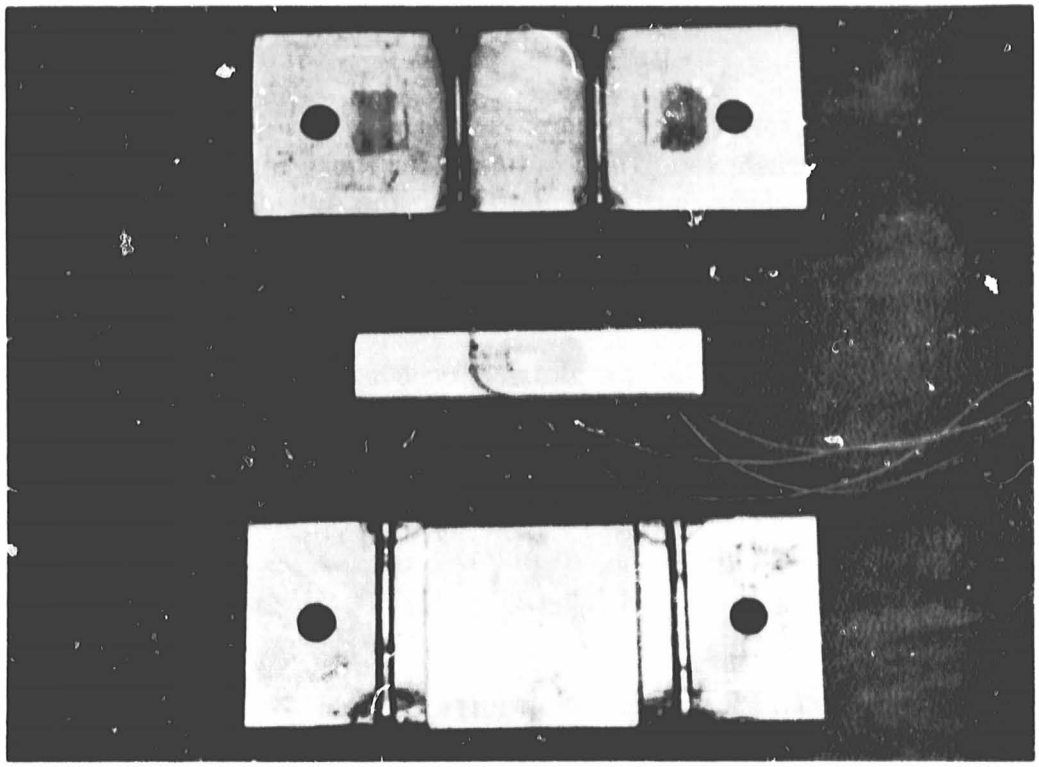

A

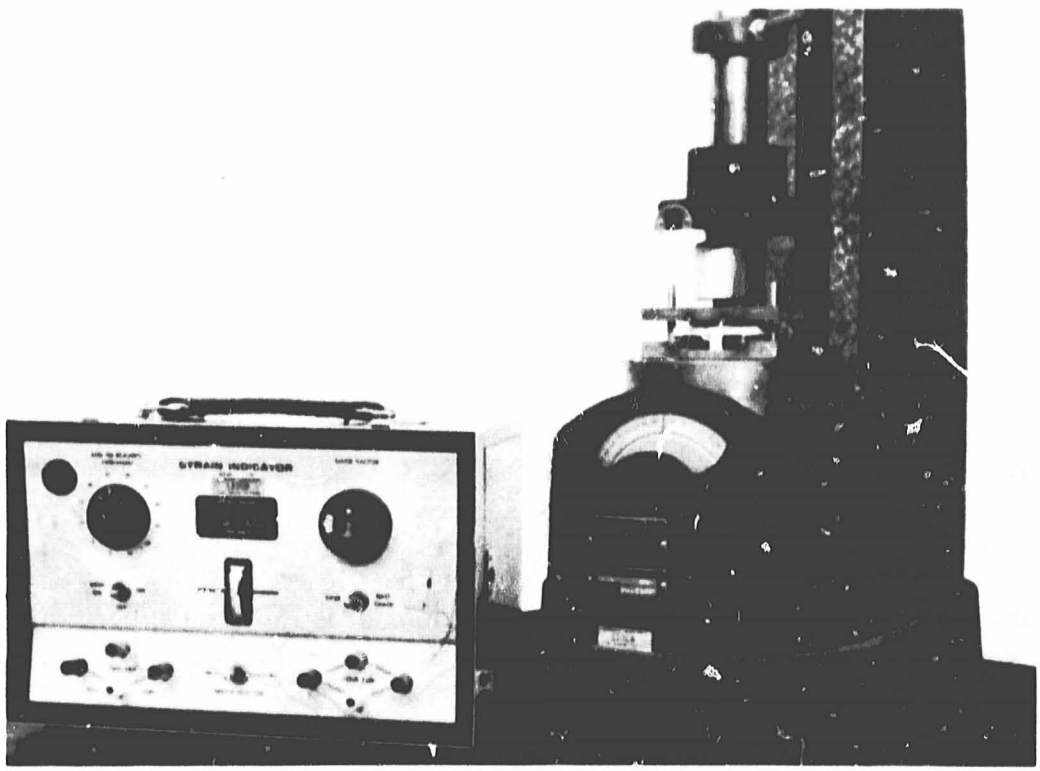

B

Figure VIII.B.4.2 (A) Four Point Bend Test Fixture and Test Specimen, (B) Strain Gauge Bridge and Spring Loaded Tester

VIII.B.4.5.5 Radial Crush Strength

VIII.B.4.5.5.1

A minimum radial crush strength is required for those regenerator assemblies in which the ring gear is elastomerically bonded to the outside diameter of the core. The actual radial crush strength is based on eight (8) separate determinations.

VIII.B.4.5.5.2

Sampling and Procedure: The sample is to be 50mm long x 50mm tangential direction x 50mm axial direction (2.0 x 2.0 x 2.0 in) and is to be located relative to the core radius and flat sheet radius of curvature as shown in Figure B.4.1 Sample "C". The specimens are outlined and saw cut from full-size matrix and the planar surface of each specimen is ground flat and parallel to within ±.03mm (±.001 in). The planar surfaces are the tangential-axial planes.

VIII.B.4.5.5.3

Radial Crush Test: The compressive strength is measured by loading the specimens to failure in a testing machine at a cross-head speed of 5mm/min (0.2 in/min). In order to provide uniform loading, thin elastomer sheets are to be incorporated on the specimen loaded surfaces.

VIII.B.4.5.5.4

Minimum Crush Strength: The results of eight specimens shall be plotted on Weibull paper, and the material shall have a B_{10} strength of 200 KPa (29 psi) with a slope, m, of the Weibull distribution curve of at least 4.0.

VIII.B.4.5.6 Open Frontal Area

VIII.B.4.5.6.1

Specification: The open frontal area must be within ±5% of the nominal value as calculated from the fired bulk density measurements and the wall density. The following will be given: bulk, displacement and skeletal density and wall porosity as obtained from conventional porosimeters.

VIII.B.4.5.6.2

Procedure: The volume used to obtain wall density is the atmospheric displacement volume in a mercury porosimeter analysis.

VIII.B.4.5.7 Assembly Strain

VIII.B.4.5.7.1

Specification: A minimum of four tangential direction strain gauges are to be mounted. One on the hot face and one on the cold face directly over each other

and a second set to be mounted in like manner 180° from the first set. Place gauges as close as possible to the outside edge.

VIII.B.4.5.7.2

Procedure: Core will be O.D. filled. Core to be saw cut radially near strain gauges, and maximum strain change measured to be less than 150 ppm.

VIII.B.4.5.8 Matrix Chemical Attack Resistance Screening

VIII.B.4.5.8.1

Cold face chemical attack (sulfuric acid cycle): Up to four standard test specimens for each candidate material shall be measured and then immersed for two hours in a 1% aqueous solution of H_2SO_4 (reagent grade) maintained at ambient temperature. At the onset of this immersion treatment, the solution and samples shall be out-gassed during two minutes of evacuation to a pressure of at least 25 inches (63.5mm) of mercury. Upon completion of the immersion cycle, the specimens shall be removed from the H_2SO_4 solution, drained gravitationally, and heated to 316°C (600°F) for a two-hour temperature soak. After cooling to room temperature, specimens shall again be measured. This constitutes one test cycle. Each test specimen shall be subjected to a minimum of three cycles.

VIII.B.4.5.8.2 Hot Face Chemical Attack (Sodium Chloride Cycle)

Duplicate standard test specimens for each candidate material shall be measured, weighed and then soaked for five minutes in a boiling 3.5% aqueous solution of sodium chloride (reagent grade). Excess moisture shall be blown out of the matrix with filtered, oil-free compressed air or nitrogen. Specimens shall be dried in air for one hour at 392°F. The treated specimens shall be weighed, measured, and then heated for three weeks total at 800°C (1472°F). The test specimens shall be introduced into the cool furnace, heated to the test temperature at a rate not greater than 50°C (90°F) per minute, maintained at the test temperature for the specified time, and cooled to room temperature at a rate not greater than 50°C (90°F) per minute. Measurements shall be taken at room temperature after 1, 3, 7, 14 and 21 days.

VIII.B.4.5.8.3 Standard Specimens

Specimens for all laboratory tests shall be of a matrix configuration and shaped as rectangular parallelopipeds with dimensions: 3 in x 1 in x 1 in (76.2mm x 25.4mm x 25.4mm). These matrix specimens shall be oriented such that the major dimension is in the axial direction. Specimen ends shall be ground to a flatness of 1 mil (0.03mm), and the opposing axial ends shall be machined so as to be parallel to one another to within 1 mil (0.03mm).

VIII.B.4.5.8.4 Measurements

Specimen lengths shall be recorded to the nearest one millionth of an inch. The type instrument used and the probable measurement accuracy shall be reported.

Measurements shall be carried out prior to the initiation of the test procedure and after each successive testing time interval. The measurement data shall be reported as parts length change per million parts original specimen length (ppm) as a function of the testing time interval and temperature. Specimen expansion shall be treated as positive, while contraction shall be expressed as a negative magnitude. The thermal expansion behavior between room temperature and the specific test temperature shall be determined for each candidate material prior to initiation and subsequent to completion of the testing program.

VIII.B.4.6 Acceptance

VIII.B.4.6.1

If any regenerator matrix or core samples, representative of the current manufacturing process, fail to meet the properties specified in Section VIII.B.4.5, supplier will request a deviation to the specification to continue shipping cores The initial core under deviation will be specified by the supplier through a relation of a material, process event or testing of retained cores under Section VIII.B.4.3.

VIII.B.5 REGENERATOR RIM FILLING PROCESS SPECIFICATIONS:

The process defined by this specification is a procedure for filling the matrix passages of regenerator cores with a ceramic coating material approximately 5.1-15mm (.20-.60 in) deep. This coating is used to fill that portion of the matrix rim of the regenerator that is in contact with the peripheral seal during operation. As a consequence, the fill or coating prevents pressure feedback under the seal shoe from the cold to the hot side. The specification for filling the matrix is as follows:

VIII.B.5.1 Filler Material:

The filler material shall be prepared as follows:

1) Obtain −100 +200 mesh size powder of matrix material.

2) Mix one part of the matrix powder with three parts by weight of an aluminum silicate low temperature setting cement. QF-180 manufactured by Carborundum Company is adequate.

3) Thoroughly blend (at least 5 minutes) in a liquid-solid blender such as a Waring blender for small quantities or a Patterson-Kelly Twin Shell blender for large quantities.

4) Store in sealed glass containers. Do not use material stored for over thirty days.

VIII.B.5.2 Preparation of the Regenerator Core:

The passages in the core matrix to be filled, shall be free of all loose dirt and any extraneous material. To ensure this, the passages shall be cleaned by blowing with filtered, oil-free, high-pressure, compressed air.

VIII.B.5.3 Filling:

The filler material shall be thoroughly mixed and applied onto the surface and worked into the passages approximately 6.4mm (1/4 in) deep. To accomplish this, spatula or an air-operated caulking gun or any such means may be used.

After filling, the surface should be wiped clean with a wet soft cloth, making sure that the filled surface is smooth and even.

VIII.B.5.4 Drying:

After filling, the core should be dried in an air circulating oven at 93°C (200°F) for 1 hour minimum and 121°C (250°F) for 1 hour minimum. The core must be positioned in the oven to expose all the filled surfaces to circulating air. After drying, air cool to room temperature. Cements other than QF-180 may require different cure temperatures and times.

VIII.B.5.5 Finishing:

If any bubbles or unevenness is present at the filled surface after drying, the surface must be cleaned using 150 grit abrasive coated screen such as "Sandscreen" (M7555) of Carborundum Company or 150 grit "Wetordry Fabricut" T04 grade of Minnesota Mining and Manufacturing Company. Care should be exercised to prevent embedding the abrasive in the filled surface.

VIII.C. Task Summary

A core material and design specification for a regenerative heat exchanger intended for operation in a gas turbine engine with a maximum of 1000°C (1832°F) inlet temperature was completed. This procurement specification evolved from experience accumulated over the last thirteen years in laboratory and engine testing of ceramic materials proposed for service as regenerator cores in the Ford 707 Gas Turbine at 800°C (1472°F) and 1000°C (1832°F) maximum inlet temperature.

The specification was written in a general sense and is intended to include a wide variety of ceramic materials fabricated into high open area cellular structures by any one of a number of viable processes. These fabrication techniques include extrusion, wrapped paper, calendering, embossing, glass tube bundling and others.

TASK IX. PROJECT MANAGEMENT

IX.A. Introduction

During the first quarter of 1978 it appeared to be desirable to test more cores at 1000°C (1832°F) regenerator inlet temperatures, rather than 800°C (1472°F), since automotive turbine and Stirling engines would have to operate at higher temperature if they are to be competitive with other power plants. It was also desirable to place more lower cost materials, like MAS, on durability test; again to allow the turbine and Stirling to be more competitive with other power plants. To meet these two new objectives, which would result in a major change in program direction, a study was initiated in January 1978. Three different plans or "cases," which would place more emphasis on higher temperature testing, were studied. Their individual impact on the overall Regenerator Program was evaluated.

During the second quarter of 1978, Ford and NASA Project Management agreed to place more emphasis on 1000°C (1832°F) testing. Two engines were then converted from 800°C (1472°F) to 1000°C (1832°F) testing. This change in direction was done at no additional cost to NASA.

During the fourth quarter of 1978, Ford and NASA Project Management agreed to extend the program an additional six months at no additional cost to NASA. This extended the completion date from June 30, 1979, to December 31, 1979. The major advantage was that additional time would permit other suppliers to develop full-size cores for test evaluation.

IX.B. Discussion

A Weibull Analysis was used to study the effect of redirecting the program to increase the amount of engine testing conducted at 1000°C (1832°F). The three different approaches or cases studied were:

Case I: The original program remains unchanged, with 4 engines operating at 800°C (1472°F), 1 at 1000°C (1832°F), and 1 engine used for accelerated chemical attack testing.

Case II: The 4 engines operating at 800°C (1472°F) converted as quickly as possible to 1000°C (1832°F) engines and all 800°C (1472°F) cores are retired. Six new, thin-wall AS and 2 new MAS cores are started on 1000°C (1832°F) test in these 4 engines.

Case III: Two of the 4 engines at 800°C (1472°F) are converted to 1000°C (1832°F) tests as quickly as possible and two new thin-wall AS cores and two new MAS cores are tested at 1000°C (1832°F) in these engines. The two highest-hour thick-wall AS cores and the two highest-hour, thin-wall AS cores are continued on test at 800°C (1472°F). In both case II and III the two cores that were on test at 1000°C (1832°F) are continued on test.

Based on the Weibull analysis for the three cases evaluated, Case III was selected. Two 800°C (1472°F) durability engines were converted to 1000°C (1832°F)

durability engines during the second quarter of 1978. Case III would allow a high confidence to be made in B_{10} life projections at 800°C, as well as allowing more AS and MAS cores to be placed on test at 1000°C. It also allowed the two high-hour 1000°C cores to be tested in separate engines, as protection in case of a disastrous engine failure.

The same analysis showed that a low confidence must be placed on any B_{10} life projections at 1000°C (1832°F) made at the end of 1978. Continuation of the 1000°C (1832°F) tests for another year would increase the confidence in the B_{10} projections to a reasonable level. Ford and NASA management agreed to extend the program from December 31, 1978, to June 30, 1979, at no additional cost to NASA.

During the fourth quarter of 1978, Ford and NASA Project Management agreed to extend the program an additional six months at no additional cost to NASA. This extended the completion date from June 30, 1979, to December 31, 1979. The major advantage was that additional time would permit other suppliers to develop full-size cores for test evaluation.

Since the original core test hour objectives at 800°C and 1000°C had been exceeded, new objectives were established for the contract completion date (December 31, 1979). The core test hour objectives at 800°C were increased from 68,000 to 76,000, while the objective at 1000°C was increased from 22,000 to 28,000.

Both of the new core hour objectives were exceeded. A total of 77,300 and 28,840 core hours were accumulated at 800°C and 1000°C, respectively.

Utilizing the total number of hours accumulated on thick- and thin-wall A-S cores at both temperatures together with an empirical reliability relationship from Weibull distribution theory, the projected confidence level for various B_{10} life objectives at 800°C was estimated (Figure I.B.1.4). The confidence level varies from 47% for a B_{10} life of 10,000 hours to 80% for a B_{10} life of 5000 hours.

IX.C. Task Summary

Program emphasis was directed to increased engine testing at 1000°C during the second quarter of 1978. In order to increase confidence level in B_{10} life projections for A-S cores, the original program was extended an additional year at no additional cost to NASA.

Based on an empirical reliability relationship from Weibull distribution theory the confidence level for A-S cores varies from 47% to 80% for B_{10} life at 800°C of 10,000 and 5000 hours, respectively.

TASK X. REPORTING REQUIREMENTS

In addition to periodic progress reports, three topical reports were required as part of the task requirements. The subjects of these reports, which were agreed upon by Ford and NASA personnel, were as follows:

1. Evaluation of Advanced Regenerator Systems — This study will tie together the major factors affecting the selection of the regenerators in a future, high-temperature, passenger-car turbine engine. Cost and size (for equal performance) will be the ultimate criteria used in this selection. The best obtainable wall thickness, open area, fin efficiency, and leakage will be estimated for each combination of ceramic material, manufacturing process and fin shape. The estimation will be based on an assumption of continued development and evolution of today's technology for a ten-year period. This Report was published in the third quarter of 1978.

2. Feasibility Study of Silicon Nitride Regenerators — If regenerator inlet temperatures exceed 1100 or 1200°C (2012 or 2192°F), something other than an oxide ceramic may be required. Silicon nitride was examined from a material, thermal stress, performance and manufacturing feasibility viewpoint. Its advantages and limitations were reviewed in detail. This report was published in the fourth quarter of 1979.

3. Regenerator Matrix Physical Property Data — The key physical property data, including F and J factors, compressive strength, coefficient of expansion, modulus of elasticity, MOR, and chemical attack results will be compiled for a limited number of key matrix configurations. This report was published in the second quarter of 1980.

REFERENCES

1. Anderson, D. H., Fucinari, C. A., Rahnke, C. J., and Rossi, L. R., Annual Summary Report, No. 2630-1, Automotive Gas Turbine Ceramic Regenerator Design and Reliability Program, ERDA Contract No. E (11-1) 2630, Sept. 15, 1975.

2. Cook, J. A., Fucinari, C. A., Lingscheit, J. N., and Rahnke, C. J., Annual Summary Report, No. 2630-18, Automotive Gas Turbine Ceramic Regenerator Design and Reliability Program, ERDA Contract No. E (11-1) 2630, Oct. 15, 1976.

3. Cook, J. A., Fucinari, C. A., Lingscheit, J. N., and Rahnke, C. J., Annual Summary Report, No. NASA CR-135330, Ceramic Regenerator Systems Development Program, NASA Contract No. DEN3-8, Dec. 1977.

4. Cook, J.A., Fucinari, C. A. Lingscheit, J. N., Rahnke, C. J., Rao, V. D., Quarterly Progress Report for Oct.-Dec. 1977, No NASA CR-135380, Ceramic Regenerator Systems Development Program, NASA Contract No. DEN3-8, Feb. 1978.

5. Cook, J. A., Fucinari, C. A., Lingscheit, J. N., Rahnke, C. J., Rao, V. D., Quarterly Progress Report for Jan.-Mar. 1978, No. NASA CR-135430, Ceramic Regenerator Systems Development Program, NASA Contract No. DEN3-8, May, 1978.

6. Cook, J. A., Fucinari, C. A., Lingscheit, J. N., Rahnke, C. J., Vallance, J. K., Quarterly Progress Report for April-June 1978, No. NASA CR-159432, Ceramic Regenerator Systems Development Program, NASA Contract No. DEN3-8, September, 1978.

7. Fucinari, C. A., Lingscheit, J. N., Vallance, J. K., Progress Report for July-December 1978, No. NASA CR-159541, Ceramic Regenerator Systems Development Program, NASA Contract No. DEN3-8, March, 1979.

8. Fucinari, C. A., Rao, V. D. N., Progress Report for January-June 1979, No. NASA CR-159707, Ceramic Regenerator Systems Development Program, NASA Contract No. DEN3-8, October 1979.

9. C. P. Howard, "Heat Transfer and Flow Friction Characteristics of Skewed Passage and Glass-Ceramic Heat Transfer Surfaces," T. R. No. 59, Department of Mechanical Engineering, Stanford University, Oct. 1963.

10. A. L. London, "Laminary Flow Gas Turbine Regenerators — Influence of Manufacturing Tolerance," Journal of Engineering for Power, Trans. ASME, Series A, Vol. 92, 1970, pp. 46-56.

11. C. A. Fucinari, "The Effect of Fin Geometry and Manufacturing Process on Ceramic Regenerator Thermodynamic Performance," American Society of Mechanical Engineers, Paper No. 77-GT-61, March, 1977.

12. R. K. Shah and A. L. London, "Laminar Flow Forced Convection Heat Transfer and Flow Friction in Straight and Curved Ducts — A Summary of Analytical Solutions," T. R. No. 75, Department of Mechanical Engineering, Stanford University.

13. Strong, G. S., "Ceramic Cements, Laminated and Methods," U.S. Patent No. 3,189,512, Corning Glass Works, Corning, N.Y.